

Thèse de doctorat

Pour obtenir le grade de Docteur de l'Université de VALENCIENNES ET DU HAINAUT-CAMBRESIS

Discipline, spécialité selon la liste des spécialités pour lesquelles l'Ecole Doctorale est accréditée :
Electronique

Présentée et soutenue par Kais, HASSAN.

Le 10/12/2012, à Villeneuve d'Ascq

Ecole doctorale :

Sciences Pour l'Ingénieur (SPI)

Equipe de recherche, Laboratoire :

Institut d'Electronique, de Micro-Electronique et de Nanotechnologie/Département d'Opto-Acousto-Electronique (IEMN/DOAE)

Institut Français des Sciences et Technologies des Transports, de l'Aménagement et des Réseaux/Laboratoire

Electronique, Ondes et Signaux pour les Transports (IFSTTAR/LEOST)

Le Laboratoire des Sciences et Techniques de l'Information, de la Communication et de la Connaissance (Lab-STICC).

Contributions aux capacités de reconnaissance de l'environnement de la Radio Cognitive pour des applications mobiles à grande vitesse

JURY

Président du jury

- Fijalkow, Inbar. Professeur des Universités. Ecole Nationale Supérieure de l'Electronique et de ses Applications (ENSEA), laboratoire ETIS, Cergy-Pontoise.

Rapporteurs

- Knopp, Raymond. Professeur des Universités. Eurocom, Sophia Antipolis.

- Cances, Jean-Pierre. Professeur des Universités. Université de Limoges, laboratoire XLIM.

Examineurs

- Fijalkow, Inbar. Professeur des Universités. Ecole Nationale Supérieure de l'Electronique et de ses Applications (ENSEA), laboratoire ETIS, Cergy-Pontoise.

- Ghannoun, Hassan. Chef de Projet Télécommunications, SNCF, Innovation & Recherche. Paris.

Directeur de thèse

- Berbineau, Marion. Directrice de Recherches, IFSTTAR LEOS. Villeneuve d'Ascq.

Co-directeur de thèse : Radoi, Emanuel. Professeur des Universités. Université de Bretagne occidentale.

Co-encadrant : Dayoub, Iyad. Maître de Conférences, HDR. Université de Valenciennes.

Co-encadrant : Gautier, Roland. Maître de Conférences. Université de Bretagne occidentale, Lab-STICC.

To my wife Lama, for her unconditional support and endless love,

To my family, who supported me in the hardest times,

To my beloved twins Wajd and Jana.

Acknowledgments

This dissertation represents three years of work with IFSTTAR, IEMN-DOAE, and Lab-STICC, and because of that, there are a large number of people to thank.

Firstly, I am very grateful to my supervisors Marion Berbineau, Emanuel Radoi, Iyad Dayoub, and Roland Gautier. Without their valuable guidance and constant encouragement this work would not have been possible. Each have contributed in significant ways to my education, either through my personal relationships or work experiences with them. Thank you all for your enthusiasm, dedication, time, positive attitude, valuable comments and suggestions.

My special thanks to Iyad Dayoub, whose encouragement and support on research, personal, and even financial levels, helped me through the most difficult times.

Also I thank the IFSTTAR, IEMN-DOAE, and Lab-STICC teams for receiving me as a Ph.D. student. Their support and warmth helped me in keeping the motivation levels high. Thank you all for both the technical and the non-technical discussions. Special thanks to my friends and colleagues in IFSTTAR-LEOST with whom I spent the most of my time.

I would like to take this opportunity to thank my scholarship donors, IFSTTAR and “Nord-Pas-de-Calais” region, for their financial support without which this research study would not have been possible. I must also thank the project CISIT which a part of these funds was in its framework.

Also, I would like to thank my reviewing committee members for accepting to dedicate their time and effort to examine this work.

Finally, and most importantly, I would like to express gratitude to my wife for her continuous support all the way to get here. Thanks to my family for being present through every step of my life and helping me to become the person I am today.

Title

Contributions to Cognitive Radio Awareness for High Mobility Applications

Abstract

An essential goal of railway operators is to increase safety, reduce operation and maintenance costs, and increase attraction and profit by offering new services to passengers. These objectives will be reached thanks to a huge increase of data fluxes exchanges between railways stakeholders and infrastructures. Interoperability, spectral efficiency, optimization of radio resource usages, and improvement of communications reliability are of significant interest for railway applications. The Cognitive Radio (CR) research has been successfully applied to meet the communication needs of the military as well as the public-safety sectors, which share many of the same needs as railway. CRs have shown significant promise to answer all of the previously listed requirements.

One of the main capabilities of a CR device is to sense and finally become aware of its environment. Three major domains define the environment of the CR, namely, the user, policy, and radio domains. This thesis highlights several contributions to radio environment awareness of a CR device. More specifically, these contributions lie in the spectrum awareness and waveform awareness functions of the CR. We designed these functions for the railways context, that is, a high speed vehicular context, besides difficult electromagnetic environments resulting a heavy-tailed impulsive noise.

An essential task in CR is to design a reliable spectrum sensing method that is able to detect the signal in the target channel, i.e. make CR aware of the spectrum resources availability. Hence, one of the main contributions of this thesis is an efficient blind non-parametric narrowband spectrum sensing method. The problem of wideband sensing is also studied and a low complexity fast solution is proposed in the thesis for this framework.

Cognitive radios are also expected to recognize different wireless networks and have capability to communicate with them. Transmission parameters of communications systems must be detected blindly if the system is not known to CR. Identifying some of the basic features of signal does enhance the CR awareness capability, i.e. giving the CR a waveform awareness dimension. Our contribution on this important CR related aspect is represented by two waveform identification methods that are introduced for two study-cases, namely, the MIMO and SIMO MC-DS-CDMA transmissions.

Last but not least, the special railways context implies some additional constraints on communications systems such as high mobility and heavy-tailed impulsive noise. These constraints are deeply analyzed and taken into account in this thesis using advanced Doppler spectrum and alpha stable models for the high mobility and impulsive noise respectively. A distribution fitting procedure of measured noise acting on GSM-R antennas is also proposed. Moreover, the effect of these special constraints on the addressed awareness functions, particularly the spectrum awareness one, is also evaluated. Another important contribution of the thesis is a method specially

designed to improve the spectrum sensing in the context of high mobility. Two methods are finally proposed to mitigate the effect of the heavy tails of impulsive noise, along with a new method to exploit the spatial correlations of multiple-antennas receiver.

Keywords : Cognitive radio, spectrum sensing, waveform identification, high mobility, heavy-tailed noise, multiple-antennas, multiple-input multiple-output systems.

Titre

Contributions aux capacités de reconnaissance de l'environnement de la radio cognitive pour des applications mobiles à grande vitesse.

Résumé

Les principaux objectifs des opérateurs ferroviaires visent à accroître la sécurité, réduire les coûts d'exploitation et de maintenance et augmenter l'attractivité et les bénéfices du transport ferroviaire en offrant de nouveaux services aux passagers. Ceci ne pourra être atteint que grâce à la multiplication des échanges de données entre les différents acteurs du monde ferroviaire. L'interopérabilité, l'efficacité spectrale, l'optimisation de l'usage des ressources radio et l'amélioration de la fiabilité des communications sont des exigences fortes pour les applications de télécommunication ferroviaires.

Les recherches dans le domaine de la radio cognitive ont vu le jour afin de répondre aux besoins de communication de l'armée ainsi qu'aux besoins dans les secteurs de la sécurité publique. Ces domaines partagent souvent les mêmes exigences que les chemins de fers. Ainsi, la radio cognitive a montré un potentiel prometteur pour répondre aux besoins listés précédemment.

Une des principales fonctionnalités d'un dispositif de radio cognitive est de prendre conscience de son environnement radioélectrique et de détecter les bandes disponibles. Trois principaux éléments définissent l'environnement de la radio cognitive : l'utilisateur, les règles d'accès au spectre radio et les domaines radio. Cette thèse met en avant plusieurs contributions relatives à la reconnaissance de l'environnement radiofréquence et la détection de bandes libres. Plus spécifiquement, ces contributions portent sur la reconnaissance par la radio cognitive de l'occupation du spectre et de la modulation des signaux présents dans les bandes analysées. Ces fonctions ont été conçues pour le contexte ferroviaire, c'est-à-dire la grande vitesse et un environnement électromagnétique difficile en présence de bruit impulsif.

Une brique essentielle de la radio cognitive repose sur des techniques fiables d'analyse du spectre capables de détecter un signal dans une bande donnée, c'est-à-dire permettre à la radio cognitive de prendre conscience des ressources spectrales disponibles dans la bande analysée. Ainsi, une des contributions principales de cette thèse consiste en une méthode aveugle non paramétrique et bande étroite d'analyse du spectre. Le cas large bande a aussi été étudié et une solution rapide et de faible complexité est aussi proposée dans ce contexte.

Les systèmes de radio cognitive doivent aussi être capables de reconnaître différents réseaux sans fils déployés dans leur environnement et de communiquer avec ces réseaux. Les caractéristiques de transmission de ces systèmes de communication doivent donc aussi être détectées de façon aveugle si le système n'est pas connu de la radio cognitive. L'identification des quelques caractéristiques clés des signaux présents dans la bande analysée permet d'améliorer considérablement les capacités cognitives de ces radios en leur permettant de prendre conscience des formes d'ondes présentes dans l'environnement. Notre contribution sur ce point important de la radio cognitive

a permis le développement de deux méthodes d'identification des formes d'ondes pour deux cas d'études : les transmissions MC-DS-CDMA dans les cas MIMO et SIMO.

Enfin, le contexte particulier du ferroviaire impose des contraintes particulières aux systèmes de communications telles que la grande vitesse et la présence de bruit impulsif. Dans ce travail nous avons analysé ces contraintes et les avons prises en compte en considérant un modèle avancé de spectre Doppler pour la grande vitesse et un modèle alpha stable pour le bruit impulsif. Nous avons ainsi proposé une méthode d'identification de la distribution statistique du bruit reçu par une antenne GSM-R validée sur des mesures réelles. En outre, les effets de ce bruit spécifique et de la grande vitesse ont été évalués sur une de nos méthodes de sondage spectral. En particulier, nous avons proposé une méthode conçue spécifiquement pour résister à la grande vitesse. Par ailleurs, nous avons aussi développé deux méthodes permettant d'atténuer les effets du bruit impulsif et une méthode qui exploite la corrélation spatiale d'un récepteur à antennes multiples

Mots Clef : Cognitive radio, sondage spectral, identification de forme d'ondes, grande vitesse ferroviaire, bruit impulsive, antennes multiple, multiple-input multiple-output.

Contents

List of Figures	xviii
List of Tables	xix
Mathematical notation and acronyms	xxvi
Introduction	1
1 Problem Foundation	9
1.1 Introduction	10
1.2 Thesis Context	10
1.2.1 Wireless Communications for Railways	10
1.2.2 Problematic, Demands, and Requirements	12
1.3 Cognitive Radio	14
1.3.1 What is a CR?	14
1.3.2 The CR Architecture	16
1.3.3 Existing CR Standards	17
1.3.4 CR Applications	18
1.4 Cognitive Radio for Railways: Merits and Challenges	19
1.4.1 Can CR be Beneficial for Railways?	19
1.4.2 How do we Propose to Apply CR for Railways?	20
1.4.3 Challenges	22
1.5 Focus of the Thesis	22
2 System Model	25
2.1 Introduction	26
2.2 Mobile Radio Channel Model	26

2.2.1	Characteristics of Mobile Radio Channels	26
2.2.2	Characterization in Time and Frequency	27
2.2.3	Mobile Radio Channels : Doppler Effect	29
2.2.4	Mobile Radio Channels Models	30
2.3	Signal Model	33
2.3.1	Received Signal Representation	33
2.3.2	Multiple-antennas Spatial Correlation	36
2.3.3	Transmission Schemes	37
2.4	Noise Model	38
2.4.1	The Gaussian Model	38
2.4.2	Heavy-tailed Impulsive Noise in Communications	38
2.4.3	Case Study : Electromagnetic Interferences Acting on GSM-R Antennas	40
2.5	Conclusions	45
3	Waveform Awareness for Cognitive Radios	47
3.1	Introduction	48
3.2	Modulation Scheme Recognition	48
3.2.1	Introduction	48
3.2.2	Preliminary Literature Review	49
3.2.3	Automatic Modulation Recognition Using Wavelet Transform	51
3.2.4	Automatic Modulation Recognition Using Higher Order Statistics	53
3.2.5	ANN Classifier	55
3.2.6	Cooperative Automatic Modulation Recognition	55
3.2.7	Case Study : Blind Digital Modulation Recognition for MIMO Systems	58
3.3	Modulation Technique Identification	69
3.3.1	Preliminary Literature Review	69
3.3.2	Case Study : Blind SIMO MC-DS-CDMA Identification	71
3.4	Conclusions	79
4	Spectrum Sensing for Cognitive Radio	81
4.1	Introduction	82
4.2	Spectrum Sensing for Cognitive Radio	82
4.2.1	Spectrum Sensing Concept	82

4.2.2	Sensing Methods Classification	83
4.2.3	Cooperative Sensing	84
4.3	Narrowband Spectrum Sensing	85
4.3.1	Introduction	85
4.3.2	Traditional Spectrum Sensing	85
4.3.3	Multiple-antenna Spectrum Sensing	87
4.3.4	Predicted Eigenvalues Threshold	91
4.3.5	Conclusions	97
4.4	Wideband Spectrum Sensing	98
4.4.1	Preliminary Literature Review	98
4.4.2	Improved Welch Periodogram Based Detection	102
4.4.3	Discussion	108
4.5	Conclusions	108
5	Narrowband Spectrum Sensing For Railways	111
5.1	Introduction	112
5.2	Weighted Covariance Value Based Spectrum Sensing for Time-Varying Channels	112
5.2.1	System Model	112
5.2.2	The Proposed Method	113
5.2.3	Performance Analysis	114
5.2.4	Numerical Results and Discussions	117
5.3	Spectrum Sensing with Spatially-Correlated Multiple-Antennas	120
5.3.1	Preliminary Literature Review	120
5.3.2	Predicted Eigenvalues Threshold Sensing Performance with Spatially-Correlated Multiple-Antennas	121
5.4	Spectrum Sensing in the Presence of Impulsive Noise	126
5.4.1	Preliminary Literature Review	127
5.4.2	Basic Properties of $S\alpha S$ Distribution	128
5.4.3	System Model	129
5.4.4	α -Stable Noise Mitigation	130
5.4.5	Generalized Covariation Coefficient Absolute Value Based Spectrum Sensing	131
5.4.6	Performance Evaluation	133
5.5	Conclusions	136

General Conclusions and Future Works	139
A α-stable Noise Generation	145
B Appendix Related to Chapter 3	147
B.1 Theoretical Values of the HOS for different modulation schemes	147
B.2 Derivation of ZF Post-processing SNR in The Presence of Channel Estimation Error	147
C Appendix Related to Chapter 4	149
C.1 Derivation Details of the SPET Missdetection Probability	149
C.2 Mathematical Derivation for the Pre-whitening Technique	151
D Appendix Related to Chapter 5	153
D.1 Derivation of Equation (5.8)	153
D.2 Optimization of the Weighting Matrix for Time-varying Channels	154
Bibliography	157

List of Figures

1.1	The conceptual model that translates information from user domain into communication system exigencies to be respected by the proposed solution.	14
1.2	Summary of spectrum band occupancy calculations [14].	15
1.3	The Cognition Loop [5].	16
1.4	Generic CR architecture [19].	17
1.5	Classification of cognitive radio applications [22].	18
1.6	Proposed “CR mobile terminal” architecture dedicated for railways communication system.	21
2.1	Characterization of mobile radio channels in time and frequency.	30
2.2	Multiple-antennas receiver at the secondary user (the moving train) in the presense of P primary users (available radio services).	34
2.3	System Model.	35
2.4	Definitions of the time characteristics of transient EM interferences acting on GSM-R antennas.	40
2.5	EM interferences measurements distribution fitting procedure.	41
2.6	Performance comparison of different stable distribution parameters estimators for different values of α (a) the NMB of α estimators. (b) the MSE of α estimators. (c) the NMB of γ estimators. (d) the MSE of γ estimators.	44
2.7	PDF of measured data	45
3.1	Block diagram of the pattern recognition based methods	50
3.2	A block diagram of the proposed HOS based modulation recognition algorithm for MIMO systems.	59
3.3	Probability of correct recognition versus SNR for AMR-ZF in the following cases (a) Θ_1 through spatially-uncorrelated channel (b) Θ_1 with Kronecker model ($ \rho_t = \rho_r = 0.5$) (c) Θ_2 through spatially-uncorrelated channel (d) Θ_2 with Kronecker model ($ \rho_t = \rho_r = 0.5$).	64

3.4	Probability of correct recognition versus SNR for different MIMO antenna configurations (AMR-ZF when considering Θ_2 through spatially-uncorrelated channel).	65
3.5	Probability of correct recognition versus SNR for different σ_e^2 (channel estimation error variance) values (AMR-ZF when considering Θ_2 with Kronecker model, $ \rho_t = \rho_r = 0.5$).	65
3.6	Probability of correct recognition versus SNR for AMR-SCMA in the following cases (a) Θ_1 through spatially-uncorrelated channel (c) Θ_1 with Kronecker model ($ \rho_t = \rho_r = 0.5$) (b) Θ_2 through spatially-uncorrelated channel (c) Θ_2 with Kronecker model ($ \rho_t = \rho_r = 0.5$).	66
3.7	AMR-ZF performance for Θ_2 with Kronecker correlation model in the following cases (a) $ \rho_t = \rho_r = 0$ (b) $ \rho_t = \rho_r = 0.3$ (c) $ \rho_t = \rho_r = 0.5$ (d) $ \rho_t = \rho_r = 0.7$ (e) and $ \rho_t = \rho_r = 0.9$	66
3.8	AMR-SCMA performance for each modulation scheme with unknown spatially-uncorrelated channel matrix for MIMO system using $P = 2$ and $M = 4$ antennas.	67
3.9	Performance comparison among different algorithms for Θ_2 with Kronecker model ($ \rho_t = \rho_r = 0.5$).	68
3.10	SIMO MC-DS-CDMA modulator scheme.	71
3.11	Autocorrelation of the CP multi-carrier signal.	75
3.12	Autocorrelation estimator fluctuations of MC-DS-CDMA signal with 1/4 cyclic prefix guard interval, SNR = -3 dB.	77
3.13	Autocorrelation estimator fluctuations of MC-DS-CDMA signal with 1/4 zero-padding guard interval, SNR = -3 dB.	77
3.14	The detection probability of the MC-DS-CDMA signals for different SNRs as a function of the number of analysis windows.	78
3.15	Performance comparison between the T_u estimation method based on the autocorrelation function and the proposed one (based on the autocorrelation estimator fluctuations). The normalized root mean square error of two estimators as a function of SNR under fading channels.	78
4.1	The general picture of the radio spectrum given each sensing interval τ_{si} . This Figure illustrates the opportunities in time and frequency.	83
4.2	The wideband of interest in the form of multi-bands. The j^{th} wideband is characterized by its band-edge frequencies $f_{l,j}, f_{u,j}$, and it can be divided into several narrowbands.	83
4.3	Spectrum sensing methods classification [81].	84
4.4	The eigenvalues of the sample covariance matrix and the adaptive PET model at $N = 1000, P = 2, M = 4$ and $L = 10$	92

4.5	(a) Missdetection probability versus SNR for OPET and SPET methods compared with the asymptotic results at different values of the number of the observed samples when $M = 4$, $L = 1$ and $P = 1$. (b) SPET missdetection probability versus SNR for different numbers of antennas when $N = 5000$, $L = 1$ and $P = 2$.	96
4.6	The MPET sensing performance (under $\mathcal{H}_{1,0}$ and $\mathcal{H}_{1,1}$) compared with SPET method when $N = 10000$, $M = 4$, $P = 2$, $L = 1$ and $C_1 = C_2 = 6$. Also, the introduced confidence metric, based on PET, is displayed.	97
4.7	Missdetection probability versus SNR for several sensing methods when $N = 10000$, $M = 4$, $P = 2$, $C_1 = C_2 = 6$ and $L = 1$	98
4.8	Block diagram of the wavelet based WSS technique (also known as the edge detector) [101].	99
4.9	Block diagram of the wavelet based WSS technique combined with compressive sensing [104].	100
4.10	The implementation of the random analog-to-digital converter (RADC) system [107].	101
4.11	Block diagram of the pseudo-random demodulator [108].	101
4.12	The block diagram of non-parametric Welch periodogram estimator combined with an optimization method to refine the spectral components	102
4.13	The detailed procedure of optimization method for refined spectral components estimation.	103
4.14	The detection of six occupied subbands of different bandwidth values at different central frequencies (total duration is $7.5 \mu\text{s}$, $K = 25$, $P_f = 0.1$, and $\text{SNR} = -5 \text{ dB}$). This Figure shows the filtered periodogram with the estimated threshold. 106	106
4.15	The missdetection probability versus SNR for Welch based algorithm at different number of segments ($K = 25, 50$, and 75) when $N_B = 6$, $\tau_{sd} = 7.5 \mu\text{s}$, and $P_f = 0.1$.	107
4.16	The missdetection probability versus SNR for different information combining approaches when $K = 25$, $N_B = 6$, $\tau_{sd} = 7.5 \mu\text{s}$ and $P_f = 0.1$	107
5.1	(a) The ACF, $r_h(\tau)$, of the complex waveform of the reference model in comparison with the corresponding ACF, $\tilde{r}_h^{(k)}(\tau)$, of the simulation model designed using the GMEDS ₁ . (b) Simulated uncorrelated Rayleigh fading waveforms ($ h^{(k)} $, $k = 1, 2, 3$) using the GMEDS ₁ ($f_d = 100\text{Hz}$, $N_i = 20$).	118
5.2	The probability of missdetection versus SNR for SPET method at different maximum Doppler frequency (f_d) values when $N = 10000$, $P = 2$, $M = 4$, $\rho_r = 0$ and $L = 20$	119
5.3	The probability of missdetection versus SNR for WCV-T method at different maximum Doppler frequency (f_d) values when $N = 10000$, $P = 2$, $M = 4$, $\rho_r = 0$ and $L = 20$	119

5.4	The probability of missdetection versus SNR for WCV-T method at different smoothing factor (L) values when $N = 10000, P = 2, M = 4, \rho_r = 0$ and $f_d = 200$. Also, the missdetection probability versus L at a fixed SNR = -14 dB.	120
5.5	(a) The eigenvalues of the receive correlation matrix for $M = 4$. (b) The expected value of the test statistic T_{SPET} , for different values of ρ_r and M , when the sample covariance matrix is calculated for noise-free signals.	125
5.6	The probability of missdetection versus SNR for SPET method at different receive spatial correlation coefficient (ρ_r) values when $N = 10000, P = 2, M = 4$, and $L = 1$	126
5.7	The probability of missdetection versus SNR for WCV-S method at different receive spatial correlation coefficient (ρ_r) values when $N = 10000, P = 2, M = 4$, and $L = 1$	126
5.8	Block diagram of the myriad filtering based spectrum sensing.	131
5.9	Myriad filtering of chirp signal corrupted with $S\alpha S$ distributed heavy-tailed noise for $\alpha = 1.253$ and GSNR = 2 dB (a) original signal (b) noisy signal (c) filtered signal. Also, the RMSE as a function of the GSNR is given for $\alpha = 1.253$ (d).	134
5.10	Missdetection probability of MyrF based spectrum sensing versus GSNR for different α values when $N = 10000, L = 1, M = 4$ and $P = 1$	134
5.11	Root minimum square error of the MFLM estimator of the covariation coefficient as a function of the parameter p	135
5.12	Generalized CCAV missdetection probability versus GSNR for different α values when $N = 10000, L = 1, M = 4$ and $P = 1$	135
A.1	Estimated CDF of simulated α -stable distributed data using the inverse transform method and the corresponding theoretical CDF.	145
C.1	The covariance matrix of Gaussian noise acting at receiver antennas after applying the narrowband filter.	152
C.2	The covariance matrix of Gaussian noise acting at receiver antennas after applying pre-whitening technique to remove the effect of the narrowband filter.	152

List of Tables

1.1	Example of frequency allocations for railways around Paris [4].	11
1.2	Frequency bands and their usage for railway communications in USA [5].	11
1.3	List of various projects of railway communication systems.	12
2.1	The estimated parameters for each assumed model besides the KL divergence between the estimated PDF and the empirical PDF.	45
4.1	Spectrum sensing requirements in IEEE 802.22	86
4.2	Comparison among some properties, advantages and drawbacks of the different traditional spectrum sensing techniques	87
5.1	Maximum Doppler frequency (Hz) as a function of some values of the train speed (Km/h) when the central frequency is 2.5 GHz and 921 MHz (the last value corresponds to the GSM-R standard).	117
B.1	Some theoretical statistical moments and cumulants values for different modulation schemes of interest.	147

Mathematical notation and acronyms

List of Mathematical Notations and Operators

$(.)^*$	Conjugate operation.
$(.)^T$	Transpose operation.
$(.)^H$	Hermitian conjugate transpose.
$(.)^\dagger$	Pseudo inverse operation of the matrix argument.
$E(.)$	Expectation operator.
$ \cdot $	Absolute value of the scalar argument.
$\ \cdot\ $	Euclidean norm of the vector argument.
$tr(.)$	Trace of the matrix argument.
\mathbf{I}_n	The $n \times n$ identity matrix.
$\mathbf{0}_n$	The $n \times n$ zero matrix.
$\text{diag}(\cdot)$	Column-vector built from the diagonal elements of the matrix argument.
\otimes	Kronecker product.
$\Re(\cdot)$	Real part of complex number.
$\Im(\cdot)$	Imaginary part of complex number.
$\lfloor \cdot \rfloor$	Floor function of the scalar argument.
$\det(\cdot)$	Determinant of the matrix argument.
$[\cdot]_{i,j}$	The $(i, j)^{th}$ entry of the matrix argument.
$\mathbb{P}(\cdot)$	Probability of the event argument.
\circ	Matrix entrywise product.

List of Notations

M	Number of antennas at SU.
N	Number of observed samples.
L	Smoothing factor.
f_c	Central frequency.
f_s	Sampling frequency.
T_s	Sampling period.
T_{sym}	Symbol period.
f_d	Maximum Doppler frequency.
$\mathbf{x}(n)$	Observation vector at the receiver.
$\mathbf{w}(n)$	Noise vector at the receiver.
\mathbf{H}	Channel matrix.
σ_w^2	Gaussian noise variance.
$\mathbf{R}_{L,x}$	Covariance matrix of the received signal.
$\mathbf{R}_{L,x}(N)$	Sample covariance matrix of the received signal, calculated based on N observed samples.
$\lambda_1, \dots, \lambda_{ML}$	Eigenvalues of the covariance matrix.
ℓ_1, \dots, ℓ_{ML}	Eigenvalues of the sample covariance matrix.
ρ_r	Receive spatial correlation coefficient.
\mathbf{R}_r	Receive spatial correlation matrix.
M_s	Number of OFDM subcarriers.
T_{chip}	Chip duration.
r_h	Autocorrelation function.
α	Characteristic exponent of α -stable distributed process.
γ	Dispersion parameter α -stable distributed process.

List of Acronyms

ACF	Autocorrelation function
ADC	Analog-to-digital converter
AMR	Automatic modulation recognition
ANN	Artificial neural network
CCAV	Covariation coefficient absolute value
CCF	Cross-correlation function
CDMA	Code division multiple access
CP	Cyclic-prefix
CR	Cognitive radio
CSI	Channel state information
CWT	Continuous wavelet transform
DSA	Dynamic spectrum access
DS-CDMA	Direct-sequence CDMA
ED	Energy detection
FLOM	Fractional lower order moments
GLRT	Generalized likelihood ratio test
GMEDS	Generalized method of exact Doppler spread
GSM-R	Global system for mobile communications-railway
GSNR	Generalized SNR
HOC	Higher order cumulants
HOM	Higher order moments
HOS	Higher order statistics
i.i.d	Independent and identically distributed
MIMO	Multiple-input multiple-output
MSE	Mean square error
MyrF	Myriad filtering
NMB	Normalized mean bias
NRMSE	Normalized root mean squared error
NSS	Narrowband spectrum sensing
OFDM	Orthogonal frequency division multiplexing

PET	Predicted eigenvalue threshold
PS	Primary source
PSD	Power spectrum density
PU	Primary user
QoS	Quality of service
RMT	Random matrix theory
RPROP	Resilient backpropagation
SCMA	Simplified constant modulus algorithm
SDR	Software defined radio
SIMO	Single-input multiple-output
SISO	Single-input single-output
SNR	Signal-to-noise-ratio
SoS	Sum-of-sinusoids
SPET	Simplified PET
SU	Secondary user
WCV-T	Weighted covariance value for time-varying channels
WCV-S	Weighted covariance value for spatially-correlated multiple-antenna systems
WRAN	Wireless regional area network
WSS	Wideband spectrum sensing
ZF	Zero-forcing
ZP	Zero-padding

Introduction

Context and Motivations

Increasing railway attraction, accessibility and productivity necessitate to increase safety, reduce operation costs, and offer new services to passengers. To reach this goal the information exchange among railways stakeholders must be largely improved. These data fluxes must cover the increasing demands of railway domain including safety-related applications, Internet access for passengers and embedded real-time closed-circuit television (CCTV), etc. On the other hand, the successive trials to answer the different railways demands results in the wide deployment of a lot of wireless communication devices operating at different frequencies in the trains and along infrastructures . There is no single technology that can replace all the other ones while still supporting the multitude of usages and needs. Thus, the integration of all these heterogeneous railway-dedicated radio services is unavoidable to improve global efficiency of railway system.

The cognitive radio (CR) concept was introduced by Mitola in 1999. The CR can be simply defined by the awareness, adaptation, and cognition capabilities. Interoperability, spectral efficiency, radio resources optimization, and improving communications reliability are all believed to be of significant interest for railway applications. CRs have shown significant promise in each of these areas. In addition, The CR research has been successfully applied to meet the communication needs of the military as well as the public-safety sectors, which share many of the same needs as railway. Despite more than a decade of research work, technical challenges, and regulations challenges, the CR is still far from being applied in many domains. However, this work is a step towards a CR based solution for railway applications.

One of the main capabilities of the CR is to sense and finally become aware of its environment. Three major domains define the environment of the CR, namely, the user, policy, and radio domains. This thesis contributes to radio domain awareness of CR. More specifically, these contributions lie in the spectrum awareness and waveform awareness functions. An essential task in CR is to design a reliable spectrum sensing method that is able to detect the presence of a signal in the target channel, i.e. make CR aware of the spectrum resources availability. Cognitive radios are expected to recognize different wireless networks and have capability to communicate with them. Transmission parameters of communications systems must be detected

blindly if the system is not known to CR. Identifying some of the basic features of signal does enhance the radio domain awareness capability, i.e. giving the CR a waveform awareness aspect.

The specificity of the railways does not lie only in its passengers and operators needs (translated into the user domain awareness) but also in its special radio environment. This special railways context implies some additional constraints on communications systems such as high mobility and heavy-tailed impulsive noise. These constraints are deeply analyzed and taken into account in this thesis using advanced Doppler spectrum and α -stable models for the high mobility and impulsive noise respectively.

Thesis Organization

This thesis is divided into five Chapters. The addressed problem is founded in Chapter 1. Then, the second Chapter presents the system model. Thereafter, the waveform awareness functions are introduced in Chapter 3, while, the spectrum awareness problem is studied in Chapter 4. Finally, the spectrum sensing methods are developed to cope with the special environment of railways in Chapter 5.

The first Chapter presents a state of the art of communication systems for railways and clarifies why the existing deployed wireless systems are not capable to answer the actual and future demands of railway domain. Then, the CR concept is introduced through its definition, architecture, possible applications, and existing standards. Thereafter, the important question on “how can CR be beneficial for railways?” is answered. The possible challenges, that could face using the CR as a solution for railway communication systems, are mentioned. Finally, this Chapter clarifies more the focus of our thesis.

The specificity of the railway context is discussed in Chapter 2 by studying the special constraints implied by the special railways environment nature, i.e. the high-speed of train, the particular electromagnetic (EM) interferences, the diversity of environments crossed by train, etc. The high mobility results in the Doppler effect, while the special EM environment results in a heavy-tailed impulsive noise. Spatial correlation among the system’s antennas is a practical issue that could influence its performance. These different aspect are deeply analyzed and modeled. Chapter 2 presents the system model, i.e. the transmitted signal model, the different effects of the wireless channel on the transmitted signal, and the noise model.

CRs are expected to recognize different wireless networks and have capability to communicate with them. That is, identifying some of the basic features of incoming signal does enhance the CR waveform awareness capability. The transmission features identified by the CR device include: a multi-carrier transmission identification, spectrum spreading detection, and modulation scheme recognition. Chapter 3 introduce two waveform identification methods. The first is a modulation recognition algorithm for spatially-correlated multiple-input multiple-output (MIMO) systems based on higher order statistics, while the second identifies the parameters of multi-carrier direct spread spectrum transmissions based on the fluctuations of the autocorrelation function estimator.

The spectrum sensing is an essential function of any cognitive radio system. Chapter 4 firstly presents a preliminary literature review of narrowband and wideband spectrum sensing techniques. This Chapter introduces a new non-parametric narrowband blind spectrum sensing method based on the predicted eigenvalue threshold. This method is simplified to reduce the complexity without leading to any performance degradation. Also, we propose to combine a non-parametric Welch periodogram spectral estimator with an optimization algorithm to better estimate spectral components in the wideband case. The performance of this method is further improved by employing multiple-antennas at the receiver.

The special constraints of railways environment were not taken into consideration when studying the problem of narrowband spectrum sensing in Chapter 4. Three particular constraints, namely, the time-varying wireless channel, the multiple-antennas spatial correlation, and the impulsive heavy-tailed noise, get more attention in Chapter 5. A new weighted covariance value based spectrum sensing method is proposed. This method exploits the properties of time-varying channel to improve the performance. Also, a new method based on a weighting covariance matrix, employed to better exploit the spatial correlation achieving higher sensing performance levels, is introduced. Two new methods are introduced to mitigate the effect of heavy-tailed impulsive noise. The first is based on filtering the received signal using the myriad concept, while, the second is based on the covariation (not covariance) coefficient matrix of the received signal.

Thesis Contributions

This thesis is a first step in a long road to design a CR based solution for railway applications. One of the main capabilities of a CR is its awareness of its environment. This awareness cover several domains. Here, we focus on the radio domain awareness translated into spectrum awareness and waveform awareness. The main contributions of this thesis are summarized as follows:

- ❖ Measurements confirm the impulsive nature of noise encountered at receivers on-board trains. The Gaussian noise assumption is not anymore valid to develop and evaluate algorithms for CR device. A distribution fitting procedure of measured noise acting on GSM-R antennas is proposed. It was found that the measured data is well modeled by the symmetric α -stable distribution. This work is presented in Chapter 2.
- ❖ The first contribution of Chapter 3 is recognizing the used modulation scheme of an available radio service. A modulation recognition algorithm for spatially-correlated MIMO systems based on higher order statistics is introduced. An artificial neural network trained with resilient backpropagation learning algorithm is employed as classifier. To the best of our knowledge, this research work is among the first ones that study the modulation recognition for MIMO systems, and the first one that studies the spatially-correlated case.
- ❖ The second contribution of Chapter 3 is to better enhance the waveform awareness by the knowledge of employment of multi-carrier or/and spectrum spread techniques. A blind

identification method of multi-carrier direct spread spectrum signals based on the autocorrelation estimator fluctuations is introduced. The described scheme leads to an efficient estimation of symbols duration, cyclic-prefix duration, and subcarriers number. The proposed method is insensitive to phase and frequency offsets. The multiple-antennas at the receiver are used to improve the performance while keeping the detection duration constant.

- ❖ Chapter 4 focus is the spectrum sensing problem which is one of the essential functions of any CR device. The spectrum sensing algorithms are classified into two main categories: narrowband sensing and wideband sensing. The narrowband sensing is based on sequentially or randomly checking the narrowband channels of the wide spectrum of interest. One of the major contributions of our thesis is a new non-parametric narrowband blind spectrum sensing method based on the predicted eigenvalue threshold. The proposed method gives good performance when compared with other existing methods.
- ❖ The entire band of interest is processed when employing the wideband sensing. Another contribution of Chapter 4 is to propose the combination of a non-parametric improved cooperative Welch periodogram spectral estimator with an optimization algorithm to better estimate spectral components in the wideband case.
- ❖ Chapter 5 is dedicated for narrowband spectrum sensing for railway applications. Several existing methods employs the covariance properties of the received signal. The time-varying wireless channels, resulting from the high-speed of trains, affects the temporal covariance properties. This could degrade the performance of the traditional narrowband spectrum sensing methods. A new weighted covariance value based spectrum sensing method is proposed to try to exploit the properties of time-varying channel to improve the performance. This method constitutes a major contribution of this thesis.
- ❖ Another constraint to cope with is the practical spatial correlations observed on the multiple-antennas of the receiver. The effect of these correlations on narrowband spectrum sensing methods was examined and it was found that these correlations do improve the performance of some methods, e.g. the PET based method proposed in Chapter 4. Another important contribution of our thesis is to introduce new method based on a weighting covariance matrix employed to better exploit the spatial correlation for higher sensing performance levels. This method is introduced in Chapter 5.
- ❖ The works presented in Chapter 2 show that the noise acting at antennas aboard trains has an impulsive nature and modeled by the symmetric α -stable distribution. The heavy tails of impulsive noise will degrade the narrowband spectrum sensing performance, and their effect must be mitigated. We contribute to this research area by introducing two new sensing methods developed based on the symmetric α -stable distributed noise assumption. The first method is based on filtering the received signal using the myriad concept, while, the second one is based on the covariation coefficient matrix of the received signal.

Publications

The following is a list of publications in refereed journals and international conference proceedings, and other publications produced during my Ph.D. candidature.

International Journal Papers

- ❖ **K. Hassan**, I. Dayoub, W. Hamouda, C. Nzeza, and M. Berbineau, “Blind Digital Modulation Identification for Spatially Correlated MIMO Systems,” *IEEE Transactions on Wireless Communications*, vol. 91, no. 2, pp. 683–693, Feb. 2012.
- ❖ **K. Hassan**, I. Dayoub, W. Hamouda, and M. Berbineau, “Automatic modulation recognition using wavelet transform and neural networks in wireless systems,” *EURASIP Journal on Advances in Signal Processing*, Article ID 532898, 13 pages, June 2010.

International Conference Papers

- ❖ **K. Hassan**, R. Gautier, I. Dayoub, E. Radoi, and M. Berbineau, “Non-parametric Multiple-Antenna Blind Spectrum Sensing by Predicted Eigenvalue Threshold,” in *Proceedings of IEEE International Conference on Communications (ICC)*, Ottawa, Canada, June 2012.
- ❖ **K. Hassan**, R. Gautier, I. Dayoub, E. Radoi, and M. Berbineau, “Predicted Eigenvalue Threshold Based Spectrum Sensing With Correlated Multiple-Antennas,” in *Proceedings of IEEE Vehicular Technology Conference (VTC) Spring*, Yokohama, Japan, May 2012.
- ❖ **K. Hassan**, C. N. Nzéza, R. Gautier, E. Radoi, M. Berbineau, and I. Dayoub, “Blind Detection of the Number of Transmitting Antennas for Spatially-Correlated MIMO Systems,” in *Proceedings of IEEE International Conference on Intelligent Transport Systems Telecommunications, ITST 2011*, Saint-Petersburg, Russia, August 2011.
- ❖ **K. Hassan**, C. N. Nzéza, M. Berbineau, W. Hamouda, and I. Dayoub, “Blind Modulation Identification for MIMO Systems,” in *Proceedings of IEEE Global Communications Conference (GLOBECOM)*, Miami, USA, December 2010.
- ❖ C. N. Nzéza, **K. Hassan**, M. Berbineau, R. Gautier, and G. Burel, “Blind MIMO MC-CDMA parameters estimation over fading channels for cognitive radio,” in *Proceedings of 10th International Conference on Intelligent Transport Systems Telecommunications, ITST 2010*, Kyoto, Japan, November 2010, pp. 1–6.
- ❖ **K. Hassan**, I. Dayoub, W. Hamouda, and M. Berbineau, “Automatic modulation recognition using wavelet transform and neural networks,” in *Proceedings of IEEE International Conference on Intelligent Transport Systems Telecommunications, ITST 2009*, Lille, France, October 2009.

Miscellaneous Publications

Scientific Reports

- ❖ **K. Hassan**, “Rapport régional d’avancement de thèse”, Décembre 2010-Décembre 2011.
- ❖ **K. Hassan**, “Rapport d’avancement de travaux de thèse”, IFSTTAR, 2011.
- ❖ **K. Hassan**, “Rapport d’avancement de thèse : Application de la radio opportuniste à la continuité de services et à la sécurité des transports dans un contexte à forte mobilité,” IFSTTAR, RA-11-702-FR, Décembre 2009-Décembre 2010.

Journées doctorales

- ❖ **K. Hassan**, “Seconde Journée des doctorants, IEMN /DOAE”, Octobre, 2011.
- ❖ **K. Hassan**, “Surveillance aveugle du spectre appliquée à un terminal radio mobile cognitif pour le domaine ferroviaire,” in Proceedings of JDD SPI-STIC, IFSTTAR, Juin 2011.
- ❖ **K. Hassan**, “Application de la radio opportuniste à la continuité de services et à la sécurité des transports,” Poster JDD SPI-STIC, IFSTTAR, May 2010.

Chapter 1

Problem Foundation

Contents

- 1.1 Introduction 10**
- 1.2 Thesis Context 10**
 - 1.2.1 Wireless Communications for Railways 10
 - 1.2.2 Problematic, Demands, and Requirements 12
- 1.3 Cognitive Radio 14**
 - 1.3.1 What is a CR? 14
 - 1.3.2 The CR Architecture 16
 - 1.3.3 Existing CR Standards 17
 - 1.3.4 CR Applications 18
- 1.4 Cognitive Radio for Railways: Merits and Challenges 19**
 - 1.4.1 Can CR be Beneficial for Railways? 19
 - 1.4.2 How do we Propose to Apply CR for Railways? 20
 - 1.4.3 Challenges 22
- 1.5 Focus of the Thesis 22**

1.1 Introduction

An essential goal of railway operators is to increase safety, reduce operation and maintenance costs, and increase attraction and profit by offering new services to passengers. This goal intersects with the target of the European rail research advisory council (ERRAC) for 2020 to double passenger traffic by rail. These objectives will be reached not only thanks to a huge increase of system wide information exchanges between railway undertakings and infrastructure managers but also thanks to an increase of information fluxes dedicated to passengers. Consequently, nowadays, a lot of wireless communication devices operating at different frequencies are widely deployed all around Europe (in the trains and along infrastructures) to answer the different railways demands. There is no single technology that is good and general enough to replace all the other ones and to support the multitude of usages and needs. Thus, the integration of all these heterogeneous railway-dedicated radio services is a technical key to improve global efficiency of global railway system [1].

Interoperability, spectral efficiency, optimization of radio resource usages, and improvement of communications reliability are of significant interest for railway applications. Cognitive radio (CR) has shown significant promise to answer these railway requirements since the CR research has been successfully applied to meet the communication needs of the military as well as the public-safety sectors, which share many of the same needs as railway. Therefore, CR technologies are able to offer solutions to railways, to ensure a continuity of communication services and network access based on a global roaming across the heterogeneous wireless networks, providing a continuous and always best service anywhere, anytime, anyhow [2, 3].

This Chapter presents the state of the art of existing communications systems for railways and the existing projects that address the problem of improving and integrating these systems. Then, the concept and the architecture of CR is presented besides the existing CR standards and possible applications. Thereafter, we analyze how CR could be applied to improve the overall performance of railway communications system, i.e. what benefits could CR offer? and what challenges to overcome before we can conduct CR for railways?. Finally, the focus of these thesis works is highlighted.

1.2 Thesis Context

1.2.1 Wireless Communications for Railways

For a long time, transmissions between ground and trains were non-existent and the only information available to the driver aboard train were provided by visual information signaling. More recently, the transmission demands had augmented due to the increasing complexity of control facilities/train control, the necessity to increase the capacity of existing lines and optimize their management and operation. Nowadays, several wireless communication networks are widely deployed along European railway lines, each of them is dedicated for a specific task in a specific context. Therefore, the integration of all these heterogeneous wireless networks deployed for railway systems is not only unavoidable but also a key to increase efficiency of global railway

Table 1.1: Example of frequency allocations for railways around Paris [4].

31-32 MHz	Voice
50-65 MHz	TV semi-embedded
70-151 MHz	Remote control
152-180 MHz	Operation, construction, analog 3RP
414-429 MHz	IRIS-safety radio
876.2-879.8 MHz	Voice and data
921.2-924.8 MHz	GSM-R, railway control systems
2.4 GHz and 5.8 GHz	WiFi access

Table 1.2: Frequency bands and their usage for railway communications in USA [5].

39-50 MHz	Data and train control
160.215-161.565 MHz	Data and voice
220-222 MHz	Positive train control (PTC)
450-460 MHz	One-way and two-way end-of-train devices, data
Six channel pairs at 896/936 MHz	Advanced train control system (ATCS), data
2.4 GHz	WiFi access

system. Table 1.1 summarizes the main frequencies allocated for specific rail services (excluding passenger service) in the Paris region [4]. Table 1.2, derived from [5], gives the frequency allocations for railway in the USA. On the other hand, improving the quality of public transport requires offering new services to customers which, in turn, results in an increasing transmission demands. So today, transport operators rely increasingly on new technologies of information and communication that allow them to modernize their image and make public transport more attractive.

Several European and national railway-dedicated projects addressed developing communication systems for operational and maintenance objectives. Table 1.3 lists some of the major projects, most of them were based on existing technologies. Mobile radio for railways networks in Europe (MORANE) project aimed to develop new telecommunication standard for railway control systems. This project successfully issued *the global system for mobile communications-railway* (GSM-R) now being deployed in Europe. This system is based on standard GSM. In Europe, a 2×4 MHz specific frequency bands (876-880 MHz for uplink, and 921-925 MHz for downlink) are allocated for GSM-R operation. The deployment of this standard is optimized to meet the performance constraints (i.e. key performance indicators) implied by the European train control system (ETCS). This standard is expected, in the coming years, to evolve to LTE-R to face its limitations, however, no specific frequency bands are yet allocated for this awaited standard. Another project MODURBAN aimed to standardize a new control and command system for urban guided transport. One of the recent FP7 European projects, InteGRail [6], has developed an intelligent communication framework, ICOM, to achieve, using middleware solutions, integration of wireless communication technologies in the railway domain. This solution is a first step toward system integration and interoperability but it will not avoid juxtaposition of communication devices along the lines and on-board the trains at very high costs.

Table 1.3: List of various projects of railway communication systems.

INTEGRAIL (2005-2008)	Integration of railway systems through intelligent interfaces and processes
MODURBAN (2005-2008)	Design, develop and evaluate an innovative, open architecture and its key interfaces (control systems, energy subsystems access) to pave the way for the next generation of urban transport guides
MODTRAIN (2004-2007)	Specification of subsystems and interfaces for modular architecture train
EUROMAIN (2002-2005)	Specifying an European railways maintenance system based on Internet technologies
TRAINCOM (2000-2004)	Integration techniques for railway train-ground communications links in order to develop new interoperable applications
MORANE (1996-2000)	Development of a uniform digital radio system for European railroad traffic. A new version of GSM called GSM-R (a platform for voice and data communications as well as for traffic control) was introduced.

Several research works also addressed the problem of providing Internet connection for passengers. Several projects rely on a set of wireless technologies instead of only one way to access the Internet, thereafter, the *gap-filler* technique is employed where one technology is used to provide the connectivity, and when this technology is no longer present, a second technology can be instead used [7]. The authors in [8] consider either a connection via a terrestrial cellular network (GSM, GPRS and UMTS), or the combination of WiFi access points and WiMAX. In [9], the proposed solution is a combination of a land link and satellite link, while the bandwidth offered to customers can be increased through access points to 802.11n WiFi [10].

1.2.2 Problematic, Demands, and Requirements

Any railway operator needs accurate and “real-time” train data (diagnostic, position, speed, etc) in order to augment safety, decrease the number of accidents and facilitate the positive train control (PTC). Better maintainability and availability of trains is a key challenge for all public transport, and certainly improving data exchange between trains and the wayside will contribute to this. Any increase in high data-rate exchange can not only improve functionality, but leads to add new services. This will help railway operators to improve public transport efficiency and quality of service (QoS), either with new and better services for passengers or secure solutions for operators and maintainers. New solutions are proposed to overcome today’s limitations and to develop efficient communication systems for railways. Any proposed communications solution must guaranty availability, continuity of service, heterogeneous traffic classes, robustness and QoS in the context of specific propagation environment and high mobility.

The three aspects that define users needs and railway systems requirements are: railways operation, safety and security, and comfort. Then, the communications applications required in the railway domain are, from services point of view, divided into two categories: safety-related

services (mainly control and command besides some maintenance applications) and non-safety-related services generally for non critical applications such as passenger information, internet on-board trains. More details on these applications are found in [11]. Some of these applications are listed below:

- ❖ Train control such as train location, all switches positions, signaling and movement authority,
- ❖ Operational communications such as connecting the trains to their maintenance centers, proactive maintenance, train diagnostics, crew connectivity and specific system information,
- ❖ Dimensioning aspects such as number of trains in a geographical zone, number of passengers in a train, percentage of passengers equipped with WiFi terminals in a train, percentage of trip time, populations, users profiles, etc,
- ❖ High data-rate Internet access service for passengers (browsing, email, VPN, P2P, streaming, live TV, etc.),
- ❖ Real time information for passengers,
- ❖ Embedded real-time closed-circuit television (CCTV).

Each one of the above mentioned applications has its own exigencies, when it comes to the communication system, in terms of throughput, delay, availability, reliability, robustness, QoS. However, only two of them require very high throughput: Internet access for passengers and embedded real-time CCTV. On the other hand, some applications are exigent en terms of delay, availability, robustness and reliability, e.g. train control applications.

In addition to the specific requirements of the above applications, the proposed communication solutions must take into consideration the specific nature of the railway domain and its resulting constraints which may degrade the global performance of communication systems. Considering the mobility aspect, the design of communication systems for high-speed trains is more “exigent” (fast fading, Doppler effects, fast handover mechanisms). Of course, it is easier to fulfill the above mentioned requirements in a mobile device that is not moving at 300 km/h. Another constraint is the electromagnetic (EM) interferences produced around the train resulting in a heavy-tailed impulsive noise generally due, not only to the converters in the engine’s motors, but also to bad contacts between the catenary and the pantograph that create electrical arcs at the vicinity of the antennas [12]. Finally, we must take into consideration the varying nature of the environments traversed by the train (rural areas, urban areas, tunnels, etc.).

Figure 1.1 explains the conceptual model that translate the information from user domain (passengers and operators) into some communication system exigencies. The proposed solution is exigencies-driven based on the information coming from the radio domain.

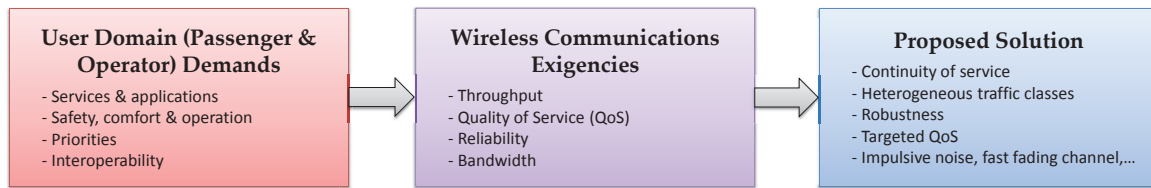


Figure 1.1: The conceptual model that translates information from user domain into communication system exigencies to be respected by the proposed solution.

1.3 Cognitive Radio

1.3.1 What is a CR?

Recently, the rapid growth in wireless communications has contributed to a huge demand on the deployment of new wireless services. The radio electromagnetic spectrum is a limited physical quantity, and only a certain part of it is suitable for radio communication. The traditional way of governing this resource has been to administer licenses for portions of the spectrum, usually by a national agency such as US federal communications commission (FCC). Almost all the usable portions of the spectrum are allocated for licensed users. Available electromagnetic spectrum for wireless transmission has become a highly valuable resource. However, recent research published by the FCC [13] shows that the traditional static frequency allocation policy is not efficient and results in poor spectrum utilization. In [14], a general survey of radio frequency bands (from 30MHz to 3 GHz) is provided. Figure 1.2 presents the average spectrum occupancy and highlights how low could be the spectrum occupancy in many bands. The dramatic increase in the demand for radio spectrum and the actual low spectral efficiency has spurred the development of a next generation wireless technology referred to as cognitive radio (CR). An early work by Mitola introducing the concept of CR is [15].

However, the revolution in processor technology in last decades allowed the design of more flexible radio systems as a larger part of the necessary signal processing could be performed digitally. This flexibility created a developing researching field which was named software defined radio (SDR). The SDR technology brings flexibility, cost efficiency and the capability to drive communications forward. A number of definitions can be found to describe SDR. The IEEE and the SDR forum have defined SDR as: "Radio in which some or all of the physical layer functions are software defined" [16]. The SDR is the technology that enables the CR.

The original definition of CR is wide, as it envisions the cognitive terminal as a SDR that is aware of its environment and its capabilities to utilize all available environmental parameters. According to [15], examples of parameters the CR can exploit are knowledge such as time, user location, user preferences, knowledge of its own hardware and limitations, knowledge of the network and knowledge of other users in the network. While there is no agreement on the formal definition of CR until now, the concept has evolved recently to include various meanings in several contexts. The definition proposed by FCC is widely adopted:

"Cognitive radio: A radio or system that senses its operational electromagnetic environment and can dynamically and autonomously adjust its radio operating parameters to modify system

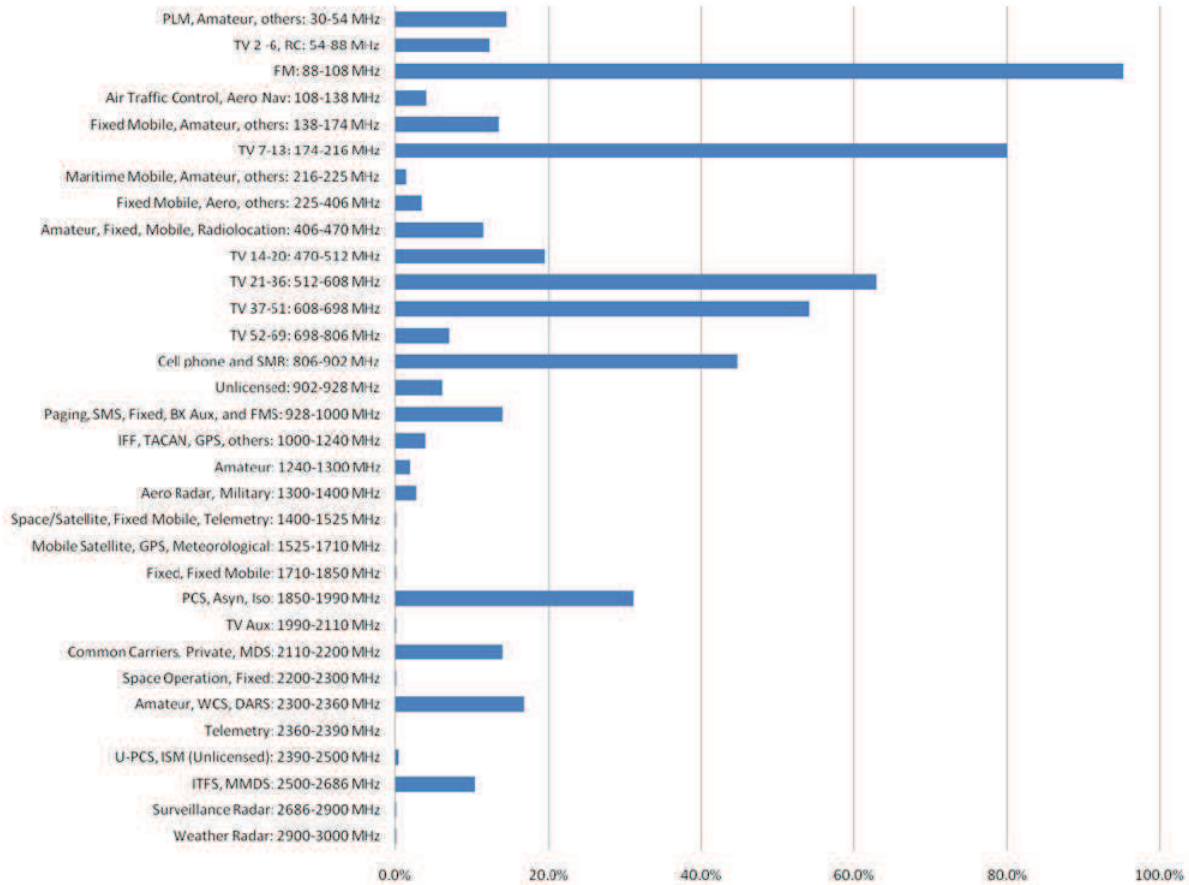


Figure 1.2: Summary of spectrum band occupancy calculations [14].

operation, such as throughput, mitigate interference, facilitate interoperability, access secondary market” [17].

There are several other definitions for CR in addition to the above one. However, three common capabilities do exist among all these definitions are:

- ❖ Awareness: the CR must be aware of itself and its operating environment. This may include that the CR is aware of the radio frequency (RF) environment, the rules that govern its operation, its user’s needs, its own capabilities, priorities and authorities, its geographic position, etc. There are three major domains that define the environment of the CR, namely, user, policy, and radio domains. Generally, awareness concept is reflected throughout these domains.
- ❖ Adaptation: this is the ability to adapt to the environment or user needs. For instance, the CR can adjust its behaviour by changing its power, modulation, waveform strategy, carrier, and signal bandwidth. This level of adaptation recalls the agility of the SDR.
- ❖ Cognition: it is the capability of understanding and learning from its environment, its inner state, the impact of its actions, and past experiences. For instance, Haykin had defined this capability as *the intelligent of wireless communication system that uses the*

methodology of understanding-by-building to learn from its surrounding environment (i.e., outside world) [18].

These three basic concepts are the soul of the CR. This soul is interpreted in the cognition loop shown in Figure 1.3. CRs are likely to make use of a goal driven observe-orient-decide-act (OODA) loop for its functionality which breaks down the basic components of how anything (here, a wireless CR device) can adapt to its environment. The cognition starts by observing the operating environment of the wireless CR device. This observation, which makes the CR more aware, could include metrics such as spectrum usage, available channels, identifying other transmitters, classifying their waveforms. This observation process is driven by the operating goals of the radio at a specific time. With this awareness and knowledge of the specific goals of the user, the CR utilizes learning algorithms to make the best possible decision. Decision making takes into consideration the history of the radio domain and past successful decisions. Finally, the CR employs the reconfigurable nature of its SDR platform to change its configuration parameters. This alters the CR inner state and enables it of reacting to perceived changes in its wireless environment.

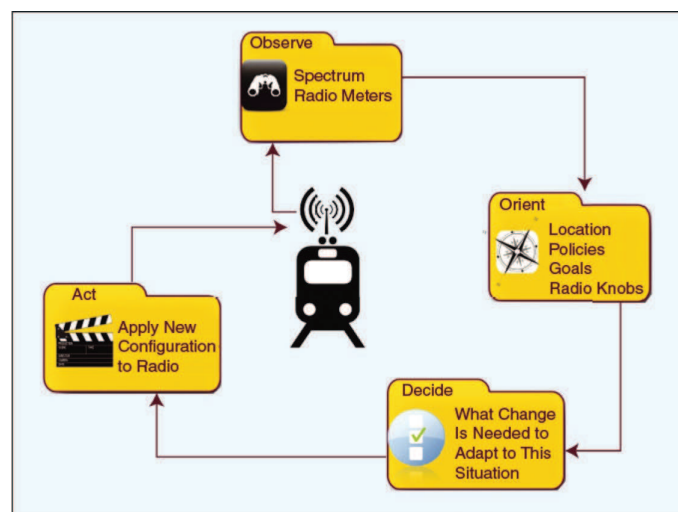


Figure 1.3: The Cognition Loop [5].

1.3.2 The CR Architecture

One of the proposed cognitive radio architectures is shown in Figure 1.4 [19]. This architecture considers that the cognitive engine represents the intelligent part of the CR. The cognitive engine performs the modeling, learning, and optimization processes necessary to reconfigure the radio communication system, which appears as the simplified open systems interconnection (OSI) stack. The cognitive engine accumulates information from the radio itself, and the three major domains of the CR environment, i.e. the user domain, the radio domain, and the policy domain. The user domain passes information relevant to the user's application and needs to help driving the cognitive engine's optimization. The radio domain information consists of RF and environmental data that could affect system performance such as propagation or interference sources. The policy engine receives policy-related information from the policy domain. These

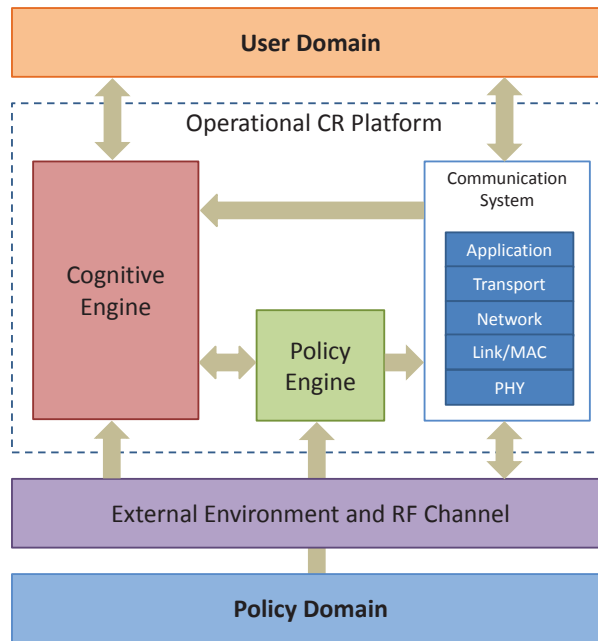


Figure 1.4: Generic CR architecture [19].

information help the CR to avoid forbidden and illegal solutions and choose the best solution from the ones that respect local regulations [19].

1.3.3 Existing CR Standards

The standardization issues have significant importance in the development of CR systems, since it encourages companies to invest in this domain. Several standards are already published or still in a draft status. The IEEE wireless regional area network (WRAN) standard, IEEE 802.22, is one of the most rising standards. Its objective is using CR techniques to allow sharing of geographically unused spectrum allocated to the television broadcast service, on a non-interfering basis, to bring broadband access to hard-to-reach low-population-density areas typical of rural environments [20]. This standard has the potential to be applied worldwide. IEEE 802.22 WRANs are designed to operate in the TV broadcast bands while ensuring that no harmful interference is caused to the incumbent operation (i.e., digital TV and analog TV broadcasting) and low-power licensed devices such as wireless microphones [20].

The IEEE P1900 standard committee was established as a result of the growing interest for dynamic spectrum access networks. Its objective was to support the standards dealing with next generation radio developments and dynamic spectrum management. The IEEE 1900 was reorganized as standards coordinating committee 41 (SCC41), dynamic spectrum access networks (DySPAN), on March 2007. The principal four working groups within SCC41 are [21]:

i) IEEE P1900.1: IEEE standard definitions and concepts for dynamic spectrum access (DSA); terminology relating to emerging wireless networks, system functionality, and spectrum management amendment.

ii) IEEE P1900.2: recommended practice for interference and coexistence analysis.

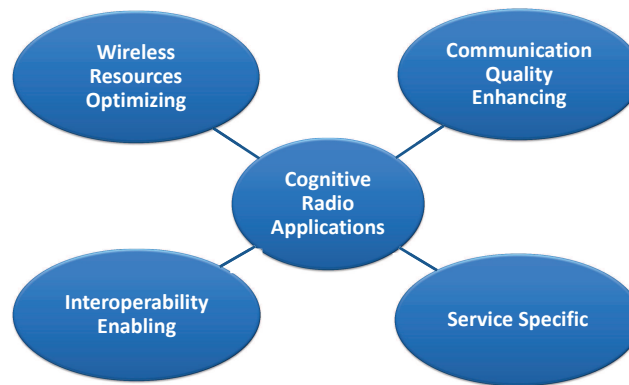


Figure 1.5: Classification of cognitive radio applications [22].

iii) IEEE P1900.3: recommended practice for testing and analysis to be used during regulatory compliance evaluation of radio systems with DSA capability.

iv) IEEE P1900.4: standard for architectural building blocks enabling network, device distributed decision making for optimized radio resource usage in heterogeneous wireless access networks, amendment: architecture and interfaces for DSA networks in white space frequency bands.

The CR research is very active also at national (France) and European level. For instance SACRA, SENDORA, LOLA, SAMURAI, CROPOLIS, SYMPA, and QOSMOS are all national projects which try to answer some of the CR challenges. E3 (end-to-end efficiency cognitive wireless networks technologies) aims to transform current wireless system infrastructures into an integrated, scalable and efficiently managed beyond 3rd generation cognitive system framework. The main issue is to introduce the cognitive systems in the wireless world, while contributing to the standardization of IEEE P1900.4. Also, CogEU (cognitive radio systems for efficient sharing of TV white spaces in European context) project aims to build the transition to digital television by developing cognitive radio systems which exploit the favorable propagation characteristics of TV white spaces through introduction and promotion of spectrum trading in real time and creating new frequencies in the upper band of the released spectrum.

1.3.4 CR Applications

Figure 1.5 represents a high level classification of possible CR applications [22]. This classification is based on the relationship between each application and the “cognitive concept”. The first group consists of CR applications contributing to the optimization of various wireless resources. These resources include spectrum, power, network, hardware/software, etc. The second group of applications address the improvement in communication quality, e.g. improving link reliability. Interoperability is one of the most desirable features of CR. Interoperability allows two or more communication systems to exchange information. The last category reflects CR applications concerning services and user needs in private, public, and military sectors. Some targeted applications are: transmit traffic congestion information to the mobile in advance, maintain communication in disaster situation, locate the rescued in the shortest time, and identify any

abnormality in the patient physical condition [22]. In general, many of these applications across groups can benefit from each other, and they can work together to improve wireless communications.

1.4 Cognitive Radio for Railways: Merits and Challenges

1.4.1 Can CR be Beneficial for Railways?

Increasing quality, reliability, and safety of railway systems while still increasing accessibility and productivity, requires ever increasing information exchange between operator's workstations, and field devices widely distributed both by the track-side and on-board trains. Hence, improving communication systems for railways is indispensable to modernize railway operations. Nowadays, a lot of wireless communication systems operating at different frequencies are deployed to reply the particular demands of railway operations. In fact, employing single universal system, among existing systems, to replace all the other ones while still being able to support the multitude of demands is not feasible. As a consequence, the integration of all these heterogeneous wireless systems is therefore a key technical challenge to improve global efficiency of railway system. This can be answered by promising CR technologies which are able to meet the requirements of future wireless communication systems: interoperability, robustness, reliability, and spectral efficiency. The first applications of CR are mainly focused in the military domain which share many of the same needs as railways [5].

Based on the above presented concept, capabilities and possible applications of CR, it is obvious that employing this emerging technology as a solution for railway operations has a significant potential to be very beneficial. Firstly, CR technology may enhance interoperability between wireless systems by sensing application needs, radio services protocols, and configuring the SDR to better meet the traffic requirements carried over the wireless link [5]. Another profits of CR based solution for railways include improving link performance by avoiding poor channels, increasing data-rates on non-occupied channels, improving spectrum efficiency, and reacting to interferences to provide more robust communications. Also, it is clear that a unique, interoperable, robust, reliable, and spectral-efficient CR based communication system brings back an economical profit to railways operators thanks to lower deployment, maintenance, and operational costs.

None of the above approaches, presented above in section 1.2.1, had yet considered the problem from the perspective of CR systems. In [5], the authors present an initiative in the US that take into account research results in CR to develop a communications platform for railways applications. The national "urbanisme des radio communications" (URC) project was one of the first project in France and in Europe to raise the problem of the optimization of spectral resources in the Paris region, taking into account the transport field and particularly the urban guided systems [4].

Recently, the French national project *cognitive radio for railway through dynamic and opportunistic spectrum reuse* (CORRIDOR) project aims to design, develop and evaluate, in real

high-speed railway conditions, innovative communication-interface CR-based solutions for vehicles/infrastructures, taking into account three characteristic types of usages (control-command, CCTV and Internet on-board) [23]. CORRIDOR is the first project dedicated to CR systems for railway applications in France and Europe. Our research works were performed partially in the framework of this project which is expected to propose a first proof of concept around 2015.

1.4.2 How do we Propose to Apply CR for Railways?

Developing CR based solution for railways covers several research fields that should be integrated towards the global CR communications system. We had recognized three main research domains [24]:

- ❖ “CR mobile terminal” (the communications device located aboard train) capable of rapidly sensing the available radio opportunities, analyzing its actual situation (position, information coming from user, radio and policy domain), to finally decide the optimal change to do. Finally, the required configuration is applied to its agile radio platform.
- ❖ “Intelligent telecommunication infrastructure” capable of selecting the adequate spectrum band, resulting from the trade-off between the QoS requirements and the spectrum characteristics. It must cope with parameters such as needed data-rate, acceptable error rate, delay bound and bandwidth, through spectrum rapid evolution (short time availability intervals, and quickly moving channel) due to the high-speed train context.
- ❖ Mobility management and end-to-end QoS solutions in the presence of “CR mobile terminal” and “intelligent telecommunication infrastructure”.

Intelligent CR mobile terminal can interact with its radio environment according to two possible strategies:

- ❖ One of the promising possibilities to increase capacity of railway communication systems is to use free frequency bands by dynamically accessing the spectrum without creating any interference with other users. That is, the CR mobile terminal interacts with the intelligent infrastructure to set up a communication link (frequency bands, waveform, power, etc.) optimized according to user needs and available spectrum opportunities while avoiding disturbing other communication systems operating in the neighborhood. The standard employed for train/infrastructure communications is specially adapted to the railways environment and needs, and could be a special version of LTE which introduces the LTE-R standard. Current regulations prevent to access dynamically to under-occupied bands. For instance, FCC removed spectrum sensing requirement for TV white space dynamic access. Despite this regulations obstacle, the design of solutions for dynamic spectrum allocation and management is a very active field of research and developments today.
- ❖ The second strategy is based on connecting to existing available radio services. These radio services could be dedicated for railway operations (control, data, voice, etc.). Connecting

the CR decisions are registered besides the success status of each decision. Historical activity can assist CR based communications system to improve its deployment decision making. This data can be further processed into information to be distributed all around railways network. The variety of railways demands (low data-rate safety-related applications, embedded real-time CCTV, and high data-rate Internet access,etc) and the variety of resources required to enable the CR concept suggests that it is more feasible to embed more than one transceiver in the CR device employed aboard the train. Based on the previous explanations, Figure 1.6 shows our proposition of the “CR mobile terminal” architecture.

1.4.3 Challenges

There are many technical challenges for cognitive radio. These challenges include the areas of spectrum management, security, policy, propagation, awareness, network management, geo-location databases management, complexity, hardware requirements, CR architecture, etc. Ten years of CR research provided some answers especially in the last four years which witnessed an acceleration in the CR development. Also, the research community is actively focused on exploiting the CR technologies in new domains, e.g. high-speed vehicular applications. However, although SDR technology is fairly near term, CR may be farther off. More effective research works, in the few coming years, must rush industry and regulators to overcome their doubts.

On the other hand, CR mobile terminal located on-board train must be able to cope with the railways environment and constraints. That is, the high speed (which means fast varying wireless channels), special EM environments (resulting in a heavy-tailed impulsive noise), and poor radio coverage in rural areas. New fast and efficient radio awareness techniques should be imagined in this special context. The opportunistic band allocation has to take into account the limited duration of band availability due to train movement. Radio domain awareness must improve the predictive aspect to allow the cognitive engine to optimize the band allocation scheduling. Finally, CR mobile terminal must assure reliability and robustness whatever is the environment encountered (tunnel, rural, urban, etc.).

1.5 Focus of the Thesis

One of the main capabilities of the CR is to sense and finally become aware of its environment. Three major domains define the environment of the CR, namely, the user, policy, and radio domains. In this Ph.D. work, we focus on designing some functions of the CR mobile terminal, and particularly we contribute to radio environment awareness of CR. More specifically, these contributions lie in the spectrum awareness and waveform awareness functions.

The proposed cognitive radio architecture is shown in Figure 1.6. Our Ph.D. works lie in the block that translates the radio domain information to the other CR blocks, i.e. detecting and estimating the radio frequency and environmental data that could affect system performance such as communications or interference sources. These works are included in the observe task of the cognition loop shown in Figure 1.3.

On one hand, an essential task in CR is to design a reliable spectrum sensing method that is able to detect the signal in the target channel, i.e. make CR aware of the spectrum resources availability. On the other hand, cognitive radios are expected to recognize different wireless networks and have capability to communicate with them. Transmission parameters of communications systems must be blindly detected if the system is not known to CR. Identifying some of the basic features of incoming signal does enhance the CR awareness capability, i.e. giving the CR a waveform awareness dimension.

Our thesis focus is sensing the spectrum to detect the used and unused spectrum bands. Also, we concentrate on the identification of transmission technologies used by available radio services through extracting several features from the received signal. These features include the modulation scheme (QAM, PSK, etc..), and the modulation technique (CDMA, OFDM, etc. . .). These detected radio-domain information are fed into the operational CR platform as shown in Figure 1.6.

One way to better clarify the focus of our thesis is by presenting its main contributions, as follows,

- ❖ As expected, observations and measurements confirm the impulsive nature of noise encountered on receivers aboard trains. The Gaussian noise assumption is not anymore valid to develop and evaluate algorithms for CR device. A distribution fitting procedure of measured noise acting on GSM-R antennas is proposed. It is found that the measured data is well modeled by the symmetric α -stable distribution.
- ❖ Recognizing the used modulation scheme of an available radio service does enhance the waveform awareness of a CR device. We introduce a modulation recognition algorithm for spatially-correlated multiple-input multiple-output (MIMO) systems based on higher order statistics (HOS). To the best of our knowledge, this research work is among the first ones that study the modulation recognition for MIMO systems, and the first one that addresses the spatially-correlated ones.
- ❖ The waveform awareness can be better enhanced by detecting multi-carrier or/and spectrum spread techniques employment. A blind identification method of multi-carrier direct spread spectrum transmission based on the autocorrelation estimator fluctuations is introduced. The described scheme leads to an efficient estimation of symbol duration, cyclic-prefix duration, and subcarriers number. The multiple-antennas at receiver are exploited to enhance the performance while keeping the detection duration constant.
- ❖ Spectrum sensing is one of the essential functions of any CR device. The narrowband sensing is based on sequentially or randomly checking the narrowband channels of the wide spectrum of interest. One of the major contributions of our thesis is introducing a new non-parametric narrowband blind spectrum sensing method based on the predicted eigenvalue threshold.
- ❖ The entire band of interest is processed when employing the wideband sensing. Here, we propose to combine a non-parametric improved cooperative Welch periodogram spectral

estimator with an optimization algorithm to better estimate spectral components in the wideband case.

- ❖ Several existing methods employ the covariance properties of the received signal. The time-varying wireless channels affect the temporal covariance properties. This may degrade the performance of the traditional narrowband spectrum sensing methods. A new weighted covariance value based spectrum sensing method is proposed to try to exploit the properties of time-varying channel to improve the performance. This method constitutes a major contribution of this thesis.
- ❖ In practice, the multiple-antenna systems suffer from the spatial correlations. The effect of these correlations on narrowband spectrum sensing methods is examined and it is found that these correlations do improve the performance of some methods. Another important contribution of our thesis is to introduce a new method based on a weighting covariance matrix employed to better exploit the spatial correlation for higher sensing performance levels.
- ❖ The heavy tails of impulsive noise degrade the narrowband spectrum sensing performance, and their effect must be mitigated. We contribute to this research area by introducing two new sensing methods developed based on the symmetric α -stable noise assumption. The first method is based on filtering the received signal using the myriad concept, while, the second one is based on the covariation coefficient matrix of the received signal.

In the following, the system model (channel, noise, signal) is presented in Chapter 2. Then, the waveform awareness functions are studied in Chapter 3, while, Chapter 4 concentrates on the spectrum sensing problem. Finally, the spectrum sensing is further analyzed and developed to cope with the special constraints of the railway domain.

Chapter 2

System Model

Contents

2.1	Introduction	26
2.2	Mobile Radio Channel Model	26
2.2.1	Characteristics of Mobile Radio Channels	26
2.2.2	Characterization in Time and Frequency	27
2.2.3	Mobile Radio Channels : Doppler Effect	29
2.2.4	Mobile Radio Channels Models	30
2.3	Signal Model	33
2.3.1	Received Signal Representation	33
2.3.2	Multiple-antennas Spatial Correlation	36
2.3.3	Transmission Schemes	37
2.4	Noise Model	38
2.4.1	The Gaussian Model	38
2.4.2	Heavy-tailed Impulsive Noise in Communications	38
2.4.3	Case Study : Electromagnetic Interferences Acting on GSM-R Antennas	40
2.5	Conclusions	45

2.1 Introduction

The railway domain, and particularly the high-speed trains context, is a special propagation environment that adds new constraints on the wireless communication systems. These constraints may degrade the performance of algorithms employed for wireless systems. This requires studying these special constraints and developing these algorithms to take into consideration the special railways environment nature.

The high-speed of trains results in the Doppler effect, also known as Doppler spectrum, which produces frequency shifts that depend on the geometrical environment of the mobile. These frequency shifts may affect the performance of wireless systems. This makes the problem of developing accurate simulators of wireless channels, that include the mobility effect, an essential key for evaluating and developing algorithms for wireless systems. This Chapter presents the existing wireless channel simulators and especially the generalized exact Doppler spread based one.

Also, the special EM environment causes the presence of a potential heavy-tailed impulsive noise. Measurements confirm the impulsive nature of noise acting on antennas aboard trains. This leads to the fact that employing the Gaussian noise model may result, in practice, non-robust algorithms. The α -stable distributed processes was widely used to model the heavy-tailed noise. The major contribution among the works presented in this Chapter is a distribution fitting procedure of measured noise encountered on GSM-R antennas. This fitting procedure confirms that the measured data is well modeled by the symmetric α -stable distribution.

Multiple-antenna systems are widely deployed to improve the transmission reliability in wireless communications. Here, multiple-antennas receiver aboard trains is employed, not only for more reliable performance, but also to improve the awareness functions of the CR radio devices. Spatial correlation among the system's antennas is a practical issue that could influence its performance. Therefore, we also present the widely accepted exponential correlation model which is employed in the following Chapters to evaluate the performance of different methods.

In the remainder of this Chapter, we will present the transmitted signal model along with the general phenomena encountered in this specific environment including the different effects of the mobile radio channel on the transmitted signal and the noise model.

2.2 Mobile Radio Channel Model

2.2.1 Characteristics of Mobile Radio Channels

The performance of any communication system is eventually affected by the medium which the message signal passes through, referred to as communication channel. The random and severe behaviour of wireless propagation channels turns communication over such channels into a difficult task and puts fundamental limitations on the performance of wireless communication systems. Wireless channels may be distinguished by the propagation environment encountered. Many propagation environments have been identified, such as rural, mountainous, urban, suburban,

indoor, underwater or orbital environments, which differ in various ways. The transmission path between the receiver and the transmitter can be altered from simple line-of-sight (LoS) to one that is drastically obstructed by buildings, mountains, etc. Furthermore, the speed of the mobile and the movement of the different objects in its environment also impact how rapidly the signal level fades and the duration of these fades.

There are a lot of mechanisms that influence the electromagnetic radio wave propagation generally attributed to the interaction between waves and material such as reflection, refraction, diffraction and scattering. The relative importance of these propagation mechanisms depends on the particular propagation scenario. Radio propagation can be roughly described by three phenomena: path loss variation with distance, shadowing, and multi-path fading. Among these phenomena, only path-loss is a deterministic effect, and it plays an important role on larger time scales, while shadowing and fading both have stochastic nature. Shadowing occurs due to the varying terrain conditions in suburban areas and due to the obstacles, such as buildings, in urban areas. Fading leads to significant attenuation changes within smaller time scales.

In other words, the mobile channel exhibits a time-varying behaviour in the received signal energy, which is called fading. In the communications literature, most often we encounter two types of fading definitions for the mobile radio channel:

- ❖ Large-scale fading usually is defined as the average signal power attenuation or path-loss due to motion over large areas. This depends on the presence of obstacles in the signal path, on the position of the mobile unit, and its distance from the transmitter. The statistics of large-scale fading provide a way of computing an estimate of path-loss as a function of distance. This is normally described in terms of a mean path-loss and a log-normally distributed variation about the mean which is known as shadowing. Hence the term large-scale fading corresponds to the combined effects of path-loss and shadowing loss.
- ❖ Small-scale fading refers to dramatic changes in signal amplitude and phase that can be experienced as a result of small changes in the spatial separation between a receiver and transmitter. Generally, small-scale fading is referred to as Rayleigh fading if the multiple reflective paths are large in number and there is no LoS signal component, hence the envelope of the received signal is statistically described by a Rayleigh probability density function (PDF). However, if there is a dominant non-fading signal component present, such as a LoS propagation path, the small scale fading envelope is described by a Rician PDF. Other PDFs, employed to describe these fades, can be encountered in the literature.

2.2.2 Characterization in Time and Frequency

The most harmful effects on the received signal in a multi-path high-mobility environment are the frequency offset (Doppler shift) of the carrier and the time delay of the envelope. This is because these frequency shifted and delayed waves might interfere destructively so that they cause severe attenuation. The time-variant impulse response of the multi-path channel can be

expressed in the equivalent baseband by

$$h(t, \varsigma) = \sum_{i=1}^{N_h(t)} h_i(t) \delta(\varsigma - \varsigma_i) \quad (2.1)$$

where $N_h(t)$ is the number of propagation paths, that equals the number of local scatterers, at time t and $h_i(t)$ stands for the complex weighting coefficient corresponding to the i^{th} path with delay ς_i .

Due to the stochastic nature of mobile radio channels, they are generally classified by their statistical properties. The autocorrelation function (ACF)

$$r_h(\tau, \varsigma) = E \{h(t, \varsigma) h^*(t + \tau, \varsigma)\} \quad (2.2)$$

This relationship can also be expressed in the frequency domain. The Fourier transformation of $r_h(\tau, \varsigma)$ with respect to τ yields the scattering function

$$S_h(\nu, \varsigma) = \mathcal{F} \{r_h(\tau, \varsigma)\} \quad (2.3)$$

The Doppler frequency ν originates from the motion of objects within the environment (which might be the transmitter, the receiver or scatterers). Integrating over ς leads to the *Doppler power spectrum*

$$S_h(\nu) = \int_0^\infty S_h(\nu, \varsigma) d\varsigma \quad (2.4)$$

describing the power distribution with respect to ν . The range over which $S_h(\nu)$ is almost nonzero is called *Doppler bandwidth* B_d . The time span that channel roughly stays constant is called the coherence time and given by

$$t_c \approx \frac{1}{B_d} \quad (2.5)$$

For $t_c \gg T$, the channel is slowly fading, for $t_c \ll T$, it changes remarkably during the processing duration T (i.e. at some instants the signal is severely attenuated). In the latter case, the channel is called time-selective. These two conditions are also named slow fading and fast fading, respectively.

Let f_d be the maximum Doppler frequency. Integrating $S_h(\nu, \varsigma)$ over ν instead of ς delivers *the power delay spread*

$$S_h(\varsigma) = \int_{-f_d}^{f_d} S_h(\nu, \varsigma) d\nu \quad (2.6)$$

that describes the power distribution with respect to ς . The delay spread is caused only by the topology of the environment itself. Let the maximum delay be denoted ς_{max} . The coherence bandwidth defined by

$$B_c = \frac{1}{\varsigma_{max}} \quad (2.7)$$

represents the bandwidth over which the channel is nearly constant.

For frequency-selective channels, $B \gg B_c$ holds, that is, the signal bandwidth B is much larger than the coherence bandwidth and the channel behaves differently in different parts of the signal's

spectrum. In this case, ς_{max} is larger than the symbol duration so that successive symbols overlap, resulting in linear channel distortions called *inter-symbol interference* (ISI). For $B \ll B_c$, the channel is frequency-non-selective, that is, its spectral density is constant within the considered bandwidth.

Since the Doppler spread is a phenomenon in frequency, the overall effect on the received signal, which is the result of interfering multiple Doppler shifted signal copies, is a time selective behaviour. The situation is exactly opposite for the delay spread. While the delay spread is a phenomenon in time, the resulting effect on the received signal indicates a frequency selective behaviour.

In the following part, the focus is on the statistics of a single channel coefficient. In the absence of LoS connection, real and imaginary parts of tap coefficient h are statistically independent and Gaussian distributed stochastic processes for a large number of propagation paths per tap. The phase of h is uniformly distributed in $[0, 2\pi]$ while the envelope $r = |h|$ is Rayleigh distributed

$$p_{|h|}(r) = \begin{cases} \frac{r}{\sigma_h^2} \cdot e^{-\frac{r^2}{2\sigma_h^2}}, & r \geq 0 \\ 0, & r < 0 \end{cases} \quad (2.8)$$

In the presence of LoS between the transmitter and the receiver, the total power of the channel coefficient is shared among a constant LoS and a Rayleigh fading component. The distribution of channel envelope is no longer Rayleigh but Rician. However, by considering Rayleigh fading, one is working with the worst possible scenario, since the Rician fading is less destructive and the performance of the communication system is better.

2.2.3 Mobile Radio Channels : Doppler Effect

Let us consider the relative velocity between the transmitter and the receiver is v and the transmitted signal arrives at the angle α . The signal's carrier frequency f_c suffers of the Doppler frequency shift

$$\nu = \frac{v}{c} f_c \cos(\alpha) = f_d \cos(\alpha) \quad (2.9)$$

where $c = 3 \cdot 10^8$ is the speed of light and $f_d = \frac{v}{c} f_c$.

Let us consider the effect of the motion in the model presented in Equation (2.1). The complex envelope is rewritten as [25]

$$h(t, \varsigma) = \sum_{i=1}^{N_h} a_i e^{j\phi_i} e^{2\pi j\nu_i t} \delta(\varsigma - \varsigma_i) \quad (2.10)$$

The real-valued quantities a_i , ϕ_i and ν_i represent the attenuation, the phase shift and the Doppler shift corresponding to the i^{th} path. Therefore relative motion introduces a frequency shift of the carrier for each path. This Doppler shift is distributed between $-f_d$ and f_d . In the case of isotropic scattering (i.e. the arrival angle α is uniformly distributed in the interval $[0, 2\pi]$), the Doppler power spectrum associated with each channel tap is given by the classical Jakes

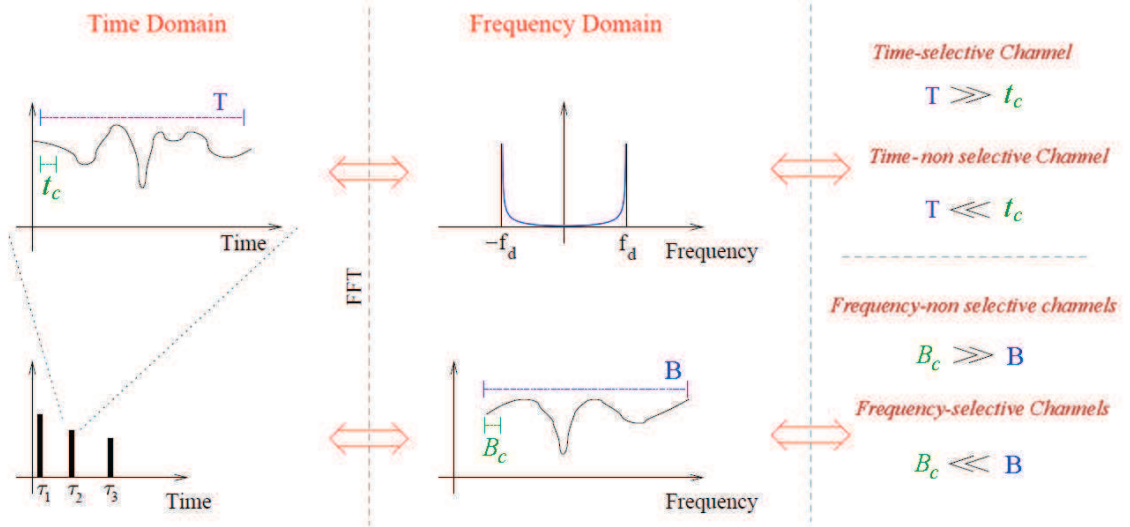


Figure 2.1: Characterization of mobile radio channels in time and frequency.

distribution

$$S_h(\nu) = \begin{cases} \frac{\sigma_h^2}{\pi f_d \sqrt{1 - (\frac{\nu}{f_d})^2}}, & |\nu| \leq f_d \\ 0, & |\nu| > f_d \end{cases} \quad (2.11)$$

where σ_h^2 is the average power of the channel tap. This is well known U shaped spectrum shown in Figure 2.1 , and it is often referred to as Jakes spectrum.

We can easily derive the autocorrelation function of the channel complex tap by taking the inverse Fourier transform of the Doppler power spectrum given in Equation (2.11)

$$r_h(\tau) = \sigma_h^2 J_0(2\pi f_d \tau) \quad (2.12)$$

where the function $J_0(\cdot)$ denotes the zero-order Bessel function of the first kind.

2.2.4 Mobile Radio Channels Models

2.2.4.1 Introduction

Mobile radio channel simulators are commonly used because they allow system tests and evaluations which are less expensive and more reproducible than field trials. The prime requirement of the simulation set-up is to capture the fading effects created by a radio channel. There are several methods in the communications literature to simulate Rayleigh fading. These methods are described in [25]. They can be based on either sum of sinusoids principle or filtering of the white Gaussian noise.

When using the filter method, a white Gaussian noise (WGN) process $w(t)$ is given to the input of a linear time-invariant filter, whose transfer function is denoted by $H(f)$. If $w(t) \sim \mathcal{N}(0, 1)$, then we obtain a zero-mean stochastic Gaussian random process $h(t)$ at the filter output, where the power spectral density $S_h(f)$ of $h(t)$ matches the squared absolute value of the transfer function, i.e., $S_h(f) = |H(f)|^2$. Hence, a colored Gaussian random process $h(t)$ can be considered as

the result of filtering WGN $w(t)$. Then, filtering Gaussian noise through appropriately designed filters, the channel Doppler power spectral density can be simulated, thereby capturing the important first and second order fading statistics. Several implementation schemes of this filtering approach exist in the literature [26].

The second approach considers that the complex channel envelope of multi-path fading channel can be represented as a “sum-of-sinusoids” (SoS) model. Each sinusoid is characterized by certain parameters (i.e., amplitude, Doppler frequency and phase). The motivation behind SoS-based fading channel simulators is that when a sinusoidal carrier is transmitted and subjected to multi-path fading, the received carrier can be modeled as a superposition of multiple possibly Doppler shifted copies of the transmitted carrier received from different paths. Being a natural representation of the channel waveform, several SoS models have been presented in the past to simulate wireless channels [25]. Rather than simulating the channel by directly applying the Clarke’s reference model [27], specialized sum of sinusoids models are proposed to efficiently simulate the channel by using a finite number of sinusoids. The philosophy of SoS modeling has been made popular after the simplified version of Clarke’s model proposed by Jakes [28].

We have to generate multiple uncorrelated Rayleigh fading processes when multiple-antennas receiver and multi-path channel is considered. It is well-known that a Rayleigh process is formed by taking the absolute value of a zero-mean complex Gaussian random process. Ideally, these different uncorrelated complex Gaussian random processes should satisfy the following criteria: i) The inphase and quadrature components of each complex process are zero-mean independent real Gaussian random processes with identical ACFs; ii) The cross-correlation function (CCF) of any pair of complex Gaussian random processes must be zero. In this thesis, we focus on the SoS based simulators. These simulators are efficient, less complex and easier to implement when employed to generate multiple uncorrelated Rayleigh fading processes [25].

2.2.4.2 Sum of Sinusoids Models

The reference model of Clarke defines the channel complex gain under non-LoS, frequency flat fading, and 2-D isotropic scattering assumptions as [27]

$$h(t) = \lim_{N_p \rightarrow \infty} \sqrt{\frac{2}{N_p}} \sum_{n=1}^{N_p} e^{j[2\pi f_d t \cos(\alpha_n) + \theta_n]} \quad (2.13)$$

where N_p denotes the number of propagation paths, $\theta_n \sim U[-\pi, \pi)$ and $\alpha_n \sim U[-\pi, \pi)$ are, respectively, the random phase and angle of arrival of the i^{th} multi-path component. When N_p becomes large, $\Re[h(t)]$ and $\Im[h(t)]$ (the real and imaginary components, respectively) are zero-mean, Gaussian and statistically independent. Due to the accurate statistical properties of Clarke’s model, it has been widely used as a reference theoretical model for simulating fading channels. However, an efficient implementation of a fading channel simulator requires using a finite and preferably a small number of sinusoids. Hence, Jakes simplified this method by exploiting the symmetry in the environment to reduce the number of sinusoids. Actually, the Jakes’s model had been the simulation model for a long time. However, several studies have

shown that the fading signals which are produced by classical Jakes simulator are not wide-sense stationary [29]. Several improvements have subsequently been proposed in the literature to make the SoS model wide-sense stationary.

SoS simulators can be classified either as “deterministic” or “stochastic” [25,30]. In deterministic SoS simulators, all the waveform parameters are held fixed for the duration of the simulation. Deterministic SoS-based models require a relatively large number N of sinusoids to achieve accurate statistical properties [25]. Also, the statistical averaging or Monte Carlo simulation results cannot be obtained since all the parameters in the model are fixed. One advantage of the deterministic channel modeling approach is that the resulting simulation model is ergodic, while stochastic methods result in non-ergodic fading simulator in most cases [25,30]. By using non-ergodic simulation models [31,32], one has to perform several simulation runs with different sets of model parameters. However, the statistics of non-ergodic simulation models can be improved by averaging over the obtained results. An ergodic stochastic SoS channel simulator has constant gains and frequencies but random phases [30]. Several ergodic stochastic methods for the generation of multiple uncorrelated Rayleigh fading processes with a SoS channel simulator exist in the literature [33]. Unfortunately, the ACFs of the inphase and quadrature parts of the designed complex waveforms are not close to the specified one.

2.2.4.3 Generalized Exact Doppler Spread Model

The usefulness of the method of exact Doppler spread (MEDS) [34] was revisited in [35]. It was shown that all the main channel model requirements can be fulfilled, but unfortunately the complexity of the resulting channel simulator increases almost exponentially with the increase of the number of uncorrelated waveforms. This makes the original MEDS less efficient if the number of waveforms is large. The authors in [36] introduced a generalized version of MEDS (GMEDS). This generalized version can be interpreted as a class of parameter computation methods, which includes many other well-known approaches as special cases. Two new special cases were introduced in [36] to enable the efficient and accurate design of multiple uncorrelated Rayleigh fading waveforms using ergodic stochastic concepts. These methods can fulfill all main requirements imposed on the correlation properties of the resulting channel simulator. Also, the computational complexity of the model parameters is low. This model is adopted in our thesis.

The K mutually uncorrelated Rayleigh fading waveforms

$$h^{(k)}(t) = h_1^{(k)}(t) + jh_2^{(k)}(t), k = 1, \dots, K \quad (2.14)$$

are generated using an SoS channel simulator

$$h_i^{(k)}(t) = \sqrt{\frac{2}{N_i}} \sum_{n=1}^{N_i} \cos\left(2\pi f_{i,n}^{(k)} t + \theta_{i,n}^{(k)}\right), i = 1, 2 \quad (2.15)$$

where N_i denotes the number of sinusoids, $f_{i,n}^{(k)}$ is called the discrete Doppler frequency, and $\theta_{i,n}^{(k)}$ is the phase of the n^{th} sinusoid of the inphase component $h_1^{(k)}(t)$ or quadrature component $h_2^{(k)}(t)$ of the k^{th} complex waveform $h^{(k)}(t)$. The phases $\theta_{i,n}^{(k)}$ are considered as outcomes of independent

and identically distributed (i.i.d.) random variables, each having a uniform distribution over the interval $[0, 2\pi)$. The problem is to find proper values for the discrete Doppler frequencies $f_{i,n}^{(k)}$ in such a way that the above mentioned two conditions on the ACFs and the CCFs are fulfilled. The discrete Doppler frequencies $f_{i,n}^{(k)}$, according to the GMEDS, are given by

$$\begin{aligned} f_{i,n}^{(k)} &= f_d \cos(\alpha_{i,n}^{(k)}) \\ &= f_d \cos\left[\frac{q\pi}{2N_i}\left(n - \frac{1}{2}\right) + \alpha_{i,0}^{(k)}\right] \end{aligned} \quad (2.16)$$

where $\alpha_{i,0}^{(k)}$ is called the angle of rotation that will be defined subsequently and $q \in \{0, 1, 2\}$. Note that the quantity q mainly determines the range of values for the angles of arrival $\alpha_{i,n}^{(k)}$. According to the GMEDS₁ (i.e. $q = 1$), the angle of rotation $\alpha_{i,0}^{(k)}$ is defined as

$$\alpha_{i,0}^{(k)} = (-1)^{(i-1)} \frac{\pi}{4N_i} \cdot \frac{k}{K+2}, \quad (2.17)$$

while the GMEDS₂ (i.e. $q = 2$) defines $\alpha_{i,0}^{(k)}$ as

$$\alpha_{i,0}^{(k)} = \frac{\pi}{4N_i} \cdot \frac{k-1}{K-1} \quad (2.18)$$

where $i = 1, 2$ and $k = 1, \dots, K$.

It was shown that the GMEDS₁ in general outperforms the GMEDS₂ with respect to the error function, which measures the accuracy of the channel simulator's ACF of the complex generated waveform [36].

This section presented the general characteristics of mobile radio channels and the Doppler effect resulting from the high-speed of trains. The development and evaluation of communication systems performance require using an accurate mobile radio channel simulator. We presented the main existing simulators in the literature before focusing on the GMEDS simulator. This ergodic effective simulator can reply all main requirements implied by the actual wireless channel model. The GMEDS simulator is designed to generate multiple uncorrelated fading channels such that the simulation model is as close as possible to the given reference model over a certain delay interval.

2.3 Signal Model

2.3.1 Received Signal Representation

We assume that there are $M \geq 1$ antennas at the CR mobile terminal aboard train, also called the secondary user (SU), as shown in Figure 2.2. The SU receiver detects several primary sources (PSs) where the PS is the signal of a licensed user, also called primary user (PU).

The continuous-time received signal at antenna i is $x_{c,i}(t) = \tilde{s}_{c,i}(t) + w_{c,i}(t)$ where $\tilde{s}_{c,i}(t)$ is the superposition of the possible continuous-time primary sources signals including the effects of

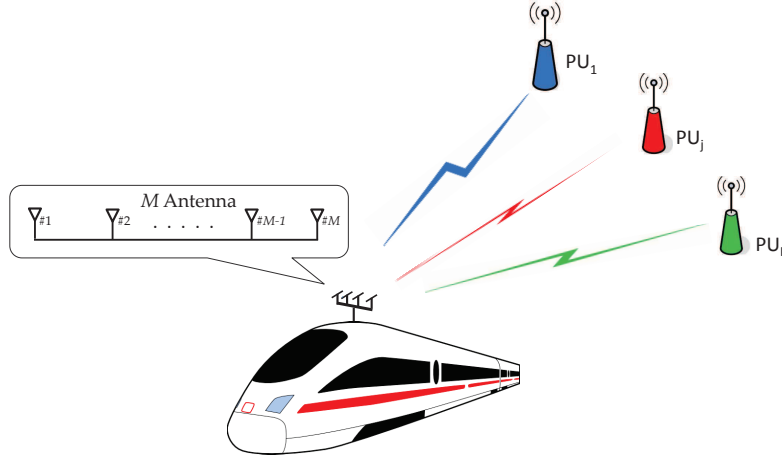


Figure 2.2: Multiple-antennas receiver at the secondary user (the moving train) in the presence of P primary users (available radio services).

path-loss, multi-path fading and time dispersion, and $w_{c,i}(t)$ is the continuous-time noise, as displayed in Figure 2.3. We sample the received signal at a sampling rate f_s . Let $T_s = 1/f_s$ be the sampling period. For notation simplicity, we define $x_i(n) \triangleq x_{c,i}(nT_s)$, $\tilde{s}_i(n) \triangleq \tilde{s}_{c,i}(nT_s)$ and $w_i(n) \triangleq w_{c,i}(nT_s)$.

In the presence of P primary sources (PS_j , $1 \leq j \leq P$), the sampled received signal at the i^{th} antenna is represented as

$$x_i(n) = \sum_{j=1}^P \sum_{k=0}^{C_j} h_{i,j}(n, k) s_j(n - k) + w_i(n), \quad n = 1, 2, \dots \quad (2.19)$$

where $s_j(n)$ is the j^{th} sampled primary source signal, C_j is the order of the channel between PS_j and each antenna, and $h_{i,j}(n, k)$ is the k^{th} tap of the channel response between PS_j and the i^{th} antenna at instant n . The $M \times 1$ observation vector at the receiver is expressed as

$$\mathbf{x}(n) = \begin{bmatrix} \mathbf{h}_{1,1}(n) & \mathbf{h}_{1,2}(n) & \cdots & \mathbf{h}_{1,P}(n) \\ \mathbf{h}_{2,1}(n) & \mathbf{h}_{2,2}(n) & \cdots & \mathbf{h}_{2,P}(n) \\ \vdots & \vdots & \vdots & \vdots \\ \mathbf{h}_{M,1}(n) & \mathbf{h}_{M,2}(n) & \cdots & \mathbf{h}_{M,P}(n) \end{bmatrix} \mathbf{s}(n) + \mathbf{w}(n), \quad n = 1, 2, \dots \quad (2.20)$$

where $\mathbf{s}(n) = [s_1(n), \dots, s_1(n - C_1), \dots, s_P(n), \dots, s_P(n - C_P)]^T$, and $\mathbf{w}(n) = [w_1(n), \dots, w_M(n)]^T$ is the $M \times 1$ received noise vector. The vector $\mathbf{h}_{i,j}(n) = [h_{i,j}(n, 0), \dots, h_{i,j}(n, C_j)]$ represents the channel taps between PS_j and the i^{th} antenna.

Let us consider L consecutive samples and define the corresponding signal/noise vectors

$$\begin{aligned} \mathbf{x}_L(n) &= [x_1(n), \dots, x_1(n - L + 1), \dots, x_M(n), \dots, x_M(n - L + 1)]^T \\ \mathbf{s}_L(n) &= [\mathbf{s}_1^T(n), \mathbf{s}_2^T(n), \dots, \mathbf{s}_P^T(n)]^T \\ \mathbf{w}_L(n) &= [w_1(n), \dots, w_1(n - L + 1), \dots, w_M(n), \dots, w_M(n - L + 1)]^T \end{aligned} \quad (2.21)$$

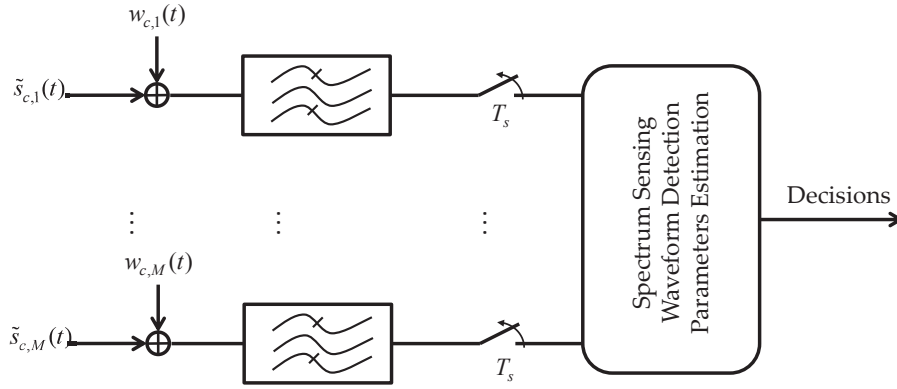


Figure 2.3: System Model.

where $\mathbf{s}_j^T(n) = [s_j(n), s_j(n-1), \dots, s_j(n-C_j-L+1)]$ and L is called the smoothing factor. The system is expressed in matrix form as

$$\mathbf{x}_L(n) = \mathbf{H}(n) \mathbf{s}_L(n) + \mathbf{w}_L(n) \quad (2.22)$$

where \mathbf{H} is an $ML \times (C + PL)$ matrix and $C = \sum_{j=1}^P C_j$.

Defining the $L \times (C_j + L)$ matrix $\mathbf{H}_{i,j}$, $1 \leq j \leq P$, $1 \leq i \leq M$, as

$$\mathbf{H}_{i,j}(n) = \begin{bmatrix} \mathbf{h}_{i,j}(n) & 0 & \cdots & 0 \\ 0 & \mathbf{h}_{i,j}(n-1) & \ddots & \vdots \\ \vdots & \ddots & \ddots & 0 \\ 0 & \cdots & 0 & \mathbf{h}_{i,j}(n-L+1) \end{bmatrix}, \quad (2.23)$$

\mathbf{H} is expressed as

$$\mathbf{H}(n) = \begin{bmatrix} \mathbf{H}_{1,1}(n) & \mathbf{H}_{1,2}(n) & \cdots & \mathbf{H}_{1,P}(n) \\ \mathbf{H}_{2,1}(n) & \mathbf{H}_{2,2}(n) & \cdots & \mathbf{H}_{2,P}(n) \\ \vdots & \vdots & \ddots & \vdots \\ \mathbf{H}_{M,1}(n) & \mathbf{H}_{M,2}(n) & \cdots & \mathbf{H}_{M,P}(n) \end{bmatrix}. \quad (2.24)$$

Let us assume $\mathbf{w}(n)$ is an additive white Gaussian noise (AWGN) vector with zero-mean and variance σ_w^2 . The covariance matrix of the received signal, set to as $\mathbf{R}_{L,x} = \mathbf{E}[\mathbf{x}_L \mathbf{x}_L^H]$, gives

$$\mathbf{R}_{L,x} = \mathbf{H} \mathbf{R}_{L,s} \mathbf{H}^H + \sigma_w^2 \mathbf{I}_{ML} \quad (2.25)$$

where $(\cdot)^H$ represents the Hermitian transpose and $\mathbf{R}_{L,s} = \mathbf{E}[\mathbf{s}_L \mathbf{s}_L^H]$ is assumed to be of full rank. Let $\lambda_1 \geq \cdots \geq \lambda_{ML}$ denote the eigenvalues of $\mathbf{R}_{L,x}$. The received signal covariance matrix is usually unknown. The sample covariance matrix is employed to overcome this difficulty, and is given by

$$\mathbf{R}_{L,x}(N) = \frac{1}{N} \sum_{k=1}^N \mathbf{x}_L(k) (\mathbf{x}_L(k))^H \quad (2.26)$$

where N is the number of observed samples. The estimated eigenvalues are ℓ_1, \dots, ℓ_{ML} such as

$$\ell_1 \geq \dots \geq \ell_{ML}.$$

The signal-to-noise-ratio (SNR) is defined as the ratio of the average received primary user's signal power to the average receiver noise power, that is

$$\text{SNR} = \frac{E[\|\mathbf{x}(n) - \mathbf{w}(n)\|^2]}{E[\|\mathbf{w}(n)\|^2]} \quad (2.27)$$

2.3.2 Multiple-antennas Spatial Correlation

Many propagation environments result in spatial correlation among antennas. Hence, spatial correlation is a crucial factor for practical systems and its effect on their performance must be evaluated. Several analytical models for multiple-antennas spatial correlations exist in the literature. For instance, the Kronecker model [37] assumes that spatial receiver and transmitter correlations are separable.

It can be shown that, under the above assumption, the Kronecker model is given by

$$\mathbf{H} = \mathbf{R}_r^{1/2} \mathbf{H}_w \mathbf{R}_t^{1/2} \quad (2.28)$$

where \mathbf{R}_t and \mathbf{R}_r are the transmitter and the receiver correlation matrices. \mathbf{H}_w is a channel gain matrix whose the structure is identical to that defined in (2.20).

When \mathbf{H}_w is a full rank gain matrix whose entries are i.i.d and follows a circularly symmetric complex Gaussian distribution with zero-mean and unit variance, the Kronecker model is equivalent to express the total correlation of the channel \mathbf{R}_H as the Kronecker product (\otimes) of the correlation matrices \mathbf{R}_t and \mathbf{R}_r , as

$$\mathbf{R}_H = \mathbf{R}_t \otimes \mathbf{R}_r \quad (2.29)$$

The effect of transmit spatial correlation is neglected when:

- ❖ the primary sources are actually well separated antennas at some primary user.
- ❖ the primary sources are actually several uncorrelated primary users.

The correlation matrices \mathbf{R}_t and \mathbf{R}_r are represented by the exponential correlation model introduced in [38]. This model defines the entries of a correlation matrix \mathbf{R} as

$$[\mathbf{R}]_{i,j} = \begin{cases} \rho^{j-i}, & i \leq j \\ [\mathbf{R}]_{j,i}^*, & i > j \end{cases}, \quad |\rho| < 1, \quad (2.30)$$

where ρ is the complex correlation coefficient of neighboring (receive or transmit) branches. This model may be not accurate for some real-world scenarios but this is a simple single-parameter model which allows us to study the effect of correlation in an explicit way. However, this model is physically reasonable in the sense that the correlation decreases with increasing distance between antennas. The two matrices \mathbf{R}_t and \mathbf{R}_r are then, respectively, defined by the transmit correlation coefficient ρ_t and the receive correlation coefficient ρ_r .

2.3.3 Transmission Schemes

Several transmission techniques are employed in the existing communications systems. These techniques were developed to achieve high data-rate multi-user robust communications. In the following, some of these techniques are presented.

2.3.3.1 Orthogonal Frequency Division Multiplexing

Orthogonal frequency division multiplexing (OFDM) is a multi-carrier modulation technique that can overcome many problems that arise from high data-rate communications, the biggest of which is time dispersion. In OFDM, carrier frequencies are chosen in such a way that there is no influence of other carriers when detecting the information in a particular carrier as long as the orthogonality between the carriers is maintained. The data bearing symbol stream is split into several lower rate streams and these streams are transmitted on different carriers. The ISI is removed by cyclically extending the OFDM symbol. The length of the cyclic extension should be at least as long as the maximum delay of the channel. OFDM is one of the key enabler technologies for very high throughputs and robustness in the emerging standards that support vehicular mobility (IEEE 802.11p, IEEE802.16e, IEEE 802.20, and LTE).

2.3.3.2 Code Division Multiple Access

Direct-sequence spread spectrum (DS-SS) is a transmission technique in which a pseudo-random sequence or pseudo-noise (PN) code, independent of the information data, is employed as a modulation waveform to spread the signal energy over a bandwidth much greater than the information signal bandwidth. This results in many benefits, such as immunity to interference and jamming and multi-user access.

DS-SS transmissions have been used in military context for secure communications for several decades due to their low probability of intercept properties. During the last couple of decades, spread spectrum technology was proposed for private and commercial use, especially the code division multiple access (CDMA) transmissions. The receiver synchronizes to the code to recover the data. The use of code independent of data and synchronous reception allows multiple users to access the same frequency band at the same time. Direct-sequence CDMA (DS-CDMA) signals are very widely used in multi-user wireless communication systems e.g. IS-95 and WCDMA. It is also used in the GPS satellite navigation system.

2.3.3.3 Multi-Carrier Spread Spectrum (MC-SS)

The success of multi-carrier modulation and spread spectrum technique motivated many researchers to investigate the advantages of possible combinations of both techniques, known as multi-carrier spread spectrum (MC-SS) which benefits from the main advantages of both schemes. Among all combination of both techniques, the so-called multi-carrier direct-sequence CDMA (MC-DS-CDMA) is considered in this thesis as a case study for some proposed algorithms. The MC-CDMA and OFDM cases can be easily inferred.

2.4 Noise Model

The performance of any communications system does not depend on the channel characteristics and the used transmission technique only, but also depends on the corrupting noise nature and its statistical properties. The most widely employed noise model in the literature is the Gaussian one. But, a wide variety of noise processes commonly found in wireless communications exhibit non-Gaussian impulsive behaviour [39]. This type of behaviour arises in the special railways environment. A brief study of some impulsive noise models is provided, followed by a statistical distribution fitting of measured impulsive noise acting on GSM-R antennas.

2.4.1 The Gaussian Model

The Gaussian distribution has been the favorite noise model in communications and signal processing literature. Despite the mathematical simplicity of this model, the ideal Gaussian model is reasonable and can be justified by the central limit theorem. This theorem explains the Gaussian nature of processes generated from superposition of many small and independent effects. This is the case for example of thermal noise, which is generated as the superposition of a large number of random independent interactions at the molecular level. In addition, the use of the Gaussian assumption is also convenient since it often leads to closed-form solutions.

Although many important processes found in the communications are non-Gaussian, a large amount of practical communications systems still live in the Gaussian world. A serious concern is that, in general, a system designed under the Gaussian assumption will show drastic performance degradations when the noise statistics depart to heavier-tailed models [39].

2.4.2 Heavy-tailed Impulsive Noise in Communications

The impulsive behaviour resulting from naturally occurring or man-made noise sources may exhibit high amplitudes for small duration time intervals. Typical examples include atmospheric radio noise (such as thunderstorms), telephone lines noise, office equipments, rotating machinery, engine ignition, and multi-user interference in mobile communication systems. Transportation systems often suffer of impulsive noise such as car ignitions, and the EM interferences in the railway environment (e.g. the transient EM noise which is produced by the sliding contact between the catenary and the pantograph).

Several distributions, with heavier than Gaussian tails, have been proposed as non-Gaussian impulsive noise models. Well credited statistical-physical models have been proposed by Middleton [40]. The most employed among these models is the class A. This model assumes that the impulsive noise is described by two PDFs: a Poisson distribution that models the number of impulses occurring in a given time interval, and a Rayleigh distribution that models the impulsive envelope. A simplified distribution commonly used in the modeling of impulsive noise is the Gaussian mixture or the contaminated Gaussian [39]. Other common physically motivated models in the literature [39,41] are based on the Laplace distribution, K -distribution, generalized Gaussian distribution, and generalized student- t distribution.

However, α -stable random processes provide a suitable model for a wide range of non-Gaussian heavy-tailed impulsive noise encountered in wireless communication channels [39, 41]. This can be justified by the generalized central limit theorem considering that the noise results from a large number of possibly impulsive effects.

Theorem 1 (generalized central limit theorem). The infinite sum of many i.i.d random variables, **not necessarily with finite variances**, converges to a α -stable distribution.

In the same way as the Gaussian model, the generalized central limit theorem constitutes a strong theoretical argument compelling the use of α -stable in practical problems. In addition, it was shown in [42] that α -stable processes provide excellent fits to measured impulsive noise. Also, recent work has experimentally verified that α -stable distribution provides an accurate model of interference in laptop embedded transceivers [43]. α -stable processes share basic characteristics with the Gaussian processes; i.e. they satisfy the stability property and the generalized central limit theorem. Also, this heavy-tailed impulsive noise model is flexible and can be controlled by few parameters.

A random variable w that follows the α -stable distribution have no closed-form of the PDF and is rather described by its characteristic function,

$$\Phi_w(t) = \exp\{j\delta t - \gamma |t|^\alpha [1 + j\beta \text{sign}(t)\kappa(t, \alpha)]\}, \quad (2.31)$$

where

$$\kappa(t, \alpha) = \begin{cases} \tan \frac{\pi\alpha}{2}, & \alpha \neq 1 \\ \frac{2}{\pi} \log |t|, & \alpha = 1 \end{cases}, \quad 0 < \alpha \leq 2, -1 \leq \beta \leq 1, 0 < \gamma.$$

Thus a stable distribution is totally determined by four parameters: (i) the characteristic exponent, α , that controls the heaviness of the tails of the stable density and hence the impulsiveness of the respective stable process (the smaller the α is, the heavier the tails are); (ii) the location parameter, δ , that represents the mean when $1 < \alpha \leq 2$ and the median when $0 < \alpha \leq 1$; (iii) the dispersion parameter, γ , that determines the spread of the distribution around its location parameter δ ; and (iv) the index of skewness, β , controls the symmetry of the distribution. A random variable w with stable distribution of parameters $\alpha, \beta, \gamma, \delta$ is noted as $w \sim \mathcal{S}_\alpha(\beta, \gamma, \delta)$.

Although some practical noise processes might be better modeled by asymmetric distributions, we will concentrate only on symmetric models since a large number of important noise and interference processes found in wireless communications are symmetric. When the stable distribution is symmetric ($\beta = 0$), Equation (2.31) is reduced to

$$\Phi_w(t) = \exp\{j\delta t - \gamma |t|^\alpha\}, \quad (2.32)$$

such symmetric α -stable process is denoted $S\alpha S$. Two well known special $S\alpha S$ distributions are the Cauchy distribution ($\alpha = 1$) and the Gaussian one ($\alpha = 2$).

In the following subsection, we will study a distribution fitting of measured impulsive noise at the output of GSM-R antennas fixed above a moving train.

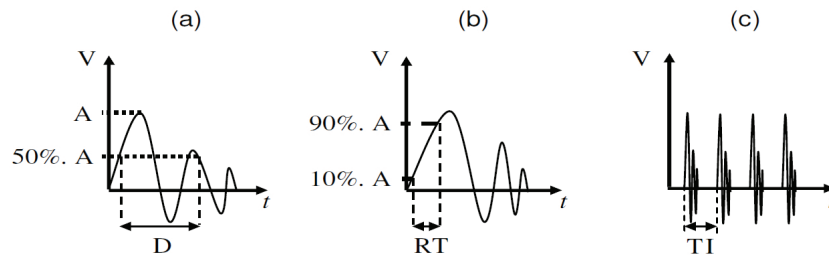


Figure 2.4: Definitions of the time characteristics of transient EM interferences acting on GSM-R antennas.

2.4.3 Case Study : Electromagnetic Interferences Acting on GSM-R Antennas

In the special railway domain, one important EM noise source that could interfere with the GSM-R communications is the transient EM disturbance which is produced by the sliding contact between the catenary and the pantograph. Indeed, the losses of contact between the catenary and the pantograph produce transient signals which are conducted along the catenary and along the power line of the train [12]. It induces transient emissions which cover wide frequency bands and which are received by the GSM-R antennas. Measurement campaigns on board trains were carried out in order to characterize these transient disturbances [12]. Experiments were carried out using a digital oscilloscope with a 20 GHz sampling frequency. The cruising speed of the train was about 160 km/h and the maximal speed was 200 km/h. For more details on the measurement campaign configuration, refer to [12].

The authors in [12] have studied some time characteristics of the transient EM interferences instead of studying the impulsive noise itself. The transient EM test signals were notably defined in terms of maximal amplitude (A) and corresponding time interval (TI), rise time (RT) and time duration (TD) as seen in Figure 2.4. It was found that the duration is lower than 20 ns and a typical duration value is 5 ns. The maximal value of the rise time of the transients is 1 ns and the most current value is 0.4 ns. It was noticed that the time interval between two successive transients can significantly vary. Nevertheless, under certain operating conditions, a typical time interval can be 25 μ s. Also, the permanent noise effect was dropped in [12].

2.4.3.1 Distribution Fitting Procedure

Figure 2.5 shows that the fitting of the measured data (the EM interferences) is performed according to the following steps:

- ❖ For each measurement dataset, 2×10^6 noise samples were used to generate a sample PDF. The empirical probability density of the measured data was estimated using kernel smoothing density estimators.
- ❖ The distribution model of the measured data is assumed Middleton class A model, $S\alpha S$ model or the Gaussian one. Based on the measured data, the parameters of the assumed distribution are estimated.

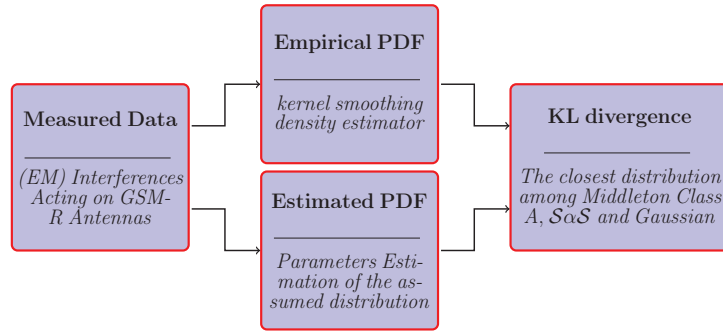


Figure 2.5: EM interferences measurements distribution fitting procedure.

- ❖ To compare the assumed distribution with the empirical one, the Kullback-Leibler (KL) divergence is used to quantify the closeness of two PDFs.

Kernel density estimation is a non-parametric way of estimating the probability density function of a random variable. Given a random sample x_1, \dots, x_N with a continuous, univariate density f . The kernel density estimator is

$$\hat{f}_h(x) = \frac{1}{Nh} \sum_{i=1}^N K\left(\frac{x - x_i}{h}\right), \quad (2.33)$$

where $K(\cdot)$ is the kernel and $h > 0$ is a smoothing parameter called the bandwidth. The bandwidth controls the smoothness or roughness of a density estimate. Kernel density estimates are closely related to histograms, but the smoothness of the kernel density estimate is evident compared to the discreteness of the histogram. Under mild conditions, the kernel estimate converges in probability to the true density.

The Kullback-Leibler divergence, also known as the relative entropy, between two probability density functions f, g ,

$$D_{KL}(f \parallel g) = \int_{-\infty}^{\infty} f(x) \log\left(\frac{f(x)}{g(x)}\right) dx, \quad (2.34)$$

is commonly used in statistics as a measure of the difference between two probability distributions. The KL divergence is non-negative (≥ 0), not symmetric in f and g , and equals zero if and only if there is an exact match of the two densities.

The last step in the fitting procedure is to introduce and evaluate the existing efficient estimation methods of the α -stable distribution parameters.

2.4.3.2 Parameters Estimation of Stable Distributions

The parameters estimation of α -stable distributed processes encounters difficulties since there are no closed form expressions for the PDF in most cases. Among many methods available in the literature for this estimation problem, we will address three reference methods. In the following, these methods are briefly introduced before examining their performances in order to choose the best one among them.

Let w_1, w_2, \dots, w_N be samples of independent random variables identically distributed according to α -stable, i.e. $w \sim \mathcal{S}_\alpha(\beta, \gamma, \delta)$.

Sample Quantile Method [44]. McCulloch provided estimators of all four stable parameters (with the restriction $\alpha \geq 0.6$) [44]. Let us denote by w_p the p^{th} population quantile of $\mathcal{S}_\alpha(\beta, \gamma, \delta)$, i.e. $\mathbb{P}[w < w_p] = p$. A quantile estimation is obtained from the $p \times 100\%$ ordered sample observation whether this value is present in the sample. Otherwise the estimator is obtained by linear interpolation.

Then the following indexes are established

$$\vartheta_\alpha = \frac{w_{0.95} - w_{0.05}}{w_{0.75} - w_{0.25}} \quad \text{and} \quad \vartheta_\beta = \frac{w_{0.95} + w_{0.05} - w_{0.5}}{w_{0.95} - w_{0.05}} \quad (2.35)$$

These two indexes don't depend on δ and γ . Moreover they are respectively decreasing and increasing function of α and β . From quantile estimates, we get index estimates $(\vartheta_\alpha, \vartheta_\beta)$, then by inversion, the corresponding estimates $(\hat{\alpha}, \hat{\beta})$. This inversion is based on the tables provided in [44] where a grid of $(\hat{\alpha}, \hat{\beta})$ values are provided for given estimated index values.

Dispersion and location parameters, δ and γ , can be estimated in a similar way depending on another two indexes, as follows

$$\vartheta_\gamma = \frac{w_{0.75} - w_{0.25}}{\gamma} \quad \text{and} \quad \vartheta_\delta = \frac{\delta + \hat{\beta}\gamma \tan \frac{\pi \hat{\alpha}}{2} - w_{0.5}}{\hat{\gamma}} \quad (2.36)$$

where ϑ_γ is a quantity which depends neither on γ nor δ and is tabulated for a grid of values of $(\hat{\alpha}, \hat{\beta})$.

Fractional Lower Order Moment Method [45]. The fractional lower order moments (FLOMs) are finite for certain parameter values of α -stable distributions [42]. The absolute and signed fractional moments can be estimated, respectively, by the sample statistics

$$A_p = \frac{1}{N} \sum_{i=1}^N |w_i|^p, \quad M_p = \frac{1}{N} \sum_{i=1}^N w_i^p \quad (2.37)$$

The *sinc* estimator for α , ratio estimator of β and FLOM γ estimator are based on the following closed form expressions [45]. Estimating α is done by solving

$$\text{sinc}\left(\frac{p\pi}{\alpha}\right) = \left[\frac{p\pi}{2} \left(\frac{A_p A_{-p}}{\tan\left(\frac{p\pi}{2}\right)} + M_p M_{-p} \tan\left(\frac{p\pi}{2}\right) \right) \right]^{-1}. \quad (2.38)$$

Given an estimate of α , the estimation of $\theta = \arctan\left(\beta \tan \frac{\pi\alpha}{2}\right)$ is calculated by

$$\frac{M_p}{A_p} = \frac{\tan\left(\frac{p\theta}{\hat{\alpha}}\right)}{\tan\left(\frac{p\pi}{2}\right)}, \quad (2.39)$$

given the θ estimate, β is estimated by: $\hat{\beta} = \frac{\tan(\hat{\theta})}{\tan(\frac{\hat{\alpha}\pi}{2})}$. The FLOM estimator of γ is given by

$$\hat{\gamma} = \left| \cos(\hat{\theta}) \right| \left[\frac{\Gamma(1-p) \cos(\frac{p\pi}{2})}{\Gamma(1-\frac{p}{\hat{\alpha}}) \cos(\frac{p\hat{\theta}}{\hat{\alpha}})} A_p \right]^{\hat{\alpha}/p} \quad (2.40)$$

All these estimators assume a zero location value ($\delta = 0$). The exponent p is chosen carefully to keep the variance of each estimator finite. It equals 0, 0.2 and $\hat{\alpha}/10$ respectively for the α , β and γ estimators. Note the α estimate is used to determine p value for γ estimator.

Empirical Characteristic Function (ECF) Method [46]. The ECF is defined by

$$\hat{\Phi}_w(t) = \frac{1}{N} \sum_{i=1}^N \exp(jtw_i) \quad (2.41)$$

The law of large numbers establishes that $\hat{\Phi}_w(t)$ is a consistent estimator of $\Phi_w(t)$. This estimation method is based on the following observations concerning the characteristic function. First, we can easily derive

$$\ln(-\ln |\Phi_w(t)|^2) = \ln(2\gamma^\alpha) + \alpha \ln |t| \quad (2.42)$$

Equation (2.42) depends only on α and γ and suggests that we can estimate these two parameters by regressing $y_1 = \ln(-\ln |\Phi_w(t)|^2)$ on $u_1 = \ln |t|$ in the model: $y_{1,k} = m + \alpha u_{1,k} + e_{1,k}$, where $u_{1,k}$ is an appropriate set of real numbers, $m = \ln(2\gamma^\alpha)$, and $e_{1,k}$ denotes an error term.

Calculating the real and imaginary parts of $\Phi_w(t)$ for $\alpha \neq 1$ leads to

$$\arctan \left(\frac{\Im[\Phi_w(t)]}{\Re[\Phi_w(t)]} \right) = \delta t + \beta \gamma^\alpha \tan \frac{\pi\alpha}{2} \text{sign}(t) |t|^\alpha \quad (2.43)$$

Once $\hat{\alpha}$ and $\hat{\gamma}$ have been obtained then estimates of δ and β can be calculated using Equation (2.43) to write another regression model: $y_{2,k} = \delta u_{2,k} + \beta \gamma^\alpha \tan \frac{\pi\alpha}{2} \text{sign}(u_{2,k}) |u_{2,k}| + e_{2,k}$ where $y_2 = \arctan \left(\frac{\Im[\Phi_w(t)]}{\Re[\Phi_w(t)]} \right)$, $u_{2,k}$ are appropriate real numbers and $e_{2,k}$ denotes the error term.

Performance Comparison Here, we propose to evaluate the different estimation methods based on two metrics: the normalized mean bias (NMB) and mean square error (MSE), which are defined as follows

$$\text{NMB}(P_r) = \frac{P_r - \overline{\hat{P}_r}}{P_r} \quad \text{and} \quad \text{MSE}(P_r) = E \left[\left(\hat{P}_r - P_r \right)^2 \right] \quad (2.44)$$

where $P_r \in \{\alpha, \beta, \gamma, \delta\}$, \hat{P}_r is the estimate of P_r , and $\overline{(\cdot)}$ is the mean value. The first metric is employed to measure the method's mean performance while the MSE measures the consistency. We generate a 1000 realizations of random stable variable for each set of parameters. The α -stable generation algorithm is explained in Appendix A. The different parameters are estimated for each realization, thereafter the NMB and MSE are calculated for each parameter. The simulations results shown in Figure 2.6 reveals that the quantile method is not efficient when $\alpha < 0.6$ (i.e.

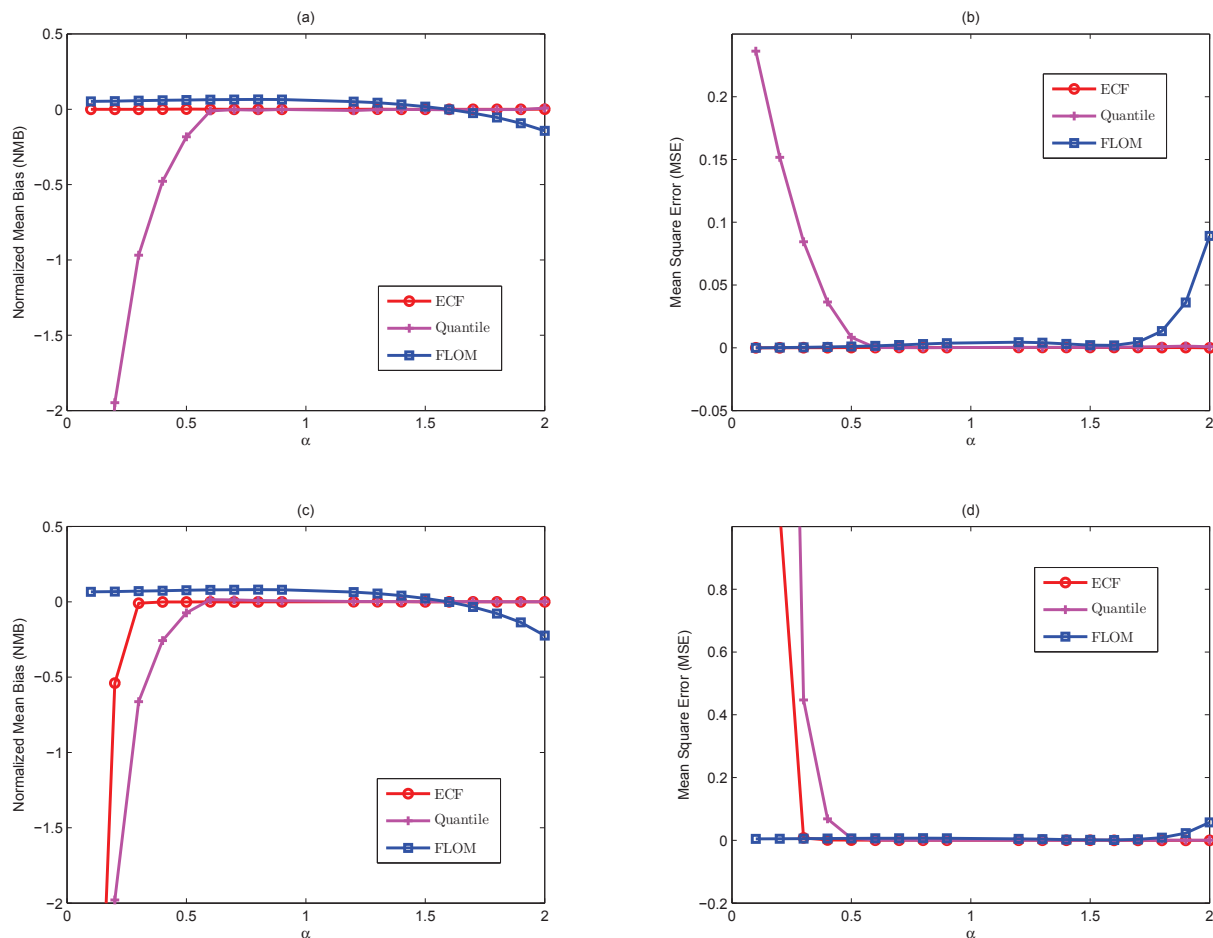


Figure 2.6: Performance comparison of different stable distribution parameters estimators for different values of α (a) the NMB of α estimators. (b) the MSE of α estimators. (c) the NMB of γ estimators. (d) the MSE of γ estimators.

the tails are very heavy). For $\alpha > 0.6$ (i.e. moderately-high impulsive noise), the FLOM has the lowest performance. The quantile method is a compromise between complexity and performance for the online applications. While the ECF method is the more consistent one among the three studied methods, it is more suitable for offline applications and it is adopted in our work.

2.4.3.3 Measured Data Fitting

The measured data is well centered around zero; i.e. its mean equals $-1.8 \times 10^{-4} \simeq 0$. Figure 2.7 shows the empirical PDF of the normalized measured data. The assumption of symmetric distribution can be easily visually justified. This fact can be confirmed by assuming stability of the impulsive noise process and estimating the skewness parameter. The β estimate equals $2.64 \times 10^{-4} \simeq 0$. The empirical distribution of the normalized measured data is compared with the three estimated models, namely, Middleton class A model, $S\alpha S$ model and Gaussian model. The distribution of the measured data and the three estimated models are shown in Figure 2.7. As seen from this Figure, both the class A model and the $S\alpha S$ model provide a better approximation to the measured data distribution as compared to the Gaussian model. Table 2.1

Table 2.1: The estimated parameters for each assumed model besides the KL divergence between the estimated PDF and the empirical PDF.

Assumed Model	Parameter	Estimated Value	KL Divergence
Gaussian	Mean	~ 0	0.1032
	Variance	1	
Class A	Overlap Index	0.891	0.0368
	Gaussian Factor	0.592	
$S\alpha S$	Location (δ)	$3.95 \times 10^{-4} \simeq 0$	0.0226
	Dispersion (γ)	0.419	
	Characteristic Exponent (α)	1.253	

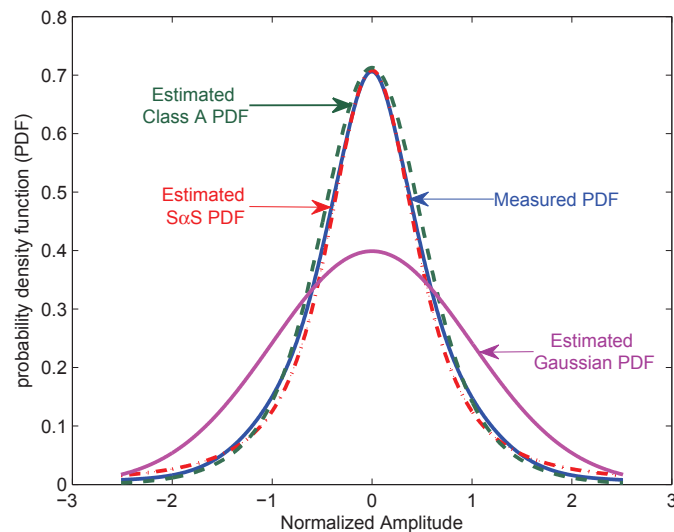


Figure 2.7: PDF of measured data

lists the estimated parameters and the corresponding KL divergence of the empirical PDF from the estimated distributions. The KL divergence values reveal that the measured data is modeled better by the $S\alpha S$ model followed by the Class A model. One value to focus on is the estimated α which equals 1.253.

2.5 Conclusions

Developing algorithms, to be employed in the CR device, suitable for railway context necessitates well modeling the special environment of this context. In this Chapter, we presented the characteristics of the mobile radio channels in time and frequency, mainly the Doppler effect related to the high mobility. The properties of the generalized exact Doppler spread model motivated us to adopt it to simulate the dynamic radio channel. The topology along the railways results in a spatial correlation at the multiple-antennas receiver. The correlation matrices of the Kronecker model are set up using an exponential correlation model. In addition, the received signal at the antennas on a moving train suffers of the EM noise interference. This implies that the traditional Gaussian noise model is not anymore valid in this context. The generalized central limit

theorem justifies employing the α -stable processes for modeling the impulsive noise. One of the contributions of our thesis works lies in the distribution fitting of the measured transient EM noise acting on GSM-R antenna. We found that the measured data is well modeled by the $S\alpha S$ distribution. Although it was very important to describe the constraints implied on the wireless communications in the railway sector, we will not consider all these constraints when developing the detection, estimation and sensing algorithms in Chapters 3 and 4. In Chapter 5, the problem of spectrum sensing will be studied when all these constraints are taken into consideration.

Chapter 3

Waveform Awareness for Cognitive Radios

Contents

3.1	Introduction	48
3.2	Modulation Scheme Recognition	48
3.2.1	Introduction	48
3.2.2	Preliminary Literature Review	49
3.2.3	Automatic Modulation Recognition Using Wavelet Transform	51
3.2.4	Automatic Modulation Recognition Using Higher Order Statistics	53
3.2.5	ANN Classifier	55
3.2.6	Cooperative Automatic Modulation Recognition	55
3.2.7	Case Study : Blind Digital Modulation Recognition for MIMO Systems	58
3.3	Modulation Technique Identification	69
3.3.1	Preliminary Literature Review	69
3.3.2	Case Study : Blind SIMO MC-DS-CDMA Identification	71
3.4	Conclusions	79

3.1 Introduction

With the rapid development of communications systems and the increasing demand of wireless services, the natural limitation of spectral resources necessitates the wireless systems to evolve towards more intelligent ones. Cognitive radio is the promising technique proposed by Mitola [47] to increase the utilization efficiency of spectrum resource. The key issue in CR is to be aware of its radio environment. Therefore, an essential task is to design reliable sensing methods which are able to detect the presence of signal in the target channel as well as to recognize different signals. CRs are expected to identify different wireless networks and have capability to communicate with them. Transmission parameters of communications system must be detected blindly if the system is not known to CR. That is, identifying some of the basic features of incoming signals does enhance the CR waveform awareness capability. Moreover, the CR should have the capability to blindly identify interference and try to mitigate its effects. Also, signal classification allows CR to select a suitable demodulation process at the receiver and to establish a communication link. Furthermore, identifying incoming signal parameters helps to conduct spectrum survey for radio monitoring systems. It allows to detect undesired and illegal transmissions.

Hence, waveform identification or waveform awareness is very beneficial to CR devices. Within this thesis, the transmission features identified by the CR device include: identification of a multi-carrier transmission, spectrum spreading detection, and recognition of the modulation type of the received signal. This Chapter introduces two important contributions of this thesis. The first one is a modulation recognition algorithm for spatially-correlated multiple-input multiple-output systems based on the higher order statistics. This research work is, to the best of our knowledge, among the first ones that study the modulation recognition problem for MIMO systems and the first that addresses the spatially-correlated case. Secondly, we introduce an algorithm for parameters identification of MC-DS-CDMA transmissions based on the fluctuations of the autocorrelation function. The identification performance of this algorithm is improved by exploiting the multiple-antennas at the receiver aboard the train. A performance comparison between this method and the one that uses directly the autocorrelation function is provided.

3.2 Modulation Scheme Recognition

3.2.1 Introduction

Automatic modulation recognition (AMR) has received international scientific attention for over three decades now. It can be considered as an intermediate step between signal interception and information recovery. Modulation recognition has its roots in military applications such as: communication intelligence (COMINT), electronic support measures (ESM), and electronic counter measures (ECM). Another group of applications that employs AMR can be found in the communications systems as spectrum monitoring, interference identification, universal demodulator. With the rapid growth of software defined radio systems, automatic digital modulation recognition (ADMR) has gained more attention than ever. As the adaptive receiver in SDR can communicate with different communications standards, the recognition of digital modulation

scheme of a signal is to be optimized and can act as front-end to SDR systems. Also recent and rapid developments in the CR technologies have given AMR more importance in civil applications, since the awareness of CR requires the recognition of the modulation scheme of desired signal.

Dozens of modulation recognizers which automatically determine incoming modulation properties have been proposed. Numerous approaches have tried to develop fast and accurate algorithms for producing acceptable results in real world applications. Some of the published algorithms are presented in this Chapter to provide a historical overview, and briefly describe the different approaches so far attempted.

The ultimate goal is to build a practical robust and lightweight classifier which must be capable of identifying almost all the different modulation schemes used in the telecommunications systems and standards (2G/3G and 4G). The type and order of modulation should be recognized at the same time and without a priori information of the received signal. The processing time must be reduced to ensure the real-time operating conditions. The different studies of AMR problem over the last decades had achieved a lot of advancement but we have never reached the ultimate classifier. Some algorithms need a priori information of the signal (e.g. carrier frequency, signal bandwidth, baud rate, offset timing, etc.), others need high value of SNR, some classifiers are limited to small number of modulation schemes, others can not be used in the real-time applications.

3.2.2 Preliminary Literature Review

Many AMR algorithms have been developed for single-input single-output (SISO) systems [48]. These algorithms are generally divided into two categories. The first category is based on decision-theoretic approach while the second on pattern recognition. The decision-theoretic approach is a probabilistic solution based on a priori knowledge of probability functions and multiple hypotheses testing problem, with each hypothesis being the modulation scheme of the received signal [48, 49]. The major drawback of this approach, besides its high complexity, is the difficulties of forming the right hypothesis as well as careful analyses that are required to set the correct threshold values. On the other hand, the pattern recognition approach is based on extracting some basic characteristics of the received signal called features [50–53]. The second approach is easier to implement and reaches a quasi-optimal performance if the proper features set is chosen. However, choosing the right feature set is still an issue.

The pattern recognition approach is generally divided into two subsystems: the features extraction subsystem and the classifier subsystem. The feature extraction subsystem is responsible of extracting prominent characteristics (the features) from the raw data. The recognition techniques, which have been employed to extract the signal features necessary for digital modulation recognition, include spectral based features set [50], higher order statistics [51], cyclostationarity signatures [52], and wavelets transforms [53]. The second subsystem is responsible of classifying the incoming signals based on the extracted features. It can be implemented in many ways, e.g. K-nearest neighbourhood classifier (KNN), probabilistic neural network (PNN), support vector machine (SVM) [48]. With their efficient performance in pattern recognition problems



Figure 3.1: Block diagram of the pattern recognition based methods

(e.g., modulation classification), many studies have proposed the application of artificial neural networks (ANNs) as classifiers [48, 50]. Figure 3.1 shows a general block diagram of a pattern recognition system. First the signal is pre-processed to determine various signal parameters such as carrier frequency, baud rate, carrier phase, SNR and timing offsets. Thereafter the features are extracted before pattern recognition.

In [54], a modulation recognizer which uses several key features obtained from the instantaneous amplitude, the instantaneous phase and the instantaneous frequency of the intercepted signal, is introduced for the 2-ASK, 4-ASK, 2-PSK, 4-PSK, 2-FSK, and 4-FSK digital modulation schemes. They proposed a single hidden layer ANN structure as a classifier. This network has a 4-node input layer, a 25 node hidden layer and a 7 node output layer. Nevertheless a degradation of performance at higher SNRs will appear when the ANN is trained on signals with lower SNR.

Hong and Ho studied the use of wavelet transform to distinguish QAM, PSK and FSK signals [55]. Their approach is to use wavelet transform to extract the transient characteristics in a digital modulation signal, and apply the distinct pattern in wavelet transform domain for simple identification. When SNR is greater than 5 dB, the percentage of correct recognition is about 97% with 50 observation symbols.

In [56], Swami and Sadler proposed a simple yet very low complexity method, based on elementary fourth-order cumulants. This method was applied in a hierarchical manner to classify various digital modulation schemes. Also classification thresholds were developed by deriving the expressions for the variance of the estimates of the cumulants. Furthermore, the statistics used by the classifier can be recursively updated. The robustness of this approach comes about not only from the resistance of HOS to additive colored Gaussian noise, but also from a natural robustness to constellation rotation and phase jitter.

The work proposed by Nandi and Azzouz [54] was extended in [50]. This study presented the use of resilient backpropagation (RPROP) as a training algorithm for multi-layer ANN recognizer, which improves the performance and epoch times by a large margin. On the other hand, additional modulation schemes (e.g. 16-QAM, V29, V32, and 64-QAM) were included, and an extra features set based on HOS of the signal is studied. Furthermore, Genetic algorithm (GA) based feature selection is used to select the best feature subset from the combined statistical and spectral features sets. RPROP ANN recognizer achieves about 99% recognition performance on most SNR values with only six features selected using GA.

Three digital modulation recognition algorithms had been investigated and compared in [57]. These algorithms are meant to identify digital modulations of type M-QAM, 8-PSK and GMSK, proposed by the ETSI-DPRS standard. The first algorithm is based on the observation of the

amplitude histograms, while the second algorithm is based on the wavelet transform and the third on the maximum-likelihood of the joint probability density of phase and amplitude. It was shown that the constellation amplitude histogram based algorithm has a good performance for inter-class modulation recognition, while the maximum-likelihood based classifier is more complex but performs well for the full-class modulation recognition. On another hand, the algorithm based on the wavelet transform has a high complexity but could perform better at lower SNR levels.

So far most of the work on modulation recognition did not address MIMO systems. For instance, Choqueuse *et. al* [58] proposed two likelihood based modulation classifiers for uncorrelated MIMO systems. The first one, called average likelihood ratio test (ALRT), is optimal in the Bayesian sense but requires a perfect channel state information (CSI). The second classifier, called hybrid likelihood ratio test (HLRT), approximates the ALRT by replacing the channel matrix with its estimate. The channel is estimated in two steps by using an independent component analysis and a phase correction algorithm respectively. Simulations showed that the two classifiers perform well, for example, perfectly recognizing 2-PSK, 4-PSK, 16-PSK and 16-QAM modulations at a SNR of 5 dB.

The ideal AMR algorithm is suitable for real-time applications, requires no prior information of the incoming signal, performs well in low SNR regime, through any channel model, and for large set of modulation schemes. Even many studies had been proposed through the last decades, the optimal AMR algorithm never achieved. Most of these studies assume an AWGN channels. Some algorithms require some prior information, or demand high SNR to perform well, while others are too complex to be employed in online applications such as modulation recognition for CR. Here, we will try to satisfy some of the aspects of ideal algorithm. After presenting, our work on modulation recognition based on wavelet transform [53], we propose a low-complexity blind (i.e. requires no prior information) AMR algorithm for MIMO fading channels based on HOS. The problem of modulation recognition for MIMO systems is rarely studied. Also, the proposed method performs well for an acceptable SNR range and considers a large modulation pool.

3.2.3 Automatic Modulation Recognition Using Wavelet Transform

In [53], we have employed the properties of the continuous wavelet transform (CWT) to extract the necessary features for modulation recognition. The main reason for our choice is due to the capability of this transform to locate, in time and frequency, the instantaneous characteristics of a signal. In the same manner as Fourier transform can be defined as being a projection on the basis of complex exponentials, the wavelet transform is introduced as projection of the signal on the basis of scaled and time-shifted versions of the original wavelet (so-called mother wavelet) in order to study its local characteristics. The importance of wavelet analysis is its scale-time view of a signal which is different from the time-frequency view and leads to the multi-resolution analysis (MRA).

The continuous wavelet transform of a received signal $x(t)$ is defined as:

$$CWT(a, \tau) = \int_{-\infty}^{\infty} x(t)\Psi_{a,\tau}^*(t)dt \quad (3.1)$$

where $a > 0$ is the scale variable, $\tau \in R$ is the translation variable, and $(\cdot)^*$ denotes complex conjugate. This defines the so-called *CWT*, where $CWT(a, \tau)$ define the wavelet transform coefficients. The Haar wavelet is chosen as the mother wavelet. The main purpose of the mother wavelet is to provide a source function to generate $\Psi_{a,\tau}(t)$, which are simply the translated and scaled versions of the mother wavelet, known as baby wavelets, as follows

$$\Psi_{a,\tau}(t) = \frac{1}{\sqrt{a}} \Psi\left(\frac{t-\tau}{a}\right) \quad (3.2)$$

The signal $x(t)$ can be presented as

$$x(t) = \tilde{x}(t)e^{j(2\pi f_c t + \theta_c)} \quad (3.3)$$

where f_c is the carrier frequency, θ_c is the carrier initial phase, and $\tilde{x}(t)$ is the baseband complex envelope of the signal $x(t)$, defined by

$$\tilde{x}(t) = \sqrt{E_x} \sum_{i=1}^N C_i e^{j(2\pi f_i t + \varphi_i)} p_T(t - iT_{sym}) \quad (3.4)$$

with N being the number of observed symbols, E_x is the average transmitted energy, and $p_T(t)$ is the pulse shaping function of duration T_{sym} . The i^{th} symbol (that belongs to the modulation constellation) is characterized by the complex amplitude $C_i = A_i + jB_i$, the frequency deviation f_i and the phase φ_i .

By extending the work of Hong and Ho [55], the magnitude of continuous wavelet transform is given by:

$$|CWT(a, \tau)| = \sum_{i=1}^N \frac{4|C_i|\sqrt{E_x}}{2\pi\sqrt{a}(f_c + f_i)} \sin^2\left[2\pi(f_c + f_i)\frac{aT_{sym}}{4}\right] p_T(\tau - iT_{sym}) \quad (3.5)$$

In what follows, the continuous wavelet transform of the normalized signal will be taken into consideration. The amplitude of the normalized signal is constant. From Equation (3.5), it is clear that the signal normalization will only affect the wavelet transform of non-constant envelope modulations (i.e., ASK and QAM), and will not affect wavelet transform of constant envelope ones (i.e., FSK and PSK). In the following, we consider the magnitude of the wavelet transforms for different modulation schemes.

The complex envelope of QAM signal is defined by $C_i = A_i + jB_i$ and $f_i = \varphi_i = 0$. It is clear from (3.5) that for a certain scale value, $|CWT|$ is a multi-step function. Considering the normalized QAM signal, the $|CWT|$ is constant since the signal loses its amplitude information. Let us consider the complex envelope of ASK signal (i.e. $C_i = A_i$ and $f_i = \varphi_i = 0$), it is clear from (3.5) that for a certain scale, $|CWT|$ of ASK signal is a multi-step function since $|C_i|$ is a variable. The magnitude of CWT of the normalized ASK signals is constant. When considering the complex envelope of PSK signals (i.e. $C_i = A$ and $f_i = 0$), $|CWT|$ is almost a constant function for a certain scale value. Given its normalized signal, $|CWT|$ is also constant. The complex envelope of FSK signal is defined by $C_i = A$ and $\varphi_i = 0$. The magnitude of CWT of FSK signal is a multi-step function with f_i being a variable. In the same manner, the $|CWT|$ of

the normalized FSK signal is also a multi-step function.

Previous discussions show that:

- ❖ The $|CWT|$ of PSK signals is constant while $|CWT|$ of ASK, FSK, and QAM signals is a multi-step function.
- ❖ The $|CWT|$ of the normalized ASK, PSK and QAM signals is constant while the $|CWT|$ of normalized FSK signals is a multi-step function.
- ❖ The statistical properties including the mean, the variance and higher order moments of wavelet transforms are different from a modulation scheme to another. These statistical properties also differ depending on the order of modulation, since the frequency, amplitude and other signal properties may change depending on the modulation order.

According to the above observations, we propose a feature extraction procedure as follows. The CWT can extract features from a digitally modulated signal. These features are collected by examining the statistical properties of wavelet transforms of both the signal and its normalized version. Our proposed classifier is a multi-layer feed-forward neural network. More details on the classifier are found in a following subsection.

The proposed CWT based recognizer is studied over AWGN channels. This recognizer have two main drawbacks: its high complexity and the rapid performance degradation in multi-path channels. One among the advantages of this method lies in the fact that it treats the signal in the RF or IF stages; i.e. it avoids the errors resulting from the carrier phase and frequency offsets.

For more details on CWT based modulation recognition refer to our published work in [53]. In what follows, we will concentrate on HOS based recognizers. The robustness of such recognizer in the presence of multi-path channel, and carrier phase and frequency offsets makes it a powerful tool.

3.2.4 Automatic Modulation Recognition Using Higher Order Statistics

One of the important aspects of modulation recognition is the selection of the proper identification features. Previous works have shown that higher order cumulants (HOC) and higher order moments (HOM) of the received signal are among the best candidates for signal recognition in SISO systems [51, 56]. Higher order moments of a signal x are defined by

$$M_{km}(x) = E[x^{k-m}(x^*)^m] \quad (3.6)$$

where k is the moment order. The cumulant of order k of the zero-mean signal x is defined by

$$C_{km}(x) = Cum[\underbrace{x, \dots, x}_{(k-m) \text{ times}}, \underbrace{x^*, \dots, x^*}_{m \text{ times}}]. \quad (3.7)$$

Also, the relation between moments and cumulants can be expressed as

$$Cum[x_1, \dots, x_n] = \sum_{\Phi} (c-1)! (-1)^{c-1} \prod_{v \in \Phi} E\left(\prod_{i \in v} x_i\right) \quad (3.8)$$

where Φ runs through the list of all partitions of $\{1, \dots, n\}$, v runs through the list of all blocks of the partition Φ , and c is the number of elements in the partition Φ . For instance, the fourth-order cumulant of zero-mean signals x, y, z and w is given by

$$Cum[x, y, z, w] = E(xyzw) - E(xy)E(zw) - E(xz)E(yw) - E(xw)E(yz). \quad (3.9)$$

Based on (3.8), moments estimation leads to estimate the cumulants. That is given a signal x with N samples, the moments are estimated as

$$\hat{M}_{km}(x) = \frac{1}{N} \sum_{i=1}^N x^{k-m}(i) x^{*m}(i). \quad (3.10)$$

We assume, without loss of generality, that the signal x is normalized to have a unity energy, i.e. $C_{21} = 1$. This will remove any scale problems in the estimators. Practically the self-normalized HOS are calculated as

$$\tilde{M}_{km}(x) = \hat{M}_{km}(x) / \hat{M}_{21}^{k/2}(x), \quad \tilde{C}_{km}(x) = \hat{C}_{km}(x) / \hat{C}_{21}^{k/2}(x). \quad (3.11)$$

Note that the complexity of (3.10) is of order N where estimating a moment of order k requires only about N complex additions and $k \times N$ complex multiplications. Based on (3.8), cumulant calculation is of order N . Of course, the computational cost of the features calculation is of the same order. Then, the features extraction process has a very low complexity $\mathcal{O}(N)$.

The hierarchical modulation recognition for SISO systems using HOS (up to four) was employed in [56]. It was shown that the probability of correct modulation recognition is a function of SNR, number of received symbols N and the considered modulation pool. The recognition performance depends on the accuracy of HOS estimation. The authors in [56] showed that adding Gaussian noise to the modulated signal will not affect the mean of the HOS estimators but will affect the variance of these estimators which depends on the SNR and N . It is clear that increasing N will decrease the variance and improves the overall performance. Anyway, simulations show that about 500 symbols are sufficient to produce good estimates of HOS. The probability of correct recognition was higher than 99% when the SNR is not lower than 5dB and 10dB when considering, respectively, four and eight modulation pools. Theoretical values of some HOS are given in Table B.1 (see Appendix B.1) to show how they can discriminate the different modulation schemes of interest. These theoretical values are calculated by averaging HOS for different digital modulation constellations under the constraints of unit variance symbols and noise free case. The robustness of this approach comes about not only from the resistance of HOS to additive impulsive non-Gaussian, but also from a natural robustness is in the presence of carrier phase and frequency offsets.

Here, the employed set of features consists of a combination of HOM and HOC up to order six

since simulations show that the statistics of order higher than six will not improve the probability of correct recognition.

3.2.5 ANN Classifier

After extracting the proper features, the modulation recognition problem can be considered as a pattern recognition problem. Knowing that ANN is one of the best solutions for pattern recognition problems, many researchers have focused on ANNs to develop high performance modulation classifiers [48, 50]. In this thesis, the proposed classifier is a multilayer feed-forward ANN. The extracted features are the inputs of this trained ANN.

The neural network structure including the number of hidden layers, the number of nodes in each layer and the transfer function of each node has been chosen through intensive simulations. This structure is directly related to network training speed and recognition precision. Speeding the learning process of the network and improving the recognition accuracy can be achieved by normalizing the features set (fifteen extracted ones) and selecting the optimal subset for the discrimination process. Here, a feature subset selection based on the principal component analysis (PCA) is applied to select the best subset of the combined HOM and HOC features set.

First, the extracted set of features are normalized before subset selection to ensure that they are of zero mean and unit variance. Then, the PCA technique constructs a low-dimensional representation of the data (normalized features) that describes as much of the variance in that data as possible. Here, only six orthogonal components (out of fifteen) are selected for both ANN training and testing. After features subset selection, the training process is triggered. The initiated ANN is trained using the RPROP introduced in [59]. Beside the fast convergence, one of the main advantages of RPROP lies in the fact that no choice of parameters and initial values is needed at all to obtain optimal or at least nearly optimal convergence times [59]. Also, RPROP is known by its high performance on pattern recognition problems. After training, a test phase is launched, and the classifier is evaluated through the probability of correct recognition.

Since the outputs of a layer in ANN are considered as linear combinations among the inputs of this layer, then the computational cost of the classifier is related to the number of nodes at each layer. Considering the static and predefined structure of ANN, and the small number of nodes at each layer, the required number of operations to obtain the classifier output is fixed and inexpensive.

3.2.6 Cooperative Automatic Modulation Recognition

In a CR network, an AMR algorithm could achieve higher recognition reliability by introducing the concept of cooperation. It is possible for several users/receivers to cooperate by sending all their data to a fusion center where they are jointly processed to make a final decision. In our context (receiver employed on-board train), this could be applied in several scenarios: i) multiple-antenna receiver, ii) several receivers distributed all around the train, and iii) the passengers aboard train could be, in the future, considered as possible secondary users. The different

antennas, receivers, and secondary users cooperating to improve the recognition performance are called sensors.

The same transmitted signal is observed differently at each sensor due to the effect of propagation distance, fading, and shadowing conditions. Cooperation overcomes the erroneous decision at a single sensor caused by badly received signal. There are two approaches for cooperation: data fusion and decision fusion. In the first approach the received signal on different sensors (antenna/receivers), some of their prominent characteristics (features), or some measurements that address the degree that the signal is close to any modulation scheme, are sent to the fusion center. While the decision fusion means that only local decisions made at each sensor are sent to the fusion center. We will assume that the transmission between each sensor and the fusion center is error-free.

To better clarify how could the cooperation be applied to improve recognition reliability, we present, in what follows, two fusion rules. The first one is the average Bayes fusion rule based on estimating the post-probabilities that a certain sensor decides a certain modulation scheme based on the observed signal. The recognized modulation scheme at the fusion center is the one which is, in average, more probable. The second fusion rule is the voting rule which is a decision fusion approach. This rule elects the modulation scheme which is more voted (decided) at different sensors. This rule has several derivatives including the majority rule and the weighted voting rule. These fusion rules can be applied to conduct cooperation regardless of the employed recognition features and/or classifier.

Let the considered modulation pool be $\Theta = \{\theta_1, \theta_2, \dots, \theta_{M_c}\}$, and $c_f, 1 \leq c_f \leq M_c + 1$ is the index of the recognized modulation scheme. Final decision $M_c + 1$ means the trial is rejected. The output of the ANN classifier at sensor k is the $1 \times M_c$ vector $\hat{C}_k, 1 \leq k \leq N_d$. The distance between this output \hat{C}_k and each modulation scheme is measured as

$$d_{k,i} = \left\| \hat{C}_k - C_i \right\| \text{ for } 1 \leq k \leq N_d, 1 \leq i \leq M_c \quad (3.12)$$

where C_i is defined as $C_i(l) = \begin{cases} 1, & l = i \\ 0, & 1 \leq l \leq M_c, l \neq i \end{cases}$.

In the following we present the two fusion rules, i.e. the average Bayes rule and the voting rule.

3.2.6.1 Averaged Bayes Fusion Rule

The Bayes classifier is based on a set of post-probabilities

$$P_k(\theta_j | x), 1 \leq k \leq N_d, 1 \leq j \leq M_c, \quad (3.13)$$

which is the probability that the sensor k recognizes the modulation scheme as θ_j when the received signal x is observed, where N_d is the number of sensors. Theoretically, the N_d recognizers are identical and these post-probabilities are independent of k . In practice, these values are not known and their estimates are employed. This will lead to that dependence of the index k . Let us assume that all modulation schemes are transmitted with the same probability, the fusion

center applies the following simple approach

$$c_f = \max_{j=1, \dots, M_c} \frac{1}{N_d} \sum_{k=1}^{N_d} P_k(\theta_j | x), \quad (3.14)$$

that is, the final average Bayes decision is based on estimating the post-probabilities $P_k(\theta_j | x)$. We estimate these probabilities by turning the classifier at each sensor to a distance classifier, either using the extracted features, or the ANN outputs. Here, the apparent post-probabilities are calculated, based on the distances introduced in Equation (3.12), as

$$P_k(j) = \frac{\frac{1}{d_{k,j}}}{\sum_{i=1}^{M_c} \frac{1}{d_{k,i}}} \quad (3.15)$$

3.2.6.2 The Voting Fusion Rule

The voting rule is a decision fusion approach. To decide locally at sensor k the following rule is applied

$$c_k = \min_{i=1, \dots, M_c} d_{k,i} \quad (3.16)$$

Let us define a binary characteristic function as

$$T_k(i) = \begin{cases} 1, & \text{if } c_k = i \\ 0, & \text{otherwise} \end{cases} \quad \text{for } 1 \leq k \leq N_d, 1 \leq i \leq M_c \quad (3.17)$$

The characteristic function of the fusion classifier is expressed as $T_F(i) = \sum_{k=1}^{N_d} T_k(i)$, this reflects how many times θ_i was recognized. The final decision is made by applying the following rule

$$c_f = \begin{cases} j, & \text{if } T_F(j) = \max_{i=1, \dots, M_c} T_F(i) \geq \eta \cdot N_d + T_2 \\ M_c + 1, & \text{otherwise} \end{cases} \quad (3.18)$$

where $0 < \eta \leq 1$.

For $T_2 = 0$, there are these special cases: i) K -out-of- N_d decision fusion rule ($\eta = \frac{K}{N_d}$), i.e. a certain modulation scheme is recognized when it is decided on K classifier among the N_d classifiers, ii) logical OR (LO) ($\eta = \frac{1}{N_d}$), iii) logical AND (LA) ($\eta = 1$), and iv) the majority ($\eta = 0.5 + \epsilon$, and $\epsilon > 0$ is arbitrary small). When decisions do not fit the fusion rule, the final decision is *rejected*, e.g. when $N_d = 3$, the majority rule is applied, and there are three different decisions, the trial is rejected.

Let $T_2 = \max_{i=1, \dots, M_c \& i \neq j} T_F(i)$ which represents the secondly most decided modulation scheme or the implicit objections to the decision j . That is, taking a reliable final decision demands to be largely chosen by the local sensors.

As mentioned above, the performance of HOS based recognizer at each sensor over AWGN channel is a function of SNR for a fixed observation duration when considering the same modulation pool. The knowledge of SNR at each sensor is beneficial to improve the overall performance.

This allows us to label sensor k with a certain degree of confidence w_k . Then, the characteristic function of the fusion classifier is redefined as

$$T_F(i) = \sum_{k=1}^{N_d} w_k \cdot T_k(i) \quad (3.19)$$

where $\sum_{k=1}^{N_d} w_k = 1$. The same rule in Equation (3.18) is applied for the final decision. Then, sensor k send the decision c_k besides its SNR_k to the fusion center. The confidence degrees can be simply defined as $w_k = \frac{\text{SNR}_k}{\sum_{i=1}^{N_d} \text{SNR}_i}$, $1 \leq k \leq N_d$. But this does not really reflect the real performance of each classifier in respect of SNR. Let $P_{d,k}(\text{SNR})$ be the overall probability of correct recognition at sensor k for a certain SNR value. Assume that $P_{d,k}$ is known at the fusion center and indexed by SNRs with a proper resolution. Then, we have

$$w_k = \frac{P_{d,k}(\text{SNR}_k)}{\sum_{i=1}^{N_d} P_{d,i}(\text{SNR}_i)} \quad (3.20)$$

In the above subsections, the following techniques were presented: how to employ HOS for modulation recognition, what is the structure of the ANN used to classify the different modulation schemes, and what fusion rules are applied to conduct cooperation among the receivers/antennas. In what follows, these techniques are used to study the case of modulation recognition for MIMO systems, i.e. the used features set is the HOS, the classifier is the above presented ANN, and the fusion centre is based on the averaged Bayes fusion rule.

3.2.7 Case Study : Blind Digital Modulation Recognition for MIMO Systems

Nowadays, MIMO technology is considered one of the essential technologies for developing the wireless systems. One essential step in the MIMO signal interception process is to blindly recognize the modulation scheme of these signals. Contrary to [58], we propose a pattern recognition approach to solve this recognition problem. Also, to the best of our knowledge, no work has yet considered the problem of modulation recognition for spatially-correlated MIMO channels. Moreover, we examine the effect of channel estimation error on our proposed modulation recognition algorithm. In our approach, the features extraction subsystem is based on the HOC and the HOM of the processed received signal.

3.2.7.1 MIMO Signal Model

A MIMO system with P transmit antennas and M receive antennas is considered ($M \geq P$). Under the assumption of a frequency flat and time invariant MIMO channel, the baseband received symbol vector at the instant k is described as

$$\mathbf{x}(k) = \mathbf{H}\mathbf{s}(k) + \mathbf{w}(k) \quad (3.21)$$

where $\mathbf{x}(k) = [x_1(k), \dots, x_M(k)]^T$ is the $M \times 1$ received signal vector without any time oversampling and optimum symbol timing, and with perfect carrier frequency and phase estimation,

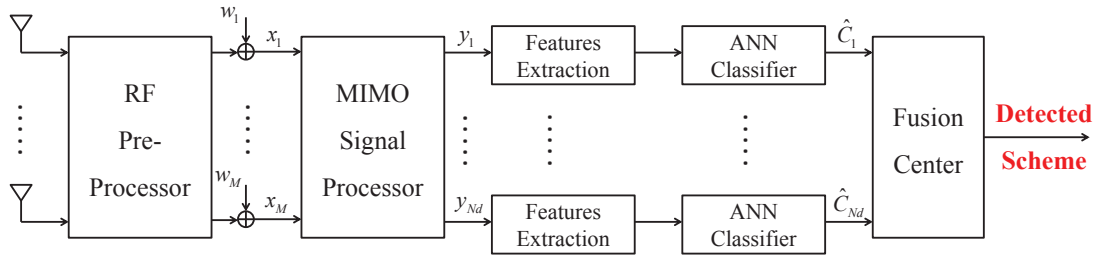


Figure 3.2: A block diagram of the proposed HOS based modulation recognition algorithm for MIMO systems.

$\mathbf{s}(k) = [s_1(k), \dots, s_P(k)]^T$ is the $P \times 1$ vector representing the transmitted source signals, and $\mathbf{w}(k) = [w_1(k), \dots, w_M(k)]^T$ is the $M \times 1$ vector corresponding to the additive zero-mean white circularly complex Gaussian noise with variance σ_w^2 ; i.e. $\mathbf{w}(k) \sim \mathcal{CN}(0, \sigma_w^2 \mathbf{I}_M)$, where \mathbf{I}_M is the identity matrix of size M . \mathbf{H} corresponds to the $M \times P$ matrix of the MIMO channel. These source symbols \mathbf{s} are i.i.d and mutually independent. The symbols are assumed to belong to the same linear modulation scheme. We will assume, without loss of generality, that the source constellations are normalized to have zero-mean and unit energy.

3.2.7.2 Channel Mixing Effect

Each stream of the received MIMO signal vector \mathbf{x} is given by: $x_j = \sum_{i=1}^P h_{ij} s_i + w_j$, where h_{ij} is the complex channel impulse response between the i^{th} transmit antenna and the j^{th} receive antenna. The noise-free case is considered to separately study how the MIMO channel affects the HOS based recognition. Since the transmitted symbols are i.i.d and mutually independent then the self-normalized HOS are given by $\tilde{M}_{km}(x_j) = \lambda_{km}(j) \tilde{M}_{km}(s^c)$ and $\tilde{C}_{km}(x_j) = \lambda_{km}(j) \tilde{C}_{km}(s^c)$, where

$$\lambda_{km}(j) = \frac{\sum_{i=1}^P h_{ij}^{k-m} h_{ij}^{*m}}{(\sum_{i=1}^P |h_{ij}|^2)^{k/2}}, \quad (3.22)$$

and s^c is an arbitrary stream of the P source ones. Then, the HOS of digitally modulated signals for the ideal noise-free case (Table B.1) are multiplied by a random factor, $\lambda_{km}(j)$, for the j^{th} equalized stream in the MIMO system. It is clear that $|\lambda_{km}(j)| < 1$, i.e. the channel mixing drives the received signals to be more Gaussian. Recognizing the modulation scheme directly for each one of the M received streams requires no CSI knowledge. However, the effect of channel mixing corrupts the HOS and hence the recognition process which in turn degrades the overall correct recognition percentage, requiring a higher SNR.

3.2.7.3 Proposed Modulation Recognition Algorithm

The block diagram of the proposed modulation recognition algorithms is shown in Figure 3.2. After the RF pre-processing, the M received MIMO streams mixed by the MIMO channel are the input of MIMO signal processor block which outputs N_d streams. The output of the MIMO signal processor block is the signal vector $\mathbf{y}(k) = [y_1(k), \dots, y_{N_d}(k)]^T$, where $N_d = (P \text{ or } M)$ depending on the considered approach. One approach is to identify the modulation directly from the received

symbols. This approach is called direct AMR (AMR-D). In this case $N_d = P$ and $\mathbf{y}(k) = \mathbf{x}(k)$. The another one is to equalize the received streams before the recognition. If a perfect CSI knowledge at the receiver side is assumed, the proposed algorithm is considered as semi-blind. Conversely, this algorithm could be considered blind when the channel is estimated. In this case $N_d = M$ and $\mathbf{y}(k) = \hat{\mathbf{s}}(k)$ where $\hat{\mathbf{s}}(k)$ is the estimated transmitted symbols vector. The features are separately extracted for each one of the N_d output streams of the MIMO signal processor. An ANN based classifier is employed to output N_d vectors. These vectors are combined for a final decision.

As seen above, the performance results of HOS based modulation recognition, for SISO systems, were given. Then the MIMO channel mixing effect was studied to show that it does degrade the recognition performance. Two equalization algorithms are used, namely, the zero-forcing (ZF) and the simplified constant modulus (SCMA) algorithms, to estimate the source streams. In what follows, we present a performance analysis of our work, i.e. the performance of modulation recognition for MIMO systems, when employing ZF or SCMA to equalize the MIMO channel, is analyzed.

3.2.7.4 AMR for MIMO Systems Using Zero-Forcing

In the following, we employ the well-known ZF equalizer, this algorithm is denoted AMR-ZF. We study the performance of the AMR-ZF algorithm when employed with or without perfect CSI. Thereafter, the effect of spatial correlation on recognition performance is analyzed.

Zero-Forcing Equalizer This technique consists of applying an equalizing matrix \mathbf{B} on the received vector. This matrix \mathbf{B} is defined by $\mathbf{B} = \mathbf{H}^\dagger = (\mathbf{H}^H \mathbf{H})^{-1} \mathbf{H}^H$ where $(\cdot)^\dagger$ denotes the pseudo inverse operation. The transmitted symbols are estimated by

$$\hat{\mathbf{s}}(k) = \mathbf{B}\mathbf{x}(k) \stackrel{\text{def}}{=} \text{ZF}(\mathbf{x}) = \mathbf{s}(k) + (\mathbf{H}^H \mathbf{H})^{-1} \mathbf{H}^H \mathbf{w}(k). \quad (3.23)$$

Then the estimated vector $\hat{\mathbf{s}}(k) = [\hat{s}_1(k), \dots, \hat{s}_P(k)]^T$ is used for features extraction. Here we assume perfect CSI at the receiver side (semi-blind classifier). If it is not the case, channel estimation has to be performed and the modulation is blindly recognized. First, we are interested in investigating the impact of channel estimation error on the modulation recognition. Hence, we model the estimated channel as

$$\hat{\mathbf{H}} = \mathbf{H} + \sigma_e \mathbf{\Omega} \quad (3.24)$$

where the entries of $\mathbf{\Omega}$ are i.i.d with zero-mean circularly symmetric complex Gaussian variables with unity variance and σ_e^2 represents the variance of the channel estimate error (i.e. how much the channel estimation is erroneous).

Zero-Forcing Performance $\text{SNR} = 10 \log_{10}(\frac{\sigma_s^2}{\sigma_w^2})$ where σ_s^2 is the average transmitted power.

The ZF equalizer estimates the P transmitted streams as given in (3.23). The post-processing

SNR of the n^{th} stream for the ZF equalizer is given by [60]

$$\eta_n = \frac{\eta_0}{[(\mathbf{H}^H \mathbf{H})^{-1}]_{n,n}} = \eta_0 \kappa_n, \quad 1 \leq n \leq P, \quad (3.25)$$

where $\eta_0 = \frac{\sigma_s^2}{\sigma_w^2}$ is the average normalised SNR at each receive antenna and σ_s^2 is the average transmitted power. Also, κ_n is a weighted chi-square distributed random variable with $K = 2(M - P + 1)$ degrees of freedom when considering uncorrelated Rayleigh fading channel. Since the distribution of κ_n is independent of the subscript n , we denote the effective post-processing SNR by η . It was shown above that the recognition performance for each detected stream is an increasing function of the effective SNR. The effect of the ZF equalizer on the overall performance is represented by the statistical properties of η which is the actual SNR at the input of each one among the P classifier branches. The cumulative distribution function (CDF), $F_K(x)$, of $\eta \sim \mathcal{X}^2(K)$ is a decreasing function of K , for any fixed $x \geq 0$; i.e. $P(\eta > x)$ increases when K increases. The overall performance depends on K and improves when $\Delta = M - P$ increases. Then, the performance for single-input multiple-output (SIMO) system is always better than that for MIMO systems having the same receiving antennas number.

Spatial Correlation Effect Based on the Kronecker correlation model presented in (2.28) and the fact that $\mathbf{H}_w \sim \mathcal{CN}(\mathbf{0}_{M \times P}, \mathbf{I}_M \otimes \mathbf{I}_P)$, we conclude that $\mathbf{H} \sim \mathcal{CN}(\mathbf{0}_{M \times P}, \mathbf{R}_r \otimes \mathbf{R}_t)$ where $\mathbf{0}_N$ is the zero matrix of order N . We will consider the presence of only transmit correlation. Since \mathbf{H} is complex normally distributed matrix, then $\mathbf{Z} = \mathbf{H}^H \mathbf{H}$ is complex Wishart matrix, i.e. $\mathbf{Z} \sim \mathbf{W}_P(M, 2\mathbf{R}_t)$. Then, the post-processing SNR of the n^{th} ZF equalized stream is a weighted Chi-squared variable distributed as [60]

$$f(\eta_n) = \frac{\exp(-\frac{\eta_n}{\eta_{0,n}})}{\eta_{0,n} \Gamma(M - P - 1)} \left(\frac{\eta_n}{\eta_{0,n}} \right)^{(M-P)}, \quad 1 \leq n \leq P, \quad (3.26)$$

where $\Gamma(\cdot)$ denotes the Gamma function and $\eta_{0,n} = \frac{\eta_0}{\lambda_{n,c}}$, i.e. $\lambda_{n,c}$ is the effective SNR degradation due to transmit correlation and it is equal to $[\mathbf{R}_t^{-1}]_{n,n}$. The matrix inversion is given by $\lambda_{n,c} = [\mathbf{R}_t^{-1}]_{n,n} = \frac{\det[\mathbf{R}_t^{n,n}]}{\det[\mathbf{R}_t]}$, where $\det(\cdot)$ denotes the determinant of a matrix and $\det[\mathbf{R}_t^{n,n}]$ is the minor of the matrix \mathbf{R}_t . It is easy to show that

$$\lambda_{n,c} = \begin{cases} 1/(1 - |\rho_t|^2), & n = 1, P \\ (1 + |\rho_t|^2)/(1 - |\rho_t|^2), & n = 2, \dots, P - 1 \end{cases} \quad (3.27)$$

It is clear that when the channel is highly correlated ($|\rho_t| \rightarrow 1$), the effective SNR degradation due to correlation is more important ($\lambda_{n,c} \rightarrow \infty$). We can see that the SNR degradation of the first and last received streams is less than the remaining $(P - 2)$ streams. The fact that the performance improves when Δ increases is also valid in the case of spatially-correlated MIMO channels as it is clear in (3.26).

Channel Estimation Error Effect Here, we are interested in investigating the impact of channel estimation error on the modulation recognition rather than the estimation process. An

erroneous channel estimation is modeled in (3.24). Hence, the ZF equalizer output is given by

$$\hat{\mathbf{s}} = \hat{\mathbf{B}} (\mathbf{H}\mathbf{s} + \mathbf{w}) \quad (3.28)$$

where $\hat{\mathbf{B}} = \hat{\mathbf{H}}^\dagger = (\mathbf{H} + \sigma_e \boldsymbol{\Omega})^\dagger$. The estimated signal can be rewritten as $\hat{\mathbf{s}} = \mathbf{s} + \hat{\mathbf{w}}$ where $\hat{\mathbf{w}}$ is given by

$$\hat{\mathbf{w}} = \mathbf{H}^\dagger \mathbf{w} - \sigma_e \mathbf{H}^\dagger \boldsymbol{\Omega} \mathbf{s} - \sigma_e \mathbf{H}^\dagger \boldsymbol{\Omega} \mathbf{H}^\dagger \mathbf{w}. \quad (3.29)$$

It was shown in [61] that the post-processing SNR for each estimated stream, when considering uncorrelated Rayleigh channel, is approximated by

$$\eta_n = \frac{\eta_0}{(1 + \sigma_e^2 P \eta_0) [(\mathbf{H}^H \mathbf{H})^{-1}]_{n,n}} = \frac{\eta_0 \kappa_n}{\lambda_e}, 1 \leq n \leq P, \quad (3.30)$$

where $\lambda_e = 1 + \sigma_e^2 P \eta_0$ is the SNR degradation owing to the imperfect CSI. This result is also valid for spatially-correlated MIMO channels when the exponential correlation model is employed as proven in Appendix B.2.

It is clear that the performance does not only depend on Δ but is also a function of P and σ_e . The reason for the dependence on P is that the inter-stream interference cannot be cancelled perfectly in the presence of channel estimation error. For large SNR ($\eta_0 \rightarrow \infty$), the percentage $\eta_0/\lambda_e \rightarrow 1/\sigma_e^2 P$, which leads to an upper bound for the correct recognition percentage contrary to the perfect CSI case.

3.2.7.5 AMR for MIMO Systems Using Simplified Constant Modulus Algorithm

The performance analysis of AMR-ZF shows that it suffers from a correct recognition upperbound when it is employed blindly. The performance is improved by blindly separating the MIMO source symbols using SCMA, before identifying the modulation. That is the transmitted symbols are estimated instead of considering erroneous channel estimation. This blind algorithm is called AMR-SCMA.

Simplified Constant Modulus Algorithm The SCMA is used to blindly recover the transmitted symbols [62]. The SCMA objective is to find an $M \times P$ matrix \mathbf{B} such as

$$\mathbf{z}(k) = \mathbf{B}^H \mathbf{x}(k) \stackrel{\text{def}}{=} \text{SCMA}(\mathbf{x}) = \mathbf{B}^H \mathbf{H}\mathbf{s}(k) + \hat{\mathbf{w}}(k). \quad (3.31)$$

The purpose is to find \mathbf{B} such that $\mathbf{z}(k) = \hat{\mathbf{s}}(k)$, but the transmitted symbols \mathbf{s} are usually determined up to a permutation and a scalar multiple, i.e. $\mathbf{B}^H \mathbf{H} = \mathbf{P}\boldsymbol{\Lambda}$ where $\boldsymbol{\Lambda}$ is a diagonal matrix and \mathbf{P} is a permutation matrix, that introduces the arbitrary phase and permutation. In fact, the SCMA simplifies the constant modulus criterion by employing a single dimension, e.g. the real part of the signal. The SCMA attempts to minimize the following cost function

$$\begin{cases} J_{\text{SCMA}}(\mathbf{B}) = \sum_{i=1}^P E \left[(\Re(z_i(k)))^2 - R \right]^2 \\ \text{Subject to : } \mathbf{B}^H \mathbf{B} = \mathbf{I}_P \end{cases} \quad (3.32)$$

where $R = \frac{E[\Re(s(k))^4]}{E[\Re(s(k))^2]^2}$ is the dispersion constant and $z_i(k)$ is the i^{th} output of the separation filter. This criterion leads to a complexity reduction and ensures a non-arbitrary constellation rotation of $\pi/2$ multiples for each data stream at the output of the equalizer. This justifies our choice of such cost function among many others that exist in the literature. In fact, any multiple $\pi/2$ rotation will not affect the statistical properties of the equalized symbols since each rotated symbol still belongs to the same constellation. Note that the SCMA is implemented using the stochastic gradient (SG) algorithm. The equalizer update equation is obtained by calculating the gradient of J_{SCMA} as follows

$$\tilde{\mathbf{b}}_i(k) = \tilde{\mathbf{b}}_i(k-1) - \mu(k) e_i(k) \mathbf{x}(k), \quad i \in \{1, \dots, P\}, \quad (3.33)$$

where \mathbf{b}_i is the i^{th} column of \mathbf{B} , μ is the SG step size which is updated by the time averaging adaptive step size (TAASS) mechanism [63], the error signal e_i is given by

$$e_i(k) = (\Re(z_i(k))^2 - R) \Re(z_i(k)), \quad i \in \{1, \dots, P\}, \quad (3.34)$$

and $\mathbf{x} = \mathbf{F}^H \mathbf{r}$ is the pre-whitened received signal. Here, the pre-whitening method proposed in [64] is used. Also, Gram-Schmidt orthogonalization algorithm allows us to satisfy the orthogonalization constraint in Equation (3.32) at each iteration [65].

We assume that the number of transmitting antennas is known at the receiver which is not true in blind scenarios. However, estimating the number of sources is well investigated in the literature. For instance, the authors in [66] reviewed and compared several source number detection methods.

3.2.7.6 Results and Discussion

The proposed algorithm was verified and validated for various orders of linear digital modulation types. In our simulations otherwise mentioned, we consider the following antenna configuration: $P = 2, M = 4$. First, 50 realizations of testing MIMO signals with $2048 \times P$ symbols for each considered modulation scheme are generated. The source messages and the channel matrix are randomly selected for each realization. These realizations are employed only for ANN training. The combined HOM and HOC of the processed signals are calculated to form the features set. Then, features normalization and subset selection is performed as a preparation of ANN training. Extensive simulations show that the optimal ANN structure to be used for these algorithms is a two hidden layers network (excluding the input and the output layers), where the first layer consists of 10 nodes and the second of 15 nodes.

In what follows, we will consider two modulation pools in all our simulations,

$$\Theta_1 = \{2\text{-PSK}, 4\text{-PSK}, 8\text{-PSK}\} \text{ and} \\ \Theta_2 = \{2\text{-PSK}, 4\text{-PSK}, 8\text{-PSK}, 4\text{-ASK}, 8\text{-ASK}, 16\text{-QAM}, 64\text{-QAM}\}.$$

Actually, Θ_1 represents the intra-class modulation recognition (i.e. only identifying the order of the modulation) and Θ_2 represents the full-class modulation recognition (i.e. identifying the

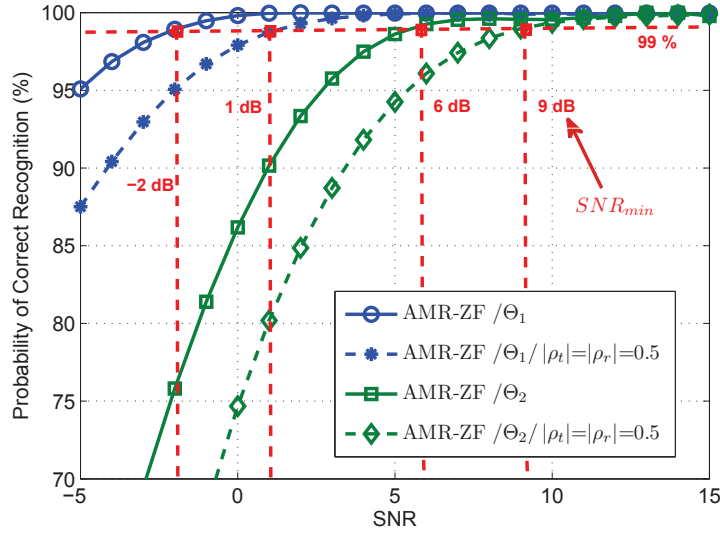


Figure 3.3: Probability of correct recognition versus SNR for AMR-ZF in the following cases (a) Θ_1 through spatially-uncorrelated channel (b) Θ_1 with Kronecker model ($|\rho_t| = |\rho_r| = 0.5$) (c) Θ_2 through spatially-uncorrelated channel (d) Θ_2 with Kronecker model ($|\rho_t| = |\rho_r| = 0.5$).

order and the type of the modulation at the same time). All results are based on 1000 Monte Carlo trials for each modulation scheme i.e. 3000 Monte Carlo trials in total for Θ_1 and 7000 Monte Carlo trials in total for Θ_2 . For each trial, P random testing streams of 2048 i.i.d symbols are generated. Also, the channel matrix is randomly generated for each trial. For different values of SNR, a white circularly complex Gaussian noise with variance σ_w^2 is added such that the $\text{SNR} = 10 \log_{10}(\frac{\sigma_s^2}{\sigma_w^2})$ where σ_s^2 is the average transmitted power. The probability of correct recognition is given in percentage and estimated by

$$P_c(\text{SNR}) = \frac{\sum_{\theta_i \in \Theta_1 \text{ (or } \Theta_2)} N_{\theta_i}}{N_{total}} \times 100 \quad (3.35)$$

where N_{total} (=3000 or 7000) is the total number of trials and N_{θ_i} being the number of trials for which the modulation $\theta_i \in \Theta_1$ (or $\in \Theta_2$) is correctly recognized. We define the minimum required SNR for close to optimal modulation recognition, SNR_{min} , by

$$\frac{P_c(\infty) - P_c(\text{SNR} > \text{SNR}_{min})}{P_c(\infty)} < \epsilon, \quad (3.36)$$

where normally, $\epsilon = 0.01$ and $P_c(\infty) = 100\%$. In what follows, we present the performance results of our proposed algorithm before introducing a performance comparison study.

AMR-ZF Performance Figure 3.3 shows the AMR-ZF performance in different scenarios. The SNR_{min} for PSK intra-class and full-class correct recognition is, respectively, -2dB and 6dB. In the presence of spatial correlation, the performance degrades where the SNR_{min} reaches 1dB and 9dB, respectively, for PSK intra-class and full-class correct recognition when $|\rho_t| = |\rho_r| = 0.5$. Also, the performance improves when the difference $\Delta = M - P$ increases as it is clear in Figure 3.4. This result is expected since increasing Δ will increase the effective post-processing SNR

and improve the recognition performance.

The effect of channel estimation error on modulation recognition has been also examined and the results are displayed in Figure 3.5. As noticed, the performance will drop rapidly for an error variance $\sigma_e^2 \geq 0.1$. That is the erroneous channel estimation leads to a performance upper bound contrary to the perfect CSI case as shown in Figure 3.5. This upper bound decreases as σ_e^2 increases. This upper bound problem is serious since even when the SNR is very large the correct recognition performance will not exceed that upper bound. The proposed solution is to use a blind source separation (BSS) technique to estimate the transmitted streams.

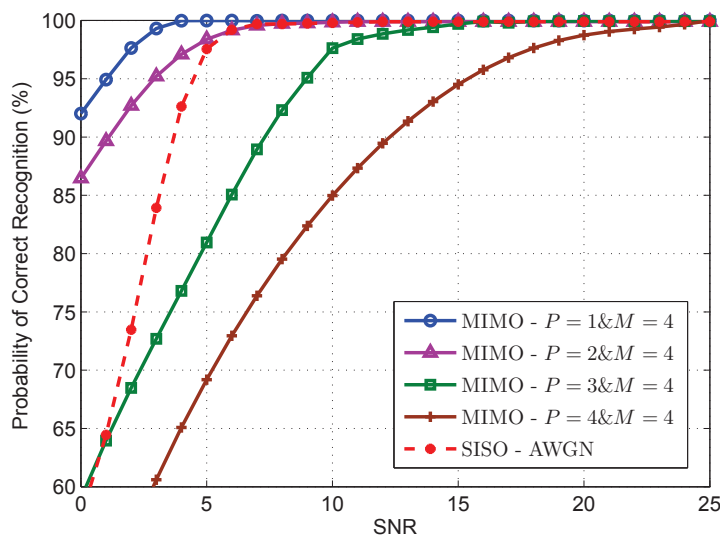


Figure 3.4: Probability of correct recognition versus SNR for different MIMO antenna configurations (AMR-ZF when considering Θ_2 through spatially-uncorrelated channel).

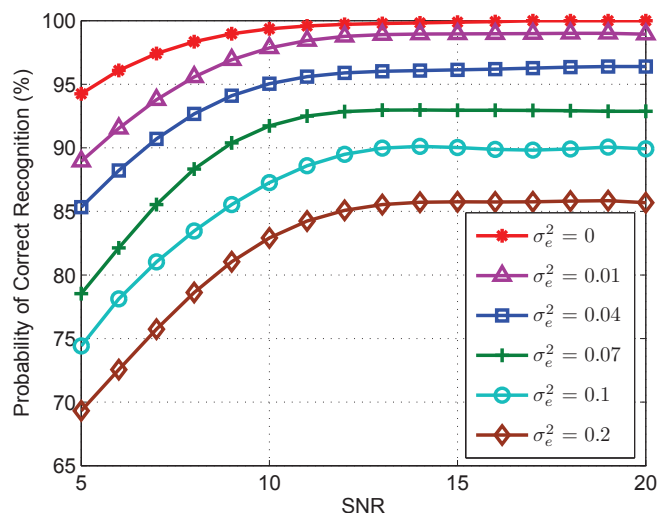


Figure 3.5: Probability of correct recognition versus SNR for different σ_e^2 (channel estimation error variance) values (AMR-ZF when considering Θ_2 with Kronecker model, $|\rho_t| = |\rho_r| = 0.5$).

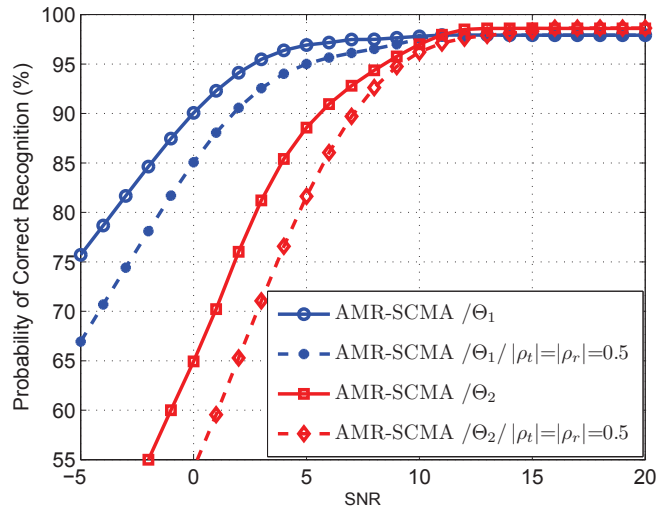


Figure 3.6: Probability of correct recognition versus SNR for AMR-SCMA in the following cases (a) Θ_1 through spatially-uncorrelated channel (c) Θ_1 with Kronecker model ($|\rho_t| = |\rho_r| = 0.5$) (b) Θ_2 through spatially-uncorrelated channel (c) Θ_2 with Kronecker model ($|\rho_t| = |\rho_r| = 0.5$) .

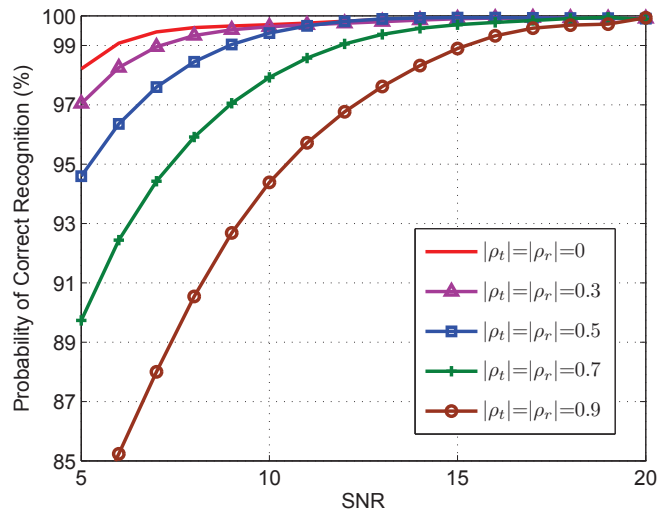


Figure 3.7: AMR-ZF performance for Θ_2 with Kronecker correlation model in the following cases (a) $|\rho_t| = |\rho_r| = 0$ (b) $|\rho_t| = |\rho_r| = 0.3$ (c) $|\rho_t| = |\rho_r| = 0.5$ (d) $|\rho_t| = |\rho_r| = 0.7$ (e) and $|\rho_t| = |\rho_r| = 0.9$.

AMR-SCMA Performance Among the different BSS algorithms available in the literature we had chosen the SCMA. The performance of the blind AMR-SCMA algorithm has been examined and the results are displayed in Figure 3.6. As noticed, the SNR_{\min} for PSK intra-class and full-class correct recognition is, respectively, 5dB and 10dB. As shown, the presence of channel correlation will degrade the performance and drive the SNR_{\min} to 9dB and 13dB, respectively, for PSK intra-class and full-class correct recognition when $|\rho_t| = |\rho_r| = 0.5$. Obviously, the blind AMR-SCMA algorithm solves the performance upper bound problem caused by the erroneous

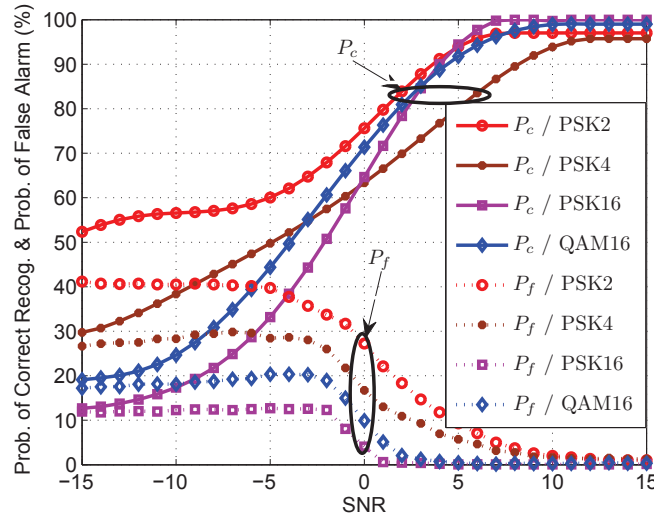


Figure 3.8: AMR-SCMA performance for each modulation scheme with unknown spatially-uncorrelated channel matrix for MIMO system using $P = 2$ and $M = 4$ antennas.

channel estimation when employing the ZF equalizer. But the blind AMR-SCMA requires a higher SNR compared to the AMR-ZF employed when perfect CSI is assumed.

Channel Correlation Effect The performance of the AMR-ZF algorithm in the presence of both transmit and receive correlations has been examined and the results are displayed in Figure 3.7. As noticed, the performance degrades when the correlation increases. The SNR_{\min} of full-class modulation recognition through spatially-uncorrelated MIMO channel is 6dB while SNR_{\min} is, respectively, 7dB and 9dB when $|\rho_t| = |\rho_r| = 0.3$ and $|\rho_t| = |\rho_r| = 0.5$. Also, the SNR_{\min} of full-class modulation recognition is, respectively, 12dB and 15dB when $|\rho_t| = |\rho_r| = 0.7$ and $|\rho_t| = |\rho_r| = 0.9$. It is clear that when $|\rho| \rightarrow 1$, the performance degrades rapidly.

Recognition Performance for each Modulation Scheme The false recognition probability P_f is the probability to recognize certain modulation scheme when it was not transmitted. Here, we separately examine P_c and P_f for each modulation scheme instead of calculating the average probability for all schemes. The modulation pool and simulations conditions are the same as that used in [58] to evaluate the performance of the ALRT and HLRT algorithms. We consider a spatially-uncorrelated MIMO system (with 2×4 antennas) and the following modulation pool: 2-PSK, 4-PSK, 16-PSK and 16-QAM.

Simulations show that the AMR-ZF algorithm performs well when compared to the optimal ALRT algorithm [58]. The AMR-SCMA algorithm is used when the channel matrix is unknown. It is clear in Figure 3.8 that, when SNR is relatively low, 2-PSK scheme has higher P_c and P_f relative to 16-PSK scheme which is the worst recognized and the less false identified. Also as seen, the performance of AMR-SCMA is good in comparison with the HLRT algorithm [58]. The major drawbacks of the methods in [58] are the high computational complexity and its need of perfect knowledge of the noise variance at the receiver side.

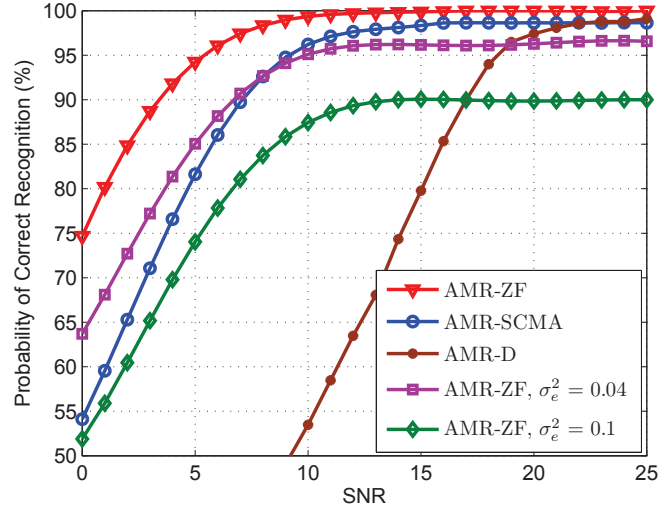


Figure 3.9: Performance comparison among different algorithms for Θ_2 with Kronecker model ($|\rho_t| = |\rho_r| = 0.5$).

Performance Comparison Finally, a comparison study among the proposed modulation recognition algorithms is introduced. The results are displayed in Figure 3.9. As noticed, the AMR-ZF algorithm offers the best performance when perfect CSI is assumed. However, the proposed AMR-ZF algorithm is sensitive to channel estimation errors. Note that the presence of erroneous channel estimation causes a rapid performance degradation when the error variance $\sigma_e^2 \geq 0.1$. Also, this erroneous estimation leads to an upper bound of the probability of correct recognition contrary to the perfect CSI case; i.e. SNR tends to infinity but the probability of correct recognition does not approach 100%. To solve this problem the totally blind AMR-SCMA algorithm was proposed. This algorithm solved the upper bound problem without any CSI knowledge. However, the AMR-SCMA requires higher SNR to achieve the same performance as the AMR-ZF employed when perfect CSI is assumed. In fact the SNR_{min} is, respectively, 9dB and 13dB when using AMR-ZF and AMR-SCMA algorithms for full-class correct recognition through MIMO channels when $|\rho_t| = |\rho_r| = 0.5$. The AMR-D algorithm has the lower complexity but offers a low performance compared to the remaining two algorithms. Simulation results show a gain in SNR_{min} of about 4dB when comparing the performance for SISO and uncorrelated SIMO systems ($M = 4$) (see Figure 3.4).

3.2.7.7 Conclusions

We introduced three new algorithms for digital modulation recognition aimed for correlated MIMO systems based on HOS as features extraction subsystem and a neural network trained with resilient backpropagation learning algorithm as classifier subsystem. The less complex AMR-D algorithm extracted the features directly from the received MIMO signal and it is a good choice when the transmitted power is very high. The AMR-ZF employs a zero-forcing equalizer before the features extraction process and it is the best algorithm when perfect CSI knowledge is assumed. The AMR-SCMA algorithm blindly separates the symbols and offers the best performance when no CSI knowledge is assumed. The proposed algorithms are examined

through correlated MIMO channels and they are shown to be capable of identifying different linear digital modulation schemes with high accuracy.

3.3 Modulation Technique Identification

OFDM, MIMO, and spectrum spreading are among the essential modulation techniques used in telecommunication systems developed over last decades. In this section, we will focus on the blind identification of signals employing these techniques. The existing identification methods of OFDM and spread spectrum signals are presented. Thereafter, we introduce a method based on the autocorrelation function (more precisely, on the fluctuations of its estimator) to identify the SIMO multi-carrier spread spectrum signals.

3.3.1 Preliminary Literature Review

Spectrum Spreading Identification Direct-sequence spread spectrum signals have been initially used in a military context for secure communications due to their well-known low probability of interception properties. During the last couple of decades, DS-SS technique has also been adopted by many civilian applications. For example, it is widely used in multi-user wireless communication systems e.g. IS-95 and WCDMA. It is also used in the GPS satellite navigation system.

The problem of blind identification and parameters estimation of spread spectrum signals was addressed in the literature. Some existing methods require some prior knowledge about users parameters such as signature waveform, the spreading code of the user to be detected, or chip rate [67]. These parameters may be unknown in a realistic blind context. DS-SS signals are similar to noise and they are often transmitted below the noise level. A detection method of a DS-SS communication has been proposed in [68]. Although the autocorrelation of a DS-SS signal is the same as the autocorrelation of a noise, the fluctuations of autocorrelation estimators are higher when a DS-SS signal is hidden in the noise [68]. This blind detection method is capable of estimating the symbol period of the DS-SS signal. In [69], a new blind method which can estimate the spreading sequence is proposed. This method is based on eigen analysis techniques. The sequence can be reconstructed from the two first eigenvectors of the signal correlation matrix, and other useful information, such as desynchronization time, can be extracted from the eigenvalues. This effective synchronization scheme based on maximizing the squared Frobenius norm of correlation matrix is extended to multi-user DS-SS case [70].

An algorithm for blind synchronization and despreading for asynchronous multi-user DS-CDMA systems is proposed in [71]. This algorithm is another multi-user extension of the algorithm proposed in [69] where single-user case was only considered. This method is based on a signal correlation matrix deflation technique in which the spreading codes and timing offsets are estimated one at a time. Then, their effect on the signal correlation matrix is iteratively removed. This way, a significant improvement over the method in [70] can be obtained since the performance of the proposed method is nearly independent of the relative timing offsets between

users. This improvement in [71] over the method in [70], comes at the expense of the increase in computing time with both the number of users and the correlation matrix size. Moreover, in [71], the number of interfering users is assumed to be known at the receiver.

A robust and efficient algorithm, with no prior knowledge needed, is proposed in [72]. The algorithm exploits the fluctuations of correlation estimator and the analysis of the signal correlation matrix to estimate the timing offsets (i.e., the synchronization process) and the number of interfering users in an iterative way, thereby improving existing methods so that sources with nearly equal timing offsets can be estimated. Thereafter, spreading codes are recovered using linear algebra techniques applied to the estimated eigenvectors of the correlation matrix. This method efficiency, even at a low SNRs through fading multi-path channel, was demonstrated in [72]. This low-complexity algorithm can be used for interference cancellation, as well as, in non-cooperative applications such as waveform awareness for CR.

OFDM Signals Identification The OFDM has received great interest for wireless broadband multimedia applications over the last decade. More recently, this technique emerges in the specific railway context. The main advantages of this technique are its flexibility and its robustness against the frequency selective fading channels. Several OFDM signals identification approaches was introduced in the literature. For instance, a method based on the statistical properties of incoming signal was proposed to discriminate between single-carrier and multi-carrier modulations propagating through AWGN channels, and to estimate their parameters [73]. This algorithm do not perform well through more realistic channels.

The cyclic-prefixed OFDM (CP-OFDM) signals are designed by prefixing the OFDM symbol with a copy of its last part. The cyclic-prefix (CP) serves as a guard interval to eliminate the inter-symbol interference from the previous symbol, and to mitigate the multi-path channel effect. Several papers proposed exploiting the autocorrelation [74] and cyclic-autocorrelation [75] features of CP-OFDM signals. These features are mainly due to the repetition of a part of the signal. These techniques are used to extract some parameters of OFDM signals propagating through frequency-selective channels and affected by carrier phase, time and frequency offsets [76]. These parameters include the power, oversampling factor, useful time interval, CP duration, and number of subcarriers.

A blind parameter estimation technique based on the power autocorrelation feature, applied to identify zero-padding time guard interval OFDM signals (ZP-OFDM), is proposed in [76]. The ZP-OFDM signals exhibit neither autocorrelation nor cyclic-autocorrelation properties since zeros are appended at the end of each OFDM symbol (instead of the CP). Therefore, the autocorrelation and cyclic-autocorrelation based techniques do not work. Hence, the authors in [76] proposed to employ the so-called power autocorrelation and given by

$$R_p(\tau) = \frac{1}{T} \int_0^T |x(t)|^2 |x(t-\tau)|^2 dt, \quad (3.37)$$

for a signal $x(t)$ observed for period T . This technique leads to an efficient estimation of the symbol duration and zero-padding duration in frequency-selective channels, and is insensitive to receiver phase and frequency offsets.

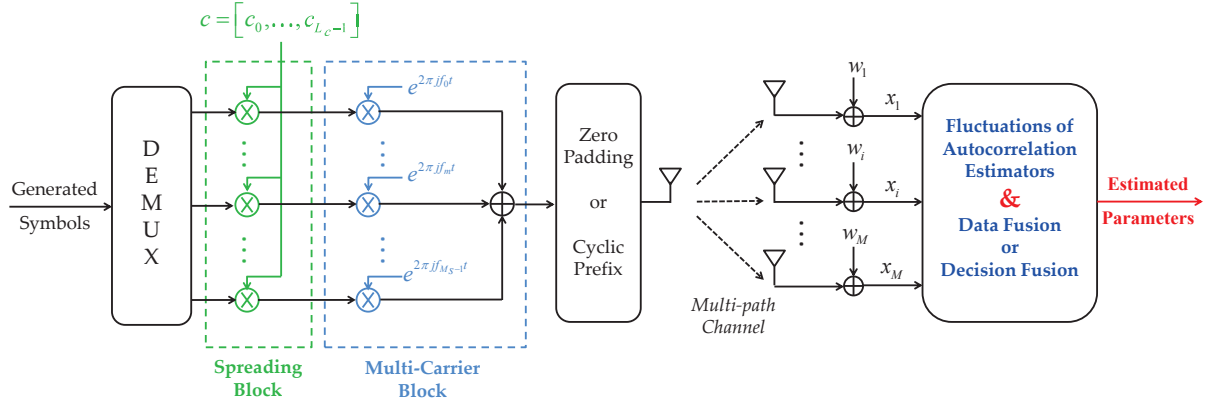


Figure 3.10: SIMO MC-DS-CDMA modulator scheme.

Nevertheless, these approaches fail when either the CP duration is small or the channel impulse response is almost as large as the CP. Therefore four new methods were proposed in [77] to estimate the parameters of OFDM modulated signal (especially the subcarrier spacing). Three of these methods need a prior synchronization step, while the fourth one doesn't require any synchronization. The methods relying on (i) the normalized kurtosis, (ii) the maximum-likelihood principle, (iii) the matched filter, do need a synchronization step. Note that this extra step increases the computational load. The fourth method exploits the second-order cyclostationarity property. The authors in [77] used these methods to blindly distinguish various OFDM based systems (e.g., WiFi, WiMAX, 3 GPP/LTE, DVB-T) from each others.

The fast and efficient blind detection scheme based on the analysis of autocorrelation estimator fluctuations, previously applied in [68], is extended to the case of multi-carrier direct spread spectrum systems [78, 79]. In what follows, we introduce an identification method applied to the case of SIMO multi-carrier DS-CDMA signals.

3.3.2 Case Study : Blind SIMO MC-DS-CDMA Identification

3.3.2.1 System Model and Assumptions

Let us consider a SIMO MC-DS-CDMA system with M receiving antenna and M_s subcarriers. Let $a_{n,m}$, $m = 0, \dots, M_s - 1$ be the complex transmitted symbol over the m^{th} subcarrier, f_m , for a duration $T_u = M_s T_{sym}$, where T_{sym} is the symbol period before demultiplexing. The transmitted symbol $a_{n,m}$ is first multiplied by a spreading code $\mathbf{c} = [c_0, \dots, c_{L_c-1}]$ of length L_c where c_ℓ stands for the ℓ^{th} sequence chip, and then sent over the m^{th} subcarrier, as illustrated on Figure 3.10. The chip duration is $T_{chip} = \frac{T_u}{L_c}$. The complex transmitted signal, $s(t)$, can be expressed as

$$s(t) = \sum_{n=-\infty}^{\infty} \sum_{m=0}^{M_s-1} a_{n,m} \psi(t - nT_u) \exp(2\pi j f_m t) \quad (3.38)$$

where $\psi(t) = \sum_{\ell=0}^{L_c-1} c_\ell p_T(t - \ell T_{chip})$ and $p_T(t)$ is the impulse response of the transmitter pulse shaping filter. The complex corrupted received signal at the i^{th} antenna, denoted $x_i(t)$, is given

by

$$x_i(t) = \sum_{n=-\infty}^{\infty} \sum_{m=0}^{M_s-1} a_{n,m} g(t - nT_u) \exp(2\pi j f_m t) + w_i(t) \quad (3.39)$$

where the following assumptions hold

- $a_{n,m}$ are assumed to be i.i.d, centered, and of variance σ_a^2 . The SNR (in dB) is negative (signal hidden in the noise).
- $w_i(t)$ is the AWGN noise at the i^{th} antenna. Without loss of generality, the noise power at different antenna is assumed to be σ_w^2 . Also, $w_i(t)$ is assumed to be independent of signals and noise components at other antennas.
- $f_m = f_c + \frac{m}{M_s T_{sym}} = f_c + \frac{m}{T_u}$, f_c stands for the central frequency. The required bandwidth is approximately $W = \frac{M_s}{T_u}$.
- Assuming an i.i.d Rayleigh block fading (i.e. the channel remains constant during the observation duration) multi-path channel of N_h taps between the transmitter and the i^{th} receiving antenna, which fading gains, $h_{i,j}$, $j = 0, \dots, N_h - 1$, have an unitary second-order moment. Also, τ_j is the j^{th} tap delay.
- $g(t) = \sum_{j=0}^{N_h-1} h_{i,j} \sum_{\ell=0}^{L_c-1} c_{\ell} p_T(t - \ell T_{chip} - \tau_j)$ stands for the global filter which represents the convolution product between transmitter shaping filter, spreading sequence waveform, and multi-path channel impulse response.

Furthermore, let us set to as T_{CP} the CP duration: $T_{cp} = \Delta_T T_u$, i.e., the CP is a fraction of the useful multi-carrier symbol duration, T_u , such as $0 \leq \Delta_T < 1$. In order to avoid the ISI, T_{CP} should be greater than the longest channel delay, i.e. $\max_{j=0, \dots, N_h-1} (\tau_j) \leq T_{cp}$. Hence, the total multi-carrier symbol is defined during $T_{MC} = T_u + T_{cp} = (1 + \Delta_T) T_u$. Therefore, Equation (3.39) can be rewritten, taking into account the CP duration, as follows

$$x_i(t) = \sum_{n=-\infty}^{\infty} \sum_{m=0}^{M_s-1} a_{n,m} g_{MC}(t - nT_{MC}) \exp(2\pi j f_m t) + w_i(t) \quad (3.40)$$

where $g_{MC}(t)$ is the global filter, and it is composed of the initial filter $g(t)$ prefixed by its last T_{cp} duration. Also, the SIMO ZP-MC-DS-CDMA signals can be easily derived from Equation (3.39) by adding a zero guard interval at the end of each multi-carrier symbol.

3.3.2.2 Proposed Blind Identification Method

Successive investigations of the contributions of noise and noise-free signal through the analysis of the second-order moment of the autocorrelation estimator computed from many windows is the key of detecting the signal and estimating its parameters. This method is compared to another one based on the correlation property between the useful part and the CP of a multi-carrier symbol.

Fluctuations of Autocorrelation Estimators First, a measurement of autocorrelation estimator fluctuations is introduced. Assume the total observed duration T is divided into K segments of duration $T_K = \frac{T}{K}$. The k^{th} segment of the received corrupted signal at the i^{th} antenna, $x_i(t)$, is given by

$$x_{i,k}(t) = x_i[t + kT_k] \quad 0 \leq t \leq T_k, 0 \leq k \leq K - 1 \quad (3.41)$$

Then, within each window k , an estimation of the received signal autocorrelation function $\widehat{R}_{i,k}$ is computed as

$$\widehat{R}_{i,k}(\tau) = \frac{1}{T_K} \int_0^{T_K} x_{i,k}(t)x_{i,k}^*(t - \tau)dt \quad (3.42)$$

Hence, the second-order moment of the estimated autocorrelation function, \widehat{R}_i , can be expressed as

$$\Phi_i(\tau) = \widehat{E} \left\{ |\widehat{R}_i(\tau)|^2 \right\} = \frac{1}{K} \sum_{k=0}^{K-1} |\widehat{R}_{i,k}(\tau)|^2 \quad (3.43)$$

where $\widehat{E}(\cdot)$ is the estimated expectation of (\cdot) . That is, $\Phi_i(\tau)$ is a measurement of the fluctuations of $\widehat{R}_i(\tau)$ since it can be easily shown that $\widehat{E} \left\{ |\widehat{R}_i(\tau)| \right\} \simeq 0$. Since symbols are assumed to be independent from the noise, Equation (3.43) can be rewritten as

$$\Phi_i(\tau) \simeq \Phi_i^s(\tau) + \Phi_i^w(\tau) \quad (3.44)$$

where the fluctuations $\Phi_i^s(\tau)$ and $\Phi_i^w(\tau)$ are, respectively, due to noise-free signals and the noise. In the sequel, we investigate both signal and noise contributions to the autocorrelation estimator fluctuations.

Analysis of the Noise Contribution to Fluctuations Firstly, let us consider the additive noise alone, i.e. there is no signal hidden in the noise. The fluctuations due to only the additive noise are uniformly distributed over all values of τ . Let us characterize the global noise fluctuations Φ_i^w by their mean $M_{\Phi_i^w}$ and standard deviation $\sigma_{\Phi_i^w}$ as described hereinafter. Let us assume the frequency response of the receiver filter, $P_R(f)$, is flat in $[-B_W/2, +B_W/2]$ and zero outside. In practice B_W is larger than the signal bandwidth W . The fluctuations mean is computed as

$$M_{\Phi_i^w} = E \left\{ |\widehat{R}_i^w(\tau)|^2 \right\} = \frac{1}{T_K} \int_{-B_W/2}^{B_W/2} \left(\frac{N_0}{2} \right)^2 |P_R(f)|^2 df = \left(\frac{N_0}{2} \right)^2 \frac{B_W}{T_K} \quad (3.45)$$

where N_0 is the power spectrum density (PSD) of the noise. Also, the fluctuations variance is given as

$$\begin{aligned} \sigma_{\Phi_i^w}^2 &= \text{var} \left\{ \widehat{E} \left[|\widehat{R}_i^w(\tau)|^2 \right] \right\} = \frac{1}{K^2} \sum_{k=0}^{K-1} \text{var} \left\{ |\widehat{R}_{i,k}^w(\tau)|^2 \right\} = \frac{1}{K} \text{var} \left\{ |\widehat{R}_i^w(\tau)|^2 \right\} \\ &= \frac{1}{K} \left\{ E \left[|\widehat{R}_i^w(\tau)|^4 \right] - M_{\Phi_i^w}^2 \right\} \end{aligned} \quad (3.46)$$

The statistical behaviour of $\widehat{R}_i^w(\tau)$ is close to a Gaussian since it is the average of a large number of random variables. Furthermore, except for small values of τ , its average value is null. Hence

$E \left[|\widehat{R}_i^w(\tau)|^4 \right] \simeq 3M_{\Phi_i^w}^2$. Therefore, we get

$$\begin{cases} M_{\Phi_i^w} = E \left\{ |\widehat{R}_i^w(\tau)|^2 \right\} = \frac{\sigma_w^4}{B_W T_K} & \text{(a)} \\ \sigma_{\Phi_i^w} = \sqrt{\frac{2}{K}} M_{\Phi_i^w} = \sqrt{2K} \frac{\sigma_w^4}{B_W T} & \text{(b)} \end{cases} \quad (3.47)$$

Analysis of the Noise-free Signal Contribution Focusing only on the noise-free signal shows that, on average, high amplitudes of the fluctuations Φ_i^s occur at multiple of T_{MC} and lower ones occur at multiple of T_{cp} . Let us also set to as $M_{\Phi_i^s}^{CP}$ their mean value at multiple of T_{MC} . By using (3.40) into (3.42), we have

$$\begin{aligned} \widehat{R}_{i,k}^s(T_{MC}) &= \frac{1}{T_K} \sum_{n_1=-\infty}^{\infty} \sum_{n_2=-\infty}^{\infty} \sum_{m_1=0}^{M_s-1} \sum_{m_2=0}^{M_s-1} a_{n_1,m_1} a_{n_2,m_2}^* \int_0^{T_K} g_{MC}(t - n_1 T_{MC}) \\ &\quad g_{MC}^*[t - (n_2 + 1)T_{MC}] \exp [2\pi j(f_{m_1} - f_{m_2})t] dt \end{aligned} \quad (3.48)$$

Since the global filter $g_{MC}(t)$ is time limited, the above Equation is simplified to

$$\widehat{R}_{i,k}^s(T_{MC}) = \frac{1}{T_K} \sum_{n=-\infty}^{\infty} \sum_{m_1=0}^{M_s-1} \sum_{m_2=0}^{M_s-1} a_{n,m_1} a_{n-1,m_2}^* \int_0^{T_K} \exp \{2\pi j(f_{m_1} - f_{m_2})t\} |g_{MC}(t - nT_{MC})|^2 dt \quad (3.49)$$

Since symbols $a_{n,m}$ are assumed independent and centered, we get $E \left\{ \widehat{R}_{i,k}^s(T_{MC}) \right\} = 0$ and

$$M_{\Phi_i^s}^{CP} = \hat{E} \left\{ |\widehat{R}_i^s(T_{MC})|^2 \right\} = \frac{1}{T_K^2} M_s \sigma_a^4 \sum_{n=-\infty}^{\infty} \left(\int_0^{T_K} |g_{MC}(t - nT_{MC})|^2 dt \right)^2 \quad (3.50)$$

Let us set $\sigma_{g,i}^2 = \frac{1}{T_{MC}} \int_0^{T_{MC}} |g_{MC}(t)|^2 dt$. The mean $M_{\Phi_i^s}^{CP}$ can be rewritten by

$$\begin{aligned} M_{\Phi_i^s}^{CP} &= \frac{1}{T_K^2} M_s \sigma_a^4 \frac{T_K}{T_{MC}} (T_{MC} \sigma_{g,i}^2)^2 \\ &= M_s K \frac{(1 + \Delta_T) T_u}{T} \sigma_a^4 \sigma_{g,i}^4 \end{aligned} \quad (3.51)$$

Furthermore, we assume the spreading code \mathbf{c} is normalized, and the transmitter pulse shaping filter $p_T(t)$ is rectangular. The variance $\sigma_{g,i}^2$ is calculated by

$$\begin{aligned} \sigma_{g,i}^2 &= \sum_{j=0}^{N_h-1} |h_{i,j}|^2 \frac{1}{T_{MC}} \int_0^{T_{MC}} \left(\sum_{\ell=0}^{L_c-1} |c_\ell p_T(t - \ell T_{chip})|^2 \right) dt \\ &= \sum_{j=0}^{N_h-1} |h_{i,j}|^2 \end{aligned} \quad (3.52)$$

Discussion Expression (3.47) shows that the noise contribution is uniformly distributed over all values of τ . Moreover, it also clarifies that its contribution can be lowered by increasing the window duration T_K . One way to do that is to increase the total observed duration T while

keeping the number of windows K constant. From Equation (3.51), we can see that an increase in the channel gain and/or the transmitted power improves the signal identification. Multi-path channel gains act as a multiplicative factor in the fluctuations curve. At constant transmit power, the lower the transmit data rate is, the higher fluctuations average amplitude is at multiple of T_{MC} .

Thus, the fluctuations curve highlights high equispaced peaks which average spacing corresponds to the symbol period T_{MC} , and also low equispaced peaks which average spacing with the high fluctuations peaks in their vicinity corresponds to an estimation of the CP duration. The analysis of Φ_i leads to a low-complexity efficient estimation method. Also, the proposed scheme is insensitive to phase and frequency offsets since only the square of the estimate of the correlation function is computed. From (3.47) and (3.51), a theoretical detection threshold is defined as: $\lambda_{\Phi_i}^{CP} = M_{\Phi_i^w} + \zeta \cdot \sigma_{\Phi_i^w}$. The ζ value is chosen $\simeq 3$ such as the false alarm probability $< 1\%$. Also, the fluctuations resulting from ZP-MC-DS-CDMA highlights high equispaced amplitude peaks, which average spacing allows the symbol period determination.

Autocorrelation Based Detection The autocorrelation function exhibits peaks resulting from the fact that the CP is a repetition of a part of the signal, as depicted in Figure 3.11. The estimated autocorrelation function is calculated by

$$|\widehat{R}_i(\tau)| = \begin{cases} \sigma_a^2 \sigma_g^2 + \sigma_w^2, & \tau = 0 \\ \sigma_a^2 \sigma_g^2 \frac{T_{CP}}{T_{MC}}, & \tau = T_u \end{cases}, \quad (3.53)$$

that is, the useful symbol duration T_u can be estimated by finding the distance between the highest peaks of the autocorrelation function. As the autocorrelation has non-zero terms only for the part that falls into the CP duration, power ratio of the guard time to the symbol duration can be used to find the CP length. However, SNR knowledge is required for a precise estimation.

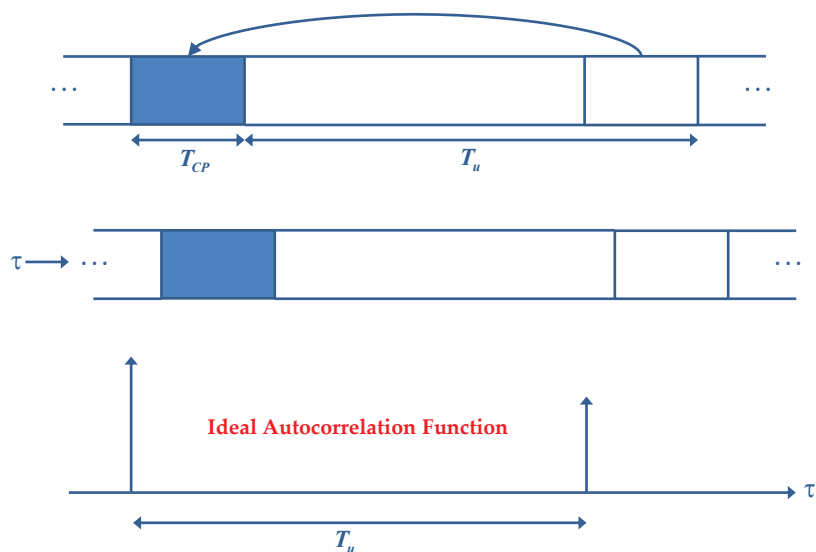


Figure 3.11: Autocorrelation of the CP multi-carrier signal.

Another CP duration estimation method exploits the cyclostationarity of the received multi-carrier signal [76]. The cyclic-autocorrelation function (CAF) is estimated as

$$\hat{R}_{i,\nu}(\tau) = \frac{1}{T} \int_0^T x_i(t)x_i^*(t-\tau)e^{-2j\pi\nu t} dt \quad (3.54)$$

Using the estimated useful symbol duration \hat{T}_u , the total symbol duration T_{MC} can be determined by using peak detection on $\hat{R}_{i,\nu}(\hat{T}_u)$. That is, our purpose is to determine the distance of two maximum peaks in ν domain, which is equal to the reciprocal of T_{MC} . It was proposed in [76] to employ the cycle frequency searching scheme to determine the two maximum peaks in the CAF pattern. After estimating T_{MC} , we can easily obtain the length of guard interval as $\hat{T}_{CP} = \hat{T}_{MC} - \hat{T}_u$.

Multiple-antenna Blind Identification Method Cooperation can also improve the MC-DS-CDMA signal identification. Let us assume a multiple-antennas receiver, or even more several multiple-antenna receivers located at both sides of the train, i.e. M receiving antenna in total. Improving signal identification is achieved by combining different information coming from all antennas at the fusion center. This combination could be done by two different approaches. The first one is the decision fusion where the signal is separately identified at each antenna. The individual decisions of the presence of MC-DS-CDMA signal and the estimated parameters are then sent to the fusion center to be combined for final decision. A literature review of existing decision fusion methods is presented in subsection 3.2.6. The final decision indicates the detection of MC-DS-CDMA signal when the majority of antennas identifies this signal. Also, the signal parameters coming from the M detectors are averaged after identifying and removing the outliers. The second approach is the data fusion. It is obvious that the detection performance improves when the number of considered segments K increases. This number could be increased by combining the received signals on all antennas at the fusion center. The total number of windows is $\sum_{i=1}^M K_i$ where K_i is the number of considered windows on the i^{th} antenna. Also, Equation (3.51) clarifies that channel gains affect the signal contribution in autocorrelation estimator fluctuations. That is, when the received signal at certain antenna is strongly faded, it is less probable to be detected. Therefore, the cooperation is more powerful when the different antennas/receivers suffer from different fading conditions.

3.3.2.3 Results and Discussion

Simulations have been carried out considering a QPSK-MC-DS-CDMA modulation, and the following parameters were set: the chip duration $T_{chip} = \frac{1}{f_{chip}}$ where $f_{chip} = 200$ MHz, $L_c=127$ (complex GOLD sequence), and the number of analysis windows is $K = 300$. The number of subcarriers is 64 with 1/4 guard interval, i.e. 16 subcarriers are allocated for the CP or ZP. The used channel model is the COST207RAx6 corresponding to rural area and a channel order of 6 [80].

Figure 3.12 illustrates the detector output of MC-DS-CDMA signal with 1/4 CP guard interval for SNR = -3 dB. This result is in accordance with theoretical developments. This Figure shows

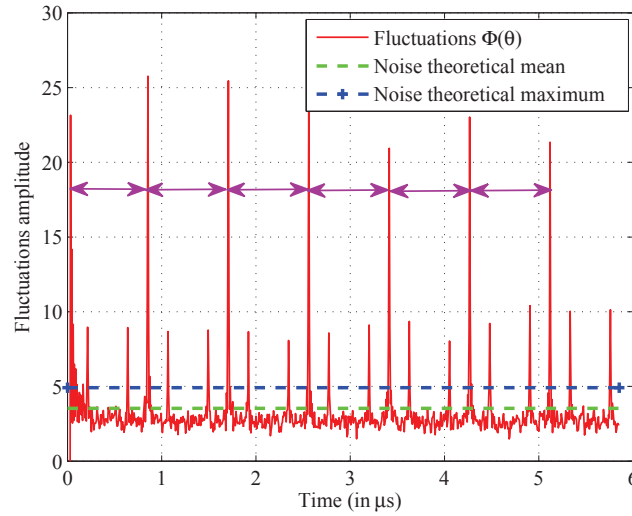


Figure 3.12: Autocorrelation estimator fluctuations of MC-DS-CDMA signal with 1/4 cyclic prefix guard interval, SNR = -3 dB.

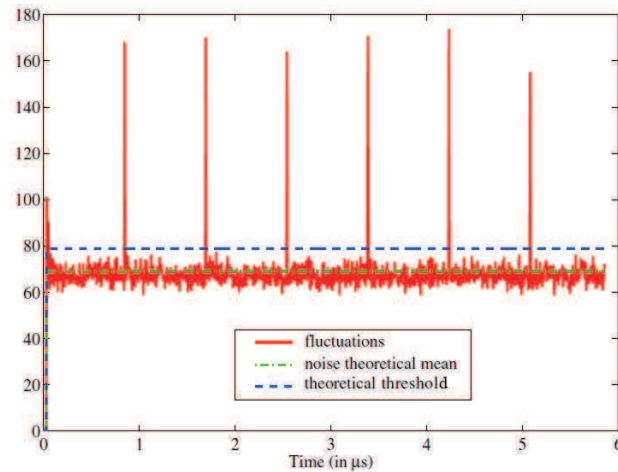


Figure 3.13: Autocorrelation estimator fluctuations of MC-DS-CDMA signal with 1/4 zero-padding guard interval, SNR = -3 dB.

high peaks regularly spaced in the autocorrelation estimator fluctuations, which average spacing is T_{MC} . Each high peak is surrounded with two low amplitude peaks, each one between them is separated from its corresponding high amplitude peak by a duration of T_{cp} . Using the average spacing between these peaks, we obtain $\hat{T}_{MC} \simeq 845.9 \text{ ns}$, while the CP duration is estimated by $\hat{T}_{cp} \simeq 211.45 \text{ ns}$. Hence, $\hat{T}_u = \hat{T}_{MC} - \hat{T}_{cp} = 634.45 \text{ ns}$ and $\hat{\Delta}_T \simeq \frac{1}{4}$. This result is very close to the real useful symbol duration value $T_u = T_{chip} \cdot L_c = 635 \text{ ns}$. The actual CP duration equals $\Delta_T \cdot T_u = \frac{1}{3} T_u = 211.667 \text{ ns}$. The total number of subcarriers can be estimated as $\hat{T}_{MC} \cdot \hat{W}$ where \hat{W} is an estimation of the signal bandwidth. The problem of estimating the bandwidth will be studied in Chapter 4. An improved Welch periodogram based method is introduced. The bandwidth is estimated by 74.5 MHz, then, The total number of subcarriers $\simeq 63$, which is very close to the real number of subcarriers.

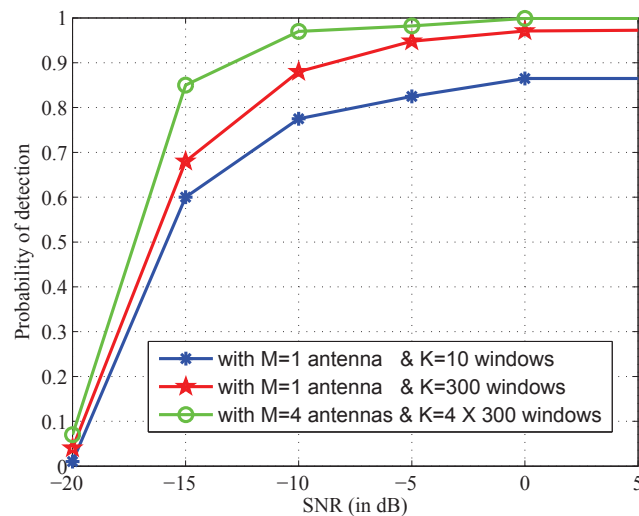


Figure 3.14: The detection probability of the MC-DS-CDMA signals for different SNRs as a function of the number of analysis windows.

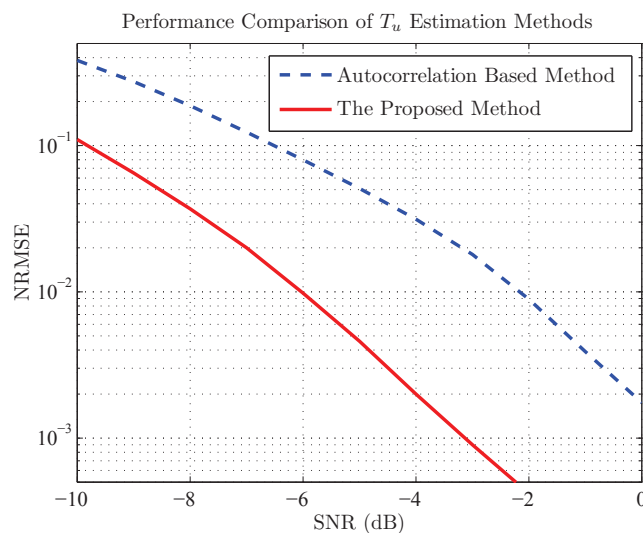


Figure 3.15: Performance comparison between the T_u estimation method based on the autocorrelation function and the proposed one (based on the autocorrelation estimator fluctuations). The normalized root mean square error of two estimators as a function of SNR under fading channels.

Furthermore, estimating the chip duration, the spreading code length, and the code itself require a synchronization process. A comprehensive study of synchronization methods can be found in [72]. Similar results are found in the case of ZP-MC-DS-CDMA transmission when using the same parameters. As expected, Figure 3.13 shows high amplitude equispaced fluctuations peaks, which average spacing gives the estimate of the symbol period $\hat{T}_{MC} \simeq 846$ ns. As suggested in [76], T_{zp} can be estimated using the power autocorrelation feature.

The performance in terms of probability of detection was examined for different SNR values, i.e. the SNR averaged at all antennas. The autocorrelation estimator fluctuations method is able to detect the MC-DS-CDMA signals even at low SNRs, as illustrated in Figure 3.14. Moreover, it also shows that the probability of detection can be strongly improved by increasing the number of analysis windows. Nevertheless, the computation cost can be very prohibitive. Also, Figure 3.14 shows that employing data fusion approach to combine the information coming from multiple-antennas ($M = 4$), while keeping the observation duration constant, does improve the performance.

A performance comparison between the useful time interval, T_u , estimators is given in Figure 3.15. This Figure depicts the normalized root mean-squared-error (NRMSE) of T_u estimation, through multi-path fading channels, using the autocorrelation function based method and the proposed autocorrelation estimator fluctuations based one. As it can be seen from this Figure, the proposed algorithm gives a good estimate of T_u in the low SNR regime. As the autocorrelation estimator is more sensitive to noise, and the autocorrelation estimator fluctuations achieve a good gain in SNRs at its output (see [68] for more details), the proposed method is more efficient, in terms of NRMSE, than that of the autocorrelation based one.

3.4 Conclusions

This Chapter focused on how to enhance the waveform awareness of a cognitive radio device by identifying several features of the received signal, for instance, recognizing the used modulation scheme. After a literature review, we propose a modulation recognition algorithm for MIMO systems based on HOS as features extraction subsystem and an ANN trained with resilient backpropagation learning algorithm as classifier subsystem. This method represents the first contribution introduced in this Chapter. To the best of our knowledge, our work is among the first ones that study the modulation recognition for MIMO systems, and the first one that addresses the spatially-correlated case. Three algorithms were introduced and studied, namely, the AMR-D, the AMR-ZF, and the AMR-SCMA algorithms. The proposed algorithms are examined through correlated MIMO channels and had shown to be capable of identifying different linear digital modulation schemes with high accuracy.

The CR waveform awareness could be further improved by detecting whether the signal is a spread spectrum one, or whether it is a multi-carrier one. We proposed a blind identification method for MC-DS-CDMA signals which forms the second contribution included in this Chapter. The autocorrelation estimator fluctuations were employed to identify the signal parameters. The described scheme leads to an efficient estimation of symbols duration, CP duration, and subcarriers number. The proposed method is insensitive to phase and frequency offsets. Simulations results confirm theoretical developments. The multiple-antennas at receiver are exploited to enhance the performance while keeping the detection duration constant. The performance of the proposed method was also compared to that of the method that directly employs the autocorrelation function. In the next Chapter, we will focus on another key capability of cognitive radio: the spectrum awareness based on spectrum sensing concept.

Chapter 4

Spectrum Sensing for Cognitive Radio

Contents

4.1	Introduction	82
4.2	Spectrum Sensing for Cognitive Radio	82
4.2.1	Spectrum Sensing Concept	82
4.2.2	Sensing Methods Classification	83
4.2.3	Cooperative Sensing	84
4.3	Narrowband Spectrum Sensing	85
4.3.1	Introduction	85
4.3.2	Traditional Spectrum Sensing	85
4.3.3	Multiple-antenna Spectrum Sensing	87
4.3.4	Predicted Eigenvalues Threshold	91
4.3.5	Conclusions	97
4.4	Wideband Spectrum Sensing	98
4.4.1	Preliminary Literature Review	98
4.4.2	Improved Welch Periodogram Based Detection	102
4.4.3	Discussion	108
4.5	Conclusions	108

4.1 Introduction

As already mentioned in Chapter 1, the spectrum sensing is an essential function of any cognitive radio system. This Chapter explains firstly the concept of spectrum sensing and highlights its importance. Spectrum sensing algorithms are divided into two main categories, namely, the narrowband spectrum sensing (NSS) and the wideband spectrum sensing (WSS). A preliminary literature review of each category is presented.

Thereafter, a new non-parametric narrowband blind spectrum sensing method based on the predicted eigenvalue threshold (PET) is introduced. This method is simplified to reduce the complexity without leading to any performance degradation. This constitutes one major contribution of our thesis. Also, we propose to combine a non-parametric Welch periodogram spectral estimator with an optimization algorithm to better estimate spectral components in the wideband case. The performance of this method is further improved by employing multiple-antennas at the receiver. This improved Welch periodogram method presents another contribution of this thesis.

The algorithms presented and proposed in this Chapter are mainly studied under the classical assumptions, i.e., a block flat fading frequency-non-selective channel in the presence of additive white Gaussian noise.

4.2 Spectrum Sensing for Cognitive Radio

4.2.1 Spectrum Sensing Concept

Here, we focus on the spectrum sensing as derived from the CR definition given in section 1.3, i.e. to monitor the activity in the radio spectrum and to identify the unoccupied frequency bands, also called *white spaces*. Sensing the spectrum and dynamically accessing the white spaces will significantly improve the spectrum utilization efficiency. In order for a CR to dynamically utilize available spectrum, it must be able to quickly and robustly determine which parts of the relevant spectrum are available or not.

A CR device must be able to give a general picture of the available medium over the entire radio spectrum of interest. All further processing and decision making performed by the communicating device is based on the results from the initial sensing. It is obvious that spectrum sensing is extremely important for a CR device to perform satisfactorily. Hence spectrum sensing is a cornerstone of CR. The most common scenario is the case of an unlicensed secondary user seeking to utilize idle parts of the spectrum when transmission from the licensed primary users is absent. In order to avoid interference with primary users, robust spectrum sensing should be performed.

Optimally, the spectrum sensing provides a full map of the spectrum occupancy on the wideband of interest $[f_{min}, f_{max}]$ at each sensing interval τ_{si} , as depicted in Figure 4.1. Actually, it is very complicated to perform that while still respecting the constraints mentioned above. Practically, the frequency support of a signal resides within several continuous intervals in a wide spectrum

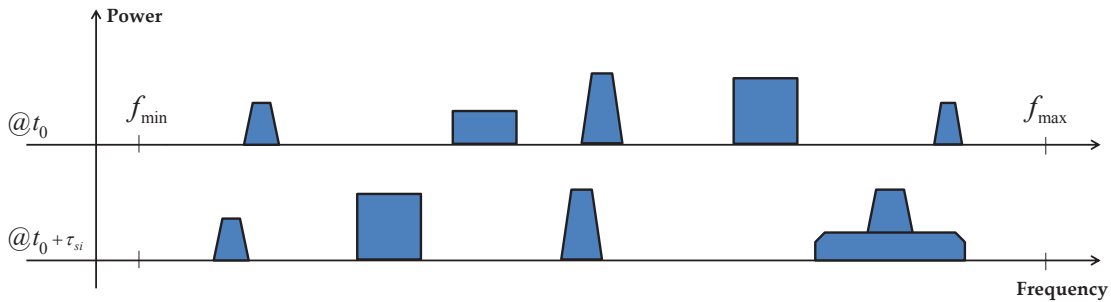


Figure 4.1: The general picture of the radio spectrum given each sensing interval τ_{si} . This Figure illustrates the opportunities in time and frequency.

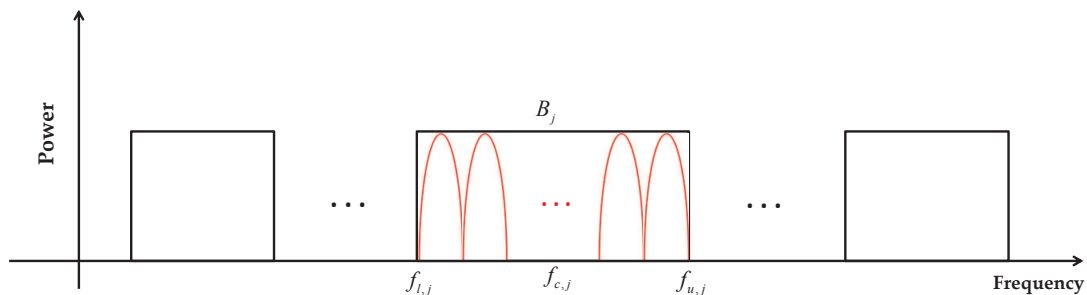


Figure 4.2: The wideband of interest in the form of multi-bands. The j^{th} wideband is characterized by its band-edge frequencies $f_{l,j}, f_{u,j}$, and it can be divided into several narrowbands.

but vanishes elsewhere. Each wideband consists of a number of narrowband transmissions as shown in Figure 4.2. The j^{th} wideband, $[f_{l,j}, f_{u,j}]$, of width B_j is divided into several subbands.

4.2.2 Sensing Methods Classification

Spectrum sensing can be classified into two categories, namely, NSS and WSS. In NSS, the entire bandwidth is modeled as a train of consecutive narrowband channels and sensing is done channel-by-channel. In order to implement this, an RF front-end with a tunable narrow bandpass filter is needed. To detect free channels in a given wideband of interest, spectrum sensing is performed over individual narrowband channels either sequentially or at random until a free channel is found. The disadvantage of NSS approach is the latency in finding a free band, since the local oscillator needs to be locked at a new frequency for every channel search.

In wideband sensing, the entire band of interest is processed at once to find a free channel. In practice, WSS systems are difficult to design, due to either high implementation complexity or high financial/energy costs.

Sensing methods are also classified, via the coherence criterion, into two categories: coherent and non-coherent sensing. In coherent sensing, the primary signal can be coherently detected by comparing the received signal or the extracted signal characteristics with a prior knowledge of primary signals. In non-coherent sensing, no prior knowledge is required. The sensing methods classification beside some examples are shown in Figure 4.3 [81].

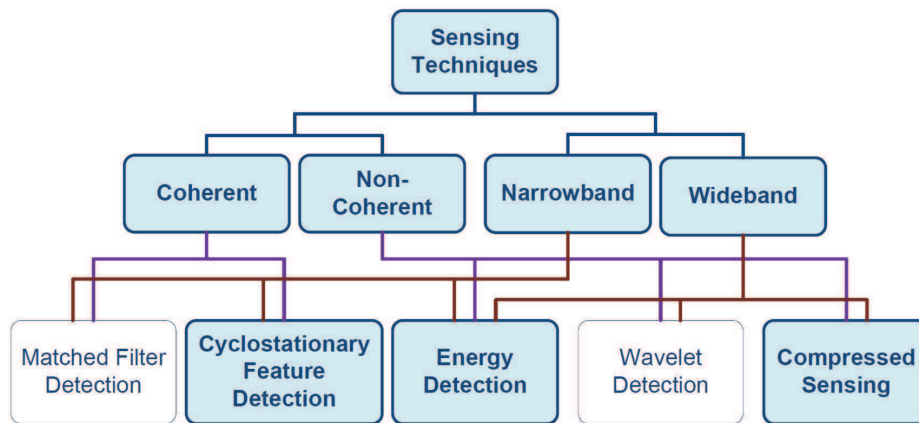


Figure 4.3: Spectrum sensing methods classification [81].

4.2.3 Cooperative Sensing

However, sensing performance in practice is often compromised with noise uncertainty, fading, and shadowing issues. Cooperation is proposed in the literature as a solution to mitigate the impact of these factors. The concept of cooperative sensing is to use multiple sensors (users/receivers) distributed in different locations and combine their measurements to one final decision. This is in essence a way of getting diversity gains.

While cooperation benefits such as improved sensing performance and relaxed sensitivity requirement can be obtained, cooperative sensing can result in cooperation overhead. This overhead refers to any extra sensing duration, delay, energy, and any performance degradation caused by cooperative sensing [81].

Generally speaking, there are two schemes to combine the observations of different sensors: data fusion and decision fusion. If each sensor sends its observed data to a specific sensor, which jointly processes the collected data and makes a final decision, this cooperation scheme is called data fusion. On the other hand, if multiple sensors process their observed data independently and send their decisions to a specific sensor, which then makes a common decision, it is called decision fusion.

Cooperative spectrum sensing is most effective when collaborating sensors observe independent fading or shadowing. It is found that it is more advantageous to have the same amount of users collaborating over a large area than over a small area [81]. Cooperation among CR users or receivers can be used to build a cooperative sensing network.

In the case of CR for railways, the cooperation can be possibly done among several receivers placed in the front, the end, and the two sides of the train. To increase the advantages of this cooperation, the positions of these receivers must be chosen to provide independent fading or shadowing. Another possibility to envisage is to employ the existing mobile users aboard train.

4.3 Narrowband Spectrum Sensing

4.3.1 Introduction

First, a bandpass filtering is applied to select the narrowband (a central frequency and bandwidth) of interest. There are two hypotheses,

$$\mathcal{H}_0, \text{ absence of PU signals, and } \mathcal{H}_1, \text{ at least one PU signal is present.} \quad (4.1)$$

and two decisions (hard decision),

$$\delta_0, \text{ no PU is present, and } \delta_1, \text{ a PU is present.} \quad (4.2)$$

In a binary hypothesis test there are two types of errors that can be made. Let $P_m = \mathbb{P}(\delta_0|\mathcal{H}_1)$ be the missdetection probability. The missed detection leads to harmful interference with existing PUs and hence degrades the performance of both the primary system and the secondary one. The probability of false alarm is defined as $P_f = \mathbb{P}(\delta_1|\mathcal{H}_0)$. In fact, false alarms lead to overlooking spectral opportunities and hence inefficient usage of the spectrum.

In general, a cognitive radio system should satisfy constraints on both P_f and P_m . A trade-off between these two probabilities has to be done knowing that protecting the PU is privileged to finding a free band. However, the probability of error ($P_f + P_m$) decreases as the number of observed signal samples increases. Hence, both constraints may be satisfied by selecting the number of samples to be large enough. But, large number of samples leads to a sensing period overhead. While selecting a sensing method, some tradeoffs among accuracy, complexity and sensing duration should be considered.

Furthermore, sensing methods should provide adequate performance at very low SNRs. For instance, the upcoming CR based standard IEEE 802.22, which is a high speed WRAN standard, requires the detector to sense a primary user at -116 dBm, usually equivalent to a SNR of -22 dB [82]. The required detection time for all three signal types (analog TV, digital TV and wireless microphones) is 2 seconds. The required sensing sensitivity is the power level at which the missdetection probability is less than 0.1, while the probability of false alarm is 0.1. Table 4.1 summarizes the required sensing receiver sensitivity for the three licensed signals types.

Many current spectrum sensing algorithms do not meet these requirements. Hence, there is a motivation to investigate why existing techniques do not provide satisfactory performance, and to propose new approaches to find a solution to this problem with a focus on the railway constraints (high speed and possible EM interferences).

4.3.2 Traditional Spectrum Sensing

Matched-filter Matched-filtering (MF) is known as the optimal method for detection of primary users when the transmitted signal is known as it maximizes the received SNR [83]. The main advantage of matched-filtering is the short time to achieve a certain level of false alarms or detection performance [84] as compared to other methods.

Table 4.1: Spectrum sensing requirements in IEEE 802.22

Parameter	Value for Wireless Microphones	Value for TV Broadcasting
Channel Detection Time	≤ 2 sec	≤ 2 sec
Sensing Sensitivity	-107 dBm (over 200KHz)	-116 dBm (over 6MHz)
Required sensing SNR	-12 dB	-21 dB
Probability of Detection	90%	90%
Probability of False Alarm	10%	10%

However, matched-filtering requires the perfect knowledge of some primary users signals features. Moreover, since CR needs receivers for all signal types, the implementation complexity of sensing unit is impractically large.

Energy Detection Energy detector (ED) based approach, also known as radiometry, is the most common spectrum sensing method because of its low computational and implementation complexities [84]. In addition, it is more generic as receivers do not need any knowledge on the PU signal. The signal is sensed by comparing the output of the energy detector with a threshold which depends on the noise floor. On the other hand, ED is very sensitive to noise uncertainty, and does not work for spread spectrum signals.

Cyclostationary Feature Detection Cyclostationary feature detection (CFD) is a method for detecting the PUs by exploiting the cyclostationary features in the modulated signals. Cyclostationarity based detectors have the potential to distinguish among the primary users, secondary users, and interference exhibiting cyclostationarity at different cyclic frequencies, in low SNR environments.

The cyclic spectral density (CSD) function of a received signal x can be calculated as [85]

$$S_x(f, \nu) = \sum_{\tau=-\infty}^{\infty} R_{x,\nu}(\tau) \exp(-j2\pi f\tau), \quad (4.3)$$

where ν is the cyclic frequency and the cyclic-autocorrelation function, $R_{x,\nu}(\tau)$, is given by the Equation (3.54).

The CSD function outputs peak values when the cyclic frequency is equal to the fundamental frequencies of transmitted signal. This method has several advantages such as: CFD is more robust to changing noise level than energy detection, and cyclostationarity detectors can work in lower SNR compared to EDs.

The main drawbacks of this method are: it requires prior knowledge on the PU's signal, if the SU does not have the knowledge of the cyclic frequencies giving the peak values of CSD, it needs to compute CSD for all possible cyclic frequencies and find the peak value. Therefore the implementation cost extremely increases [83]. Also, cyclostationarity based detection is very sensitive to synchronization errors, such as carrier frequency and sampling clock frequency offsets [86]. Table 4.2 lists advantages and drawbacks of the different traditional sensing techniques.

Table 4.2: Comparison among some properties, advantages and drawbacks of the different traditional spectrum sensing techniques

	Advantages	Drawbacks	Required N ^(*)
ED	- Non-coherent blind detection - Simplicity and low complexity	- Very sensitive to noise variations - Does not work for CDMA	$\mathcal{O}(\text{SNR})^{-2}$ [84]
MF	- Optimum method for detection - Short sensing duration	- Prior information about PU's signal - Implementation complexity - Large power consumption	$\mathcal{O}(\text{SNR})^{-1}$ [84]
CFD	- Higher performance than ED	- Known cyclic frequencies \Rightarrow unless very high complexity - Vulnerable to synchronization errors	Function of SNR and cyclic frequencies

^(*)Required N is defined by the number of samples needed to reach a certain level of P_m and P_f .

4.3.3 Multiple-antenna Spectrum Sensing

Multiple-antenna systems have been widely deployed to improve the transmission reliability in wireless communications. In a cognitive radio network, multiple-antenna SUs are beneficial not only for a reliable communications but also to improve the performance of spectrum sensing. Indeed, multiple-antennas at the receiver can cooperate to achieve higher sensing reliability. Therefore, in this thesis, we assume a multiple-antenna system model. In addition to being spatially correlated, the received signal samples are usually correlated in time due to several reasons [83]: the received signal is oversampled, the propagation channel is time-dispersive or the transmitted signal is correlated in time. Then, we can combine space and time correlations to improve the detection. That is why the smoothing factor was introduced in Equation (2.21). In the following, the different existing multiple-antenna spectrum sensing techniques are described.

Note that the signal model, used for NSS throughout this section, was presented in subsection 2.3.1.

The Likelihood Ratio Test It is the optimal solution since the Neyman-Pearson (NP) theorem states that, for a given probability of false alarm, the test statistic that maximizes the probability of detection is the likelihood ratio test (LRT) defined as $M_{\text{LRT}} = \frac{P(\mathbf{x}|\mathcal{H}_1)}{P(\mathbf{x}|\mathcal{H}_0)}$. Such a likelihood ratio test decides δ_1 when T_{LRT} exceeds a threshold λ_{LRT} , and δ_0 otherwise. The major difficulty in using the LRT is its requirements on the knowledge of the exact distributions of the signal and the noise as well as the channels, which is practically difficult to acquire.

If we assume that the noise and signal samples are both Gaussian distributed, the LRT becomes the estimator-correlator (EC) detector [83] for which the test statistic is given by

$$T_{\text{EC}} = \sum_{k=1}^N \mathbf{x}^T(k) \mathbf{R}_s (\mathbf{R}_s + \sigma_w^2 \mathbf{I}_M)^{-1} \mathbf{x}(k) \underset{\delta_0}{\overset{\delta_1}{\gtrless}} \lambda_{\text{EC}} \quad (4.4)$$

where $\mathbf{w}(k) \sim \mathcal{N}(0, \sigma_w^2 \mathbf{I}_M)$ and $\mathbf{s}(k) \sim \mathcal{N}(0, \mathbf{R}_s)$ (see Equation (2.20)); i.e. $\mathbf{R}_s = \mathbf{E}[\mathbf{s} \mathbf{s}^H]$. From Equation (4.4), we see that $\mathbf{R}_s (\mathbf{R}_s + \sigma_w^2 \mathbf{I}_M)^{-1} \mathbf{x}(k)$ is actually the minimum-mean-squared-error (MMSE) estimation of the source signal $\mathbf{s}(k)$. Thus, M_{EC} can be seen as the correlation of the

observed signal $\mathbf{x}(k)$ with the MMSE estimation of $\mathbf{s}(k)$. The EC detector needs to know the source signal covariance matrix \mathbf{R}_s and noise power σ_w^2 .

Energy Detector The EC detector needs the knowledge of \mathbf{R}_s which is unrealistic. Thus, if we further assume that $\mathbf{R}_s = \sigma_s^2 \mathbf{I}_M$, the EC detector is reduced to the energy detector for which the test statistic is given as follows:

$$T_{\text{ED}} = \sum_{k=1}^N \mathbf{x}^T(k) \mathbf{x}(k) \underset{\delta_0}{\overset{\delta_1}{\gtrless}} \lambda_{\text{ED}} \quad (4.5)$$

Note that for the multiple-antenna case, T_{ED} is actually the energy summation of signals from all antennas, which is a straightforward cooperative sensing scheme [83].

Let η_w be the noise uncertainty factor. The noise power estimation error (in dB) is assumed to be uniformly distributed in the interval $[-B, B]$ [84] (i.e. $B = \sup \{10 \log(\eta_w)\}$). The ED is denoted "ED-U(B dB)". The ED suffers of noise sensibility and its performance degrades when the noise uncertainty increases. Furthermore, it was shown in [84] that robust sensing is impossible for energy detector if SNR is lower than a certain threshold. This threshold is denoted SNR_{wall} and given, in dB, by

$$\text{SNR}_{\text{wall}} = 10 \log \left(\eta_B - \frac{1}{\eta_B} \right) \quad (4.6)$$

where $\eta_B = 10^{B/10}$.

The authors in [87] shown that the magnitude of the noise uncertainty without considering interference is at least $B = 1$ dB. So we see that for this noise uncertainty, the SNR wall is -3.3 dB. As a consequence, it is impossible for the ED to sense the presence of a primary user signal if its power is 3.3 dB less than that of the noise.

Generalized Likelihood Ratio Test In most practical scenarios, it is impossible to know the likelihood functions exactly, because of the existence of uncertainty about one or more parameters in these functions. The assumptions on the noise and signal simplify LRT to ED and EC detectors. The ED suffers of noise uncertainty while the EC detector is not blind.

The generalized likelihood ratio test (GLRT) is one efficient method [88, 89] to solve the above problem. For this method, the maximum likelihood estimation of the unknown parameters under \mathcal{H}_i ($i = 1, 2$) is first obtained as $\hat{\Theta}_i = \arg \max_{\Theta_i} P(\mathbf{x} | \mathcal{H}_i, \Theta_i)$, where Θ_i is the set of unknown parameters under \mathcal{H}_i . Then, the GLRT statistic is formed as

$$T_{\text{GLRT}} = \frac{P(\mathbf{x} | \hat{\Theta}_0, \mathcal{H}_1)}{P(\mathbf{x} | \hat{\Theta}_1, \mathcal{H}_0)} \underset{\delta_0}{\overset{\delta_1}{\gtrless}} \lambda_{\text{GLRT}} \quad (4.7)$$

In [88], the primary user signal is modeled as colored Gaussian with unknown covariance matrix. A GLRT procedure is applied to the problem. The resulting detector computes the arithmetic to geometric mean (AGM) of the eigenvalues of a sample covariance matrix and compares it with

a threshold

$$T_{\text{AGM}} = \frac{\frac{1}{M} \sum_{i=1}^M \ell_i}{\left(\prod_{i=1}^M \ell_i \right)^{1/M}} \underset{\delta_0}{\overset{\delta_1}{\gtrless}} \lambda_{\text{AGM}}, \quad (4.8)$$

where $\ell_1 \geq \dots \geq \ell_M$ are the eigenvalues of the sample covariance matrix. The AGM is a sphericity test. In [89, 90], the authors derive the GLRT detector when channel gains, and PU and noise powers are unknown under the form given below

$$T_{\text{GLRT}} = \frac{\ell_1}{\sum_{i=1}^M \ell_i} \underset{\delta_0}{\overset{\delta_1}{\gtrless}} \lambda_{\text{GLRT}}. \quad (4.9)$$

Optimally Combined Energy Detection The multiple-antenna techniques are employed to exploit the spatial correlations of multiple received signals. The maximum ratio combining (MRC), the equal gain combining (EGC) and the selection combining (SC) techniques are applied to better sense the spectrum [83]. These methods are ED based and suffers of the noise uncertainty. The authors in [91] proposed an optimal combining energy detection (OCED) method. The idea behind OCED is to find a linear combining transformation such that the resultant signal has the largest SNR. The signals from all antennas are combined with a matrix \mathbf{C} such as $\mathbf{z}(k) = \mathbf{C}^T \mathbf{x}(k)$, $k = 1, 2, \dots, N$. The test is defined as $T_{\text{OCED}} = \frac{1}{N} \sum_{k=1}^N \|\mathbf{z}(k)\|^2$. It is obvious that the SNR after combining is [91]

$$\eta(\mathbf{C}) = \frac{E \left[\|\mathbf{C}^T [\mathbf{x}(k) - \mathbf{w}(k)]\|^2 \right]}{E \left[\|\mathbf{C}^T \mathbf{w}(k)\|^2 \right]} = \frac{\text{tr}(\mathbf{C}^T \mathbf{R}_s \mathbf{C})}{\sigma_w^2 \text{tr}(\mathbf{C}^T \mathbf{C})},$$

where $\text{tr}(\cdot)$ is the trace of the matrix argument. Hence, the optimal combining matrix should maximize the value of function $\eta(\mathbf{C})$. Let \mathbf{v}_1 be the corresponding eigenvector to λ_{\max} the maximum eigenvalue of \mathbf{R}_s . It can be proved that the optimal combining matrix degrades to the vector \mathbf{v}_1 [91]. Therefore, $T_{\text{OCED}} = \frac{\lambda_{\max}}{\sigma_w^2}$. This test statistic is optimal in terms of SNR. The OCED needs the knowledge of the noise power and the maximum eigenvalue of \mathbf{R}_s , which is usually unknown.

Eigenvalue and Covariance Based Sensing The structure of the covariance matrix at the receiver is not the same in the absence/presence of primary signals. From Equation (2.25), if no signal is present, the off-diagonal elements of $\mathbf{R}_{L,x}$ are all zeros. If there is at least one signal, $\mathbf{R}_{L,s}$ is not a diagonal matrix. Hence, some of the off-diagonal elements of $\mathbf{R}_{L,x}$ should be nonzero. This property could be exploited for spectrum sensing either directly (using the entries of the sample covariance matrix $\mathbf{R}_{L,x}(N)$) or indirectly (using the eigenvalues of $\mathbf{R}_{L,x}(N)$).

Let $r_{n,m}$ denotes the $(n, m)^{\text{th}}$ element of the sample covariance matrix $\mathbf{R}_{L,x}(N)$. Two covariance based sensing methods were proposed in [92]: the covariance absolute value (CAV), and the

covariance Frobenius norm (CFN) detection . The test statistics of these methods are given by

$$T_{\text{CAV}} = \frac{\sum_{n=1}^{ML} \sum_{m=1}^{ML} |r_{n,m}|}{\sum_{m=1}^{ML} |r_{m,m}|} \underset{\delta_0}{\overset{\delta_1}{\geq}} \lambda_{\text{CAV}}, \quad T_{\text{CFN}} = \frac{\sum_{n=1}^{ML} \sum_{m=1}^{ML} |r_{n,m}|^2}{\sum_{m=1}^{ML} |r_{m,m}|^2} \underset{\delta_0}{\overset{\delta_1}{\geq}} \lambda_{\text{CFN}} \quad (4.10)$$

The authors in [93] introduced two eigenvalue based sensing methods, namely, the maximum-minimum eigenvalue (MME) detection algorithm and energy with minimum eigenvalue (EME) detection algorithm as

$$T_{\text{EME}} = \frac{\frac{1}{MLN} \sum_{k=1}^N \mathbf{x}_L^T(k) \mathbf{x}_L(k)}{\ell_{ML}} \underset{\delta_0}{\overset{\delta_1}{\geq}} \lambda_{\text{EME}}, \quad T_{\text{MME}} = \frac{\ell_1}{\ell_{ML}} \underset{\delta_0}{\overset{\delta_1}{\geq}} \lambda_{\text{MME}} \quad (4.11)$$

Each test statistic is compared to a threshold to decide the presence of a primary signal.

Blind Spectrum Sensing by Information Theoretic Criteria This technique is an approach originally introduced to estimate the number of source signals [94]. Then, the information theoretic criteria (ITC) method can be directly applied to conduct spectrum sensing, as proposed in [95]. The basic idea is when the primary user is absent, the estimated number of source signals via ITC should be zero. Hence, by comparing the estimated number of source signals with zero, the presence of the primary user can be detected. The estimated number of source signals is determined by

$$\hat{k}_{\text{ITC}} = \arg \min_{k=0, \dots, q-1} \text{ITC}(k) = \arg \min_{k=0, \dots, q-1} -\log \left(\frac{\prod_{i=k+1}^q \ell_i^{1/q-k}}{\frac{1}{q-k} \sum_{i=k+1}^q \ell_i} \right)^{N(q-k)} + b(k) \quad (4.12)$$

where $b(k)$ is a penalty function and $q = ML$. The well-known criteria, Akaike information criterion (AIC) and minimum description length (MDL) criterion, are defined by $b(k) = k(2q - k)$ and $b(k) = [\frac{1}{2}k(2q - k) + \frac{1}{2}] \log N$, respectively [94]. This method produces the exact number of sources while it is sufficient to check if this number is larger than zero or not. In [95], the authors propose a simplified ITC (SITC) algorithm to conduct the spectrum sensing. This algorithm is based on the fact that if there is one value \hat{k} (> 0) that minimizes the ITC metric, then $\text{ITC}(0) > \text{ITC}(1)$ with high probability. Then, the decision metric is

$$\text{ITC}(0) \underset{\delta_0}{\overset{\delta_1}{\geq}} \text{ITC}(1)$$

In SITC algorithm, only two criterion values ($k = 0, 1$) should be computed and compared. It can significantly reduce the computational complexity while having almost no performance loss.

Analysis and Motivations The above methods can be summarized as follows:

1. the likelihood test (LRT), its simplified versions (ED and EC), and its generalized ones (AGM and GLRT),
2. the methods based on combining the received signals from all the antennas (EGC, MRC, and OCED),
3. the methods based on the sample covariance matrix structure (CAV and CFN) or its eigenvalues structure (EME and MME),
4. the methods derived from the sources number estimation ones (ITC).

Some of these methods are not blind (LRT, EC and OCED) or sensitive to noise power variations (ED, EGC and MRC). Several existing methods need no information on the transmitted signal and the channel. Also, these methods do not need noise power estimation and overcome the sensibility to noise uncertainty. Some among these methods give a less detection performance when compared to the rest (EME, ITC, CAV, and CFN). Among the remaining methods (GLRT, AGM and MME) the GLRT detector gives the best detection performance in the low SNR region. But, the GLRT was derived in the presence of only one primary user signal. The objective of our work is to find another fast and blind method that outperforms these methods in the low SNR region and remains valid in a more general scenario.

In what follows, we introduce a non-parametric blind spectrum sensing method based on the PET originally introduced in [96]. This method was employed to detect the number of communications sources. Here, the PET method is applied for spectrum sensing, since it is a special case of source number detection problem. Thereafter, we will simplify the PET method to reduce the complexity with no performance loss. This simplified PET (SPET) method represents one of the major contributions of this thesis.

4.3.4 Predicted Eigenvalues Threshold

4.3.4.1 Mathematical Preliminaries

The rank of the part of the covariance matrix that represents the signal (i.e., $\mathbf{H}\mathbf{R}_{L,s}\mathbf{H}^H$) is $C + PL$. Hence, the lowest eigenvalue of $\mathbf{R}_{L,x}$ is equal to σ_w^2 and its multiplicity order is equal to $(M - P)L - C$ [97]. By applying the eigenvalue decomposition, the matrix $\mathbf{R}_{L,x}$ has a diagonal form,

$$\mathbf{U}^H \mathbf{R}_{L,x} \mathbf{U} = \text{diag}(\vartheta_1, \dots, \vartheta_{C+PL}, 0, \dots, 0) + \sigma_w^2 \mathbf{I}_{ML} \quad (4.13)$$

in the basis \mathbf{U} , where $\vartheta_1 \geq \vartheta_2 \geq \dots \geq \vartheta_{C+PL} > 0$. Obviously, $\lambda_k = \vartheta_k + \sigma_w^2$ for $1 \leq k \leq C + PL$. This result requires that the matrix \mathbf{H} is overdetermined, i.e., $L > \frac{C}{M-P}$. For simplicity, we define $q = ML$ for the rest of the Chapter.

Theorem 2. *Suppose $N\mathbf{R}_{L,x}(N)$ has the complex Wishart distribution $\mathbf{W}_q(N, \mathbf{R}_{L,x})$, and the eigenvalues of $\mathbf{R}_{L,x}(N)$ and $\mathbf{R}_{L,x}$ are $\ell_1 \geq \dots \geq \ell_q$ and $\lambda_1 \geq \dots \geq \lambda_k = \dots = \lambda_q = \lambda$ respectively. The limiting distribution of ℓ_k^{av} , the average of the lowest $q - k$ eigenvalue, as $N \rightarrow \infty$, is*

$$(N(q - k))^{(1/2)} (\ell_k^{av} - \lambda) / \lambda \xrightarrow{\text{dist}} \mathcal{N}(0, 1). \quad (4.14)$$

In the absence of signal, the matrix $N\mathbf{R}_{L,x}(N)$ follows a Wishart complex distribution, i.e. $N\mathbf{R}_{L,x}(N) \sim \mathbf{W}_q(N, \mathbf{R}_{L,x})$. Based on that, the authors in [96] proposed an upper bound for each eigenvalue of the noise subspace. The upper threshold of ℓ_k is predicted as

$$\ell_k^{up} = \underbrace{\left[(m_k + 1) \frac{1 + t[N(m_k + 1)]^{1/2}}{1 - t(N \cdot m_k)^{-1/2}} - m_k \right]}_{\eta_k(t)} \underbrace{\frac{1}{q - k} \sum_{i=k+1}^q \ell_i}_{\ell_k^{av}} \quad (4.15)$$

where ℓ_k^{av} is the average of the $m_k (= q - k)$ lowest eigenvalues, $\eta_k(t)$ is the prediction factor and t is a two-direction threshold that represents the confidence interval of the averaged eigenvalue. The eigenvalue ℓ_k is considered in the noise subspace when it satisfies the following condition

$$\ell_k \leq \ell_k^{up}. \quad (4.16)$$

Figure 4.4 shows the adaptive PET model of the sample covariance matrix eigenvalues. It is clear that the noise subspace dimension is $(M - P)L$, while each PU is represented by L eigenvalues (PL in total). Each signal eigenvalue exceeds its own predicted threshold.

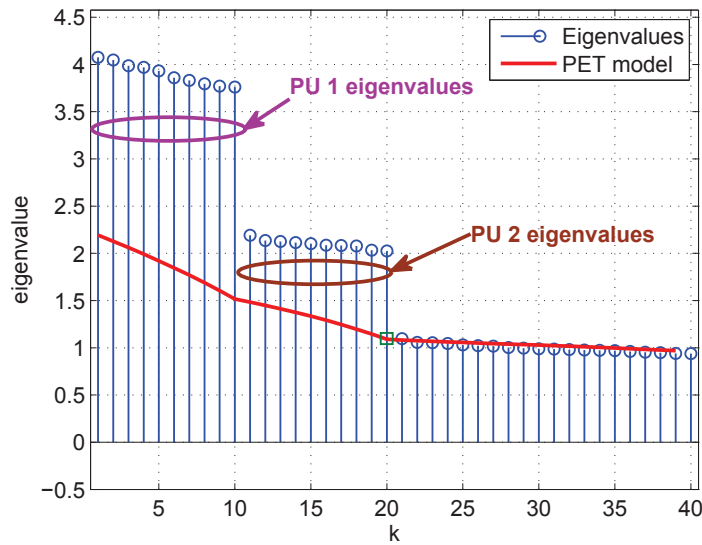


Figure 4.4: The eigenvalues of the sample covariance matrix and the adaptive PET model at $N = 1000$, $P = 2$, $M = 4$ and $L = 10$.

Remark on the noise-only covariance matrix

Under the assumption that the noise samples are i.i.d, the covariance matrix is given by $\sigma_w^2 \mathbf{I}_{ML}$ in the absence of PUs. This is usually true if no narrowband filtering is applied at the receiver. However, if it is the case, the noise samples may be correlated. To solve this problem, a pre-whitening technique is applied on the noise samples to transform the covariance matrix to a diagonal one [92]. The used pre-whitening technique is presented in Appendix C.2.

4.3.4.2 Predicted Eigenvalues Threshold Based Spectrum Sensing

The PET method is employed for detecting the communications sources number. It is based on (4.16) and consists in adaptively modeling the noise eigenvalues increase to determine the dimension of the noise subspace, and hence, the signal subspace dimension. Actually, the PET model is controlled by a single parameter t . Spectrum sensing problem is a special case of the sources number detection one. In the absence of PUs, the estimated number of source signals should be zero. The original PET (OPET) method, as described above, can be applied directly to conduct spectrum sensing. Based on that, the two hypotheses in (4.1) are reformulated as,

$$\begin{aligned} \mathcal{H}_0 : \hat{k} &= 0, \ell_k \leq \ell_k^{up}, k = 1, 2, \dots, q-1 \\ \mathcal{H}_1 : \hat{k} &\geq 1, \hat{k} = \arg \max_{k=1, \dots, q-1} \ell_k > \ell_k^{up}. \end{aligned} \quad (4.17)$$

In the presence of P primary users, the dimension of signal subspace is $PL + \sum_{j=1}^P C_j$ (i.e., the contribution of PU_j is equivalent to $L + C_j$ eigenvalues). The idea is to detect *at least* one PU under \mathcal{H}_1 . Since C_j is unknown and difficult to be estimated, the presence of PUs is reflected by *at least* L signal eigenvalues.

It is clear from (4.13) that when a certain eigenvalue $\lambda_{\hat{k}}$ belongs to the signal subspace, then $\lambda_1, \dots, \lambda_{\hat{k}}$ are all signal eigenvalues. This leads to the fact that when ℓ_1 is noise eigenvalue then \mathcal{H}_0 is detected, i.e., there is no PU signal when every eigenvalue does not exceed its own predicted threshold. Also, \mathcal{H}_1 is detected when ℓ_L corresponds to signals. Therefore, the spectrum sensing problem as defined in (4.1) is modified to

$$\begin{aligned} \mathcal{H}_0 : \ell_1 / \ell_1^{av} &\leq \eta_1(t), \\ \mathcal{H}_{1,0} : \ell_1 / \ell_1^{av} &> \eta_1(t), \\ \mathcal{H}_{1,1} : \ell_L / \ell_L^{av} &> \eta_L(t). \end{aligned} \quad (4.18)$$

where ℓ_k^{av} is defined in (4.15). The $\mathcal{H}_{1,0}$ hypothesis indicates the presence of a weak PU's signal, while $\mathcal{H}_{1,1}$ is the sensing state for the presence of relatively non-weak signal. This method is called the modified PET (MPET).

This extra information is either sent to the media access control (MAC) layer of the CR to be employed for the adaptive joint scheduling of spectrum sensing and data transmission, or sent to the fusion center when multiple sensors are cooperating for a final decision by combining their spectrum sensing results.

Furthermore, this extra information could be provided more precisely through a confidence metric which is a measure of the confidence that the spectrum sensor has in the signal presence decision. The confidence metric is obtained as,

$$\text{confidence metric} = \frac{k_c}{L}, 0 \leq k_c \leq L \quad (4.19)$$

where k_c is the index of the lowest eigenvalue, among the first L of the decreasingly ordered eigenvalues, that does exceed its predicted threshold. A confidence metric varies between a min-

imum of zero indicating no confidence in the signal presence and one indicating total confidence in the signal presence [82].

4.3.4.3 Simplified Predicted Eigenvalues Threshold Method

The above discussion indicates that the PET method could be simplified to employ only the largest eigenvalue of the sample covariance matrix. Indeed, when ℓ_1 corresponds to noise, we are confident that all eigenvalues belong to the noise subspace. On the other hand, if ℓ_1 is a signal eigenvalue, the PU detection must not be missed even though all the other eigenvalues corresponds to noise. This is due to the privilege of protecting PUs over spectrum utilization efficiency. Then, the PET method is simplified to test the largest eigenvalue against its own predicted threshold. Hence, the sensing problem can be expressed as $\ell_1/\ell_1^{av} \underset{\delta_0}{\overset{\delta_1}{\gtrless}} \eta_1(t)$, and is altered to

$$T_{\text{SPET}} = \frac{\ell_1}{\frac{1}{q} \sum_{i=1}^q \ell_i} \underset{\delta_0}{\overset{\delta_1}{\gtrless}} \lambda_{\text{SPET}} \quad (4.20)$$

This decision statistic was found in [89,90] based on GLRT for a single source through memoryless channel. Our work extends this decision statistic to a more general scenario. The outline of the proposed SPET method is described by the Algorithm 4.1.

Algorithm 4.1 SPET sensing method.

1. Compute $\mathbf{R}_{L,x}(N)$, the sample covariance matrix of received signals, as defined in (2.26).
 2. Obtain the ML eigenvalues of $\mathbf{R}_{L,x}(N)$ such as $\ell_1 \geq \dots \geq \ell_{ML}$.
 3. Calculate the decision statistic T_{SPET} introduced in (4.20).
 4. Decide the presence of PU's signal when $T_{\text{SPET}} > \lambda_{\text{SPET}}$, otherwise, the absence of signals is stated, where λ_{SPET} is chosen to achieve a certain level of false alarm probability.
-

4.3.4.4 Performance Analysis and Discussion

The performance of OPET method is controlled by t . The two-direction threshold t is chosen to satisfy a certain level of the false alarm probability P_f . For more details on the expressions of P_m and P_f of OPET refer to [96]. Here, we will focus on performance analysis of SPET.

Probability of False Alarm New results in random matrix theory (RMT) revealed that ℓ_1 converges in distribution to a Tracy-Widom distribution of order β ($\beta=1, 2$ for real or complex observations, respectively) when $\mathbf{R}_{L,x}(N)$ follows a Wishart distribution of order N [98]. The authors in [90] established that these results imply that asymptotically T_{SPET} also follows a Tracy-Widom distribution.

Theorem 3. *Let $\mathbf{R}_{L,x}(N)$ follows a Wishart distribution with parameters N, q and T_{SPET} be the ratio of largest eigenvalue to the average trace. Then, as $N, q \rightarrow \infty$, with $c_N = \frac{q}{N} \rightarrow c \geq 0$, the*

following holds

$$\mathbb{P} \left[\frac{T_{\text{SPET}} - \mu_{N,q}}{\sigma_{N,q}} < \lambda_{\text{SPET}} \right] \approx F_{\beta}(\lambda_{\text{SPET}}) - \frac{1}{\beta q N} \left(\frac{\mu_{N,q}}{\sigma_{N,q}} \right)^2 F_{\beta}''(\lambda_{\text{SPET}}) \quad (4.21)$$

where the centering and scaling constants are

$$\mu_{N,q} = (1 + \sqrt{c_N})^2, \quad \sigma_{N,q} = N^{-\frac{2}{3}} (1 + \sqrt{c_N}) \left(1 + \frac{1}{\sqrt{c_N}} \right)^{1/3}, \quad (4.22)$$

and $F_{\beta}(\cdot)$ is the cumulative distribution function of the Tracy-Widom law of order β , while F_{β}'' denotes the second derivative of F_{β} .

In [99], it was established that this approximation is accurate for finite value of N and q , even when $N \gg q$. Hence, the probability of false alarm is given by

$$P_f = \mathbb{P} [T_{\text{SPET}} > \lambda_{\text{SPET}} | \mathcal{H}_0] = 1 - F_{\beta} \left(\frac{\lambda_{\text{SPET}} - \mu_{N,q}}{\sigma_{N,q}} \right) + \frac{1}{\beta q N} \left(\frac{\mu_{N,q}}{\sigma_{N,q}} \right)^2 F_{\beta}'' \left(\frac{\lambda_{\text{SPET}} - \mu_{N,q}}{\sigma_{N,q}} \right) \quad (4.23)$$

Now for a given P_f , the threshold λ_{SPET} is obtained based on (4.23). Obviously, the decision threshold is independent of the noise power and the channel gains, and depends only on N , M , L and P_f .

Missdetection Probability The sample covariance matrix is no longer a Wishart matrix in the presence of a signal. Here, we try to approximate the missdetection probability in the presence of single strong source, i.e., the signal subspace contains an eigenvalue of multiplicity L . Under this assumption, it is clear that $\frac{1}{q} \sum_{i=1}^q \ell_i \simeq \frac{1}{q} [L\ell_1 + \sum_{i=L+1}^q \ell_i]$ and the missdetection probability is given by

$$P_m = \mathbb{P} [T_{\text{SPET}} < \lambda_{\text{SPET}} | \mathcal{H}_1] = 1 - \mathbb{P} \left[\frac{\ell_1}{\sigma_w^2} > \frac{(q-L)\lambda_{\text{SPET}}}{q-L\lambda_{\text{SPET}}} \xi \right] \quad (4.24)$$

where $\xi = \frac{\frac{1}{q-L} \sum_{i=L+1}^q \ell_i}{\sigma_w^2}$ is asymptotically approximated to unity [89]. Also the largest eigenvalue has a limiting Gaussian distribution as follows [100]

$$\ell_1 \xrightarrow{\text{dist}} \mathcal{N} \left(\lambda_1 + \frac{(q-L)\lambda_1\sigma_w^2}{N(\lambda_1 - \sigma_w^2)}, \frac{\lambda_1^2}{N} \right), \quad (4.25)$$

which implies that $\frac{\ell_1}{\sigma_w^2} \xrightarrow{\text{dist}} \mathcal{N}(\mu_n, \sigma_n^2)$, where $\mu_n = (1 + M\rho) \left(1 + \frac{L(M-1)}{MN\rho} \right)$, $\sigma_n^2 = \frac{(1+M\rho)^2}{N}$ and ρ is the instantaneous received SNR. Hence, P_m is approximated as

$$P_m = 1 - \text{Q} \left(\frac{\sqrt{N}}{1 + M\rho} \frac{M-1}{M} \lambda_{\text{SPET}} - \sqrt{N} - \frac{L(M-1)}{M\rho\sqrt{N}} \right) \quad (4.26)$$

The average missdetection probability is computed by averaging over the distribution of ρ . Calculations of the missdetection probability are more detailed in Appendix C.1.

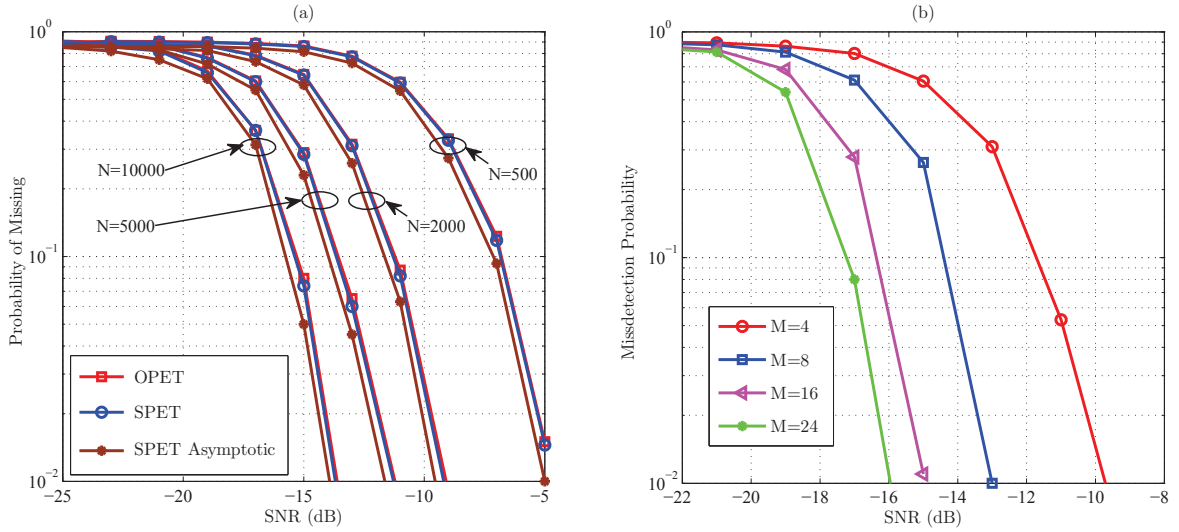


Figure 4.5: (a) Missdetection probability versus SNR for OPET and SPET methods compared with the asymptotic results at different values of the number of the observed samples when $M = 4$, $L = 1$ and $P = 1$. (b) SPET missdetection probability versus SNR for different numbers of antennas when $N = 5000$, $L = 1$ and $P = 2$.

4.3.4.5 Numerical Results and Discussion

Here, we present some simulations results to demonstrate the effectiveness of the proposed sensing methods. These methods are evaluated through the missdetection probability at a false alarm probability of $P_f = 0.1$. All results are based on 1000 Monte Carlo trials for each method. For each realization, the binary phase-shift keying modulated PU signals are randomly generated. Also, the random channel taps follow a Gaussian distribution. For different values of SNR, a random additive white Gaussian noise is added.

Figure 4.5(a) compares the sensing performance of OPET and SPET with the asymptotic results in (4.23) and (4.26). These simulations are done for different values of N . Based on simulations, the two-direction threshold t is chosen 1.108 to achieve a false alarm probability of 0.1. It is clear that the SPET method simplifies the original one to reduce the complexity without leading to any performance loss. Also, the simulations reveal that the asymptotic results provides a good approximation of the SPET sensing performance. Comparing the missdetection probability for different values of N shows that the performance improves when the number of the observed samples at the receiver is larger.

Furthermore, Figure 4.5(b) shows that as the degree of freedom M increases, the missdetection probability decreases, while the false alarm probability is still under certain level, without sacrificing any other metrics such as sensing duration or secondary user throughput. On the other hand, increasing M does increase the computational complexity of the SPET method.

The performance of MPET method is illustrated in Figure 4.6. This performance is evaluated by the detection probability of weak signals and that of relatively non-weak signals, set to as $P_{d,0} = \mathbb{P}(\mathcal{H}_{1,0} \text{ is decided} | \mathcal{H}_1)$ and $P_{d,1} = \mathbb{P}(\mathcal{H}_{1,1} \text{ is decided} | \mathcal{H}_1)$ respectively. This Figure depicts the detection probability and the false alarm probability of MPET, SPET methods. Obviously,

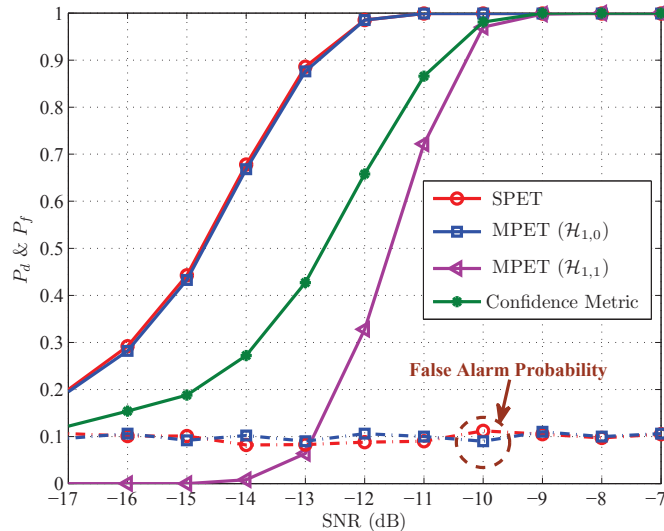


Figure 4.6: The MPET sensing performance (under $\mathcal{H}_{1,0}$ and $\mathcal{H}_{1,1}$) compared with SPET method when $N = 10000$, $M = 4$, $P = 2$, $L = 1$ and $C_1 = C_2 = 6$. Also, the introduced confidence metric, based on PET, is displayed.

the detection probability of a weak signal is identical to that of SPET which is well confirmed by simulation results. On the other hand, the presence of relatively non-weak signal is stated with a detection probability of 0.9 when the SNR is about -10 dB. Also, it is clear that the proposed confidence metric converges to $P_{d,1}$ when the SNR is relatively not-very-low (> -10 dB). For lower values of SNR, we are a little confident of the PU presence but the statement that its signal is relatively non-weak can not be declared.

A performance comparison among several sensing methods is provided in Figure 4.7. The optimal, but not blind, OCED method [91] outperforms the ED as it maximizes the SNR. The ED suffers of noise uncertainty. It is clear that the performance significantly degrades when $B = 1$ dB; i.e. for ED-U(1 dB). Among the different blind methods the SPET one has the best performance followed by the AGM method [88]. The MME detection [93] is a bit less effective than the AGM detector but outperforms the CAV detector [92]. The CAV detection is directly based on the entries of the sample covariance matrix. Therefore, this method has a smaller complexity but it is less representative of the signals. Even though the ITC based methods [95] offer a low false alarm probability, they are not as efficient as the other blind methods.

4.3.5 Conclusions

The PET method, originally used for number of communications sources detection, is employed for multiple-antenna spectrum sensing. This method is simplified to significantly reduce the computational complexity without any performance loss compared with the original PET. The detection performance is well predicted by the asymptotic analysis which is based on new results in random matrix theory. The SPET test statistic generalizes that of the GLRT [89] to a more general scenario. The blind non-parametric SPET detector outperforms the other blind detectors existing in the literature.

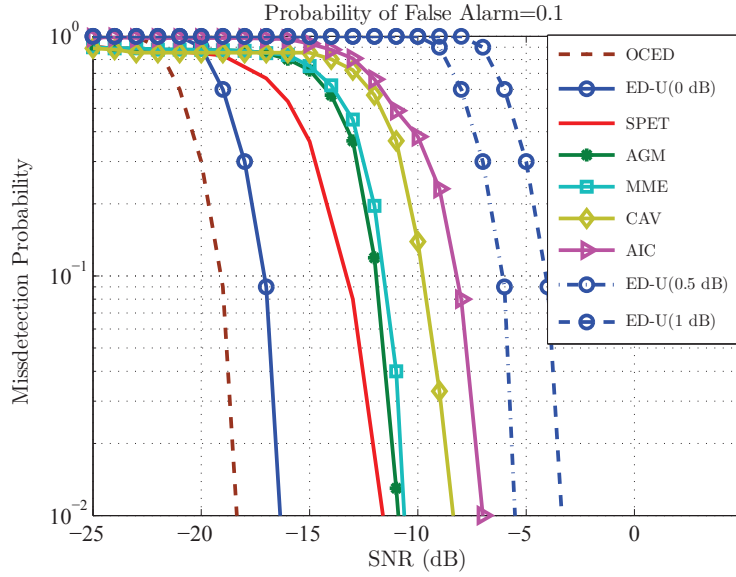


Figure 4.7: Missdetection probability versus SNR for several sensing methods when $N = 10000$, $M = 4$, $P = 2$, $C_1 = C_2 = 6$ and $L = 1$.

4.4 Wideband Spectrum Sensing

The traditional way for detecting holes in a wideband spectrum is subband-by-subband scanning using NSS techniques, while in WSS, the entire band of interest is processed at once to determine the occupied portions of the spectrum.

4.4.1 Preliminary Literature Review

Several existing WSS approaches in the literature are discussed. This includes: *i*) wavelet detection [101], *ii*) spectral estimation based detection [102,103], and *iii*) compressed sensing [104,105]. Thereafter, we propose an improved Welch periodogram based WSS by introducing a second refined estimation of the spectral properties, and by employing multiple-antennas to reduce complexity and sampling rates. This improved method is another important contribution of our thesis.

4.4.1.1 Wavelet Based Sensing

In [101], a wavelet approach for efficient WSS was developed. As a powerful mathematical tool for analyzing singularities and edges, the wavelet transform is employed to detect spectrum singularities such as band edges. Hence, this method is also called edge detection.

The signal spectrum over a wide frequency band contains several occupied subbands (see Figure 4.2), where the PSD is smooth within each subband B_k and exhibits irregularities on the border of two adjacent subbands. Once the edges, which correspond to transitions from an occupied band to an empty band or vice versa, are detected, the powers within bands between two edges are estimated. Then, the problem is reduced to the estimation of the edge frequencies of each

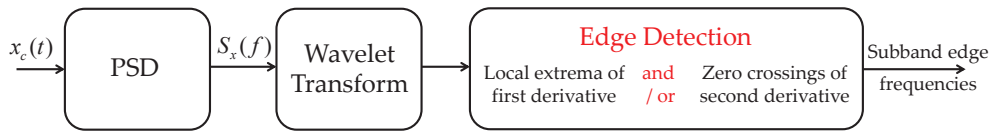


Figure 4.8: Block diagram of the wavelet based WSS technique (also known as the edge detector) [101].

subband. Discontinuities in the frequency domain (i.e. the boundaries of each subband) are given by the extrema of the first derivative and/or by the zero crossings values of the second derivative of the wavelet transform. Figure 4.8 illustrates the block diagram of this technique. However, this method demands sampling the signal at Nyquist rate (f_{Nyq}) which results in energy expensive analog-to-digital converters (ADCs). Practically, the PSD is smoother and does not exhibit exactly sharp discontinuities along the frequency axis. This will make the use of wavelet transform more difficult.

4.4.1.2 Spectral Estimation Based Detection

Various spectral estimation approaches can be found in the literature. While non-parametric methods usually estimate the PSD directly from the signal and require less computational complexity, the parametric ones produce better results when the available data records of the signal are relatively short. The simplest non-parametric method is the periodogram and its different versions.

A more advanced non-parametric method is the multitaper spectrum estimation (MTSE) [103]. In MTSE, the PSD is estimated by averaging over output of several filters or tapers. The tapers are orthogonal to each other and are centered on central frequency f_c . These filters are a Slepian base vectors. The remarkable property of Slepian sequences is that their Fourier transforms have the maximal energy concentration in the bandwidth $2W$ (centered on f_c) under a finite sample-size constraint. After MTSE, by analyzing this feature, CR users can identify whether there is spectrum opportunity or not. This method is efficient for small sample spaces, but it is regarded as a computationally intensive procedure.

Filter bank based spectrum estimation (FBSE) is done by introducing only one prototype filter for each band, and is proposed for cognitive radio networks in [102]. The wideband spectrum is considered as the output of a bank of prototype filters (with different shifted central frequencies). Based on the filters outputs, spectrum occupancy can be obtained to identify the spectrum opportunities. For the comparison, MTSE is better for small sample spaces whereas FBSE is better for large number of samples [102]. Furthermore, MTSE approach increases the computational complexity and hence might not be suitable for CR systems in which the wideband has to be quickly sensed. However, the implementation of the filter bank approach requires a large number of RF components for sensing a wideband spectrum. The spectral estimation methods propose solutions to accelerate the spectrum scanning while still demand a high sampling rate (i.e. \geq Nyquist sampling rate).

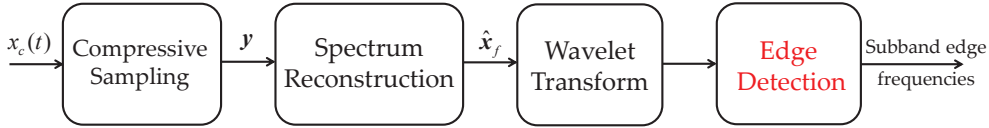


Figure 4.9: Block diagram of the wavelet based WSS technique combined with compressive sensing [104].

4.4.1.3 Compressive Sensing

Compressive sensing (CS) technique is based on acquiring the signals through a few non-adaptive linear measurements at a rate lower than f_{Nyq} . Thereafter, the signal spectrum is reconstructed efficiently from this incomplete set of measurements [106]. It is possible to reconstruct an arbitrary signal from an incomplete set of linear measurements when it is constrained to be sparse in some basis (the sparsifying basis), i.e., the signal only have a few non-zero coordinates in this basis. Let us consider that the frequency representation of the signal is sparse (i.e. assuming that majority of the subbands are unoccupied). Then, the signal can be sampled at a sub-Nyquist rate while its spectrum can be reconstructed with a high probability. The reconstructed spectrum is called *sparsogram*.

Let the wideband received signal, $x_c(t)$, be sampled at the rate f_s . A sampled signal vector \mathbf{x} of length N is obtained. The signal is represented in the frequency domain by \mathbf{x}_f which is obtained using the discrete Fourier transform (DFT) by

$$\mathbf{x}_f = \mathbf{F}\mathbf{x} \quad (4.27)$$

where \mathbf{F} is the discrete Fourier matrix. The samples vector is compressed into a vector of lower dimension $d < N$ as follows

$$\mathbf{y} = \mathbf{\Phi}\mathbf{x} \quad (4.28)$$

where $\mathbf{\Phi}$ is the $d \times N$ measurement matrix, i.e. $N - d$ samples are skipped. Based on the compressive sensing theory [106], the sparsogram can be recovered from the d samples by solving the l_1 -norm optimization problem

$$\hat{\mathbf{x}}_f = \arg \min \|\mathbf{x}_f\|_1, \quad \text{subject to } \mathbf{y} = \mathbf{\Phi}\mathbf{F}^{-1}\mathbf{x}_f \quad (4.29)$$

The idea behind CS is to combine both the signal acquisition and the compression process by directly sensing the essential part of the signal using fewer linear measurements. The assumptions made in [101] for wavelet edge detection are relaxed for building a practical sensing algorithm. The method proposed in [101] is extended in [104] by assuming that the signal spectrum is sparse, and employing sub-Nyquist sampling (via non-uniform sampling or random sampling) to obtain coarse spectrum knowledge in an efficient way; see Figure 4.9.

To practically realize the CS by sub-Nyquist rate sampling the analog-to-information convertors (AICs) were proposed. In [107] the AIC is based on random sampling system that can be implemented in practical hardware, before applying an efficient information recovery algorithm

to compute the sparsogram. The proposed implementation of this random AIC uses a parallel bank of low-rate ADCs that have equal shifts between their starting conversion points. This creates a shift in the samples that are produced from each of the parallel ADCs. The switching mechanism among their outputs is then pseudo-randomly controlled. The implementation of this random analog-to-digital converter (RADC) system is shown in Figure 4.10. This can be viewed as a random selection compression matrix.

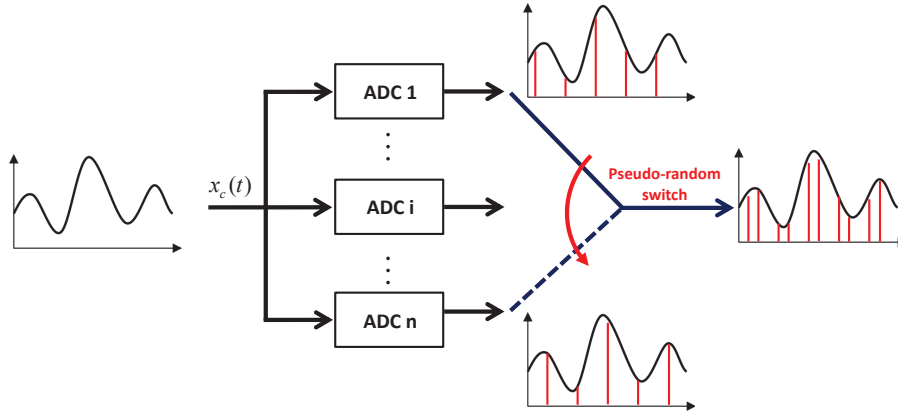


Figure 4.10: The implementation of the random analog-to-digital converter (RADC) system [107].

In [108] AICs were realized by pseudo-random demodulation. Here, the signals were initially spread with a high-rate pseudo-random discrete-time sequence called the chipping sequence. This random sequence takes values of ± 1 with equal probability. The chipping sequence should randomly alternate at or above the Nyquist rate. The output of the pseudo-random sequence generator, $p_c(t)$, is employed to demodulate a continuous-time input $x_c(t)$ by a mixer. Then, a low-pass anti-aliasing filter is applied by accumulating the sum of the demodulated signal for $1/f_s$ seconds. The filtered signal is sampled at a relatively low sub-Nyquist rate of f_s . The block diagram of this method is shown in Figure 4.11. The overall action of the random demodulator is described in matrix form (i.e. via Φ) [108]. The sampling rate is proportional to the number of non-zero tones. The main drawback of the random demodulator is that it can easily be influenced by design imperfections or model mismatches [109].

The compression rate is denoted r_c and given by $\frac{\text{sub-Nyquist rate } (f_s)}{\text{Nyquist rate } (f_{Nyq})}$.

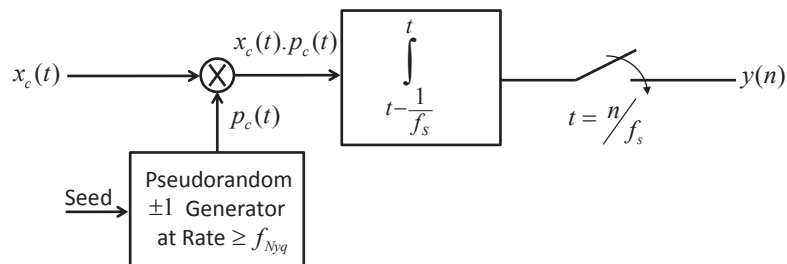


Figure 4.11: Block diagram of the pseudo-random demodulator [108].

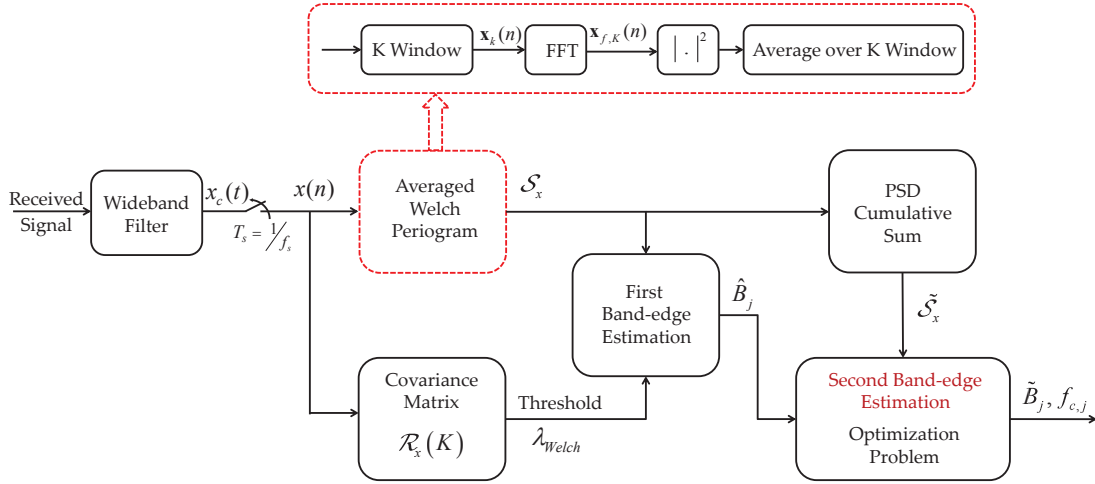


Figure 4.12: The block diagram of non-parametric Welch periodogram estimator combined with an optimization method to refine the spectral components

4.4.2 Improved Welch Periodogram Based Detection

4.4.2.1 Welch Periodogram Based Detection

The Welch method was introduced to reduce the variance of the periodogram. We have proposed in [79] to employ the non-parametric Welch periodogram spectral estimator combined with an optimization method to refine the spectral components. The block diagram of the proposed method is shown in Figure 4.12. Thereafter, a cooperative scheme is introduced to relax the high sampling rates constraint.

Assume the sensing duration τ_{sd} is divided into K non-overlapping segments of duration $T_K = \frac{\tau_{sd}}{K}$, i.e. the sampled corrupted received sequence is given as $\mathbf{x} = [\mathbf{x}_0^T, \dots, \mathbf{x}_{K-1}^T]^T$. The k^{th} segment, represented by the $N_K \times 1$ vector \mathbf{x}_k , is given by

$$\mathbf{x}_k(n) = r_K(n)x[n + kN_K] \quad 0 \leq n \leq N_K - 1, 0 \leq k \leq K - 1 \quad (4.30)$$

where r_K is a window of width T_k , the samples number per window is $N_k = \lfloor \frac{\tau_{sd}}{K} \cdot f_s \rfloor$ and $\lfloor \cdot \rfloor$ denotes the floor function. Let $\mathbf{x}_{f,k} = \text{DFT}(\mathbf{x}_k)$ be the Fourier transform in the k^{th} segment. The non-overlapping Welch periodogram \mathcal{S}_x gives an estimate of the received signal PSD by

$$\mathcal{S}_x(n) = \frac{1}{K} \sum_{k=0}^{K-1} |\mathbf{x}_{f,k}(n)|^2. \quad (4.31)$$

The band edge frequencies are detected by comparing the PSD with a predetermined threshold λ_{Welch} as shown in Figure 4.13. Under hypothesis \mathcal{H}_0 (i.e. \mathbf{x}_k is just noise), the Fourier spectrum follows a complex Gaussian distribution when the noise is assumed to be AWGN, i.e. $\mathbf{x}_{f,k}(k) \sim \mathcal{CN}(0, \sigma_N^2 \mathbf{I}_{N_k})$ when $\mathbf{x}_k(k) \sim \mathcal{CN}(0, \sigma_w^2 \mathbf{I}_{N_k})$, where $\sigma_N^2 = N_k \frac{\sigma_w^2}{2}$. This is due to the fact that the noise samples are i.i.d, the DFT is a linear transform and the window is considered rectangular. Then, the averaged periodogram is a weighted Chi-square distributed random variable with $2K$

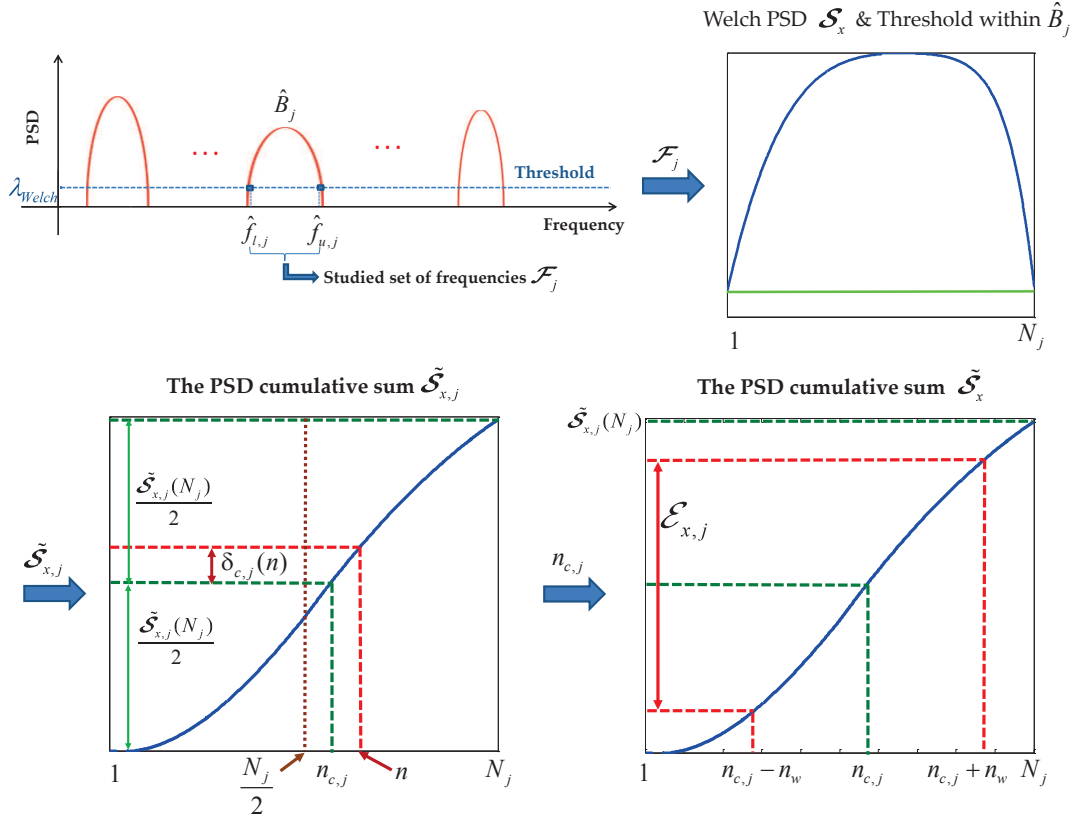


Figure 4.13: The detailed procedure of optimization method for refined spectral components estimation.

degrees of freedom. The false alarm probability is given by

$$P_f = \mathbb{P}(\mathcal{S}_x(n) > \lambda_{\text{Welch}} | \mathcal{H}_0) = \frac{\Gamma\left(K, \frac{K\lambda_{\text{Welch}}}{N_K \sigma_w^2}\right)}{\Gamma(K)} \quad (4.32)$$

where $\Gamma(\cdot)$ denotes the Gamma function, and $\Gamma(\cdot, \cdot)$ is the upper incomplete gamma function. The proof of Equation (4.32) comes directly from the CDF of the chi-square distribution. The noise power is unknown and must be estimated. Here, the estimation method is based on the PET. An estimate of the covariance matrix of the received sequence is computed as

$$\mathcal{R}_x(K) = \frac{1}{K} \sum_{k=0}^{K-1} \mathbf{x}_k \mathbf{x}_k^H \quad (4.33)$$

Then, applying the PET method proposed in [96] in Equation (4.33), the noise power estimate $\hat{\sigma}_w^2$ is given by the average of the lowest eigenvalues (the noise eigenvalues). Thereafter, a power threshold λ_{Welch} is calculated based on Equation (4.32), the targeted P_f and the noise power estimate $\hat{\sigma}_w^2$. Then, using λ_{Welch} in Equation (4.31), the estimated band-edge frequencies ($\hat{f}_{l,j}$ and $\hat{f}_{u,j}$) are those which average power are above the threshold while scanning the PSD estimate \mathcal{S}_x .

Thereafter, signals within each occupied subband of interest are separately processed to identify

their spectral characteristics (carrier frequency and bandwidth) as shown in Figure 4.13. In each detected subband \hat{B}_j , the set of frequencies is denoted \mathcal{F}_j and assumed to be of length N_j . The PSD cumulative sum is computed and set to as: $\tilde{\mathcal{S}}_{x,j}$. We propose the following successive steps to allow fine spectral components estimation. The central frequency $f_{c,j}$ in each occupied band is traditionally given by $\frac{\hat{f}_{l,j} + \hat{f}_{u,j}}{2}$. Here, it is refined to be $f_{c,j} = \mathcal{F}_j(n_{c,j})$, where $n_{c,j}$ is obtained by solving the following optimization problem

$$n_{c,j} = \arg \min_{1 \leq n \leq N_j} [\delta_{c,j}(n)] = \arg \min_{1 \leq n \leq N_j} \left\{ \left| \tilde{\mathcal{S}}_{x,j}(n) - \frac{\tilde{\mathcal{S}}_{x,j}(N_j)}{2} \right| \right\}, \quad (4.34)$$

i.e. the central frequency is the one that equally divides the total power in the studied subband. This optimization problem is explained in Figure 4.13. Moreover, the band-edge estimation \hat{B}_j can be improved by finding the set of frequencies containing 95% of the signal energy and centered around the frequency $f_{c,j}$. Then, the refined bandwidth defined as $\tilde{B}_j = \mathcal{F}_j(n_{c,j} + n_{b,j}) - \mathcal{F}_j(n_{c,j} - n_{b,j})$ is estimated by solving the following optimization problem

$$n_{b,j} = \arg \min_{n_w} \{ \mathcal{E}_{x,j} > 0.95 \cdot \tilde{\mathcal{S}}_{x,j}(N_j) \} \quad (4.35)$$

where the signal power in the refined band is calculated as follows: $\mathcal{E}_{x,j} = \tilde{\mathcal{S}}_{x,j}(n_{c,j} + n_w) - \tilde{\mathcal{S}}_{x,j}(n_{c,j} - n_w)$ and $1 \leq n_w \leq \min(N_j - n_{c,j} + 1, n_{c,j})$.

The probability of detection can be strongly improved by increasing the number of analysis windows and/or the sensing duration. Nevertheless, the computation cost can be very prohibitive. Therefore, a compromise must be made between both expected performance and computational cost. The non-parametric Welch periodogram based sensing gives good performances but requires high sampling rates which results in large complexity and high power consumption.

4.4.2.2 Multiple-antenna Welch Periodogram Based Detection

Cooperation can also improve the WSS performance. Let us assume a multiple-antennas receiver or even more several multiple-antennas receivers located at both sides of the train (this makes the cooperation more powerful), i.e. M receiving antenna in total. Improving sensing is achieved by combining different information coming from all antennas at the fusion center. This combination could be done by three different approaches.

Decision Fusion One way to improve the performance is to detect the occupied bands using the received signal at each antenna separately, these information are then sent to the fusion center to be combined for final decision. A literature review of existing decision fusion methods is presented in subsection 3.2.6. Here, the employed method tries to find the intersection among the subbands detected on the majority of antennas.

Data Fusion The performance of WSS based on Welch periodogram improves when the number of considered segments K increases. This number could be increased without decreasing

the window width or leading to sensing duration overhead by combining the received signals on all antennas at the fusion center. The total number of windows is $\sum_{i=1}^M K_i$ where K_i is the number of considered windows on the i^{th} antenna.

Compressive Sensing The two above approaches still require a high sampling rate even though they lead to a better performance. This makes the Welch periodogram based WSS impractical for large wideband. The compressive sensing is employed to overcome this difficulty and to enable detecting the occupied bands with lower sampling rate. The required compression rate to achieve certain sensing performance depends on the compression method and the spectrum occupancy. However, the performance improves when the compression rate increases.

Multiple-antennas at the receiver are beneficial to either increase the compression rate, or to reach the required r_c with lower-rate ADCs. The compression ratio at the fusion center is given by $\frac{\sum_{i=1}^M f_{s,i}}{f_{Nyq}}$ where $f_{s,i}$ is the sub-Nyquist sampling rate at the i^{th} antenna.

We propose to employ multiple-antennas for compressive sensing in several ways

- ❖ Perform a compressive sensing and spectrum reconstruction locally. Thereafter, the spectrum decisions are either taken locally, and then are sent to the fusion center for combining, or taken at the fusion center after combining all the reconstructed spectrum versions coming from different antennas.
- ❖ Combining the sub-Nyquist sampled signals collected from all antennas at the fusion center. This can be employed to reconstruct a more accurate spectrum estimation, or to reduce the sampling rates. One of the compressive sensing that can be applied to realize this method is the RADC.

Here, the received signal at each antenna is sampled at a sub-Nyquist rate equal to $\frac{f_{Nyq}}{M}$. The sampled signals are transmitted to the fusion center without any additional requirements (receivers at all antennas are connected to the fusion center with wires). Then, the total compression rate is 100% which leads to avoid the NP-hard optimization problem needed for spectrum reconstruction. That is, the spectrum is calculated directly from the collected samples.

The received signal at the i^{th} antenna sampled as

$$x_i(n) = \begin{cases} x(\frac{n}{f_{Nyq}}), & n = mM + t_i \\ 0, & \text{otherwise} \end{cases} \quad (4.36)$$

where $\frac{t_i}{f_{Nyq}}$ is the offset of the i^{th} ADC. Without loss of generality, we choose $t_i = i$.

Here, we improved the Welch periodogram based sensing by introducing the refined spectral characteristics optimization. This method is extended to exploit the multiple-antennas at receivers to achieve better performance.

4.4.2.3 Simulation Results

The studied wideband of width 5 GHz includes $N_B = 6$ occupied subband of different bandwidths and at different central frequencies. The bandwidth varies in the range of $B_j = 5 \sim 50$ MHz. The total observation time is $\tau_{sd} = 7.5 \mu\text{s}$ divided into $K = 25$ segments. To sense a band of 5 GHz width, a Nyquist sampling rate of 10 GSPS is required; i.e. the length of each segment is $N_k = 3000$ while the total number of samples is 75000. The detection threshold is chosen to achieve a false alarm probability of 0.1.

Figure 4.14 shows that the proposed improved welch based method provides good estimate of the spectral characteristics of the received signal. This Figure shows the Welch periodogram compared to the predetermined threshold for $\text{SNR} = -5$ dB. The refined central frequency and band-edges are optimized as explained in Equations (4.34) and (4.35).

This optimization method shows high accuracy for an acceptable range of SNR (> -5 dB, when $\tau_{sd} = 7.5 \mu\text{s}$, $K = 25$, and $P_f = 0.1$). Comparing the estimated spectral characteristics with the generated ones shows that the normalized mean bias of the central frequency estimator $\simeq 5 \times 10^{-4}$ while the NMB of the edges estimator is $\simeq 10^{-2}$.

Moreover, Figure 4.15 shows that the missdetection probability P_m can be improved by increasing the number of analysis segments. However, achieving a good performance ($P_m \leq 0.1$) for very low SNRs ($\text{SNR} = -12$ dB) requires a large number of segments ($K = 75$). Nevertheless, the computation cost can be very prohibitive. For a small number of segments ($K = 25$), the sensing performance is poor and needs to be enhanced while keeping the complexity and the sampling rates sufficiently low. The cooperation concept was introduced to solve this problem.

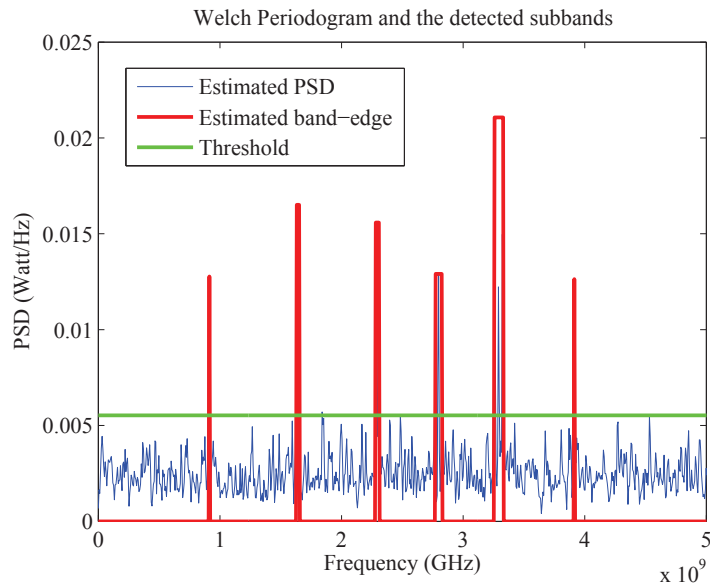


Figure 4.14: The detection of six occupied subbands of different bandwidth values at different central frequencies (total duration is $7.5 \mu\text{s}$, $K = 25$, $P_f = 0.1$, and $\text{SNR} = -5$ dB). This Figure shows the filtered periodogram with the estimated threshold.

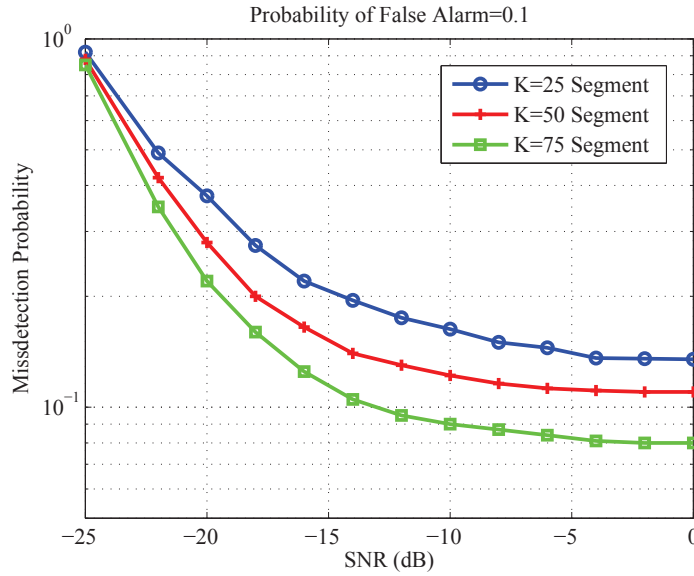


Figure 4.15: The missdetection probability versus SNR for Welch based algorithm at different number of segments ($K = 25, 50,$ and 75) when $N_B = 6$, $\tau_{sd} = 7.5 \mu s$, and $P_f = 0.1$.

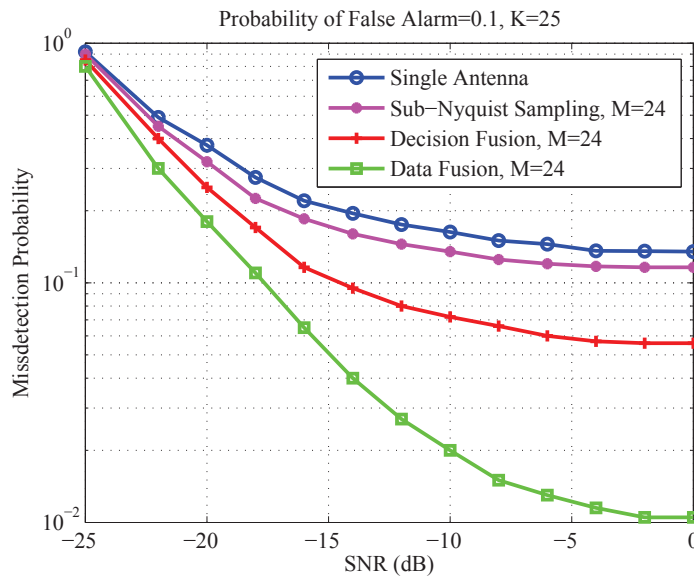


Figure 4.16: The missdetection probability versus SNR for different information combining approaches when $K = 25$, $N_B = 6$, $\tau_{sd} = 7.5 \mu s$ and $P_f = 0.1$.

Figure 4.16 shows a performance comparison among different multiple-antenna Welch periodogram based WSS approaches. This result is obtained when 6 receivers located all around the train are employed, each receiver has 4 antennas, i.e. the total number of antennas is $M = 24$. The fading conditions moderately varies from receiver to receiver, and also from subband to subband. For different values of SNR, a white circularly complex Gaussian noise is added. It is clear that cooperation among several antennas does improve the sensing performance. Collecting the samples obtained at Nyquist rate from all antennas dramatically increases K (up to $25 \times 24 = 600$) without any sensing duration overhead are window width re-

duction. This results in an effective improvement in sensing performance. Nevertheless, this approach has a huge complexity (total number of samples collected at the fusion center is $75000 \times 24 = 1,800,000$ samples) and requires high sampling rate. The performance of the decision fusion approach is better when compared to that of the single antenna case. However, this approach does not reduce computational complexity and still requires high sampling rates. The proposed sub-Nyquist sampling approach does slightly improve the performance (in comparison to the single antenna case) while considerably reducing the the sampling rate at each antenna to $f_{s,i} = \frac{f_{Nyq}}{M} = 416.66$ MSPS. The slight performance improvement is due to the cooperation among different receivers suffering from different levels of fading. In fact, this approach is a combination of sub-Nyquist sampling and data fusion.

4.4.3 Discussion

The classical Welch periodogram based WSS suffers from prohibitive complexity and high sampling rate ($\geq f_{Nyq}$). Also, this method does not perform well for very low SNRs. Decision fusion approach improves performance but still has the same drawbacks. Data fusion approach, or increasing the sensing duration, strongly improves the performance at the cost of huge increase in the complexity. One solution to decrease the sampling rate is the joint use of multiple-antennas and sub-Nyquist sampling. One drawback of this approach is the sampling time offsets errors. This problem could be extremely complicated to solve in a cognitive radio network, conversely, synchronization requirements can be easily fulfilled in our context (different receivers distributed all around the train). Our approach has a compression ratio of 100%, i.e. its computational complexity is the same as in the case of a single antenna. To reduce this complexity a lower compression ratio is needed. But, reducing the compression ratio traditionally demands solving a complex l_1 -norm optimization problem. One of our under-development research works is how to estimate the PSD directly from the sub-Nyquist sampled signals when the compression ratio is lower ($\sim 50\%$), this will decrease more the sampling rates. Obviously, designing the Welch periodogram based wideband detector is a compromise among several parameters: the sensing duration, the sampling rates, the computational complexity and the targeted performance (P_m and P_f).

All existing WSS methods suffer from performance degradation in the low SNR regime. Furthermore, the receiver sensitivity is an essential parameter in spectrum sensing. The NSS is still more reliable than the wideband one. This is due to the fact that the receiver sensitivity is lower when the receiver bandwidth is larger as the noise power increases with the bandwidth. Increasing the receiver sensitivity with wideband detection is a real challenge.

4.5 Conclusions

Cognitive radio should be flexible to adaptively operate over a wide range of frequencies. The occupied bands consist of several continuous narrowband intervals over a wide spectrum. Spectrum sensing is divided into two categories: narrowband sensing and wideband sensing. The NSS is based on dividing the wide spectrum of interest into consecutive subbands (narrowband

channels). These subbands are sequentially or randomly checked to decide their occupancy until a free band is found. Contrary to the wideband sensing where the entire band of interest is processed. This Chapter has presented a preliminary literature review of these two categories. It is clear that the WSS is still in its early stages, while the NSS problem is well studied in the literature. We have also proposed a narrowband sensing method based on the predicted eigenvalue threshold. Our blind non-parametric method gives good performance when compared with other existing blind methods. The main drawback of the NSS is the latency in finding a free band which leads to sensing duration overhead. This overhead increases when the spectrum occupancy is higher. To overcome this problem the wideband sensing was motivated. High power consumption, high sampling rates and computational complexity are the drawbacks that make the WSS impractical. An improved cooperative Welch periodogram based sensing was also proposed in this Chapter. This method is a compromise between reducing complexity and sampling rates (compression rate 100%), i.e. using sub-Nyquist sampling while still avoiding the NP-hard problem of spectrum reconstruction. Furthermore, note that improving the WSS performance requires more antennas than that required in the NSS. In fact, wideband sensing is a hot subject and still demands a lot of research. One of our perspectives is to develop the proposed WSS method to work with lower compression rates without the need of spectrum recovery. This will relax the constraints on ADCs and reduce the complexity and consequently cut down energy cost.

Chapter 2 introduced the system model and the constraints related to the special railways environment. However, these constraints were not taken into consideration when studying the problem of spectrum sensing in this Chapter. The next Chapter studies the NSS problem taking into account these constraints.

Chapter 5

Narrowband Spectrum Sensing For Railways

Contents

5.1	Introduction	112
5.2	Weighted Covariance Value Based Spectrum Sensing for Time-Varying Channels	112
5.2.1	System Model	112
5.2.2	The Proposed Method	113
5.2.3	Performance Analysis	114
5.2.4	Numerical Results and Discussions	117
5.3	Spectrum Sensing with Spatially-Correlated Multiple-Antennas	120
5.3.1	Preliminary Literature Review	120
5.3.2	Predicted Eigenvalues Threshold Sensing Performance with Spatially-Correlated Multiple-Antennas	121
5.4	Spectrum Sensing in the Presence of Impulsive Noise	126
5.4.1	Preliminary Literature Review	127
5.4.2	Basic Properties of $S\alpha S$ Distribution	128
5.4.3	System Model	129
5.4.4	α -Stable Noise Mitigation	130
5.4.5	Generalized Covariation Coefficient Absolute Value Based Spectrum Sensing	131
5.4.6	Performance Evaluation	133
5.5	Conclusions	136

5.1 Introduction

Three particular railways environment constraints had got more attention, namely, the time-varying wireless channel, the multiple-antenna spatial correlation, and the impulsive heavy-tailed noise. In this Chapter new methods are introduced either to exploit these constraints or to mitigate their effect. The time-varying wireless channels affect the time correlation properties. This could degrade the performance of the traditional narrowband spectrum sensing methods presented in Chapter 4. A new weighted covariance value based spectrum sensing method is proposed to try to exploit the properties of time-varying channel to improve the performance. The practical multiple-antenna systems always suffer from spatial correlations. The effect of the presence of spatial correlations on NSS methods is examined. It is found that the performance of some methods do improve when these correlations are larger. A new method based on a weighting covariance matrix, employed to better exploit the spatial correlation to achieve higher sensing performance levels, is introduced. This method represents another important contribution of our thesis. As seen in Chapter 2, the special EM environment around the train results in an impulsive noise with heavy tails. It was also shown that the $S\alpha S$ distributed processes are fitted to model the noise behaviour. The heavy tails of impulsive noise will degrade the NSS performance. Two new methods are introduced to mitigate their effect. The first is based on filtering the received signal using the myriad concept, while, the second is based on the covariation (not covariance) coefficient matrix of the received signal. These two algorithms are the last contribution provided by our thesis.

5.2 Weighted Covariance Value Based Spectrum Sensing for Time-Varying Channels

To the best of our knowledge, no work has yet considered the problem of spectrum sensing for time-varying channels. In what follows, we will try to exploit the temporal correlations of the time-varying channel taps to improve the sensing performance. The proposed approach employs the weighted covariance matrix.

5.2.1 System Model

The following assumptions hold in this section. A secondary user possessing M antennas is sensing the presence of P primary users. The source signals $s_p, 1 \leq p \leq P$ are assumed to be centered and i.i.d. The received signal at the i^{th} antenna is given by

$$x_i(n) = \sum_{p=1}^P \sum_{k=0}^{C_p} h_{i,p}(n, k) s_p(n - k) + w_i(n), \quad n = 1, 2, \dots \quad (5.1)$$

where $w_i(n)$ is the AWGN with zero-mean and variance σ_w^2 , C_p is the order of the channel between the p^{th} primary source (PS_p) and each antenna, and $h_{i,p}(n, k)$ is the n^{th} sample of the

k^{th} tap of the time-varying channel response between PS_p and the i^{th} antenna. The channel taps satisfy the following criteria,

- ❖ Antennas are spatially-uncorrelated, i.e. $E \left\{ h_{i_1,p}(n,k) h_{i_2,q}^*(m,l) \right\} = 0$, for $i_1 \neq i_2$,
- ❖ The channel between PS_p and the i^{th} antenna is uncorrelated with the channel between PS_q and the same antenna, i.e. $E \left\{ h_{i,p}(n,k) h_{i,q}^*(m,l) \right\} = 0$, for $p \neq q$,
- ❖ The inter-tap correlation is insignificant, i.e. $E \left\{ h_{i,p}(n,k) h_{i,p}^*(m,l) \right\} = 0$, for $k \neq l$,
- ❖ The complex envelop $|h_{i,p}(n,k)|$ is Rayleigh distributed,
- ❖ Adopting isotropic scattering Jakes reference model, we have

$$r_h(m) \triangleq E \left\{ h_{i,p}(n,k) h_{i,p}^*(n-m,k) \right\} = \sigma_h^2 J_0(2\pi f_d m T_s), \quad (5.2)$$

where f_d is the maximum Doppler frequency, σ_h^2 is the average power of the channel tap, and $J_0(\cdot)$ is the zero-order Bessel function of the first kind.

- ❖ The inphase and quadrature components of $h_{i,p}(n,k)$ are zero-mean independent real Gaussian random processes with identical autocorrelation functions. Let $h_{i,p}^{\Re}(n,k)$, $h_{i,p}^{\Im}(n,k)$, respectively, be the real and imaginary parts of $h_{i,p}(n,k)$, then

$$\begin{aligned} E \left\{ h_{i,p}^{\Re}(n,k) h_{i,p}^{\Re}(m,k) \right\} &= E \left\{ h_{i,p}^{\Im}(n,k) h_{i,p}^{\Im}(m,k) \right\} = \frac{\sigma_h^2}{2} J_0 \{ 2\pi f_d (n-m) T_s \} \\ E \left\{ h_{i,p}^{\Re}(n,k) h_{i,p}^{\Im}(m,k) \right\} &= E \left\{ h_{i,p}^{\Im}(n,k) h_{i,p}^{\Re}(m,k) \right\} = 0 \end{aligned}$$

5.2.2 The Proposed Method

In the absence of antenna spatial correlation, we focus on the time correlation to enhance spectrum sensing performance. In the first time, let us examine the signal received on one antenna only. The obtained result can be easily generalized for all antennas. Let us denote the $L \times 1$ smoothed observation vector at the i^{th} antenna by $\mathbf{x}_{L,i}(k) = [x_i(k), \dots, x_i(k-L+1)]^T$. The sample covariance matrix is employed to estimate the unknown covariance matrix, and is given, for N observed samples, by

$$\begin{aligned} \mathbf{R}_{L,i}(N) &= \frac{1}{N} \sum_{k=1}^N \mathbf{x}_{L,i}(k) \mathbf{x}_{L,i}^H(k) \\ &= \begin{bmatrix} R_i(1,1) & R_i(1,2) & \cdots & R_i(1,L) \\ R_i(2,1) & R_i(2,2) & \cdots & R_i(2,L) \\ \vdots & \vdots & \ddots & \vdots \\ R_i(L,1) & R_i(L,2) & \cdots & R_i(L,L) \end{bmatrix} \end{aligned} \quad (5.3)$$

where $R_i(n,m) = \frac{1}{N} \sum_{k=1}^N x_i(k-n+1) x_i^*(k-m+1)$, $1 \leq n, m \leq L$. In what follows, the index “ i ” is omitted, since the statistical properties of sources and channel are identical and independent of the receiving antenna. This omission will be also justified by the obtained results. The existing

covariance-based spectrum sensing methods consider that all the entries of this matrix have the same contribution in its test statistic. However, it is a good idea to employ a weighted sample covariance matrix when the temporal correlation structure is known. The weighted sample covariance matrix can be introduced as an entrywise product of the covariance matrix $\mathbf{R}_L(N)$ and the weights matrix \mathbf{T} , and is represented by

$$\mathbf{R}_{L,T}(N) = \mathbf{T} \circ \mathbf{R}_L(N) = \begin{bmatrix} t_{1,1}R(1,1) & t_{1,2}R(1,2) & \cdots & t_{1,L}R(1,L) \\ t_{2,1}R(2,1) & t_{2,2}R(2,2) & \cdots & t_{2,L}R(2,L) \\ \vdots & \vdots & \ddots & \vdots \\ t_{L,1}R(L,1) & t_{L,2}R(L,2) & \cdots & t_{L,L}R(L,L) \end{bmatrix} \quad (5.4)$$

The weights $t_{i,j} = [\mathbf{T}]_{i,j}$ are optimized based on the prior knowledge of the time correlation structure to improve sensing performance. In fact the channel temporal variations are faster when the maximum Doppler frequency is larger. The statistical properties of temporal correlation lags are known when the train speed and the central frequency of the sensed subband are known, which is usually the case. We can easily show that $E[R(n,m)]$ is real and $E[R(n,m)] = E[R(m,n)]$, $1 \leq l \leq L$. Also, $\mathbf{R}_L(N)$ is Hermitian, hence, we assume, without loss of generality, $t_{n,n} = t_0$, $1 \leq n \leq L$ and $t_{n,m} = t_{m,n}$, $1 \leq n, m \leq L$.

The weighted covariance value based method for time-varying (WCV-T) channels has the following test statistics

$$T_{\text{WCV-T}} = \frac{\sum_{n=1}^L \sum_{m=1, m \neq n}^L t_{n,m} R(n,m)}{\sum_{n=1}^L t_{n,n} R(n,n)} \underset{\delta_0}{\overset{\delta_1}{\geq}} \lambda_{\text{WCV-T}} \quad (5.5)$$

The matrix $\mathbf{R}_L(N)$ has nearly zero off-diagonal entries when there is no PU's signal. Contrary, in the presence of, at least, one PU, it has some non-zero off-diagonal entries. Then, if there is no signal, $T_{\text{WCV-T}} \simeq 0$. When, at least, one PU's signal is detected $T_{\text{WCV-T}} > 0$. In what follows, the index "WCV-T" could be omitted for simplicity.

5.2.3 Performance Analysis

Let Δ be defined as

$$\Delta_{\text{WCV-T}} = \sum_{n=1}^L \sum_{m=1, m \neq n}^L t_{n,m} R(n,m) - \lambda_{\text{WCV-T}} \sum_{n=1}^L t_{n,n} R(n,n) \quad (5.6)$$

Then, $P_m = \mathbb{P}[\Delta < 0 | \mathcal{H}_1]$ and $P_f = \mathbb{P}[\Delta > 0 | \mathcal{H}_0]$. Finding the optimal \mathbf{T} is achieved by solving the following optimization problem,

$$\begin{cases} \text{Minimize: } P_m(\mathbf{T}) \\ \text{Subject to: } P_f(\mathbf{T}) \leq \xi \end{cases} \quad (5.7)$$

where ξ is the targeted level of P_f . This objective requires to study the statistical properties of Δ , which in turn needs the statistical properties of $R(n,m)$. In fact, we assume that the temporal correlation coefficients $R(n,m)$, $1 \leq n, m \leq L$ are jointly Gaussian. This approximation can be

justified, for a large N , by the central limit theorem and will be confirmed by the performance of the proposed method.

Under \mathcal{H}_η for $\eta = 0, 1$, we can easily demonstrate, based on the above assumptions, that $r(n, m) = E[x_i(n)x_i^*(m)]$ is obtained as

$$r(n, m) = \eta \underbrace{(P + C)\sigma_s^2}_{\triangleq P_s} r_h(n - m) + \sigma_w^2 \delta(n - m) \quad (5.8)$$

where $r_h(n)$ is defined in Equation (5.2). It is clear that $r(n, m)$ depends on the difference $(n - m)$ and is denoted $r(n - m)$.

The sample time autocorrelation mean is calculated as $E[R(n, m)] = r(n - m)$. Also, the covariance, $c(n, m, d, q) \triangleq \text{Cov}[R(n, m), R^*(d, q)]$ $1 \leq n, m, d, q \leq L$, is determined by,

$$\begin{aligned} c(n, m, d, q) &= \text{Cov} \left\{ \frac{1}{N} \sum_{k_1=1}^N x_i(k_1 - n + 1) x_i^*(k_1 - m + 1), \frac{1}{N} \sum_{k_2=1}^N x_i(k_2 - d + 1) x_i^*(k_2 - q + 1) \right\} \\ &= \frac{1}{N^2} \sum_{k_1=1}^N \sum_{k_2=1}^N \{ r(k_1 - k_2 + q - n) r(k_2 - k_1 + m - d) \\ &\quad + r(k_1 - k_2 + d - n) r(k_2 - k_1 + m - q) \} \end{aligned} \quad (5.9)$$

The statistical properties of Δ are given by its mean and its variance, such as

$$E(\Delta) = \sum_{n=1}^L \sum_{m=1, m \neq n}^L t_{n,m} r(n - m) - \lambda L t_0 r(0), \quad (5.10)$$

and the variance is calculated by

$$\begin{aligned} \text{Var}(\Delta) &= \sum_{n=1}^L \sum_{m=1, m \neq n}^L \sum_{d=1}^L \sum_{q=1, q \neq d}^L t_{n,m} t_{d,q} c(n, m, d, q) \\ &\quad - 2\lambda \sum_{n=1}^L \sum_{m=1, m \neq n}^L \sum_{d=1}^L t_{n,m} t_{d,d} c(n, m, d, d) + \lambda^2 \sum_{n=1}^L \sum_{m=1}^L t_{n,n} t_{m,m} c(n, n, m, m) \end{aligned} \quad (5.11)$$

Let us, respectively, denote $m_{\Delta,i} = E[\Delta|\mathcal{H}_i]$ and $\sigma_{\Delta,i}^2 = \text{Var}[\Delta|\mathcal{H}_i]$. Then the missdetection probability and the false alarm probability are, respectively, calculated by

$$P_m = 1 - Q\left(-\frac{m_{\Delta,1}}{\sigma_{\Delta,1}}\right) \quad \text{and} \quad P_f = Q\left(-\frac{m_{\Delta,0}}{\sigma_{\Delta,0}}\right) \quad (5.12)$$

Under \mathcal{H}_0 , we have $r(n - m) = \sigma_w^2 \delta(n - m)$. Hence, $E[R(n, m)] = \sigma_w^2 \delta(n - m)$ and

$$c(n, m, d, q) = \frac{\sigma_w^4}{N} \{ \delta[n - m + q - d] + \delta[n - m + d - q] \} \quad (5.13)$$

Hence, $m_{\Delta,0} = -\lambda L t_0 r(0)$ and

$$\sigma_{\Delta,0}^2 = \frac{2\sigma_w^4}{N} \left[L^2 t_0^2 \lambda^2 + \sum_{n=1}^L \sum_{m=1, m \neq n}^L \sum_{d=d_{min}}^{d_{max}} t_{n,m} t_{d,d-n+m} \right] \quad (5.14)$$

where $d_{min} = \max(1+n-m, 1)$ and $d_{max} = \min(L+n-m, L)$.

Let us denote $\Lambda_t^2 = \frac{1}{L^2} \sum_{n=1}^L \sum_{m=1, m \neq n}^L \sum_{d=d_{min}}^{d_{max}} \tilde{t}_{n,m} \tilde{t}_{d,d-n+m}$ where $\tilde{t}_{n,m} = \frac{t_{n,m}}{t_0}$. Then, Equation (5.14) is reformulated as,

$$\sigma_{\Delta,0}^2 = \frac{2\sigma_w^4}{N} L^2 t_0^2 [\lambda^2 + \Lambda_t^2] \quad (5.15)$$

The false alarm probability is calculated as,

$$P_f = Q \left(\frac{\lambda_{\text{WCV-T}} \sqrt{\frac{N}{2}}}{\sqrt{\lambda_{\text{WCV-T}}^2 + \Lambda_t^2}} \right) \quad (5.16)$$

Now for a given false alarm level ξ , the threshold λ is obtained based on (5.16), as follows

$$\lambda_{\text{WCV-T}}(\xi) = \frac{\Lambda_t \cdot Q^{-1}(\xi)}{\sqrt{\frac{N}{2} - [Q^{-1}(\xi)]^2}} \quad (5.17)$$

Obviously, the decision threshold is independent of the noise power and the channel gains, and depends only on the weights, L, N, M and ξ .

It is clear from Equation (5.16) that fixing the false alarm probability to a certain level requires that Λ_t^2 remains constant (while choosing the proper threshold). Also, note that missdetection probability, given in Equation (5.12), decreases when $\frac{m_{\Delta,1}}{\sigma_{\Delta,1}}$ increases. Hence, the optimization problem in (5.7) is reformulated as

$$\begin{cases} \text{Maximize: } J = \frac{m_{\Delta,1}}{\sigma_{\Delta,1}} \\ \text{Subject to: } \Lambda_t^2 = \Lambda_{t,0}^2 \end{cases} \quad (5.18)$$

where $\Lambda_{t,0}$ is an arbitrary constant.

The real objective is to maximize the performance in the low SNR regime. The optimal covariance matrix entries are calculated in Appendix D.2 and are given by

$$t_{n,m} = \frac{L r_h(n-m)}{L - |n-m|}, 1 \leq n, m \leq L. \quad (5.19)$$

The above analysis justifies the previous omission of the antenna index "i" and enables the generalization of the obtained results to other antennas.

Let us consider the received signal on all antennas as $\mathbf{x}_L(k) = [\mathbf{x}_{L,1}^T(k), \dots, \mathbf{x}_{L,M}^T(k)]^T$. In the

Table 5.1: Maximum Doppler frequency (Hz) as a function of some values of the train speed (Km/h) when the central frequency is 2.5 GHz and 921 MHz (the last value corresponds to the GSM-R standard).

	50 Km/h	100 Km/h	200 Km/h	300 Km/h
$f_c = 921$ MHz	43	85	171	256
$f_c = 2.5$ GHz	116	232	463	695

absence of any spatial correlation, the sample covariance matrix is represented by,

$$\begin{aligned} \mathbf{R}_L(N) &= \frac{1}{N} \sum_{k=1}^N \mathbf{x}_L(k) \mathbf{x}_L^H(k) \\ &= \begin{bmatrix} \mathbf{R}_{L,1}(N) & \mathbf{0}_L & \cdots & \mathbf{0}_L \\ \mathbf{0}_L & \mathbf{R}_{L,2}(N) & \cdots & \mathbf{0}_L \\ \vdots & \vdots & \ddots & \vdots \\ \mathbf{0}_L & \mathbf{0}_L & \cdots & \mathbf{R}_{L,M}(N) \end{bmatrix} \end{aligned} \quad (5.20)$$

We can directly conclude that the performance based on the test statistic,

$$T_{\text{WCV-T}} = \frac{\sum_{n=1}^{ML} \sum_{m=1, m \neq n}^{ML} t_{n,m} R(n, m)}{\sum_{n=1}^{ML} t_{n,n} R(n, n)}, \quad (5.21)$$

can be maximized by weighting $\mathbf{R}_L(N)$ as,

$$\mathbf{R}_{L,T}(N) = \begin{bmatrix} \mathbf{T} \circ \mathbf{R}_{L,1}(N) & \mathbf{0}_L & \cdots & \mathbf{0}_L \\ \mathbf{0}_L & \mathbf{T} \circ \mathbf{R}_{L,2}(N) & \cdots & \mathbf{0}_L \\ \vdots & \vdots & \ddots & \vdots \\ \mathbf{0}_L & \mathbf{0}_L & \cdots & \mathbf{T} \circ \mathbf{R}_{L,M}(N) \end{bmatrix} \quad (5.22)$$

where \mathbf{T} is defined in Equation (5.19).

5.2.4 Numerical Results and Discussions

In this subsection, we present numerical results for weighted covariance value based spectrum sensing over time-varying channels. Throughout this subsection, we assume $P_f = 0.1$, the PU signals are random binary phase-shift keying modulated. The random AWGN is added such that $\text{SNR} = \frac{E[\|\mathbf{x}(n) - \mathbf{w}(n)\|^2]}{E[\|\mathbf{w}(n)\|^2]}$. The Rayleigh channel taps respect the assumptions made in 5.2.1.

The uncorrelated ($C + P$) complex channel taps are generated using generalized exact Doppler spread model (GMEDS₁) method presented in 2.2.4. This method is designed such that the ACF, $\tilde{r}_h^{(k)}(\tau)$, of the simulation model must be as close as possible to the ACF, $r_h(\tau)$, of a given reference model over a certain domain $[0, \tau_{max}]$. Studies have shown that for the GMEDS₁, the quantity τ_{max} is given by $\tau_{max} = N_i / (2f_d)$ where N_i is the number of summed sinusoids [36]. At the price of increased simulations complexity, the GMEDS₁ enables an excellent fitting to both the quadrature ACFs and the ACF of the complex waveform over larger domain of interest, i.e.

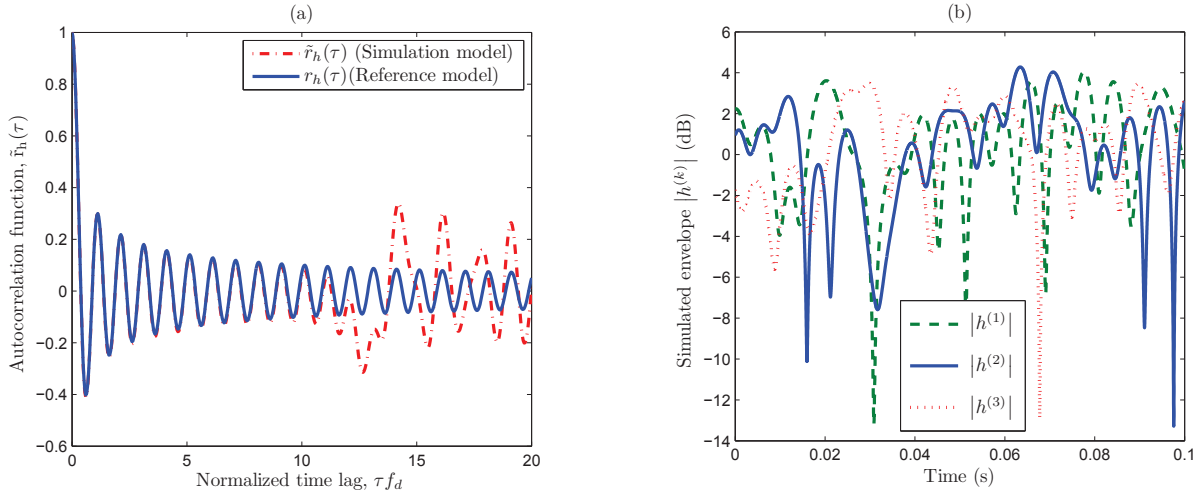


Figure 5.1: (a) The ACF, $r_h(\tau)$, of the complex waveform of the reference model in comparison with the corresponding ACF, $\tilde{r}_h^{(k)}(\tau)$, of the simulation model designed using the GMEDS₁. (b) Simulated uncorrelated Rayleigh fading waveforms ($|h^{(k)}|$, $k = 1, 2, 3$) using the GMEDS₁ ($f_d = 100\text{Hz}$, $N_i = 20$).

$\tau_{max} \nearrow \Rightarrow N_i \nearrow \Rightarrow$ simulation complexity \nearrow . The performance of most mobile communication systems is only sensitive to errors of the ACF if the time lag is small, meaning $\tau f_d \leq 0.3$ [25]. Here, the value of τ_{max} is proportional to the smoothing factor L . Hence, larger L does require increasing N_i and results in longer simulation times. Figure 5.1(a) depicts the ACF, $r_h(\tau)$, of the complex waveform of the reference model in comparison with the corresponding ACF, $\tilde{r}_h^{(k)}(\tau)$, of the simulation model designed by using the GMEDS₁ for $N_i = 20$. The simulated ACF, $\tilde{r}_h^{(k)}(\tau)$, represents an excellent fitting to the reference model when $\tau \in [0, N_i/(2f_d)]$ or, equivalently, $\tau f_d \in [0, 10]$. Also, Figure 5.1(b) illustrates a simulation of the temporal behaviour of the resulting uncorrelated fading envelopes for $K = 3$. This Figure shows that the complex envelope could be attenuated to a level that is lower than -10 dB for short duration. In fact the rate of variations in channel gains increases as the maximum Doppler frequency increases.

The performance of detection algorithms are usually evaluated for the values of the normalized frequency Doppler $f_d T_{sym}$ where T_{sym} is the symbol duration. Here, T_{sym} is fixed and the performance of sensing algorithms is examined as a function of SNR for different f_d values. Knowing that each f_d value corresponds to a certain speed value depending on the carrier frequency. Table 5.2.4 shows the maximum Doppler frequency values for different train speed values and two carrier frequencies 921 MHz (corresponding to the GSM-R standard) and 2.5 GHz.

Figure 5.2 illustrates the missdetection probability of SPET method as a function of SNR for different f_d values. It is clear that best performance is that of $f_d = 0\text{Hz}$ (i.e. channel is constant during the observation duration) as the channel provides the maximum correlation level. The performance degrades as maximum Doppler frequency increases since increasing f_d does attenuate the correlation level as seen in Figure 5.1(a). The rate of attenuation is larger when f_d increases which explains the sensing performance degradation. For instance, a detection probability of 0.9 is reached for SNR = -15 dB when the train is not moving, while a SNR larger than -8 dB is required to reach the same level of detection when $f_d = 500\text{Hz}$.

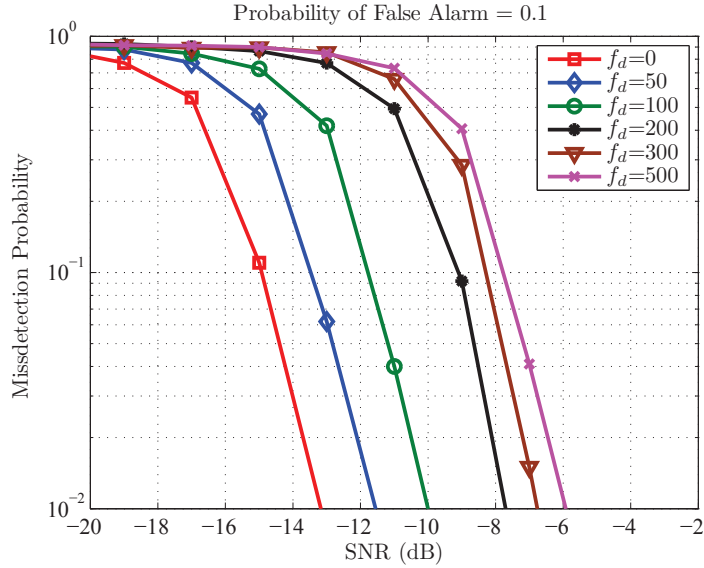


Figure 5.2: The probability of missdetection versus SNR for SPET method at different maximum Doppler frequency (f_d) values when $N = 10000$, $P = 2$, $M = 4$, $\rho_r = 0$ and $L = 20$.

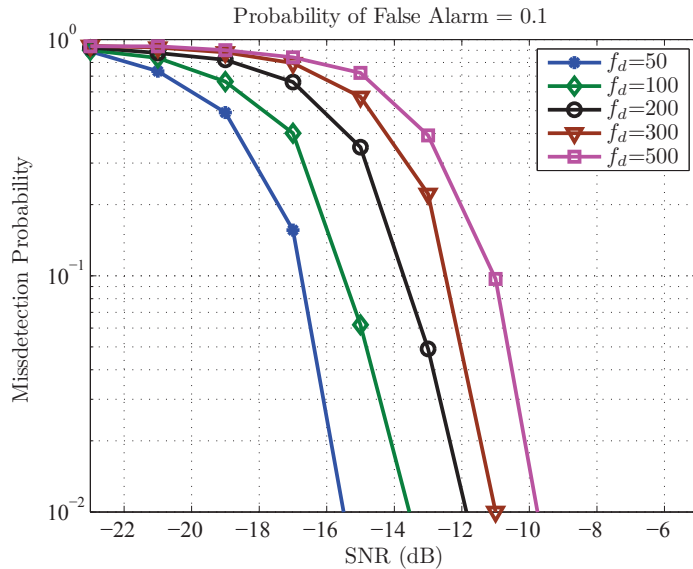


Figure 5.3: The probability of missdetection versus SNR for WCV-T method at different maximum Doppler frequency (f_d) values when $N = 10000$, $P = 2$, $M = 4$, $\rho_r = 0$ and $L = 20$.

The performance of WCV-T method is examined as a function of SNR for different maximum Doppler frequency values and the results are depicted in Figure 5.3. It is clear that the proposed method does improve the performance when compared to the SPET one. The average improvement is represented by a SNR gain of about 3 dB for a level of missdetection probability of 0.1. Also, this Figure shows that the performance of this method degrades when the train moves faster, i.e. for larger f_d values. The WCV-T method requires an SNR level of -11 dB to reach a detection probability of 0.9 for a fast train ($f_d = 500$ Hz), while this level of SNR is approximately -17 dB when the train is moving slowly ($f_d = 50$ Hz).

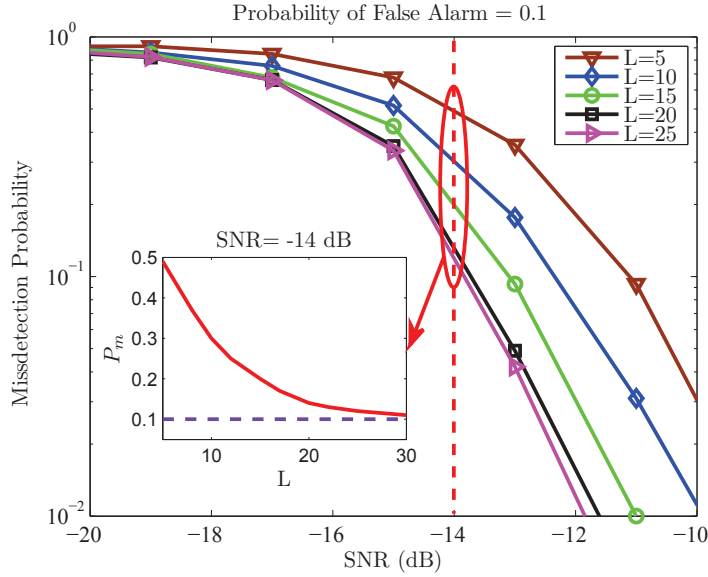


Figure 5.4: The probability of missdetection versus SNR for WCV-T method at different smoothing factor (L) values when $N = 10000$, $P = 2$, $M = 4$, $\rho_r = 0$ and $f_d = 200$. Also, the missdetection probability versus L at a fixed SNR = -14 dB.

In Figure 5.4, the missdetection probability versus SNR for WCV-T method at different smoothing factor values ($L = 5, 10, 15, 20$ and 25) is shown. As can be seen from this Figure, increasing the smoothing factor up to 20 does improve the detection performance. On the other hand, the missdetection probability is almost constant when $L > 20$. For a SNR value of -14 dB, the missdetection probability varies from ~ 0.5 to ~ 0.13 as L goes from 5 to 20, but does not vary a lot for L values larger than 20. In fact, the computational complexity of the proposed method increases when L is larger. Hence, the smoothing factor is chosen relatively low as a compromise between decreasing complexity and performance degradation.

5.3 Spectrum Sensing with Spatially-Correlated Multiple-Antennas

5.3.1 Preliminary Literature Review

Currently, the multiple-antenna techniques are widely used in wireless communications owing to their promise of high data rate and high effectiveness. In CR, using multiple antennas for spectrum sensing is one possible approach to improve detection reliability by exploiting the spatial diversity. The energy detector (ED) [84] is a simple and popular detector for spectrum sensing that gives high performance when the noise variance is known. Another methods that investigates the covariance matrix structure (or its eigenvalues analysis) were used for spectrum sensing when the noise variance is unknown. For instance, we mention the CAV method [92], the MME detector [93], the AGM detector [88], and the proposed SPET method. These detectors were derived and examined for spatially-uncorrelated antennas and may be not appropriate for the correlated case. However, for most practical propagation environments, the antennas are spatially-correlated. Thus, it is worthy to evaluate these methods for the correlated multiple

antennas scenario.

However, for the correlated multiple antennas scenario, the sensing performance of an ED was shown to degrade greatly [110]. The authors analyzed the sensing performance of energy detectors in CR networks when multiple antennas are correlated. It is verified that the sensing performance of the energy detector is degraded when the antennas are spatially-correlated and the performance degradation is proportional to the antennas correlation. In fact, the emergence of the PU's signal changes not only the detected energy, but also the correlation structure of the received signal. Can spatial correlation help? this was the question asked and answered in [111]. The authors studied the GLRT detector performance with spatially-correlated multiple antennas. It was verified that the sensing performance of the GLRT detector does improve with the antenna correlation.

A weighted ED and correlated-GLRT (C-GLRT) detector are proposed for spectrum sensing assisted with correlated multiple antennas in [112]. Compared with the ED and eigenvalue-based detectors, the detection performance of the weighted ED and C-GLRT algorithms does improve. It was seen that the sensing performance of the weighted ED is better than that of the ED under the correlated antennas scenario, while these performances are the same under the independent antennas scenario. In fact, when the antennas are independent, the weighted ED becomes the ED. Also, the C-GLRT detector is more appropriate for correlated multiple antennas assisted spectrum sensing than that of the eigenvalue-based detectors.

The covariance matrix of the received signal was exploited in [113]. The authors define a test statistic as the ratio of the sum of the off-diagonal terms to the sum of the diagonal terms in correlation matrix. The exact sensing performance and the corresponding threshold were derived in closed form in a simple case, i.e. the SU employs two antennas to sense one PU's signal. In [114], the authors analyze the performance of energy detection based spectrum sensing in a CR possessing multiple correlated antennas when the channel from the PU to the CR is Nakagami- m faded. The detection probability of the CR by employing square law combining (SLC) was derived by using the MGF-based approach. Again, it was found that antenna correlation degrades the energy detection performance of the CR. In [115], the spectrum sensing is conducted using an estimate of the cross-correlation among the signals received at different spatially-correlated antenna elements, the authors proposed a blind detection method, which assumes no prior knowledge of the signaling scheme used by the PU, the noise power, or the channel path coefficients.

5.3.2 Predicted Eigenvalues Threshold Sensing Performance with Spatially-Correlated Multiple-Antennas

The following assumptions hold in this section. A secondary user possessing M antenna is sensing the presence of P primary users. The received signal at the i^{th} antenna is given by

$$x_i(n) = \sum_{p=1}^P \sum_{k=0}^{C_p} h_{i,p}(k) s_p(n-k) + w_i(n), \quad n = 1, 2, \dots \quad (5.23)$$

where C_p is the order of the channel between the p^{th} primary source (PS $_p$) and each antenna, and $h_{i,p}(k)$ is the k^{th} tap of the channel response between PS $_p$ and the i^{th} antenna. The taps of the block-fading channel are assumed to be uncorrelated and constant during the observation time. We assume that the source signals $s_p, 1 \leq p \leq P$ are centered and i.i.d. The $M \times 1$ observation vector at the receiver is expressed in matrix form as:

$$\mathbf{x}(n) = \mathbf{H}\mathbf{s}(n) + \mathbf{w}(n) \quad (5.24)$$

where $\mathbf{w}(n) = [w_1(n), \dots, w_M(n)]^T$ is the $M \times 1$ additive white Gaussian noise vector with zero-mean and variance σ_w^2 .

Due to its simplicity and good agreement when describing the spatial correlation, the exponential correlation model is generally used to describe the spatial correlation among multiple antennas. This model was introduced in section 2.3.2.

The channel matrix \mathbf{H} can be rewritten as

$$\mathbf{H} = \mathbf{R}_r^{1/2} \mathbf{H}_w \quad (5.25)$$

where \mathbf{R}_r is the receiver correlation matrices and \mathbf{H}_w is a channel gain matrix whose entries are i.i.d and follows a circularly symmetric complex Gaussian distribution with zero-mean and unit variance. The exponential correlation model defines the receive correlation matrix \mathbf{R}_r with its entries given by

$$[\mathbf{R}_r]_{i,j} = \begin{cases} \rho_r^{j-i}, & i \leq j \\ [\mathbf{R}_r]_{j,i}^*, & i > j \end{cases}, \quad 1 \leq i, j \leq M, |\rho_r| < 1, \quad (5.26)$$

where ρ_r is the receive correlation coefficient between two adjacent antennas.

The covariance matrix of the received signal, set to as $\mathbf{R}_x = \mathbf{E}[\mathbf{x}\mathbf{x}^H]$, gives

$$\mathbf{R}_x = \mathbf{H}\mathbf{R}_s\mathbf{H}^H + \sigma_w^2 \mathbf{I}_M = \mathbf{R}_r^{1/2} \underbrace{\mathbf{H}_w \mathbf{R}_s \mathbf{H}_w^H}_{\mathbf{R}_r^{1/2}} + \sigma_w^2 \mathbf{I}_M \quad (5.27)$$

where $\mathbf{R}_s = \mathbf{E}[\mathbf{s}\mathbf{s}^H]$ is assumed to be of full rank.

The sample covariance matrix is employed to estimate the unknown covariance matrix, and is given, for N observed samples, by

$$\mathbf{R}_x(N) = \frac{1}{N} \sum_{k=1}^N \mathbf{x}(k)\mathbf{x}^H(k) \quad (5.28)$$

In Chapter 4, we proposed a non-parametric multiple-antennas assisted spectrum sensing method based on the predicted eigenvalue threshold. Thereafter, a simplified PET sensing method, which needs to compare only the largest eigenvalue to its threshold, was introduced. The test statistics of the proposed SPET method is represented by

$$T_{\text{SPET}} = \frac{\ell_1}{\frac{1}{q} \sum_{i=1}^q \ell_i} \underset{\delta_0}{\overset{\delta_1}{\gtrless}} \lambda_{\text{SPET}}, \quad (5.29)$$

The eigenvalues of \mathbf{R}_r are approximated as [116]

$$\lambda_{r,i} = \frac{1 - |\rho_r|^2}{1 + 2|\rho_r|\psi_{r,i} + |\rho_r|^2}, 1 \leq i \leq M \quad (5.30)$$

where $\psi_{r,i}$ are roots of the following Equation

$$\frac{\sin(M+1)\psi - 2|\rho_r|\sin M\psi + |\rho_r|^2\sin(M-1)\psi}{\sin\psi} \quad (5.31)$$

It can be shown that $\lambda_{r,1}$, the largest eigenvalue of matrix \mathbf{R}_r , verifies $\lambda_{r,1} \rightarrow \text{tr}(\mathbf{R}_r)$ when $|\rho_r| \rightarrow 1$. Also, the following holds $\sum_{i=1}^M \lambda_{r,i} = \text{tr}(\mathbf{R}_r) = M$, i.e. when $\lim_{|\rho_r| \rightarrow 1} \lambda_{r,i} = 0$ for $2 \leq k \leq M$.

When the multiple-antennas are more correlated, the received power is accumulated in a virtual channel associated with the largest eigenvalue of the covariance matrix. Hence, the diversity effect decreases leading to a capacity loss when using the traditional maximum ratio combiner. On the other hand, any increase in the spatial correlation improves any detection approach based on the largest eigenvalue, e.g. the SPET method. The expected value of the largest eigenvalue of the covariance matrix increases when the channel is more spatially correlated, while the sum of the eigenvalues of this matrix remain almost constant. That is, the test statistic T_{SPET} increases when ρ_r is larger. On the other hand, the decision threshold is chosen under \mathcal{H}_0 , and is found to be independent of the noise power and the channel gains, i.e. this threshold does not change when the level of spatial correlation changes. Obviously, the SPET performance improves when the antennas are more correlated.

Nevertheless, this improvement is limited. In the high SNR region, the missdetection probability is already low and can not be much improved. The largest eigenvalue can be formed as $\lambda_1 = \vartheta_1 + \sigma_w^2$, where ϑ_1 is the largest eigenvalue of the covariance matrix due to noise-free signal. Hence, the improvement resulting from increasing the spatial correlation is reflected in ϑ_1 . Then, the increase of λ_1 is limited when the SNR is very low, i.e. the noise power level is high compared to ϑ_1 . Also, this performance improvement is attested by an increase of the confidence metric. In fact, this improvement is not due to a method development and results from the presence of spatial correlation. In the following, we will propose a method that tries to exploit the spatial correlation structure in a way that the performance is more improved when the correlation level is higher.

Let us consider \mathbf{x}_i the observed signal vector at the i^{th} antenna, i.e. $\mathbf{x}_i = [x_i(1), x_i(1), \dots, x_i(N)]$. The sample covariance matrix of the received signal defined in Equation (5.28) can be reformulated as

$$\mathbf{R}_{\mathbf{x}}(N) = \begin{bmatrix} R_{1,1} & R_{1,2} & \cdots & R_{1,M} \\ R_{2,1} & R_{2,2} & \cdots & R_{2,M} \\ \vdots & \vdots & \ddots & \vdots \\ R_{M,1} & R_{M,2} & \cdots & R_{M,M} \end{bmatrix} \quad (5.32)$$

where $R_{i,j}$ is the estimated spatial cross-correlation between the observed signal at the i^{th} antenna

and that on the j^{th} antenna, and is given as

$$R_{i,j} = \frac{1}{N} \sum_{k=1}^N x_i(k)x_j^*(k) = \frac{1}{N} \mathbf{x}_i \mathbf{x}_j^H. \quad (5.33)$$

The previous methods that exploit the covariance matrix (directly or via the eigenvalue analysis) for spectrum sensing gives all the entries of this matrix the same weight. On the other hand, it could be more beneficial to employ a weighted sample covariance matrix when the spatial correlation coefficient is not negligible. The weighted sample covariance matrix can be introduced as an entrywise product of the covariance matrix $\mathbf{R}_x(N)$ and the weights matrix \mathbf{S} , and is represented by $\mathbf{R}_{x,s}(N) = \mathbf{S} \circ \mathbf{R}_x(N)$. The weights $s_{i,j} = [\mathbf{S}]_{i,j}$ are chosen to improve the sensing performance. The test statistics of the proposed weighted covariance value method for spatially-correlated (WCV-S) multiple-antennas, is defined by

$$T_{\text{WCV-S}} = \frac{\sum_{i=1}^M \sum_{j=1, j \neq i}^M s_{i,j} R_{i,j}}{\sum_{i=1}^M s_{i,i} R_{i,i}} \underset{\delta_0}{\overset{\delta_1}{\geq}} \lambda_{\text{WCV-S}}, \quad (5.34)$$

In fact the spatial cross-correlation between the signals received at two antennas is larger when these antennas are closer. Hence, this cross-correlation must be more involved in PU's signals sensing, i.e. the cross-correlation $R_{i,j}$ must be more weighted when the antennas are closer. Based on this analysis, we propose the following weighting matrix,

$$s_{i,j} = \begin{cases} 1 + \rho_r^{|i-j|}, & i \neq j \\ 1, & \text{otherwise} \end{cases}, 1 \leq i, j \leq M. \quad (5.35)$$

The proposed WCV-S method outperforms the SPET one in the presence of moderately spatially-correlated antennas.

Yet the weighting matrix of WCV-S method has to be optimized. This optimization problem is one of our research perspectives. Also, we assume that the spatial correlation coefficient ρ_r is known at the SU receiver or can be estimated. It can be easily proven that the above analysis is still valid when using smoothing factor $L > 1$. The proposed method is evaluated and its performance is compared with that of other methods that employ the standard sampled covariance matrix.

5.3.2.1 Simulations Results and Discussion

Here, we present some simulations results to demonstrate the effectiveness of the proposed sensing methods. These methods are evaluated through the probability of missdetection at a false alarm probability of 0.1. All results are based on 1000 Monte Carlo trials for each method. For each realization, binary phase-shift keying modulated PU signals have been considered. Also, the channel is block-fading whose taps follow a Rayleigh distribution. The spatial correlation is modeled via the exponential correlation model. For different values of SNR, a random additive white Gaussian noise is added.

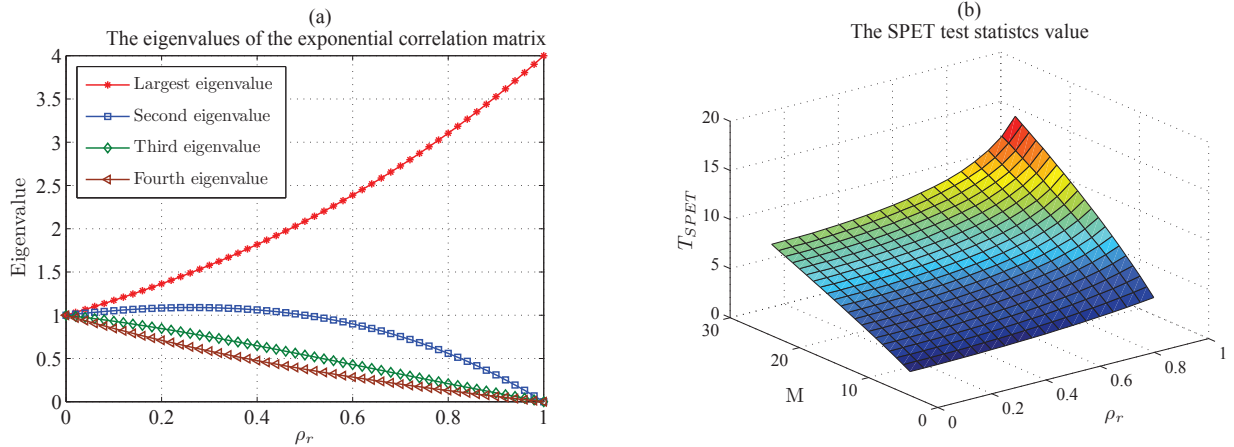


Figure 5.5: (a) The eigenvalues of the receive correlation matrix for $M = 4$. (b) The expected value of the test statistic T_{SPET} , for different values of ρ_r and M , when the sample covariance matrix is calculated for noise-free signals.

Figure 5.5(a) illustrates the eigenvalues of the receive correlation matrix for $M = 4$. We note that the first eigenvalue tends to $\text{tr}(\mathbf{R}_r) = M$ as the correlation coefficient goes to 1. This reflects a tendency to accumulate the received power in the first eigenvalue. Also, simulations reveals that the sum of \mathbf{R}_r eigenvalues always equals to M .

Figure 5.5(b) depicts the expected value of the test statistic T_{SPET} , for different values of ρ_r and M , when the sample covariance matrix is calculated for noise-free signals. This Figure confirm the above analysis, i.e. T_{SPET} increases when the correlation coefficient increases. This increment is more significant when the SU has more receiving antennas.

The impact of the spatial correlation on SPET performance is evaluated and the results are depicted in Figure 5.6. The detection performance improves when the antennas are spatially correlated and becomes ever more improved as the correlation increases. Obviously, the eigenvalues of the spatial correlation matrix \mathbf{R}_r strengthen the largest eigenvalue of the signal subspace and reflect time accumulation of SNR. This reinforce the contribution of signals eigenvalues in T_{SPET} compared to the noise eigenvalues and decrease the probability of missdetection. Note an SNR gain of 3 dB when the channel is heavily spatially-correlated. Also, the false alarm probability is not affected by the spatial correlation since it is not reflected in the covariance matrix when there is no signal.

Giving a more important contribution to the cross-correlation components corresponding to the closer antennas leads us to the proposed WCV-S method. This method is evaluated in the presence of moderately spatial correlation coefficient values ($\rho_r \geq 0.4$). The simulations results are depicted in Figure 5.7. The same as the SPET method, increasing the spatial correlation coefficient improves the sensing performance. On the other hand, the WCV-S method provides, in average, an SNR gain of about 2 dB for the missdetection level of 0.1 when compared to the SPET one.

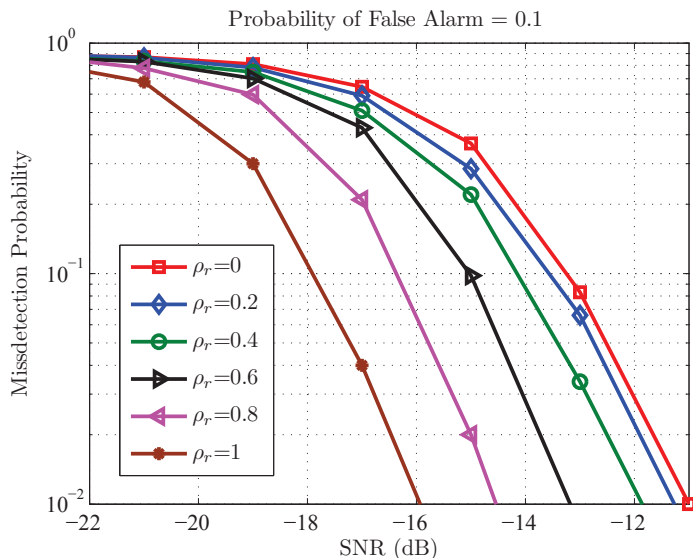


Figure 5.6: The probability of missdetection versus SNR for SPET method at different receive spatial correlation coefficient (ρ_r) values when $N = 10000$, $P = 2$, $M = 4$, and $L = 1$.

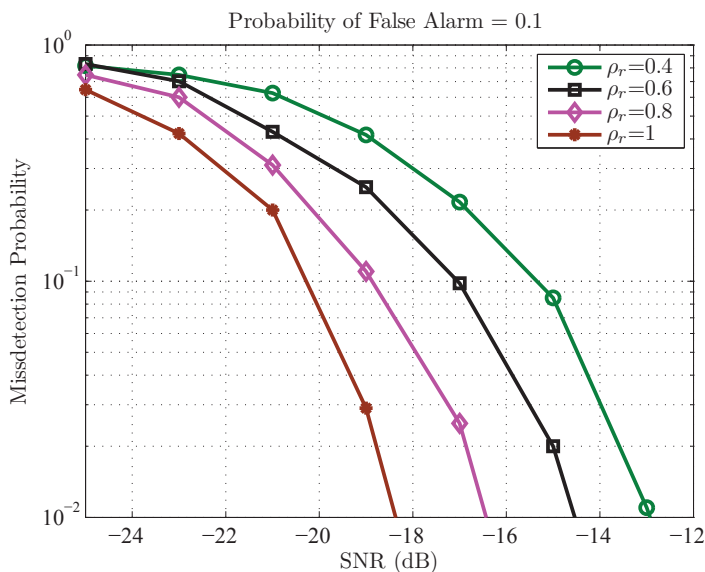


Figure 5.7: The probability of missdetection versus SNR for WCV-S method at different receive spatial correlation coefficient (ρ_r) values when $N = 10000$, $P = 2$, $M = 4$, and $L = 1$.

5.4 Spectrum Sensing in the Presence of Impulsive Noise

The impulsive nature of the noise processes is commonly found in wireless communications. Transportation systems often suffer of impulsive noise such as car ignitions, and the transient EM noise which is produced by the sliding contact between the catenary and the pantograph. The later non-Gaussian heavy-tailed impulsive noise was demonstrated to be characterized by $S\alpha S$ random processes.

The algorithms developed for wireless communication systems under the favorite assumption of Gaussian noise exhibit performance degradation in the presence of non-Gaussian heavy-tailed impulsive noise. Spectrum sensing algorithms are not an exception, the question is, how much their performance is affected by heavy noise tails? However, we will propose two sensing methods. The first one is based on myriad filtering and tries to mitigate the effect of the heavy-tailed noise before sensing, while the second method is based on the covariation absolute value and tries to exploit the noise properties.

5.4.1 Preliminary Literature Review

Some spectrum sensing algorithms are developed to address the problem of spectrum sensing under impulsive noise circumstances [117–120]. In [118], a robust non-parametric cyclic correlation estimator based on the multivariate (spatial) sign function is proposed. However, this method requires prior information about the PU. A class of spectrum-sensing schemes for CR with receive diversity was proposed in [117]. The authors employ the GLRT in the detectors at each antenna branch and exploit a nonlinear diversity-combining strategy. Closed-form expressions of the GLRT was introduced under Gaussian, Cauchy and contaminated Gaussian environments, while calculating the GLRT in the $S\alpha S$ case requires numerical simulations. In [119], a suboptimal l_p -norm primary signal detector in the presence of non-Gaussian noise was proposed. This method provides tunable parameters that allow the detector to adapt to the underlying type of noise. This analysis is valid for arbitrary l_p -norm metric parameters and all types of circularly symmetric noise with finite moments, e.g. AWGN, Gaussian mixture noise, Middleton's class A noise, generalized Gaussian noise, and co-channel interference. The only major exception is α -stable noise. The decision statistic of the proposed detector also requires the knowledge of the power of the fading channel gains. In [120], the authors consider the application of the non-parametric polarity-coincidence-array detectors to sense the primary signal in the presence of non-Gaussian (heavy-tailed) noise when a SU is equipped with multiple antennas. However, this research paper considers the generalized Gaussian noise and Gaussian mixture noise only.

On the other hand, several impulsive noise mitigation methods exist in the literature [43]. The maximum a posteriori (MAP) detector was used in [121] with the $S\alpha S$ noise assumption. The $S\alpha S$ random variable does not have a closed form PDF. This complicates the design of the MAP detector. The PDF is approximated to overcome this difficulty. A well-behaved and computationally tractable approximation was proposed in [121]. Hole punching is a nonlinear filter that emulates the functionality of a hard limiter by setting a received sample to zero when it exceeds some threshold [122]. The advantage of hole punching is the significantly reduced computational complexity. It can be used as a nonlinear filter preceding the sensing algorithm. In [123], the simplified Cauchy-based l_p -norm filter was presented. This filter operates in a wide range of impulsive noise due to the proper adjustment of p exponent of the l_p -norm. The authors applied their filter to suppress an impulsive noise in testing chirp signal and in power line communications environment.

The myriad filter is a robust filter which is very useful in suppressing impulsive noise [124]. It represents a wide class of maximum likelihood type estimators, i.e. the M-estimator. These

estimators were developed in the theory of robust statistics. The selection myriad filtering achieves a good balance between the complexity and the performance for $S\alpha S$ noise mitigation [43]. In the following, we present some of the beneficial properties of α -stable processes.

5.4.2 Basic Properties of $S\alpha S$ Distribution

The $S\alpha S$ random variables are assumed centered at the origin. They have no closed-form of the PDF and are rather described by the characteristic function given by

$$\Phi_w(t) = \exp(-\gamma |t|^\alpha). \quad (5.36)$$

Two well known special $S\alpha S$ distributions are the Cauchy distribution ($\alpha = 1$) and the Gaussian one ($\alpha = 2$). An important difference between the Gaussian and the other distributions of the $S\alpha S$ family is that only moments of order less than α exist for the non-Gaussian $S\alpha S$ family members. The fractional lower order moments of a $S\alpha S$ random variable are given by Zolotarev's theorem.

Theorem 4 (Zolotarev's Theorem). Let $w \sim \mathcal{S}_\alpha(\beta, \gamma, \delta)$. Then,

$$E(|w|^p) = \begin{cases} C_\alpha(p) \gamma^{p/\alpha}, & \text{for } 0 < p < \alpha \\ \infty, & \text{for } p \geq \alpha \end{cases}, \quad (5.37)$$

where $C_\alpha(p) = \frac{2^{p+1}\Gamma(\frac{p+1}{2})\Gamma(\frac{-p}{\alpha})}{\alpha\sqrt{\pi}\Gamma(\frac{-p}{2})}$ is a function of α and p .

One important observation we can make from this theorem is that other than the Gaussian case, α -stable random variable do not have finite variance; and for $\alpha \leq 1$, even the absolute mean, $E(|w|)$, is not finite, i.e. covariances do not exist on the space of $S\alpha S$ random variables. Instead a quantity called *covariation* plays an analogous role, for statistical signal processing problems involving $S\alpha S$ processes, to the role played by covariance in the case of second order processes. For jointly $S\alpha S$ random variables X and Y with $1 < \alpha \leq 2$, the covariation of X with Y is defined by

$$[X, Y]_\alpha \triangleq \int_{\mathcal{S}} x y^{(\alpha-1)} d\Gamma(S) \quad (5.38)$$

where \mathcal{S} is the unit circle, $d\Gamma(S)$ is the spectral measure of the $S\alpha S$ random vector (X, Y) , and the notation " $\cdot^{(\cdot)}$ " denotes the following operation

$$y^{(\alpha)} = \begin{cases} |y|^\alpha \text{sign}(y), & \text{for } y \in \mathbb{R} \\ |y|^{\alpha-1} y^*, & \text{for } y \in \mathbb{C} \end{cases}. \quad (5.39)$$

The *covariation coefficient* of X with Y is described by

$$\lambda_{X,Y} \triangleq \frac{[X, Y]_\alpha}{[Y, Y]_\alpha} \quad (5.40)$$

Contrary to the covariance, the covariation is not symmetric other than for $\alpha = 2$, i.e. $[X, Y]_\alpha \neq [Y, X]_\alpha$, $1 < \alpha < 2$. These definitions has practical use since covariation is expressed as a function

of FLOMs as explained in the following theorem.

Theorem 5. Let X and Y be jointly $S\alpha S$ with $1 < \alpha \leq 2$. Suppose that the dispersion of Y is γ_y . Then

$$[Y, Y]_\alpha = \gamma_y, \quad (5.41)$$

$$\lambda_{X,Y} = \frac{E(XY^{(p-1)})}{E(|Y|^p)}, 1 \leq p < \alpha, \quad (5.42)$$

$$[X, Y]_\alpha = \frac{E(XY^{(p-1)})}{E(|Y|^p)} \gamma_y, 1 \leq p < \alpha. \quad (5.43)$$

The covariation has the following properties:

- ❖ If X_1, X_2 and Y are jointly $S\alpha S$, then

$$[aX_1 + bX_2, Y]_\alpha = a[X_1, Y]_\alpha + b[X_2, Y]_\alpha, \forall (a, b),$$

- ❖ If Y_1 and Y_2 are independent and X, Y_1 and Y_2 are jointly $S\alpha S$, then

$$[aX, bY_1 + cY_2]_\alpha = ab^{(\alpha-1)} [X, Y_1]_\alpha + ac^{(\alpha-1)} [X, Y_2]_\alpha, \forall (a, b, c),$$

- ❖ If X and Y are independent $S\alpha S$, then $[X, Y]_\alpha = 0$.

Let $\mathbf{x} = [X_1, \dots, X_M], \mathbf{y} = [Y_1, \dots, Y_M]$ be $M \times 1$ vectors whose entries are jointly $S\alpha S$, then the covariation matrix of \mathbf{x} with $\mathbf{y}, \mathbf{\Gamma}_{x,y} = [\mathbf{x}, \mathbf{y}]_\alpha$, is defined by $[\mathbf{\Gamma}_{x,y}]_{i,j} \triangleq [X_i, Y_j]_\alpha$. Also, the covariation of \mathbf{x} is formed as $\mathbf{\Gamma}_x = [\mathbf{x}, \mathbf{x}]_\alpha$.

Quick review of traditional spectrum sensing techniques reveals that they employ second and higher order moments. These techniques cannot be applied in impulsive noise environments modeled under the α -stable law, since these processes do not possess finite p^{th} order moments for $p \geq \alpha$. Instead properties of FLOMs and covariations should be used.

5.4.3 System Model

The following assumptions hold in this section. A SU possessing M antenna is sensing the presence of P PUs. The source signals $s_j, 1 \leq j \leq P$ are assumed to be centered and i.i.d. The received signal at the i^{th} antenna is given by

$$x_i(n) = \tilde{s}_i(n) + w_i(n) = \sum_{j=1}^P h_{i,j} s_j(n) + w_i(n), \quad n = 1, 2, \dots \quad (5.44)$$

where $w_i(n)$ is additive noise, and $h_{i,j}$ is block-fading channel response between PS_j and the i^{th} antenna.

The $M \times 1$ observation vector at the receiver is expressed as,

$$\mathbf{x}(n) = \mathbf{H}\mathbf{s}(n) + \mathbf{w}(n) \quad (5.45)$$

where \mathbf{H} is the $M \times P$ matrix of the block-fading channel. Also, $\mathbf{w}(n) = [w_1(n), \dots, w_M(n)]^T$ is the $M \times 1$ additive centered $S\alpha S$ distributed noise vector. The noise components are assumed to have the same characteristic exponent α . Also, the noise samples are assumed i.i.d, independent from received signals, and has covariation matrix $\mathbf{\Gamma}_w = \gamma_w \mathbf{I}_M$.

5.4.4 α -Stable Noise Mitigation

Myriad filters provide a flexible filtering framework with high statistical efficiency in bell-shaped impulsive distributions encountered in practice like the $S\alpha S$ distribution. Myriad filters present important optimality properties along the α -stable family [124]. Myriad filtering is the M-estimator of Cauchy distribution ($\alpha = 1$), and its associated cost function is given by,

$$\varphi(x) = \log(k^2 + x^2), \quad (5.46)$$

where the free-tunable parameter k is called the *linearity parameter* of the myriad and controls the impulse-resistance, i.e. the outlier rejection capability. The maximum likelihood estimator of location associated with this cost function is called the *sample myriad*. Let us consider a set of samples $\{x(i)\}_{i=1}^{N_w}$, the sample myriad of order $k > 0$ is calculated by,

$$\begin{aligned} \hat{\beta}_k &= \text{myriad} \{k; x(1), x(2), \dots, x(N_w)\} \\ &= \arg \min_{\beta} \sum_{i=1}^{N_w} \log \{k^2 + [x(i) - \beta]^2\} \\ &= \arg \min_{\beta} \prod_{i=1}^{N_w} \{k^2 + [x(i) - \beta]^2\} \end{aligned} \quad (5.47)$$

The linearity parameter determines the behaviour of the myriad filter: an infinite value of k makes the myriad filter a linear estimator, as the value of k decreases this estimator becomes more resilient to the presence of impulsive noise and finally converts into the so-called mode-myriad when k tends to zero. The selection myriad filter is based on the properties of mode-myriad. The selection property means that the output of the filter does always belong to \mathcal{M} , the set of most repeated values in the input window, and is introduced by,

$$\begin{aligned} \hat{\beta}_0 &= \text{mod-myriad} \{x(1), x(2), \dots, x(N_w)\} \\ &\triangleq \arg \min_{x_j \in \mathcal{M}} \prod_{i=1, i \neq j}^{N_w} |x(i) - x(j)| \end{aligned} \quad (5.48)$$

The myriad filter is used as a non-linear filter to mitigate the heavy tails effects. This filter is defined as a sliding window filter whose output is the sample myriad of the elements in the window. The filtered signal x_f can be interpreted as an estimate of location based on signal samples,

$$x_f(n) = \text{myriad} \{k; x(n - N_1), \dots, x(n + N_2)\}, 1 \leq n \leq N \quad (5.49)$$

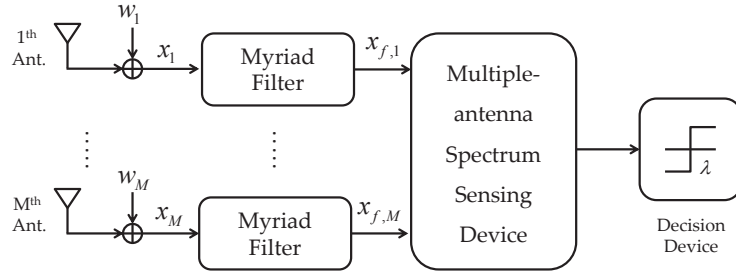


Figure 5.8: Block diagram of the myriad filtering based spectrum sensing.

where N is the number of observed samples of signal x , and N_1, N_2 are chosen such as $N_1 + N_2 = N_w - 1$.

Figure 5.8 shows the block diagram of the myriad filtering (MyrF) based spectrum sensing. The traditional spectrum sensing methods, presented in Chapter 4, are employed to conduct the spectrum sensing. Here, we will apply the SPET method on the filtered signal to sense the spectrum. Its performance is examined for different impulsive noise parameters.

5.4.5 Generalized Covariation Coefficient Absolute Value Based Spectrum Sensing

We assume that the primary signals are independent $S\alpha S$ random processes with zero locations such that $[s_k(n), s_l(n)]_\alpha = \gamma_{s,k} \delta(k - l)$. The covariation of $x_i(n)$ with $x_j(n)$ is calculated by,

$$\begin{aligned} [x_i(n), x_j(n)]_\alpha &= [\tilde{s}_i(n) + w_i(n), \tilde{s}_j(n) + w_j(n)]_\alpha \\ &= [\tilde{s}_i(n), \tilde{s}_j(n)]_\alpha + [\tilde{s}_i(n), w_j(n)]_\alpha + [w_i(n), \tilde{s}_j(n)]_\alpha + [w_i(n), w_j(n)]_\alpha \end{aligned} \quad (5.50)$$

By the independence assumption of signal and noise components, we have $[\tilde{s}_i(n), w_j(n)]_\alpha = [w_i(n), \tilde{s}_j(n)]_\alpha = 0$. Also, by using (5.44) and covariation properties, it holds that,

$$\begin{aligned} [\tilde{s}_i(n), \tilde{s}_j(n)]_\alpha &= \left[\sum_{k=1}^P h_{i,k} s_k(n), \tilde{s}_j(n) \right]_\alpha \\ &= \sum_{k=1}^P h_{i,k} [s_k(n), \tilde{s}_j(n)]_\alpha \\ &= \sum_{k=1}^P h_{i,k} \left[s_k(n), \sum_{l=1}^P h_{j,l} s_l(n) \right]_\alpha \\ &= \sum_{k=1}^P h_{i,k} \sum_{l=1}^P h_{j,l}^{(\alpha-1)} [s_k(n), s_l(n)]_\alpha \end{aligned} \quad (5.51)$$

Finally, we have $[w_i(n), w_j(n)]_\alpha = \gamma_w \delta(i - j)$. This can be easily justified by the above noise assumptions. Hence, the covariation of $x_i(n)$ with $x_j(n)$ is calculated by,

$$[x_i(n), x_j(n)]_\alpha = \sum_{k=1}^P h_{i,k} h_{j,k}^{(\alpha-1)} \gamma_{s,k} + \gamma_w \delta(i - j), \quad 1 \leq i, j \leq M \quad (5.52)$$

Hence,

$$\lambda_{x_i(n), x_j(n)} = \frac{\sum_{k=1}^P h_{i,k} h_{j,k}^{(\alpha-1)} \gamma_{s,k} + \gamma_w \delta(i-j)}{\sum_{k=1}^P |h_{j,k}|^\alpha \gamma_{s,k} + \gamma_w}, 1 \leq i, j \leq M \quad (5.53)$$

The covariation matrix of the observation vector is given, in matrix form, by the following expression,

$$\mathbf{\Gamma}_x = \mathbf{H} \mathbf{\Gamma}_s \mathbf{H}^{(\alpha-1)} + \gamma_w \mathbf{I}_M \quad (5.54)$$

where $\mathbf{\Gamma}_s = \text{diag}(\gamma_{s,1}, \dots, \gamma_{s,P})$ and $[\mathbf{H}^{(\alpha-1)}]_{i,j} = [\mathbf{H}]_{j,i}^{(\alpha-1)}, 1 \leq i \leq P, 1 \leq j \leq M$. The covariation coefficient matrix $\mathbf{\Lambda}_x$ is defined by $[\mathbf{\Lambda}_x]_{i,j} = \lambda_{x_i(n), x_j(n)}$.

Hence, some traditional covariance matrix based signal processing methods could be extended to the covariation matrices. For instance, the authors in [125] proposed a robust covariation-based multiple signal classification (ROC-MUSIC) method to estimate the direction of arrival. Several estimators for the covariation coefficient exist in the literature. Therefore, in the following, we focus on the covariation coefficient matrix to conduct spectrum sensing.

Let X, Y be two random variables, the *generalized covariation coefficient* (GCC) function of X with Y is defined by,

$$\lambda_{\alpha,p}(X, Y) = \frac{E(XY^{(p-1)})}{E(|Y|^p)}, 0 < p < \alpha, \quad (5.55)$$

Obviously, $\lambda_{\alpha,p}(X, Y)$ is identical to the covariation coefficient when X, Y are jointly $S\alpha S$. We have $\lambda_{\alpha,p}[x_i(n), x_j(n)] = \gamma_w \delta(i-j)$ when no PU is present. On the other hand, under \mathcal{H}_1 , $\lambda_{\alpha,p}[x_i(n), x_j(n)]$ exists, when $E(|s_j(n)|^p), 0 < p < \alpha, 1 \leq j \leq P$ does exist. This assumption is realistic and relax the constraints on the source signals.

In fact, the GCC is unknown at the receiver and has to be estimated. The sample GCC is introduced to overcome this difficulty, and is obtained by,

$$\hat{\lambda}_{\alpha,p}(i, j) = \frac{\sum_{k=1}^N x_i(k) [x_j(k)]^{(p-1)}}{\sum_{k=1}^N |x_j(k)|^p} \quad (5.56)$$

This estimator has the same form of the modified FLOM (MFLOM) estimator for jointly $S\alpha S$ random variables [125].

Ideally, under \mathcal{H}_0 , the GCC matrix is a diagonal, while some off-diagonal entries are not zeros under \mathcal{H}_1 . This property is exploited to introduce the generalized covariation coefficient absolute value (CCAVAL) based spectrum sensing. The proposed test statistic is calculated by,

$$T_{\text{CCAVAL}}(p) = \frac{\sum_{i=1}^M \sum_{j=1}^M |\hat{\lambda}_{\alpha,p}(i, j)|}{\sum_{i=1}^M |\hat{\lambda}_{\alpha,p}(i, i)|} \underset{\delta_0}{\overset{\delta_1}{\geq}} \lambda_{\text{CCAVAL}}(p) \quad (5.57)$$

In fact this non-parametric sensing method requires a rough estimation of α .

5.4.6 Performance Evaluation

In this subsection we evaluate the performance of the two proposed methods, namely, the generalized CCAV and the myriad filtering based spectrum sensing methods. These methods are evaluated through the probability of missdetection at a false alarm probability of 0.1. In order to determine the threshold for this given P_f , the decision statistic is calculated for 10^6 independent random trials under \mathcal{H}_0 , i.e. when there is no signal. We sort the decision statistic values in descending order to choose the detection threshold such as $P_f \times 10^6$ samples of the generated statistic values are above the chosen threshold.

All results are based on 1000 Monte Carlo trials for each method. For each realization, the channel is block-fading whose taps follow a Rayleigh distribution. Also, the P primary signals are binary phase-shift keying modulated ones. A random additive i.i.d $S\alpha S$ noise vector is added.

The second order moment is widely accepted as a measure of signal strength which defines the popular SNR measure. This distortion measure is not valid in the presence of α -stable noise, since this noise processes do not have finite second order statistics. In our simulations, we employ the generalized SNR (GSNR). The GSNR is calculated by the ratio of the average received signal power and average dispersion of the stable noise [42], such that,

$$\text{GSNR (dB)} = 10 \log_{10} \frac{E \left[\|\mathbf{x}(n) - \mathbf{w}(n)\|^2 \right]}{M\gamma}. \quad (5.58)$$

We had shown that the measured EM interferences acting on GSM-R Antennas can be fitted to $S\alpha S$ random variable with $\alpha = 1.253$. This value is adopted throughout our simulations.

The performance of MyrF based spectrum sensing is a reflection of the performance of the myriad filter itself. That is, for a chosen multiple-antenna spectrum sensing (e.g. the SPET method), the performance already degrades in low SNR regime under Gaussian noise conditions. This degradation could be extended in the presence of impulsive noise, when the filter fails to properly remove the heavy tails.

The performance of myriad filtering is examined by chirp signals employed as the same deterministic component corrupted with $S\alpha S$ distributed heavy-tailed noise. The performance is evaluated by the root mean square error (RMSE) between the deterministic part of the signal and the filtered signal. Figure 5.9(c) show an example of filtered chirp signal, while Figure 5.9(a) and Figure 5.9(b) shows the original and corrupted signals. Also, It is clear, from Figure 5.9(d), that in the very low SNR region (i.e. $\text{GSNR} < -10$ dB), the myriad filter performance does degrade dramatically.

Figure 5.10 illustrates the missdetection probability of the MyrF based spectrum sensing as a function of GSNR for different values of $1 < \alpha < 2$. The filter output is sensed using the SPET detector to decide the PU signals presence/absence. The performance of MyrF based method, in one way or another, reflects the performance of myriad filter itself shown in Figure 5.9(d). In average, the sensing performance degrades rapidly for SNR values lower than certain level which is around -10 dB. On the other hand, it is clear that this performance depends on α where the missdetection probability is lower for higher α values, i.e. heavier tails more affect the sensing

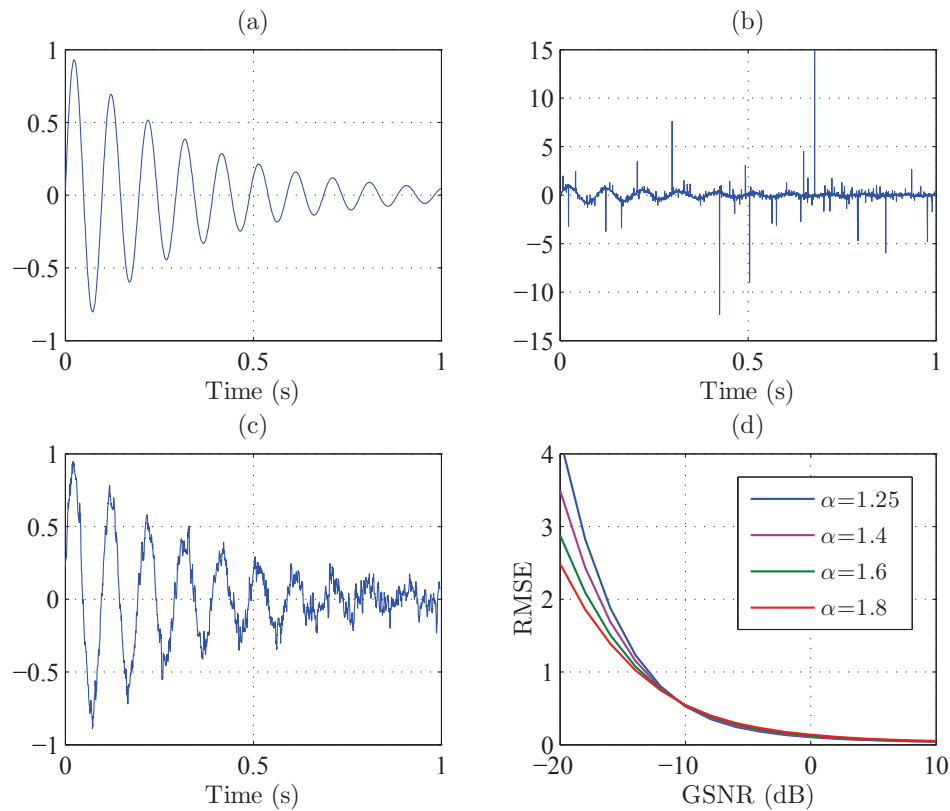


Figure 5.9: Myriad filtering of chirp signal corrupted with $S\alpha S$ distributed heavy-tailed noise for $\alpha = 1.253$ and $\text{GSNR} = 2$ dB (a) original signal (b) noisy signal (c) filtered signal. Also, the RMSE as a function of the GSNR is given for $\alpha = 1.253$ (d).

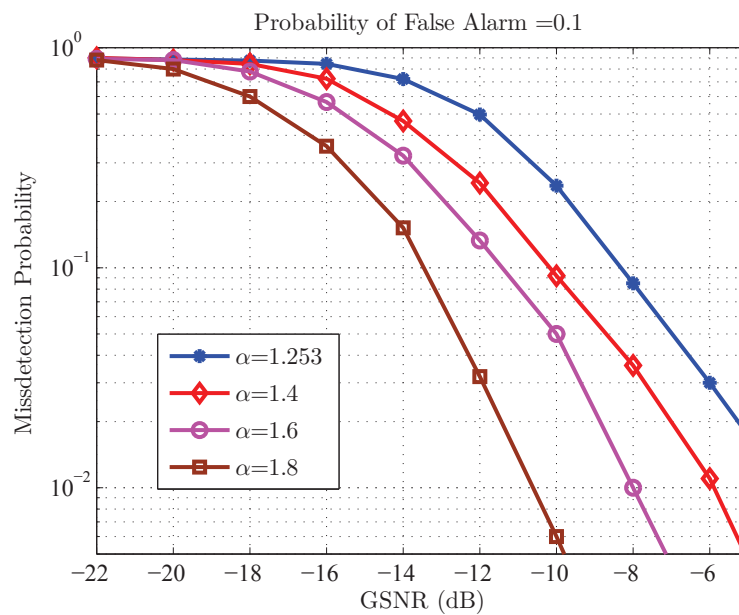


Figure 5.10: Missdetection probability of MyrF based spectrum sensing versus GSNR for different α values when $N = 10000$, $L = 1$, $M = 4$ and $P = 1$.

performance even when filtered. Yet this influence can be considered reasonable when comparing to other methods. To reach a detection probability value of 0.9, an extra GSNR, about 4 dB, is required when α varies from 1.8 to 1.253.

The performance of generalized CCAV method depends on the p value employed to obtain its test statistic, i.e. the p value used in Equation (5.57) to estimate the covariation coefficients. In other words, the generalized CCAV performance depends on the performance of the MFLOM estimator for $S_{\alpha S}$ processes. This covariation coefficient estimator was deeply studied in [125]. Figure 5.11 shows that this estimator is very robust for the values of p in the range $[1/2, \alpha/2]$, $1 < \alpha < 2$.

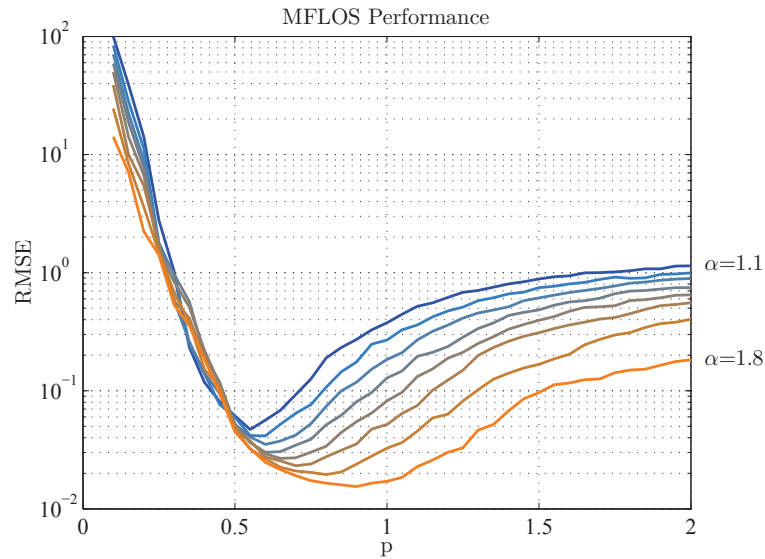


Figure 5.11: Root minimum square error of the MFLOM estimator of the covariation coefficient as a function of the parameter p .

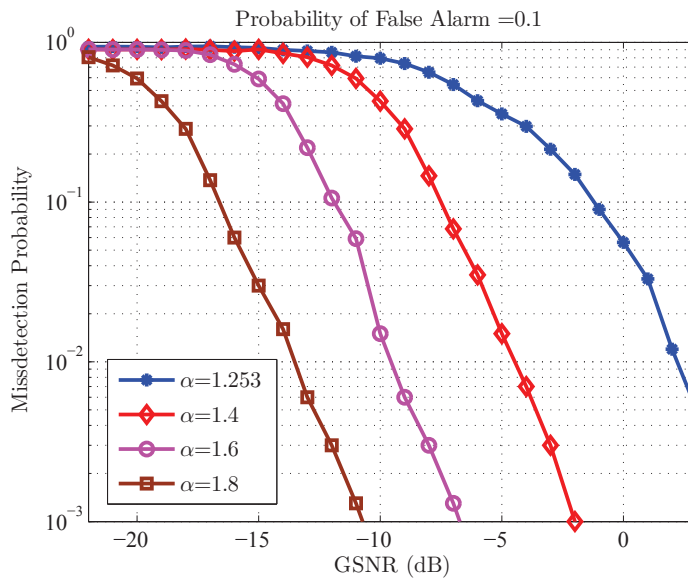


Figure 5.12: Generalized CCAV missdetection probability versus GSNR for different α values when $N = 10000$, $L = 1$, $M = 4$ and $P = 1$.

The best p value is the one that minimize the root minimum square error of the MFLOM estimator. This value belongs to the previous range but more close to $\alpha/2$. For instance, the best p is about 0.57, 0.61, and 0.7 when α equals, respectively, 1.2, 1.3, and 1.6. Hence, the chosen p value is 0.6 when $\alpha = 1.253$.

The performance of generalized CCAV method is shown Figure 5.12 where the missdetection probability is depicted as a function of GSNR for different α values. It is clear that the performance degradation is larger for lower α values and that the amount of degradation is considerable. For instance, the probability of detection is larger than 0.9 even for very low GSNR value of -17 dB when $\alpha = 1.8$, while reaching the same level of detection probability is not possible when $\text{GSNR} < -2$ dB for $\alpha = 1.253$. On the other hand, this method provides better performance when compared to MyrF based method under moderately heavy-tailed noise conditions (i.e. $\alpha > 1.5$). The generalized CCAV is preferred in this α region not only due to the previous reason but also due to its lower complexity. In the other α region (i.e. $1 < \alpha < 1.5$), the MyrF based method gives better performance and is preferred. The dramatic degradation of generalized CCAV for $1 < \alpha < 1.5$ is caused by the lower performance of the MFLOM estimator in this region. One way to enhance its sensing performance is to improve the estimator performance.

5.5 Conclusions

This Chapter contents are based on studying the problem of spectrum sensing in the special context of railways, i.e. to cope with: the time-varying nature of wireless channel resulting from high speed of train, the presence of multiple-antenna spatial correlation, and the heavy tails of the impulsive noise modeled with $S\alpha S$ distribution.

First, it was found that the time-varying channel degrades the performance of the NSS methods presented in Chapter 4. Therefore, a new NSS method based on the weighted covariance matrix is introduced. The weighting matrix is optimized to improve the sensing performance in the low SNR regime. The proposed weighted covariance value for time-varying channels method provides an average SNR gain of 3 dB when the train is moving.

Also, the effect of the spatial correlations on NSS methods was examined. It was found that these correlations do improve the sensing performance of some methods, e.g. the SPET method. Another weighting matrix was proposed to better exploit the spatial correlation to achieve higher detection levels. The proposed weighted covariance value for spatially-correlated multiple-antenna systems method provides an average SNR gain of 2 dB when antennas are moderately correlated.

Finally, it was found that the presence of heavy-tailed impulsive noise degrades the performance of NSS methods developed based on the Gaussian noise assumption. Two method were proposed to mitigate the effect of the heavy noise tails when the $S\alpha S$ distributed noise is assumed. The first method is based on the myriad filtering while the second one tries to exploit the covariation properties of the $S\alpha S$ distributed noise. The first method was found to be more efficient when the noise tails are heavier.

General Conclusions and Future Works

Both railway operators and European rail research advisory council target increasing passenger traffic by rail. This objective is infeasible without developing the communication systems for railways such as the information fluxes can reply the demands of operations and safety-related applications (control, command, and maintenance), and that of the various application necessary to guarantee the attraction of rails (passenger information, Internet on-board trains). The integration of the various existing railway-dedicated communication systems represents a key technical challenge for railways in the context of interoperability and efficiency.

The next generation wireless technology referred to as cognitive radio emerged originally to improve the radio spectrum utilization efficiency. CR based solution for railways has the potential for providing significant benefits, including interoperability, improved spectral efficiency, optimization of radio resource usages, lower deployment and operational costs, and improvement of communications reliability. This thesis is a step towards that solution.

In the following, the most important topics discussed in each Chapter are summarized, and the main conclusions and contributions of this thesis are highlighted. Thereafter, we present a list of possible near future work and perspectives that could lead to the continuation of some of our propositions.

Summary and conclusions

In Chapter 1, we discussed the problematic, the context and the motivations of this work. First, the existing communication systems for railways were surveyed, and the special needs of operators and passengers were explained. Then, we presented the concept and the architecture of the CR, before exploring the possibility of developing a communication system for railways based on the CR. The focus of the last section of this Chapter was to highlight the areas of the CR research where this thesis contributions belong, i.e. developing waveform awareness and spectrum awareness functions.

Our first task was modeling the radio environment of railways such as the developed methods must respect the characteristics of this special context. These characteristics come mainly from the high mobility, the EM interferences, and the topology of the environment. Chapter 2 presented the resulting constraints from these phenomena. The characteristics of the mobile radio channels mainly the Doppler effect related to the high mobility was presented. We adopted the

generalized exact Doppler spread model to simulate the dynamic radio channel due to its properties which are well matched to the theoretical model. Furthermore, practical multiple-antenna receivers suffer from the spatial correlation which may degrade the performance of wireless systems. These correlations were modeled by the Kronecker model based on the exponential correlation model. This model is physically reasonable in the sense that the correlation decreases with increasing distance between antennas. Also, the EM noise interferences were modeled by the α -stable processes. This model was justified not only by the generalized central limit theorem, but also by the proposed distribution fitting of the measured transient EM noise acting on GSM-R antenna. The importance of this new result lies in the fact that it confirms the validity of the wide use of α -stable processes to model impulsive noise. These constraints were taken into consideration in Chapter 5 where the problem of narrowband spectrum sensing was studied.

Thereafter, the waveform awareness of a CR device was the focus of Chapter 3. This awareness can be improved by identifying several features of the received signal, e.g. the used modulation scheme, whether spectrum spreading is employed or not, and whether the signal is a multi-carrier one or not. Literature review of existing waveform identification algorithms is presented. Then we proposed a modulation recognition algorithm for MIMO systems based on HOS. This method, to the best of our knowledge, is among the first ones that studied the modulation recognition for MIMO systems, and the first one that addressed the spatially-correlated case. Three new algorithms were introduced and studied: the AMR-D, the AMR-ZF, and the AMR-SCMA algorithms. The proposed algorithms showed to be capable of identifying different linear digital modulation schemes with good accuracy. Thereafter, a blind identification method of MC-DS-CDMA signals based on autocorrelation estimator fluctuations was proposed. The described scheme efficiently estimates symbol duration, CP duration, and subcarriers number. We proposed to enhance the identification performance by exploiting the multiple-antennas at receiver while keeping the detection duration constant. A performance comparison between this method and the one that directly employs the autocorrelation function reveals that this method gives a better identification performance.

The CR based solution for railways requires having a general image of the frequency bands of interest through the spectrum sensing function. Two approaches of spectrum sensing exist, namely, the narrowband sensing and the wideband sensing. Chapter 4 presented a preliminary literature review of these two approaches. The obvious conclusion was that the wideband sensing is still in its early stages, contrary to the narrowband sensing which is well studied in the literature. As a contribution to the narrowband sensing activity, we proposed a new narrowband spectrum method based on the predicted eigenvalue threshold. The proposed method is blind non-parametric and gives good performance when compared with other existing methods. On the other hand, we proposed an improved cooperative Welch periodogram based wideband sensing. This method is a compromise between reducing complexity and sampling rates (compression rate 100%), i.e. using sub-Nyquist sampling while still avoiding the NP-hard problem of spectrum reconstruction. However, improving the wideband sensing performance is a tradeoff with using more antennas than that required in the narrowband sensing. Nowadays wideband spectrum sensing is a very active research area and may become preferred to the narrowband spectrum sensing in the near future.

Sensing the spectrum for railway-dedicated CR application faces some special constraints to cope with. That is, the high-speed results in a time-varying wireless channel, and the EM interferences makes the Gaussian noise assumption (assumed in Chapter 4) invalid. First, it was found that the time-varying channel degrades the performance of the NSS methods presented in Chapter 4. Therefore, we introduced a new NSS method based on the weighted covariance matrix, and optimized to improve the sensing performance in the low SNR regime. The new weighted covariance value for time-varying channels method provides an average SNR gain of 3 dB when the train is moving. Also, we found that spatial correlations do improve the sensing performance of some methods, e.g. the SPET method. However, higher detection levels were achieved by exploiting the spatial correlation phenomenon. We proposed the new weighted covariance value for spatially-correlated multiple-antenna systems method. This method provided an average SNR gain of 2 dB when antennas are moderately correlated. Finally, we had found that the presence of heavy-tailed impulsive noise degrades the performance of NSS methods developed based on the Gaussian noise assumption. Two method were proposed to mitigate the effect of the heavy noise tails when the $S\alpha S$ distributed noise is assumed. The first method is based on the myriad filtering while the second one tries to exploit the covariation properties of the $S\alpha S$ distribution. The first method was found to be more efficient when the noise tails are heavier.

Perspectives

Beyond the contributions presented in this thesis, some questions remain open issues and need further investigations. Below, we list some topics that may be viewed as the natural continuity of our work:

- ❖ We assumed the isotropic scattering when modeling the Doppler power spectrum, i.e., each channel tap is associated with the classical Jakes Doppler spectrum. In practice, this assumption may be not always valid. Measurements has to be done in different scenarios to confirm which model to be employed to characterize the wireless channel. These measurements are beyond our research wok, however, some new results published in [126] may be taken into consideration. Also, our algorithms must be evaluated in other existing Doppler power spectrum models like asymmetrical Jakes spectrum, bi-Gaussian spectrum, bell-shaped spectrum, etc.
- ❖ The proposed waveform awareness methods, presented in Chapter 3, had not taken into consideration the effects of the high mobility and the heavy-tailed impulsive noise. Developing modulation scheme recognition and modulation technique identification algorithms, that take these phenomena into account, is an important perspective of our research work.
- ❖ The sub-Nyquist sampling is used for the proposed cooperative Welch periodogram based wideband sensing while still avoiding the NP-hard problem of spectrum reconstruction. One of our perspectives is to develop the proposed wideband sensing method to work with lower compression rates without the need of spectrum recovery. This will relax the constraints on ADCs and reduce the complexity and consequently cut down energy cost.

- ❖ We have shown in Chapter 5 that the presence of spatial correlation improves the sensing performance of some methods. However, we proposed a weighting matrix to better exploit these correlations to enhance the sensing performance. This improvement was confirmed by the simulations results. Yet the weighting matrix of WCV-S method has to be optimized. This optimization problem is one of our near future research perspectives.
- ❖ Theoretically, the covariation properties well characterize the $S\alpha S$ processes. The performance of the covariation based spectrum sensing was not as high as expected because of the low performance of the modified fractional lower order estimator. An improved covariations estimator will certainly improves the sensing performance.
- ❖ Our thesis contributions were restricted to the physical layer functions. Our research work will be extended, by employing the knowledge obtained during this Ph.D. candidature and the developed methods, to the area of the cross-layer design. The objectives are to develop techniques for resource management, priorities organization, and the joint scheduling of sensing and transmission durations.
- ❖ Some of the proposed methods in this thesis will be implemented and evaluated on the OpenAir Interface platform in the framework of the ANR project CORRIDOR. This platform is developed by EURECOM and other partners within several collaborative projects [127].

Appendix A

α -stable Noise Generation

In order to generate α -stable distributed data $\{w_k\}_{k=1,\dots,N}$, we have used the inverse transform method, whose principle is briefly described below.

Let U be a random variable uniformly distributed over the interval $[0, 1]$ and consider N of its realizations $\{u_k\}_{k=1,\dots,N}$. Then, if $F_U(u)$ stands for the cumulative distribution function (CDF) of U , we can write that $F_U(u_k) = u_k$.

Let's now consider that our data samples are obtained from $\{u_k\}_{k=1,\dots,N}$, via the transformation $w_k = G(u_k)$, where the function G is the inverse of, H , the CDF of α -stable distributed data, so that $G = H^{-1}$.

The cumulative distribution function of W can be then readily derived as follows

$$\begin{aligned} F_W(w) &= \mathbb{P}[W \leq w] = \mathbb{P}[G(U) \leq w] \\ &= \mathbb{P}[U \leq G^{-1}(w)] = \mathbb{P}[U \leq H(w)] \\ &= F_U\{H(w)\} = H(w) \end{aligned} \tag{A.1}$$

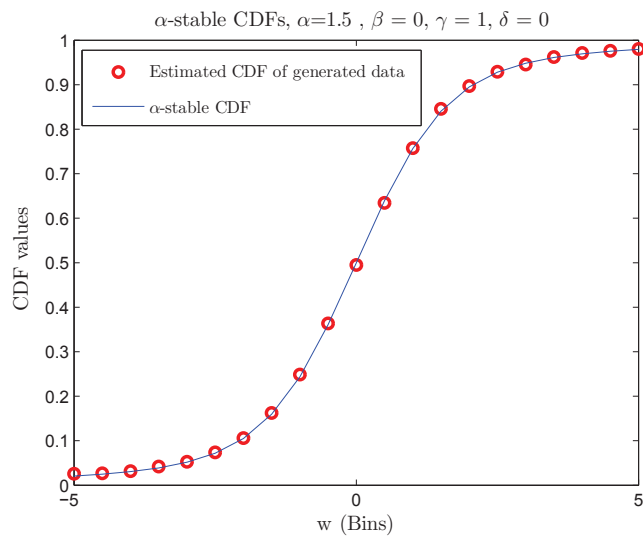


Figure A.1: Estimated CDF of simulated α -stable distributed data using the inverse transform method and the corresponding theoretical CDF.

Consequently, we can conclude from Equation (A.1) that the data samples given by $w_k = H^{-1}(u_k)$ are α -stable distributed.

Figure A.1 displays the estimated CDF of generated α -stable distributed data using the inverse transform method and the corresponding theoretical CDF.

Appendix B

Appendix Related to Chapter 3

B.1 Theoretical Values of the HOS for different modulation schemes

The theoretical values of higher order cumulants and higher order moments for $k = 2, 4$ and 6 , and 2-PSK, 4-PSK, 8-PSK, 4-ASK, 8-ASK, 16-QAM, and 64-QAM signals, are given in B.1. These values are computed for noise-free constellations with unit variance and equiprobable symbols [48, 56].

Table B.1: Some theoretical statistical moments and cumulants values for different modulation schemes of interest.

	2-PSK	4-PSK	8-PSK	4-ASK	8-ASK	16-QAM	64-QAM
C20	1	0	0	1	1	0	0
M40	1	1	0	1.64	1.77	-0.67	-0.18
M41	1	0	0	1.64	1.77	0	0
M42	1	1	1	1.64	1.77	1.32	1.34
C40	-2	1	0	-1.36	-1.24	-0.68	-0.62
C41	-2	0	0	-1.36	-1.24	0	0
C42	-2	-1	-1	-1.36	-1.24	-0.68	-0.62
M60	1	0	0	2.92	3.62	0	0
M61	1	-1	0	2.92	3.62	-1.32	0.38
M63	1	1	1	2.92	3.62	1.96	2.08
C60	16	0	0	8.32	7.19	0	0
C61	16	-4	0	8.32	7.19	2.08	1.8
C62	16	0	0	8.32	7.19	0	0
C63	16	4	4	8.32	7.19	2.08	1.8

B.2 Derivation of ZF Post-processing SNR in The Presence of Channel Estimation Error

The ZF equalizer output is given by

$$\hat{\mathbf{s}} = \hat{\mathbf{B}} (\mathbf{H}\mathbf{s} + \mathbf{w}) \quad (\text{B.1})$$

where $\hat{\mathbf{B}} = \hat{\mathbf{H}}^\dagger = (\mathbf{H} + \sigma_e \mathbf{\Omega})^\dagger$. Assume $\sigma_e \ll 1$, then the pseudo-inverse of the estimated channel matrix can be approximated by the linear part of the Taylor expansion as $\hat{\mathbf{B}} = \mathbf{H}^\dagger (\mathbf{I}_M - \sigma_e \mathbf{\Omega} \mathbf{H}^\dagger)$. Hence, the estimated signal can be written as $\hat{\mathbf{s}} = \mathbf{s} + \hat{\mathbf{w}}$ where $\hat{\mathbf{w}}$ is given by

$$\hat{\mathbf{w}} = \mathbf{H}^\dagger \mathbf{w} - \sigma_e \mathbf{H}^\dagger \mathbf{\Omega} \mathbf{s} - \sigma_e \mathbf{H}^\dagger \mathbf{\Omega} \mathbf{H}^\dagger \mathbf{w}. \quad (\text{B.2})$$

The last two terms in the above expression are additional noise introduced by the channel estimation error. To calculate the effective post-processing SNR for each estimated stream we need to calculate the covariance matrix of the effective post-processing noise, i.e. $\mathbf{E}[\hat{\mathbf{w}} \hat{\mathbf{w}}^H]$. This covariance matrix is computed as,

$$\begin{aligned} \mathbf{E}[\hat{\mathbf{w}} \hat{\mathbf{w}}^H] &= \mathbf{E} \left[\left(\mathbf{H}^\dagger \mathbf{w} - \sigma_e \mathbf{H}^\dagger \mathbf{\Omega} \mathbf{s} - \sigma_e \mathbf{H}^\dagger \mathbf{\Omega} \mathbf{H}^\dagger \mathbf{w} \right) \times \left(\mathbf{H}^\dagger \mathbf{w} - \sigma_e \mathbf{H}^\dagger \mathbf{\Omega} \mathbf{s} - \sigma_e \mathbf{H}^\dagger \mathbf{\Omega} \mathbf{H}^\dagger \mathbf{w} \right)^H \right] \\ &= \sigma_w^2 \mathbf{H}^\dagger \left(\mathbf{H}^\dagger \right)^H - \sigma_e \sigma_w^2 E \left[\mathbf{H}^\dagger \left(\mathbf{H}^\dagger \right)^H \mathbf{\Omega}^H \left(\mathbf{H}^\dagger \right)^H \right] + \sigma_e^2 \sigma_s^2 \mathbf{H}^\dagger E \left[\mathbf{\Omega} \mathbf{\Omega}^H \right] \left(\mathbf{H}^\dagger \right)^H \\ &\quad - \sigma_e \sigma_w^2 E \left[\mathbf{H} \mathbf{H}^\dagger \mathbf{\Omega} \left(\mathbf{H}^\dagger \right)^H \right] + \sigma_e^2 \sigma_w^2 \mathbf{H}^\dagger E \left[\mathbf{\Omega} \mathbf{H}^\dagger \left(\mathbf{H}^\dagger \right)^H \mathbf{\Omega}^H \right] \left(\mathbf{H}^\dagger \right)^H \\ &= \sigma_w^2 \left(\mathbf{H}^H \mathbf{H} \right)^{-1} + \sigma_e^2 \sigma_s^2 \mathbf{H}^\dagger P \mathbf{I}_M \left(\mathbf{H}^\dagger \right)^H + \sigma_e^2 \sigma_w^2 \mathbf{H}^\dagger E \left[\mathbf{\Omega} \left(\mathbf{H}^H \mathbf{H} \right)^{-1} \mathbf{\Omega}^H \right] \left(\mathbf{H}^\dagger \right)^H \\ &= \left[\sigma_w^2 + P \sigma_e^2 \sigma_s^2 + \sigma_e^2 \sigma_w^2 \text{tr} \left(\left(\mathbf{H}^H \mathbf{H} \right)^{-1} \right) \right] \left(\mathbf{H}^H \mathbf{H} \right)^{-1} \end{aligned} \quad (\text{B.3})$$

where $\mathbf{E}[\mathbf{s} \mathbf{s}^H] = \sigma_s^2 \mathbf{I}_P$, $\mathbf{E}[\mathbf{w} \mathbf{w}^H] = \sigma_w^2 \mathbf{I}_M$, $\mathbf{E}[\mathbf{\Omega} \mathbf{\Omega}^H] = P \mathbf{I}_M$, $\mathbf{H}^\dagger \left(\mathbf{H}^\dagger \right)^H = \left(\mathbf{H}^H \mathbf{H} \right)^{-1}$, and $E \left[\mathbf{\Omega} \left(\mathbf{H}^H \mathbf{H} \right)^{-1} \mathbf{\Omega}^H \right] = \text{tr} \left(\left(\mathbf{H}^H \mathbf{H} \right)^{-1} \right) \mathbf{I}_M$.

Based on the above Equation, the post-processing SNR per symbol of the n^{th} stream can be expressed as,

$$\eta_n = \frac{\sigma_s^2 / \sigma_w^2}{\left[1 + P \sigma_e^2 \sigma_s^2 / \sigma_w^2 + \sigma_e^2 \text{tr} \left(\left(\mathbf{H}^H \mathbf{H} \right)^{-1} \right) \right] \left[\left(\mathbf{H}^H \mathbf{H} \right)^{-1} \right]_{nn}}, 1 \leq n \leq P, \quad (\text{B.4})$$

The probability of $\left[\left(\mathbf{H}^H \mathbf{H} \right)^{-1} \right]_{nn}$ to be large is still small. The term $\sigma_e^2 \text{tr} \left(\left(\mathbf{H}^H \mathbf{H} \right)^{-1} \right)$ in the above Equation can be neglected. Finally, the post-processing SNR for each estimated stream is approximated by,

$$\eta_n = \frac{\eta_0}{(1 + \sigma_e^2 P \eta_0) \left[\left(\mathbf{H}^H \mathbf{H} \right)^{-1} \right]_{nn}} = \frac{\eta_0 \kappa_n}{\lambda_e}, 1 \leq n \leq P, \quad (\text{B.5})$$

This derivation was introduced in [61] for uncorrelated Rayleigh channel. Here, we proved that this result is still valid for correlated MIMO systems when the exponential correlation model is assumed.

Appendix C

Appendix Related to Chapter 4

C.1 Derivation Details of the SPET Missdetection Probability

The objective of this Appendix is to prove Equation (4.26). Here, we try to approximate the missdetection probability in the presence of single strong source, i.e., the signal subspace contains an eigenvalue of multiplicity L . Under this assumption, it is clear that $\frac{1}{q} \sum_{i=1}^q \ell_i = \frac{1}{q} [L\ell_1 + \sum_{i=L+1}^q \ell_i]$ and the missdetection probability is given by

First, T_{SPET} is altered to,

$$\begin{aligned} T_{\text{SPET}} &= \frac{\ell_1}{\frac{L\ell_1}{q} + \frac{1}{q} \sum_{i=L+1}^q \ell_i} \\ &= \frac{\ell_1}{\frac{L\ell_1}{q} + \frac{q-L}{q} \frac{1}{q-L} \sum_{i=L+1}^q \ell_i} \\ &= \frac{\ell_1}{\frac{L\ell_1}{q} + \frac{q-L}{q} \sigma_w^2 \xi} \end{aligned} \tag{C.1}$$

where $\xi = \frac{\frac{1}{q-L} \sum_{i=L+1}^q \ell_i}{\sigma_w^2}$ is asymptotically approximated to 1 [89]. The missdetection probability is given by,

$$\begin{aligned} P_m &= \mathbb{P}[T_{\text{SPET}} < \lambda_{\text{SPET}} | \mathcal{H}_1] \\ &= \mathbb{P}\left[\ell_1 < \lambda_{\text{SPET}} \left(\frac{L\ell_1}{q} + \frac{q-L}{q} \sigma_w^2 \xi\right)\right] \\ &= \mathbb{P}\left[\ell_1 \left(1 - \frac{\lambda_{\text{SPET}} L}{q}\right) < \lambda_{\text{SPET}} \frac{q-L}{q} \xi\right] \\ &= \mathbb{P}\left[\frac{\ell_1}{\sigma_w^2} < \frac{\lambda_{\text{SPET}} \frac{q-L}{q} \xi}{1 - \frac{\lambda_{\text{SPET}} L}{q}}\right] \\ &= 1 - \mathbb{P}\left[\frac{\ell_1}{\sigma_w^2} > \frac{(q-L)\lambda_{\text{SPET}}}{q-L\lambda_{\text{SPET}}} \xi\right] \end{aligned} \tag{C.2}$$

The instantaneous received SNR ρ is obtained as,

$$\begin{aligned}\rho &= \frac{E[\|\mathbf{x}(n) - \mathbf{w}(n)\|^2]}{E[\|\mathbf{w}(n)\|^2]} \\ &= \frac{L(\lambda_1 - \sigma_w^2)}{ML\sigma_w^2} \\ &= \frac{1}{M} \left(\frac{\lambda_1}{\sigma_w^2} - 1 \right)\end{aligned}\tag{C.3}$$

This implies that $\frac{\lambda_1}{\sigma_w^2} = 1 + M\rho$. The largest eigenvalue has a limiting Gaussian distribution as follows [100],

$$\ell_1 \xrightarrow{\text{dist}} \mathcal{N} \left(\lambda_1 + \frac{(q-L)\lambda_1\sigma_w^2}{N(\lambda_1 - \sigma_w^2)}, \frac{\lambda_1^2}{N} \right),\tag{C.4}$$

which implies that $\frac{\ell_1}{\sigma_w^2} \xrightarrow{\text{dist}} \mathcal{N}(\mu_n, \sigma_n^2)$, where

$$\begin{aligned}\mu_n &= \frac{\lambda_1}{\sigma_w^2} + \frac{(q-L)\lambda_1}{N(\lambda_1 - \sigma_w^2)} \\ &= \frac{\lambda_1}{\sigma_w^2} + \frac{q-L}{N} \frac{\lambda_1/\sigma_w^2}{\lambda_1/\sigma_w^2 - 1} \\ &= \frac{\lambda_1}{\sigma_w^2} \left(1 + \frac{q-L}{N} \frac{1}{\lambda_1/\sigma_w^2 - 1} \right) \\ &= (1 + M\rho) \left(1 + \frac{q-L}{N} \frac{1}{M\rho} \right) \\ &= (1 + M\rho) \left[1 + \frac{L(M-1)}{MN\rho} \right]\end{aligned}\tag{C.5}$$

and

$$\begin{aligned}\sigma_n^2 &= \frac{\lambda_1^2}{N\sigma_w^4} \\ &= \frac{(1 + M\rho)^2}{N}\end{aligned}\tag{C.6}$$

Let us denote $x = \frac{(q-L)\lambda_{\text{SPET}}}{q-L\lambda_{\text{SPET}}}$, the missdetection probability is calculated by,

$$\begin{aligned}P_m &= \mathbb{P} \left[\frac{\ell_1}{\sigma_w^2} < x \right] \\ &= 1 - \text{Q} \left(\frac{x - \mu_n}{\sigma_n} \right) \\ &= 1 - \text{Q} \left[\frac{\sqrt{N}}{1 + M\rho} x - \sqrt{N} \left(1 + \frac{q-L}{M\rho N} \right) \right] \\ &= 1 - \text{Q} \left(\frac{\sqrt{N}}{1 + M\rho} \frac{M-1}{M} \lambda_{\text{SPET}} - \sqrt{N} - \frac{L(M-1)}{M\rho\sqrt{N}} \right)\end{aligned}\tag{C.7}$$

C.2 Mathematical Derivation for the Pre-whitening Technique

The received signal is filtered by a narrowband filter. Therefore, the noise embedded in the received signal is also filtered. Let $w(n)$ be the noise samples before the filter, which are assumed to be i.i.d. Let $g(k), k = 0, 1, \dots, N_f$ be the employed filter. After filtering, the noise samples turn to,

$$\tilde{w}(n) = \sum_{k=0}^{N_f} g(k)w(n-k) \quad (\text{C.8})$$

Let us Consider L consecutive outputs as follows,

$$\tilde{\mathbf{w}}_L(n) = [\tilde{w}(n), \dots, \tilde{w}(n-L+1)]^T \quad (\text{C.9})$$

The statistical covariance matrix of the filtered noise becomes,

$$\mathbf{R}_{L, \tilde{\mathbf{w}}} = \mathbf{E}[\tilde{\mathbf{w}}_L \tilde{\mathbf{w}}_L^H] = \sigma_w^2 \mathbf{G} \mathbf{G}^H \quad (\text{C.10})$$

where \mathbf{G} is an $L \times (L + N_f)$ matrix defined as,

$$\mathbf{G} = \begin{bmatrix} g(0) & \dots & g(N_f - 1) & g(N_f) & \dots & 0 \\ & \ddots & & & \ddots & \\ 0 & \dots & g(0) & \dots & g(N_f - 1) & g(N_f) \end{bmatrix} \quad (\text{C.11})$$

Let $\mathbf{D} = \mathbf{G} \mathbf{G}^H$. Note that \mathbf{D} is a positive-definite symmetric matrix. It can be decomposed to $\mathbf{D} = \mathbf{Q}^2$

where \mathbf{Q} is also a positive-definite symmetric matrix. Hence, we can transform the statistical covariance matrix into,

$$\mathbf{Q}^{-1} \mathbf{R}_{L, \tilde{\mathbf{w}}} \mathbf{Q}^{-1} = \sigma_w^2 \mathbf{I}_L \quad (\text{C.12})$$

Note that \mathbf{Q} is only related to the filter. Furthermore, since \mathbf{Q} is not related to signal and noise, we can pre-compute its inverse \mathbf{Q}^{-1} and store it for later usage. This pre-whitening technique was used in [92, 93].

Let us consider M antennas at the receiver. The $M \times L$ matrix \mathbf{G} is replaced by the matrix \mathbf{G}_M as

$$\mathbf{G}_M = \begin{bmatrix} \mathbf{G} & \mathbf{0}_L & \dots & \mathbf{0}_L \\ \mathbf{0}_L & \ddots & \ddots & \vdots \\ \vdots & \ddots & \ddots & \mathbf{0}_L \\ \mathbf{0}_L & \dots & \mathbf{0}_L & \mathbf{G} \end{bmatrix} \quad (\text{C.13})$$

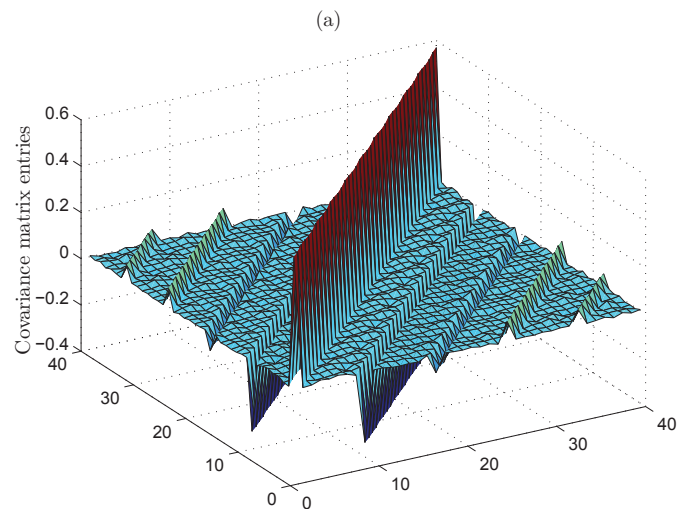


Figure C.1: The covariance matrix of Gaussian noise acting at receiver antennas after applying the narrowband filter.

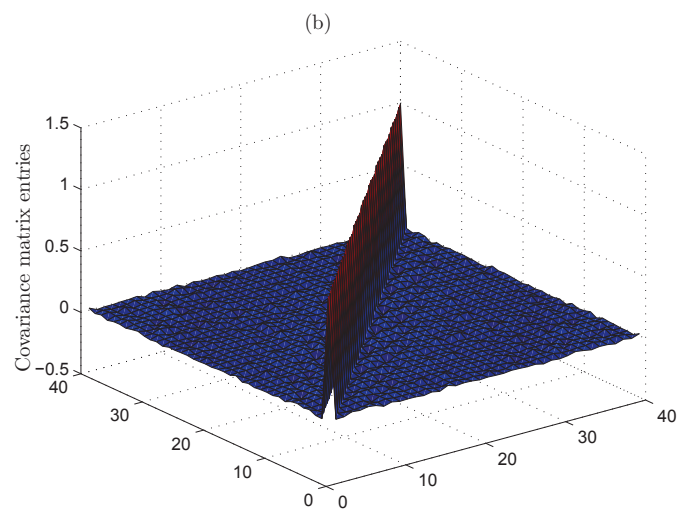


Figure C.2: The covariance matrix of Gaussian noise acting at receiver antennas after applying pre-whitening technique to remove the effect of the narrowband filter.

Figure C.1 displays the noise-only covariance matrix when the narrowband filter is used. It is clear that this filter turns the noise samples to be correlated. Also, Figure C.2 shows the pre-whitened covariance matrix of the noise. This matrix is transformed to a diagonal one.

Appendix D

Appendix Related to Chapter 5

D.1 Derivation of Equation (5.8)

The received signal at the i^{th} antenna is given by

$$x_i(n) = \sum_{p=1}^P \sum_{k=0}^{C_p} h_{i,p}(n, k) s_p(n - k) + w_i(n), \quad n = 1, 2, \dots \quad (\text{D.1})$$

where $w_i(n)$ is the AWGN with zero-mean and variance σ_w^2 , C_p is the order of the channel between the p^{th} primary source (PS $_p$) and each antenna, and $h_{i,p}(n, k)$ is the n^{th} sample of the k^{th} tap of the time-varying channel response between PS $_p$ and the i^{th} antenna.

The term $r(n, m) = E[x_i(n) x_i^*(m)]$ is obtained as,

$$\begin{aligned} r(n, m) &= \mathbf{E} \left[\left(\sum_{p_1=1}^P \sum_{k_1=0}^{C_{p_1}} h_{i,p_1}(n, k_1) s_{p_1}(n - k_1) + w_i(n) \right) \left(\sum_{p_2=1}^P \sum_{k_2=0}^{C_{p_2}} h_{i,p_2}(m, k_2) s_{p_2}(m - k_2) + w_i(m) \right) \right] \\ &= \sum_{p_1=1}^P \sum_{k_1=0}^{C_{p_1}} \sum_{p_2=1}^P \sum_{k_2=0}^{C_{p_2}} \mathbf{E} [h_{i,p_1}(n, k_1) s_{p_1}(n - k_1) h_{i,p_2}(m, k_2) s_{p_2}(m - k_2)] + \sigma_w^2 \delta(n - m) \end{aligned} \quad (\text{D.2})$$

Here we used the fact that the noise and signal components are uncorrelated. The inter-tap correlation is insignificant, and source signals are assumed uncorrelated, hence, we have,

$$\begin{aligned} r(n, m) &= \sum_{p=1}^P \sum_{k=0}^{C_p} \sigma_s^2 r_h(n - m) + \sigma_w^2 \delta(n - m) \\ &= (P + C) \sigma_s^2 r_h(n - m) + \sigma_w^2 \delta(n - m) + \sigma_w^2 \delta(n - m) \end{aligned} \quad (\text{D.3})$$

where $r_h(n - m) \triangleq E \{ h_{i,p}(n, k) h_{i,p}^*(m, k) \}$ and $C = \sum_{p=1}^P C_p$. In the absence of primary signals, we have $\sigma_s^2 = 0$. This proves Equation (5.8), i.e., Under \mathcal{H}_η for $\eta = 0, 1$, $r(n, m)$ is given by,

$$r(n, m) = \eta \underbrace{(P + C)\sigma_s^2}_{\triangleq P_s} r_h(n - m) + \sigma_w^2 \delta(n - m) \quad (\text{D.4})$$

D.2 Optimization of the Weighting Matrix for Time-varying Channels

Under \mathcal{H}_1 , we have $r(n - m) = P_s r_h(n - m) + \sigma_w^2 \delta(n - m)$.

The studied problem is optimized in the low SNR regime, i.e. $P_s \ll \sigma_w^2$. Thus, the variance $\sigma_{\Delta,1}^2$ is approximated as

$$\sigma_{\Delta,1}^2 \simeq \frac{2\sigma_w^4 t_0^2 L^2}{N} (\lambda^2 + \Lambda_t^2) \quad (\text{D.5})$$

The cost function is reformulated as

$$J = \alpha_{t,a} \sum_{n=1}^L \sum_{m=1, m \neq n}^L \tilde{t}_{i,j} r(n - m) + \alpha_{t,b} \quad (\text{D.6})$$

where $\tilde{t}_{i,j} = \frac{t_{i,j}}{t_0}$, $\alpha_{t,a} = \frac{1}{\sqrt{\frac{2}{N}\sigma_w^2 L \sqrt{\lambda^2 + \Lambda_t^2}}}$, and $\alpha_{t,b} = \frac{-\lambda r(0)}{\sqrt{\frac{2}{N}\sigma_w^2 \sqrt{\lambda^2 + \Lambda_t^2}}}$. The Lagrange function is calculated by,

$$\begin{aligned} \Omega_t &= J + \eta_t (\Lambda_t^2 - \Lambda_{t,0}^2) \\ &= \alpha_{t,a} \sum_{n=1}^L \sum_{m=1, m \neq n}^L \tilde{t}_{n,m} r(n - m) + \alpha_{t,b} + \frac{\eta_t}{L^2} \sum_{n=1}^L \sum_{m=1, m \neq n}^L \sum_{d=d_{min}}^{d_{max}} \tilde{t}_{n,m} \tilde{t}_{d,d-n+m} - \eta_t \Lambda_{t,0}^2 \end{aligned} \quad (\text{D.7})$$

The partial derivative is given by

$$\frac{d\Omega_t}{d\tilde{t}_{n,m}} = \alpha_{t,a} r(n - m) + \frac{\eta_t}{L^2} \sum_{d=d_{min}, d \neq n}^{d_{max}} \tilde{t}_{d,d-n+m} + \frac{2\eta_t}{L^2} \tilde{t}_{n,m}, \quad 1 \leq n, m \leq L, n \neq m \quad (\text{D.8})$$

Setting the partial derivative to zero gives

$$\tilde{t}_{n,m} + \sum_{d=d_{min}}^{d_{max}} \tilde{t}_{d,d-n+m} = -\frac{\alpha_{t,a} L^2 P_s}{\eta_t} r_h(n - m) \quad (\text{D.9})$$

where $r(n - m) = P_s r_h(n - m)$, $n \neq m$. Applying the equality constraint, the arbitrary constant $\Lambda_{t,0}$ is chosen such as,

$$\tilde{t}_{n,m} + \sum_{d=d_{min}}^{d_{max}} \tilde{t}_{d,d-n+m} = L r_h(n - m), \quad 1 \leq n, m \leq L, n \neq m \quad (\text{D.10})$$

At first, we consider $n > m$, the above Equation is rewritten as,

$$\tilde{t}_{n,m} + \sum_{d=1+n-m}^L \tilde{t}_{d,d-n+m} = Lr_h(n-m), \quad 1 \leq n, m \leq L, n > m \quad (\text{D.11})$$

Let us denote $\tau = n - m$, we have

$$\tilde{t}_{n,n-\tau} + \sum_{d=1+\tau}^L \tilde{t}_{d,d-\tau} = Lr_h(\tau), \quad 1 \leq \tau \leq L-1, 1+\tau \leq n \leq L-1 \quad (\text{D.12})$$

The optimal weighting coefficients are determined by solving this system of linear equations. The following is straightforward proved,

$$\tilde{t}_{n_1,n_1-\tau} = \tilde{t}_{n_2,n_2-\tau}, \quad 1 \leq \tau \leq L-1, 1+\tau \leq n_1, n_2 \leq L-1, \quad (\text{D.13})$$

which results in $\tilde{t}_{n,n-\tau} = \frac{Lr_h(\tau)}{L-\tau}$. Finally, we conclude,

$$\tilde{t}_{n,m} = \frac{Lr_h(n-m)}{L-(n-m)}, \quad 1 \leq n, m \leq L, n > m \quad (\text{D.14})$$

Repeating the same steps when $n < m$, the optimal weighting coefficients are given by,

$$\tilde{t}_{n,m} = \frac{Lr_h(n-m)}{L-|n-m|}, \quad 1 \leq n, m \leq L, n \neq m \quad (\text{D.15})$$

Bibliography

- [1] J. Billion, D. V. den Abeele, C. Gransart, and M. Berbineau, "ICOM: Toward integrated communications for global railway systems," in *WCRR 08*, Seoul, Korea, 2008.
- [2] F.-U. Andersen, H. Berndt, H. Abramowicz, and R. Tafazolli, "Future internet from mobile and wireless requirements perspective, emobility technology platform," 2007, White Paper. [Online]. Available: http://www.ist-emobility.org/WorkingGroups/PostIP/WhitePaper_v0-6.pdf
- [3] M. Kassab, "Optimisation des handovers de niveau 2 pour une mobilité intra et inter technologies," Ph.D. dissertation, Université de Rennes 1, Télécom Bretagne, December 2008.
- [4] "Architecture générique de gestion des ressources et des protocoles associés," Urban Planing for Radio Communications, URC-SP1-D1,2,3, November 2007.
- [5] A. Amanna, M. G. M. J. Price, J. H. Reed, W. P. Siriwongpairat, and T. K. Himsoon, "Railway cognitive radio, future wireless communication systems for railways," *IEEE Vehicular Technology Magazine*, vol. 5, no. 3, pp. 82–89, 2010.
- [6] <http://www.integrail.info/>.
- [7] J.-C. Maureira, "Internet on rails," Ph.D. dissertation, University of Nice - Sophia Antipolis, January 2011.
- [8] T. Manabe and H. Hojo, "Technologies for railway internet services in japan," in *ITST2010*, Kyoto, Japan, November 2010.
- [9] D. Sanz, B. Villeforceix, D. Duchange, P. Pasquet, and P. Mercier, "Tgv communicant research program: from reasearch to industrialisation of onboard broadband internet services for high-speed trains," in *World Congress on Railway Research*, Seoul, Korea, May 2008.
- [10] D. Sanz, H. Ghannoum, and B. Villeforceix, "Delivering broadband internet access for high speed trains passengers using the new wifi standard 802.11n for train-to-ground communications," in *UIC Conference*, Banff, Canada, September 2011.
- [11] M. Berbineau, *Les systèmes de télécommunication existants ou émergents et leur utilisation dans le domaine des transports guidés*. IFSTTAR/INRETS, 2002.

- [12] N. B. Slimen, V. Deniau, J. Rioult, S. Dudoyer, and S. Baranowski, "Statistical characterisation of the EM interferences acting on GSM-R antennas fixed above moving trains," *The European Physical Journal Applied Physics*, vol. 48, no. 2, p. 21202 (7 pages), Nov. 2009.
- [13] "Spectrum policy task force," Federal Communications Commission, ET Docket No. 02-135, November 2002.
- [14] "General survey of radio frequency bands (30 MHz to 3 GHz): Vienna, virginia," Shared Spectrum Company, Tech. Rep. 20100323, September 2010. [Online]. Available: <http://www.sharespectrum.com/papers/spectrum-reports/>
- [15] J. Mitola, "Cognitive radio," Ph.D. dissertation, Roy. Inst. Technol., Stockholm, Sweden, 1999.
- [16] "SDRF cognitive radio definitions working document," Software Defined Radio Forum, SDRF-06-R-0011-V1.0.0, November 2007.
- [17] "Notice of proposed rule making and order: Facilitating opportunities for flexible, efficient, and reliable spectrum use employing cognitive radio technologies," Federal Communications Commission, ET Docket No. 03-108, Feb. 2005.
- [18] S. Haykin, "Cognitive Radio: Brain-Empowered Wireless Communications," *IEEE Journal on Selected Area in Communications*, vol. 23, no. 2, pp. 201–220, February 2005.
- [19] B. Fette, *Cognitive Radio Technology*, 2nd ed. Academic Press, Elsevier Inc., 2009.
- [20] C. Stevenson, G. Chouinard, Z. Lei, W. Hu, S. Shellhammer, and W. Caldwell, "IEEE 802.22: The first cognitive radio wireless regional area network standard," *IEEE Communications Magazine*, vol. 47, no. 1, pp. 130–138, 2009.
- [21] <http://grouper.ieee.org/groups/dyspan/>.
- [22] H. Arslan, Ed., *Cognitive Radio, Software Defined Radio, and Adaptive Wireless Systems*. Springer, 2007.
- [23] <http://corridor.ifsttar.fr/>.
- [24] K. Hassan, "Rapport d'avancement de thèse : Application de la radio opportuniste à la continuité de services et à la sécurité des transports dans un contexte à forte mobilité," IFSTTAR, RA-11-702-FR, 2010.
- [25] M. Patzold, *Mobile Radio Channels*, 2nd ed. John Wiley & Sons, Ltd., 2011.
- [26] K. E. Baddour and N. C. Beaulieu, "Autoregressive modeling for fading channel simulation," *IEEE Transactions on Wireless Communications*, vol. 4, no. 4, pp. 1650–1662, 2005.
- [27] R. H. Clarke, "A statistical theory of mobile-radio reception," *Bell Syst. Tech. J.*, vol. 47, pp. 975–1000, August 1968.
- [28] W. C. Jakes, *Microwave Mobile Communications*, 2nd ed. Piscataway, NJ: Wiley-IEEE Press., 1994.

- [29] D. J. Young and N. C. Beaulieu, "Limitations of sum-of-sinusoids fading channel simulators," *IEEE Transactions on Communications*, vol. 49, no. 4, pp. 699–708, 2001.
- [30] M. Patzold and B. O. Hogstad, "Classes of sum-of-sinusoids rayleigh fading channel simulators and their stationary and ergodic properties - part i," *WSEAS Transactions on Mathematics*, vol. 5, no. 1, pp. 222–230, Feb. 2006.
- [31] Y. R. Zheng and C. Xiao, "Simulation models with correct statistical properties for rayleigh fading channels," *IEEE Transactions on Communications*, vol. 51, no. 6, pp. 920–928, June 2003.
- [32] A. G. Zajic and G. L. Stuber, "Efficient simulation of rayleigh fading with enhanced decorrelation properties," *IEEE Transactions on Wireless Communications*, vol. 5, no. 7, pp. 1866–1875, July 2006.
- [33] Y. X. Li and X. J. Huang, "The simulation of independent rayleigh faders," *IEEE Transactions on Communications*, vol. 50, no. 9, pp. 1503–1514, Sept. 2002.
- [34] M. Patzold, U. Killat, F. Laue, and Y. Li, "On the statistical properties of deterministic simulation models for mobile fading channels," *IEEE Transactions on Vehicular Technology*, vol. 47, no. 1, pp. 254–269, Feb. 1998.
- [35] C.-X. Wang, M. Patzold, and D. Yuan, "Accurate and efficient simulation of multiple uncorrelated rayleigh fading waveforms," *IEEE Transactions on Wireless Communications*, vol. 6, no. 3, pp. 833–839, Mar. 2007.
- [36] M. Patzold, C.-X. Wang, and B. O. Hogstad, "Two new sum-of-sinusoids-based methods for the efficient generation of multiple uncorrelated rayleigh fading waveforms," *IEEE Transactions on Wireless Communications*, vol. 8, no. 6, pp. 3122–3131, June 2009.
- [37] D.-S. Shiu, G. J. Foschini, M. J. Gans, and J. M. Kahn, "Fading correlation and its effect on the capacity of multielement antenna systems," *IEEE Transactions on Communications*, vol. 48, no. 3, pp. 502–13, 2000.
- [38] S. Loyka, "Channel capacity of mimo architecture using the exponential correlation matrix," *IEEE Communications Letters*, vol. 5, no. 9, pp. 369–371, September 2001.
- [39] J. G. Gonzalez, "Robust techniques for wireless communications in non-gaussian environments," Ph.D. dissertation, University of Delaware, 1997.
- [40] D. Middleton, "Non-gaussian noise models in signal processing for telecommunications: New methods and results for class a and class b noise models," *IEEE Trans. Info. Theory*, vol. 45, no. 4, pp. 1129–1149, May 1999.
- [41] J. Ilow, "Signal processing in alpha-stable noise environments noise modeling, detection and estimation," Ph.D. dissertation, University of Toronto, 1995.
- [42] C. Nikias and M. Shao, *Signal processing with alpha-stable distribution and application*. John Wiley and Sons, New York, 1995.

- [43] M. Nassar, K. Gulati, M. R. DeYoung, B. L. Evans, and K. R. Tinsley, "Mitigating near-field interference in laptop embedded wireless transceivers," *Journal of Signal Processing Systems*, vol. 36, no. 1, pp. 1–12, March 2009.
- [44] J. H. McCulloch, "Simple consistent estimators of stable distribution parameters," *Communications in Statistics - Simulation and Computation*, vol. 15, no. 4, pp. 1109–1136, 1986.
- [45] E. E. Kuruoglu, "Density parameter estimation of skewed α -stable distributions," *IEEE Transactions on Signal Processing*, vol. 49, no. 10, pp. 2192–2201, 2001.
- [46] S. M. Kogon and D. B. Williams, "A practical guide to heavy tails," R. J. Adler, R. E. Feldman, and M. S. Taqqu, Eds. Cambridge, MA, USA: Birkhauser Boston Inc., 1998, ch. Characteristic function based estimation of stable distribution parameters, pp. 311–335.
- [47] J. Mitola and G. Q. Maguire, "Cognitive radio: making software radios more personal," *IEEE Personal Commun. Mag.*, vol. 6, no. 4, pp. 13–18, Aug. 1999.
- [48] O. A. Dobre, A. Abdi, Y. Bar-Ness, and W. Su, "Survey of automatic modulation classification techniques: classical approaches and new trends," *IET Communications*, vol. 1, pp. 137–156, 2007.
- [49] J. L. Xu, W. Su, and M. C. Zhou, "Likelihood ratio approaches to automatic modulation classification," *IEEE Transactions on Systems, Man, and Cybernetics: Part C*, vol. 41, pp. 455–469, July 2011.
- [50] M. L. D. Wong and A. K. Nandi, "Automatic digital modulation recognition using artificial neural network and genetic algorithm," *Signal Processing*, vol. 84, pp. 351–365, 2004.
- [51] H.-C. Wu, M. Saquib, and Z. Yun, "Novel automatic modulation classification using cumulant features for communications via multipath channels," *IEEE Transactions on Wireless Communications*, vol. 7, no. 8, pp. 3098–3105, August 2008.
- [52] O. A. Dobre, A. Abdi, Y. Bar-Ness, and W. Su, "Cyclostationarity-based modulation classification of linear digital modulations in flat fading channels," *Wireless Personal Communications Journal*, vol. 54, no. 4, pp. 699–717, September 2010.
- [53] K. Hassan, I. Dayoub, W. Hamouda, and M. Berbineau, "Automatic modulation recognition using wavelet transform and neural networks in wireless systems," *EURASIP Journal on Advances in Signal Processing*, Article ID 532898, 13 pages, June 2010.
- [54] A. K. Nandi and E. E. Azzouz, "Algorithms for automatic modulation recognition of communication signals," *IEEE Transactions on Communications*, vol. 46, pp. 431–436, 1998.
- [55] L. Hong and K. C. Ho, "Identification of digital modulation types using the wavelet transform," in *IEEE Military Communications Conference (MILCOM '99)*, Atlantic City, NJ, USA, October 1999, pp. 427–431.

- [56] A. Swami and B. Sadler, "Hierarchical digital modulation classification using cumulants," *IEEE Trans. Communications*, vol. 48, no. 3, pp. 416–429, 2000.
- [57] I. Dayoub, A. Okassa-MFoubat, R. Mvone, and J. M. Rouvaen, "A blind modulation type detector for DPRS standard," *Wireless Personal Communications*, vol. 41, pp. 225–241, 2007.
- [58] V. Choqueuse, S. Azou, K. Yao, L. Collin, and G. Burel, "Blind modulation recognition for MIMO systems," *Journal of the ATM Bucharest*, vol. XIX, no. 2, pp. 183–196, 2009.
- [59] M. Riedmiller and H. Braun, "A direct adaptive method for faster backpropagation learning: the rprop algorithm," in *Proc. IEEE International Conference on Neural Networks*, San Francisco, CA, October 1993.
- [60] D. A. Gore, R. W. H. Jr., and A. J. Paulraj, "Transmit selection in spatial multiplexing systems," *IEEE Communications Letters*, vol. 6, no. 11, pp. 491–493, Nov 2002.
- [61] C. Wang and *et al.*, "On the performance of the MIMO zero-forcing receiver in the presence of channel estimation error," *IEEE Transactions on Wireless Communications*, vol. 6, no. 3, pp. 805–810, March 2007.
- [62] A. Ikhlef and D. L. Guennec, "A simplified constant modulus algorithm for blind recovery of MIMO QAM and PSK signals: a criterion with convergence analysis," *EURASIP Journal on Wireless Communications and Networking*, Article ID 90401, 13 pages, 2007.
- [63] L. Wang, R. C. de Lamare, and Y. L. Cai, "Low-complexity adaptive step size constrained constant modulus SG algorithms for adaptive beamforming," *Signal Processing*, vol. 89, pp. 2503–2513, December 2009.
- [64] S. Douglas, "Combined subspace tracking, prewhitening, and contrast optimization for noisy blind signal separation," in *2nd int. workshop Indept. Component Analysis Source Separation*, Helsinki, Finland, June 2000, pp. 579–584.
- [65] C. Papadias, "Globally convergent blind source separation based on a multiuser kurtosis maximization criterion," *IEEE Transactions on Signal Processing*, vol. 48, no. 12, pp. 3508–3519, December 2000.
- [66] K. Hassan, C. N. Nzéza, R. Gautier, E. Radoi, M. Berbineau, and I. Dayoub, "Blind detection of the number of transmitting antennas for spatially-correlated mimo systems," in *IEEE International Conference on Intelligent Transport Systems Telecommunications (ITST)*, Saint-Petersburg, Russia, August 2011.
- [67] S. Buzzi, L. Venturino, A. Zappone, and A. D. Maio, "Blind user detection in doubly dispersive DS-CDMA fading channels," *IEEE Transactions on Signal Processing*, vol. 58, no. 3, pp. 1446–1451, March 2010.
- [68] G. Burel, "Detection of spread spectrum transmission using fluctuations of correlation estimators," in *IEEE ISPACS*, Honolulu, Hawaii, USA, November 2000.

- [69] C. Boudier, S. Azou, and G. Burel, "Performance analysis of a spreading sequence estimator for spread spectrum transmissions," *J. Franklin Inst.*, vol. 341, no. 7, pp. 595–614, October 2004.
- [70] C. N. Nzéza, R. Gautier, and G. Burel, "Blind Multiuser Detection in Multirate CDMA Transmissions Using Fluctuations of Correlation Estimators," in *IEEE-GlobeCom06*, San Francisco, California, USA, 2006.
- [71] T. Koivisto and V. Koivunen, "Blind despreading of short-code DS-CDMA signals in asynchronous multi-user systems," *Signal Processing*, vol. 87, pp. 2560–2568, April 2007.
- [72] C. N. Nzéza and R. Gautier, "Blind detection, parameters estimation and despreading of DS-CDMA signals in multirate multiuser cognitive radio systems," in *Advances in Cognitive Radio Systems*, C.-X. Wang and J. Mitola, Eds. InTech, July 2012, pp. Chapter 6, 105–130. [Online]. Available: <http://www.intechopen.com/books/advances-in-cognitive-radio-systems/>
- [73] W. Akmouche, "Detection of multicarrier modulations using 4th-order cumulants," in *Proceedings of IEEE Military Communications Conference (MILCOM'99)*, vol. 1, 1999, pp. 432–436.
- [74] S. Chaudhari, V. Koivunen, and H. V. Poor, "Autocorrelation-based decentralized sequential detection of ofdm signals in cognitive radios," *IEEE Transactions on Signal Processing*, vol. 57, no. 7, pp. 2690–2700, July 2009.
- [75] A. Punchihewa, Q. Zhang, O. A. Dobre, C. Spooner, S. Rajan, and R. Inkol, "On the cyclostationarity of OFDM and single carrier linearly digitally modulated signals in time dispersive channels: Theoretical developments and application," *IEEE Transactions on Wireless Communications*, vol. 9, no. 8, pp. 2588–2599, August 2010.
- [76] V. L. Nir, T. V. Waterschoot, M. Moonen, and J. Duplicy, "Blind CP-OFDM and ZP-OFDM parameter estimation in frequency selective channels," *EURASIP Journal on Wireless Communications and Networking*, vol. 2009, p. 10, 2009.
- [77] A. Bouzegzi, P. Ciblat, and P. Jallon, "New algorithms for blind recognition of OFDM based systems," *Signal Processing*, vol. 90, no. 3, pp. 900–913, 2010.
- [78] C. N. Nzéza, M. Berbineau, G. Moniak, R. Gautier, G. Burel, and I. Dayoub, "Blind MC-DS-CDMA parameters estimation in frequency selective channels," in *IEEE GLOBECOM Workshops*, Honolulu, HI, November 2009, pp. 1–6.
- [79] C. N. Nzéza, K. Hassan, M. Berbineau, R. Gautier, and G. Burel, "Blind MIMO MC-CDMA parameters estimation over fading channels for cognitive radio," in *Proceedings of 10th International Conference on Intelligent Transport Systems Telecommunications, ITST 2010*, Kyoto, Japon, November 2010, pp. 1–6.
- [80] 3GPP, "TS 45.005," 3GPP Technical Specification, Tech. Rep., 2007-2, v7.9.0.

- [81] I. F. Akyildiz, B. F. Lo, and R. Balakrishnan, "Cooperative spectrum sensing in cognitive radio networks: A survey," *Physical Communication (Elsevier) Journal*, vol. 4, no. 1, pp. 40–62, March 2011.
- [82] C. R. Stevenson, C. Cordeiro, E. Sofer, and G. Chouinard, "Functional requirements for the 802.22 WRAN standard," *IEEE Std. 802.22-05/0007r46*, Sep. 2005.
- [83] Y. H. Zeng, Y.-C. Liang, A. T. Hoang, and R. Zhang, "A review on spectrum sensing for cognitive radio: Challenges and solutions," *EURASIP Journal on Advances in Signal Processing*, pp. 1–16, Oct. 2010.
- [84] R. Tandra and A. Sahai, "SNR walls for signal detection," *IEEE Journal of Selected Topics in Signal Processing*, vol. 2, no. 1, pp. 4–17, Feb. 2008.
- [85] T. Yucek and H. Arslan, "A survey of spectrum sensing algorithms for cognitive radio applications," *IEEE Communications Surveys & Tutorials*, vol. 11, no. 1, pp. 116–130, First Quarter 2009.
- [86] Y. Zeng and Y.-C. Liang, "Robustness of the cyclostationary detection to cyclic frequency mismatch," in *IEEE 21st International Symposium on Personal Indoor and Mobile Radio Communications (PIMRC)*, Istanbul, Turkey, September 2010, pp. 2704–2709.
- [87] S. Shellhammer and R. Tandra, *Performance of the Power Detector With Noise Uncertainty*, IEEE 802.22-06/0134r0 Std., July 2006. [Online]. Available: http://ieee802.org/22/Meeting_documents/2006_July/22-06-0134-00-0000_Performance-of-the-powerdetector-with-Noise-Uncertainty.ppt
- [88] R. Zhang, T. J. Lim, Y.-C. Liang, and Y. Zeng, "Multi-antenna based spectrum sensing for cognitive radios: A GLRT approach," *IEEE Transactions on Communications*, vol. 58, no. 1, pp. 84–88, Jan. 2010.
- [89] A. Taherpour, M. Nasiri-Kenari, and s. Gazor, "Multiple antenna spectrum sensing in cognitive radios," *IEEE Transactions on Wireless Communications*, vol. 9, no. 2, pp. 814–823, Feb. 2010.
- [90] P. Bianchi, M. Debbah, M. Maida, and J. Najim, "Performance of statistical tests for single-source detection using random matrix theory," *IEEE Transactions on Information theory*, vol. 57, no. 4, pp. 1–20, April 2011.
- [91] Y. H. Zeng, Y.-C. Liang, and R. Zhang, "Blindly combined energy detection for spectrum sensing in cognitive radio," *IEEE Signal Processing Letters*, vol. 15, pp. 649–652, Oct. 2008.
- [92] Y. H. Zeng and Y.-C. Liang, "Spectrum-sensing algorithms for cognitive radio based on statistical covariances," *IEEE Transactions on Vehicular Technology*, vol. 58, no. 4, pp. 1804–1815, 2009.
- [93] —, "Eigenvalue-based spectrum sensing algorithms for cognitive radio," *IEEE Transactions on Communications*, vol. 57, no. 6, pp. 1784–1793, 2009.

- [94] M. Wax and T. Kailath, "An information theoretic approach to source enumeration in array signal processing," *IEEE Trans. Acoust., Speech, Signal Process.*, vol. 33, no. 2, pp. 387–392, Apr. 1985.
- [95] R. Wang and M. Tao, "Blind spectrum sensing by information theoretic criteria for cognitive radios," *IEEE Transactions on Vehicular Technology*, vol. 59, no. 8, pp. 3806–3817, Oct. 2010.
- [96] W. Chen, K. M. Wong, and J. P. Reilly, "Detection of the number of signals: A predicted eigen-threshold approach," *IEEE Transactions on Signal Processing*, vol. 39, no. 5, pp. 1088–1098, 1991.
- [97] J. F. C. E. Moulines, P. Duhamel and S. Mayrargue, "Subspace methods for the blind identification of multichannel fir filters," *IEEE Transactions on Signal Processing*, vol. 43, no. 2, pp. 516–525, 1995.
- [98] I. Johnstone, "On the distribution of the largest eigenvalue in principal components analysis," *The Annals of Statistics*, vol. 29, no. 2, pp. 295–327, 2001.
- [99] B. Nadler, "On the distribution of the ratio of the largest eigenvalue to the trace of a wishart matrix," *Journal of Multivariate Analysis*, vol. 102, no. 2, pp. 363–371, Feb. 2011.
- [100] F. Haddadi, M. M. Mohammadi, M. M. Nayebi, and M. R. Aref, "Statistical performance analysis of MDL source enumeration in array processing," *IEEE Transactions on Signal Processing*, vol. 58, no. 1, pp. 452–457, Jan. 2010.
- [101] Z. Tian and G. B. Giannakis, "A wavelet approach to wideband spectrum sensing for cognitive radios," in *Proceedings of International Conference on Cognitive Radio Oriented Wireless Networks and Communications (CrownCom 2006)*, June 2006, pp. 1–5.
- [102] B. Farhang-Boroujeny, "Filter bank spectrum sensing for cognitive radios," *IEEE Transactions on Signal Processing*, vol. 56, no. 5, pp. 1801–1811, May 2008.
- [103] S. Haykin, D. J. Thomson, and J. H. Reed, "Spectrum sensing for cognitive radio," *Proceedings of the IEEE*, vol. 97, no. 5, pp. 849–877, May 2009.
- [104] Z. Tian and G. B. Giannakis, "Compressed sensing for wideband cognitive radios," in *Proceedings of IEEE International Conference on Acoustics, Speech, and Signal Processing (ICASSP 2007)*, Honolulu, Hawaii, Apr. 2007, pp. 1357–1360.
- [105] M. Mishali and Y. C. Eldar, "Wideband spectrum sensing at sub-nyquist rates," *IEEE Signal Processing Magazine*, vol. 28, no. 4, pp. 102–135, July 2011.
- [106] E. J. Candes and M. B. Wakin, "An introduction to compressive sampling," *IEEE Signal Processing Magazine*, vol. 25, no. 2, pp. 21–30, Mar. 2008.
- [107] J. N. Laska, S. Kirolos, Y. Massoud, R. G. Baraniuk, A. C. Gilbert, M. Iwen, and M. J. Strauss, "Random sampling for analog-to-information conversion of wideband signals," in *Proceedings of the IEEE Dallas Circuits and Systems Workshop (DCAS)*, Oct. 2006.

- [108] J. A. Tropp, J. N. Laska, M. F. D. J. K. Romberg, and R. G. Baraniuk, "Beyond nyquist: Efficient sampling of sparse bandlimited signals," *IEEE Transactions on Information Theory*, vol. 56, no. 1, pp. 520–544, Jan. 2010.
- [109] M. Mishali and Y. C. Eldar, "From theory to practice: Sub-nyquist sampling of sparse wideband analog signals," *IEEE Journal of Selected Topics in Signal Processing*, vol. 4, no. 2, pp. 375–391, Apr. 2010.
- [110] S. Kim, J. Lee, H. Wang, and D. Hong, "Sensing performance of energy detector with correlated multiple antennas," *IEEE Signal Processing Letters*, vol. 16, no. 8, pp. 671–674, August 2009.
- [111] X. Yang, K. Lei, S. Peng, and X. Cao, "Sensing performance analysis of GLRT detector with multiple antennas: does correlation help?" in *IET 3rd International Conference on Wireless, Mobile and Multimedia Networks (ICWMNN 2010)*, Beijing, China, 26-29 Sept. 2010.
- [112] L. Luo, P. Zhang, G. Zhang, and J. Qin, "Spectrum sensing for cognitive radio networks with correlated multiple antennas," *Electronics Letters*, vol. 47, no. 23, pp. 1297–1298, November 2011.
- [113] D.-C. Oh, J.-H. Lee, and Y.-H. Lee, "Spectrum sensing based on antenna correlation in cognitive radio systems," *Wirel. Pers. Commun.*, vol. 63, no. 3, pp. 703–712, Apr. 2012. [Online]. Available: <http://dx.doi.org/10.1007/s11277-010-0161-y>
- [114] V. R. S. Banjade, N. Rajatheva, and C. Tellambura, "Performance analysis of energy detection with multiple correlated antenna cognitive radio in nakagami-m fading," *IEEE Communications Letters*, vol. 16, no. 4, pp. 502–505, April 2012.
- [115] M. Orooji, R. Soosahabi, and M. Naraghi-Pour, "Blind spectrum sensing using antenna arrays and path correlation," *IEEE Transactions on Vehicular Technology*, vol. 60, no. 8, pp. 3758–3767, October 2011.
- [116] R. Gray, "On the asymptotic eigenvalue distribution of toeplitz matrices," *IEEE Transactions Information Theory*, vol. 18, no. 6, pp. 725–730, November 1972.
- [117] H. G. Kang, I. Song, S. Yoon, and Y. H. Kim, "A class of spectrum-sensing schemes for cognitive radio under impulsive noise circumstances: Structure and performance in nonfading and fading environments," *IEEE Transactions on Vehicular Technology*, vol. 59, no. 9, pp. 4322–4339, 2010.
- [118] J. Lundén, S. A. Kassam, and V. Koivunen, "Robust nonparametric cyclic correlation-based spectrum sensing for cognitive radio," *IEEE Transactions on Signal Processing*, vol. 58, no. 1, pp. 38–52, 2010.
- [119] F. Moghimi, A. Nasri, and R. Schober, "Adaptive l_p norm spectrum sensing for cognitive radio networks," *IEEE Transactions on Communications*, vol. 59, no. 7, pp. 1934–1945, 2011.

- [120] T. Wimalajeew and P. K. Varshney, "Polarity-coincidence-array based spectrum sensing for multiple antenna cognitive radios in the presence of non-gaussian noise," *IEEE Transactions on Wireless Communications*, vol. 10, no. 7, pp. 2362–2371, 2011.
- [121] E. Kuruoglu, "Signal processing in alpha stable environments: A least l_p approach," Ph.D. dissertation, University of Cambridge, 1998.
- [122] S. Ambike, J. Ilow, and D. Hatzinakos, "Detection for binary transmission in a mixture of gaussian noise and impulsive noise modeled as an alpha-stable process," *IEEE Signal Processing Letters*, vol. 1, pp. 55–57, Mar 1994.
- [123] T. Pander and T. Przybyla, "Impulsive noise cancelation with simplified cauchy-based l_p -norm filter," *Signal Processing*, vol. 92, no. 9, pp. 2187–2198, September 2012.
- [124] J. Gonzalez and G. Arce, "Statistically-efficient filtering in impulsive environments: Weighted myriad filters," *EURASIP Journal on Applied Signal Processing*, vol. 2002, no. 1, pp. 4–20, 2002.
- [125] P. Tsakalides and C. Nikias, "The robust covariation-based music (roc-music) algorithm for bearing estimation in impulsive noise environments," *IEEE Transactions on Signal Processing*, vol. 44, no. 7, pp. 1623–1633, 1996.
- [126] L. Liu, C. Tao, T. Zhou, Y. Zhao, X. Yin, and H. Chen, "A highly efficient channel sounding method based on cellular communications for high-speed railway scenarios," *EURASIP Journal on Wireless Communications and Networking*.
- [127] <http://www.openairinterface.org/>.

Titre : Contributions aux capacités de reconnaissance de l'environnement de la radio cognitive pour des applications mobiles à grande vitesse.

Résumé

Les principaux objectifs des opérateurs ferroviaires visent à accroître la sécurité, réduire les coûts d'exploitation et de maintenance et augmenter l'attractivité et les bénéfices du transport ferroviaire en offrant de nouveaux services aux passagers. Ceci ne pourra être atteint que grâce à la multiplication des échanges de données entre les différents acteurs du monde ferroviaire. L'interopérabilité, l'efficacité spectrale, l'optimisation de l'usage des ressources radio et l'amélioration de la fiabilité des communications sont des exigences fortes pour les applications de télécommunication ferroviaires. Les recherches dans le domaine de la radio cognitive ont vu le jour afin de répondre aux besoins de communication de l'armée ainsi qu'aux besoins dans les secteurs de la sécurité publique. Ces domaines partagent souvent les mêmes exigences que les chemins de fers. Ainsi, la radio cognitive a montré un potentiel prometteur pour répondre aux besoins listés précédemment. Une des principales fonctionnalités d'un dispositif de radio cognitive est de prendre conscience de son environnement radioélectrique et de détecter les bandes disponibles. Trois principaux éléments définissent l'environnement de la radio cognitive : l'utilisateur, les règles d'accès au spectre radio et les domaines radio. Cette thèse met en avant plusieurs contributions relatives à la reconnaissance de l'environnement radiofréquence et la détection de bandes libres. Plus spécifiquement, ces contributions portent sur la reconnaissance par la radio cognitive de l'occupation du spectre et de la modulation des signaux présents dans les bandes analysées. Ces fonctions ont été conçues pour le contexte ferroviaire, c'est-à-dire la grande vitesse et un environnement électromagnétique difficile en présence de bruit impulsif.

Mots Clef : Cognitive radio, sondage spectral, identification de forme d'ondes, grande vitesse ferroviaire, bruit impulsive, antennes multiple, multiple-input multiple-output.

Title : Contributions to Cognitive Radio Awareness for High Mobility Applications

Abstract

An essential goal of railway operators is to increase safety, reduce operation and maintenance costs, and increase attraction and profit by offering new services to passengers. These objectives will be reached thanks to a huge increase of data fluxes exchanges between railways stakeholders and infrastructures. Interoperability, spectral efficiency, optimization of radio resource usages, and improvement of communications reliability are of significant interest for railway applications. The Cognitive Radio (CR) research has been successfully applied to meet the communication needs of the military as well as the public-safety sectors, which share many of the same needs as railway. CRs have shown significant promise to answer all of the previously listed requirements. One of the main capabilities of a CR device is to sense and finally become aware of its environment. Three major domains define the environment of the CR, namely, the user, policy, and radio domains. This thesis highlights several contributions to radio environment awareness of a CR device. More specifically, these contributions lie in the spectrum awareness and waveform awareness functions of the CR. We designed these functions for the railways context, that is, a high speed vehicular context, besides difficult electromagnetic environments resulting a heavy-tailed impulsive noise.

Keywords : Cognitive radio, spectrum sensing, waveform identification, high mobility, heavy-tailed noise, multiple-antennas, multiple-input multiple-output systems.